University of Strathclyde

Strathclyde Institute of Pharmacy and Biomedical Science

Combined chemo-radiotherapy utilising Olaparib and Mirin in combination with X-rays and targeted radionuclide therapy

Rhona Jane Galloway

A thesis submitted in fulfilment of the requirements for the degree of Doctor of Philosophy

2016

Declaration

This thesis is the result of the author's original research. It has been composed by the author and has not been previously submitted for examination which has led to the award of a degree.

Signed:

Date:

Acknowledgements

Firstly, I would like to thank my supervisor Dr Marie Boyd for giving me this opportunity and allowing me to be part of her group. I would also like to thank SULSA and AstraZeneca without whom this research could not have been undertaken.

Immeasurable thanks have to go to my second supervisor Dr Annette Sorensen whose patience, encouragement, unequivocal hard work and immense knowledge have contributed so much to this project. What a star!

Thanks also to Dr Anthony McCluskey for his guidance and expertise throughout the project and to Dr Richard Cox for giving up his valuable time to cast an expert eye over my thesis.

A special thanks also to Dr Nicola McGinely, who is hands down the best export Inverness ever had! We have had so many laughs, tears and tantrums along the way and I look forward to so many more throughout life! We are two peas in a pod and I can't wait for the next chapter! First things first though….Do you hear a yeehaw?

Special thanks also to Kay McMillan (top flatmate!), Dr Felicity Lumb, Dr Jenny Crowe, Dr Kara Bell and Dr Jamie Doonan. You have all given me some smashing (and some questionable!) advice and support over the last 4 (and a bit) years, and some absolutely hilarious times. You're the best friends a girl could ask for and this is just the beginning. ☺

Also to Hannah Terrance, Elaine Eadie, all the other Strathys and in particular Anne-Marie Hughes for giving great advice, fantastic support, listening to all my moans and providing a great place for escapism! I'll always bleed maroon!

Additional thanks also go to my new(ish) work mates, Rachel Everett, Eilish Wells, Stephanie Vallot and Mari Eltermann who stepped in to provide fantastic support, encouragement and ears for a moan (despite only knowing me for 6 months!) You're all bonkers and make work so much fun. ☺

Finally, and most importantly, massive thanks must go to my family: Mum, Dad, Auntie Linda, Uncle Ken, Fraser, Jennifer, Auntie Anne and Papa for unwavering encouragement and support on those not always chipper phone calls and for all the free food, laughs and entertainment. ☺

Table of Contents

Table of Figures

List of Abbreviations

3DCRT	3D Conformal Radiotherapy
[^{131}I]MIBG	^{131}Iodine-labelled meta-iodobenzylguanidine
[^{211}At]MABG	^{211}Astatine-labelled meta-astatobenzylguanidine
µg	Microgram
µl	Microlitre
µM	Micromole
ADP	Adenosine diphosphate
APE-1	Apurinic/Apyrimidinic (AP) endonuclease-1
ATM	Ataxia Telengiectasia Mutated
ATP	Adenosine Triphosphate
ATR	Ataxia Telengiectasia and Rad3 related protein
BASC	BRCA1 Associated Genome Surveillance Complex
BER	Base Excision Repair
bNAT	Bovine Noradrenaline Transporter
BRCA	Breast Cancer 1
BSA	Bovine serum albumin
Cdc25c	Cell Division Cycle 25c
cDNA	Complementary DNA
CHK1	Checkpoint Kinase 1
CHK2	Checkpoint Kinase 2
CNS	Central Nervous System
CO_2	Carbon Dioxide
CtIP	CTBP Interacting Protein
DDR	DNA Damage Response
DDT	Dichlorodiphenyltrichloroethane
DEF	Dose Enhancement Factor
dH_2O	Distilled Water
DMSO	Dimethyl Sulfoxide

DNA	Deoxyribonucleic acid
DNA-PKcs	DNA Dependent Protein Kinase Catalytic Subunit
DSB	Double-strand DNA break
dsDNA	Double stranded DNA
EDTA	Ethylene-diamine-tetra-acetic acid
EGTA	Ethylene Glycol Tetra Acetic Acid
ERCC1	Excision repair cross-complementation group 1
FACS	Fluorescence-activated cell sorting
FAT	FRAP-ATM-TRAAP Domain
FCS	Foetal calf serum
FRAP	FKBP-Rapamycin-Associated Protein
g	Force of terrestrial gravity
Gy	Gray
h	Hours
H2AX	H2A Histone Family Member X
H_2O_2	Hydrogen Peroxide
HCl	Hydrochloric acid
HEPES	4-(2-hydroxyethyl)-1-piperazineethanesulfonic acid
HR	Homologous Recombination
IC_{10}	Inhibitory concentration (10%)
IC_{30}	Inhibitory concentration (30%)
IC_{50}	Inhibitory concentration (50%)
IC_{70}	Inhibitory concentration (70%)
IC_{90}	Inhibitory concentration (90%)
IGRT	Intensity Guided Radiotherapy
IMRT	Intensity Modulated Radiotherapy
LET	Linear energy transfer
l	Litre
LET	Linear Energy Transfer
mAb	Monoclonal antibody

MBq	Megabequerel
mg	Milligram
MIBG	Metaiodobenzylguanidine
mins	Minutes
ml	Millilitre
mM	Millimole
MRE11	Meiotic Recombination 11
MRN	MRE11-RAD50-NBS1
Na Cl	Sodium Chloride
NAD+	Nicotinamide adenine dinucleotide
NAT	Noradrenaline transporter
NBS1	Nibin
NER	Nucleotide Excision Repair
ng	Nanogram
NHEJ	Non Homologous End Joining
NIS	Sodium Iodide Co-transporter
nm	Nanometre
^{o}C	Degrees centigrade
p21	Cyclin Dependent Kinase Inhibitor 1
PARP-I	Poly(ADP-ribose)polymerase-1
PARP-II	Poly(ADP-ribose)polymerase-2
pATM	Phosphorylated ATM
PBS	Phosphate buffered saline
PMSF	Phenyl methyl sulfonyl fluoride
PI	Propidium Iodide
RAD50	DNA Repair Protein RAD50
RAD51	RAD51 Recombinase
RECIST	Response Evaluation Criteria In Solid Tumours
RIBBE	Radiation-induced biological bystander effect
ROS	Reactive Oxygen Species

RPA	Replication Protein A
RPM	Revolutions per minute
RNA	Ribonucleic Acid
SCID	Severe Combined Immunodeficiency
SD	Standard Deviation
SF	Surviving fraction
siRNA	Small Interfering RNA
SSB	Single-strand DNA break
ssDNA	Single Strand DNA
T_3	Triiodothyronine
T_4	Thyroxine
TFIIH	Transcription Factor IIH
TMB	3,3',5,5' - tetramethylbenzidine
TRRAP	Transformation/Transcription Domain Associated Protein
TRT	Targeted Radionuclide Therapy
XBR	External Beam Radiotherapy
XPA	Xeroderma Pigmentosum, Complementation Group A
XPC	Xeroderma Pigmentosum, Complementation Group C
XPF	Xeroderma Pigmentosum, Complementation Group F
XPG	Xeroderma Pigmentosum, Complementation Group G

Abstract

Introduction: Conventional radiotherapy efficacy is hampered by inefficient dose delivery to the target and normal tissue toxicity. Thus the use of more targeted radiotherapeutic tools such as targeted radionuclide therapy utilising for example ^{131}I conjugated to metaiodobenzylguanidine (MIBG) is a more effective approach. Additionally, the development of new radiosensitising compounds is also at the forefront of cancer research. Mirin, an MRN complex inhibitor, and Olaparib, a PARP-1 inhibitor, are two such compounds that have been predicted to enhance radiotherapy

Aims: The aims of the present study were to determine the radiosensitising potential of Mirin and Olaparib in combination with X-ray radiation and [^{131}I]MIBG *in vitro* and interrogate the molecular mechanisms underpinning the cellular response to combination treatments.

Results: Despite both X-ray radiation and [^{131}I]MIBG eliciting a dose dependent reduction in cell survival, the pattern of activation of DNA repair proteins including ATM kinase, γ-H2AX and RAD51 varied greatly, demonstrating that the dynamics of DNA damage and repair, was much more prolonged with [^{131}I]MIBG with respect to activation of DNA repair pathway components. There was also a variation in cells response to the two radiation qualities in combination with Mirin and Olaparib, with Mirin showing no radiosensitising effect with X-rays, however, significant radiosensitisation was observed in those exposed to Mirin and [^{131}I]MIBG. Olaparib demonstrated effective radiosensitising potential when combined with both X-ray radiation and [^{131}I]MIBG despite the difference in duration of DNA damaging effects.

Conclusions: The radiosensitising potential of Mirin was dependant on radiation quality with a greater radiosensitisation seen with [^{131}I]MIBG over X-irradiation. Conversely, Olaparib exerted tumour cell radiosensitisation regardless of radiation type. Additionally, mechanistic analyses indicated that Mirin is acting to efficiently inhibit the MRN-ATM directed DNA repair pathway in both cases therefore the lack of radiosensitisation produced with X-ray radiation is possibly as a result of residual or compensatory DNA repair.

Chapter 1

1.1 Introduction to Cancer

Cancer is a disease on the increase and currently affects approximately 1 in 3 people at some point in their lifetime. Despite major advances in disease understanding and therapeutics, many cancers remain refractory to treatment making the development of novel therapeutic strategies of high priority. Currently radiotherapy plays an integral part in the treatment schedules of 50% of cancer patients, however conventional radiotherapy has a plethora of well documented limitations, including normal tissue toxicity and an inability to target metastatic disease [1], [2]. More targeted radiotherapeutic tools that have the potential to treat advanced systemic disease and reduce normal tissue toxicity, are therefore of increasing interest. Coupled with the development of more tumour targeted radiotherapeutics is the development of radiosensitising agents that have the potential to target important components of pathways involved in DNA repair, cell growth, and cell proliferation and apoptosis. Dysfunction in any of the aforementioned coordinated pathways can lead to the initiation and progression of cancer therefore manipulation of vital components is an attractive prospect for cancer therapeutics [3].

Proto-oncogenes are genes within normal cells that have the potential to induce a cancerous state upon mutation into oncogenes [4]. Proto-oncogenes frequently encode proteins that are responsible for cell division, differentiation and cell death, therefore mutation of these regulatory genes results in uncontrolled cell division, and decreased cell differentiation and death [4]. These phenotypes are synonymous with cancer cells. Normal cells also contain tumour suppressor genes, which as the name suggests, act to prevent the development of tumours [5]. However, these genes are also susceptible to mutation and when this occurs they lose their ability to act as inhibitors of tumour development [5]. It is therefore hypothesised that cancer originates as a single cell that becomes functionally modified resulting in its excessive,

uncontrolled growth into a neoplasm [6]. A neoplasm was described by the British oncologist Willis as 'having growth which exceeds and is uncoordinated with that of the normal tissues and persists in the same excessive manner after cessation of the stimulation that evoked the change' [7]. The neoplasm relies on an efficient vascular supply to provide it with the necessary nutrients for growth and it is through this vascular system that cells from the tumour can enter the circulation and migrate to distant sites resulting in new metastatic neoplasm formation [8]. Cancer metastasis can occur through one of three mechanisms, direct seeding of body cavities (where cells enter open cavities such as the peritoneal cavity), lymphatic spread (cells gain access to the lymphatic system) and haematogenous spread (via arteries and veins) [8]. Venous invasion is generally the most common form of haematogenous spread as the walls of arteries are much thicker and harder to penetrate therefore the liver and lungs are frequently the most common sites of secondary tumours due to their heavy venous blood supply [8]. Metastasis is the final stage of cancer development and the prognosis following this is often poor for many cancers due to resistance of the evolved cells to conventional therapies, and the heterogeneity of cells within the metastatic tumour and primary tumour [8].Nevertheless, cancer treatment success has improved exponentially over the last 50 years and the development of novel therapeutic approaches remains an ongoing objective.

1.2 Radiotherapy

Radiation medicine has progressed significantly since the initial discovery of X-rays by Wilhelm Roentgen in 1895 and continues to be developed to the present day [9]. Following this initial discovery there was an exponential increase in the knowledge surrounding radiation medicine, from Becquerel's theory on radioactivity and the Curies' discovery of radium, to the hugely influential and compelling findings by Regaud and Coutard, which led to the implementation of fractionated radiation dosing [10]. Primitive X-ray radiotherapeutics were only considered useful for the treatment of superficial masses due to the low energy of these particular X-rays. Therefore, the development of a higher energy source was paramount for the

treatment of deep seated tumours [10]. After addressing this limitation many higher energy X-ray radiation sources were designed culminating in the discovery of electron beam therapy in 1940 [10].

1.2.1 Current Methods

Currently, second to surgery, radiotherapy is one of the most common therapeutic approaches for cancer patients, with approximately 40-50% requiring radiotherapy at some stage in their treatment regime [1]. Conventional 2D external beam radiotherapy, such as that delivered by electron linear accelerators, involves the direction of radiation toward the tumour from a source outside the body. Electron linear accelerators were widely utilised for cancer therapy between the 1960s and 1970s. However, although they allowed for irradiation of deep set tumours and produced less damaging effects to the skin, the nature of the beam was such that the radiation source was unpredictable with lateral dissemination and increased penetration depth being problematic resulting in disproportionate irradiation of the healthy tissue adjacent to the tumour [10]. This system, however, has proven beneficial in the treatment of many cancers and was therefore regarded as the standard therapeutic approach in certain situations [11].

More recently the focus of radiation based cancer treatment has shifted to the implementation of computer controlled radiotherapeutic techniques in an attempt to deliver effective radiation doses to the tumour cells whilst sparing the healthy tissues surrounding the tumour [2]. This has resulted in the evolution of radiation delivery away from basic 2D directionality of the beam to more sophisticated 3D conformal radiotherapy (3DCRT) [2]. By employing imaging technologies such as CT imaging and MRI scanning in order to determine the precise shape and size of the target mass, 3DCRT technology has gone some way to alleviate the problems associated with inadequate dose penetration [2][12]. Based on the imaging information, it is possible for multiple radiation beams to be directed towards the tumour at varying angles therefore maximising the amount of radiation reaching the tumour core. However, it does not address the problem of normal tissue toxicity [2].

The principle of 3DCRT has therefore been further developed in order to attempt to ameliorate the issue of healthy tissue toxicity. The resulting next generation of 3DCRT was Intensity modulated radiotherapy (IMRT), which has allowed the dose of radiation delivered to the tumour to be controlled (by computers) and varied based on the 3D shape of the tumour [2]. This delivery system, allows for more precise targeting of malignancies by increasing beam intensity where a large part of the tumour volume is easily accessible and reducing intensity to adjacent sites with healthy tissue [13]. IMRT does, however, take a great deal of planning and execution is complicated; therefore, there is a significant margin for error that can contribute its own problems [2]. 3DCRT is, therefore, still the preferred technique for the more specific administration of external beam radiotherapy. However, the IMRT system has a growing niche in the treatment of CNS, head and neck, and prostate cancers where the surrounding tissue, such as the spinal cord, is more precious [2]. Another problem associated with IMRT is the treatment of tumours with high mobility such as those in the lungs whereupon respiration results in tumour movement or in patients who are not adequately immobilised [14]. This has led to the development of image-guided radiation therapy (IGRT) which also employs imaging technologies in order to deliver radiation more specifically to the tumour [15]. In this instance, however, volumetric and temporal imaging is carried out at the time of treatment in order to allow the radiation beam to be adapted in response to variations in the tumour itself or the adjacent healthy tissues that can occur throughout the treatment programme [15].

Although the use of more targeted delivery systems for external beam radiotherapy have shown successes, there is still a focus on developing other means of radiation delivery. One such approach, targeted radionuclide therapy (TRT) aims to exploit the body's own intricate network of cell surface receptors and antigens, in order to facilitate tumour cell specific uptake of radiolabelled molecules, such as tumour specific antibodies, peptides and specific small molecules. The predicted outcome of such a technique is the enhancement of radiation dose administration specifically to the tumour with minimal exposure to surrounding normal healthy tissues.

1.2.2 Targeted radionuclide therapy (TRT)

In more recent times, progression in the knowledge of the molecular biology underpinning cancer has led to the discovery of several potential targeted therapeutic strategies which have the potential to deliver radioactivity more specifically to malignant cells, both in the primary tumour and secondary metastatic disease. Current external beam radiation (XBR) techniques cannot target metastatic disease, which is the most common cause of patient death. However, targeted radionuclide therapy (TRT) employs the principle that, by using a specific tumour seeking agent as a conjugate for cytotoxic radionuclides, more selective irradiation of the primary malignant tissue and disseminated disease will result [16]. This is hypothesised to reduce the level of damage elicited within normal healthy tissues that do not express the required cell surface receptor, or do not overexpress it to the same level as the tumour cells, thus creating a therapeutic differential. The other advantage of TRT is the ability to choose from a variety of isotopes with different characteristics to allow specific targeting of different clinical scenarios in cancer.

Beta (β) emitting (Figure 1.1) radionuclides are the most commonly used radionuclides in human cancer therapeutics owing to their low linear energy transfer (LET) (the rate at which energy is transferred from ionising radiation to tissues) and therefore more desirable path length for targeting whole tumours [17]. β-emitting radiopharmaceuticals generate damage upon traversing the tissue by interacting with water molecules within cells, thus dropping their high energy state and inducing formation of ionised atoms and free radicals within the cell [17]. These charged particles subsequently interact with DNA molecules, causing single and double stranded breaks and other cell components and macromolecules, such as lipids in the membrane of the cell or mitochondria, resulting in a loss of cell integrity and initiation of apoptotic and necrotic cell death pathways [17].

^{131}Iodine is a β-emitter with a tissue range of approximately 0.8mm [18] that makes it a desirable radioisotope for cancer therapeutics, as it has the potential to target tissues that have poor accessibility; that is, they cannot be directly targeted by the radiopharmaceutical. As a consequence, large tumours, those located in less

accessible areas (CNS) and those that have a poor vascular supply, have the potential to be more effectively treated [17]. Many tumours are also heterogeneous in nature and so not all cells in the tumour volume will express the target antigen or receptor complementary to the radiopharmaceutical. This makes an emitter with a longer path length an attractive candidate for these scenarios as there is greater potential to elicit damage to a larger cell population including those that have not themselves internalised the radioisotope and accrue direct damage via radiation cross fire [19]. Boyd *et al.,* (2002) utilised transfectant mosaic spheroid and transfectant mosaic monolayer models in order to assess radiation crossfire and radiation-induced biological bystander effects (RIBBE) following exposure to the β emitter [^{131}I]MIBG. This study demonstrated that the spheroid model was more susceptible to [^{131}I]MIBG than the monolayer cells which they hypothesise was attributable to greater radiation crossfire and radiation induced biological bystander effects (RIBBEs) [20]. ^{131}Iodine also has a half-life of approximately eight days, making it more advantageous than other shorter half-life emitters, as there is a more prolonged damaging effect elicited within the cell resulting in greater efficiency of tumour cell kill through a diminished capacity to activate repair responses [21]. However a key factor in the success of targeted radionuclides is how long they are retained within tumour cells in order to elicit these long term damaging effects.

Alpha (α)-emitters (Figure 1.1) elicit their damaging effects within a much smaller tissue range compared to β-emitters. However, as a result of their high LET values, they are significantly more cytotoxic than their β-emitting counterparts [22]. Greater damage to the DNA is potentially exerted by α-emitters than β-emitters and is hypothesised to be due to the creation of multifaceted, clustered complex DNA damage lesions resulting in production of irreparable DNA double strand breaks [17][23]. Furthermore, the short path length of α-emitters (50-100μm) allows for more precise targeting of tumour cells without eliciting excessive damaging effects to adjacent healthy tissues due to less radiation cross fire [22]. Whilst this is a desirable property for targeted cancer therapeutics, it can be problematic when treating larger heterogeneous tumour masses. Thus, it has been documented that α-

emitters are often used primarily for destruction of homogeneous tumours or cases of micro-metastases where tumour volume is reduced [22].

It has long since been postulated that auger emitters (Figure 1.1) must be positioned within the DNA to elicit any significant damage as their emission range extends only nanometres, thereby limiting their use to targeting single tumour cells [24]. However, it has been suggested that, despite their nanometre emission range, auger emitters still have the potential to elicit biological radiation induced bystander effects (described in more detail in section 1.2.2.1) [25], [26]. Neshasteh-Riz *et al*., (1998), demonstrated that auger emitter labelled (^{123}I and ^{125}I) IUdR elicited a dose dependent reduction in spheroid volume at low doses <20kBq, however at higher doses >40kBq this effect plateaued [27]. In contrast to [^{123}I] and [^{125}I]IUdR, β-emitting [^{131}I]IUdR produced increasingly cytotoxic effects upon escalation of dose across the entire dose range [27]. Therefore, despite the effectiveness of auger emitters, increasing dose elicits no additional toxicity due to their short range activity [27].

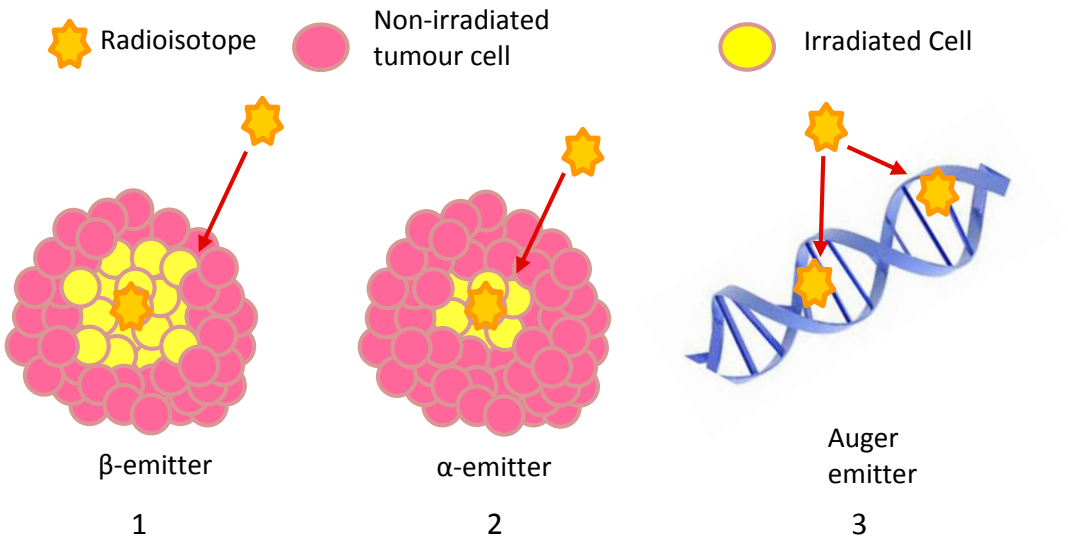

Figure 1.1 Cell damaging potential of the 3 emitter types

1. β-emitters have the longest path length and can elicit damaging effects to surrounding cells a significant distance from the target cells.
2. α-emitters have a shorter path length and can elicit damage to surrounding cells in the near vicinity to the target cell
3. Auger emitters mainly produce damaging effects within the DNA of the target

Targeted radiotherapy, more specifically therapy with radioactive iodine, has been used successfully for the treatment of thyroid cancer for decades. Cure rates are exceeding 80% for papillary and follicular thyroid cancer with total thyroidectomy followed by adjuvant ablative therapy with radioiodine [28]. This therapeutic approach seeks to selectively ablate all thyroid cancer tumour tissue and lower the rate of relapse [21]. The tumour specificity of this approach is due to the uptake of iodine into the follicular cells of the thyroid gland via the sodium iodide co-transporter (NIS), a transmembrane glycoprotein, which is also expressed in the kidney, ovaries and breast tissue [28]. Once inside the cell, iodine subsequently forms the thyroid hormones, thriiodothyronine (T_3) and thyroxine (T_4). Due to the overexpression of NIS in thyroid tissue and other tissues, such as oxytocin dependent expression in breast tissue [29] it is considered that exploitation of this natural active uptake system will result in the selective accumulation of radiolabelled iodine in these cells. Thus, making it an effective and, more importantly, targeted treatment for NIS expressing cancers [21]. However, although this has been successful in the treatment of thyroid cancers it has been less successful in breast cancers due to lack of retention of ^{131}I in breast tissue. This concept has consequently been applied to the possible treatment of other cancers using different targets, radionuclides and conjugates. These include small molecules such as [^{131}I]MIBG, radiolabelled peptides such as somatostatin analogues and radiolabelled monoclonal antibodies [21], [30].
The use of somatostatin peptides in TRT has been investigated in the treatment of gastroenteropancreatic neuroendocrine tumours as they express high levels of the somatostatin receptor [21]. Unfortunately due to the expression of somatostatin receptor subtypes in the kidneys and its involvement in the clearance of these molecules nephrotoxicity has been reported [21].
Monoclonal antibodies have also been radiolabelled and used to direct radiation specifically to tumour cells. Monoclonal antibodies are however large in size therefore tumour mass penetration is poor making them most useful for blood borne cancers such as lymphoma rather than bulky solid tumours where antibody penetration is limited [31]. Zevalin *(Ibritumomab tiuxetan)* and Bexxar (*tositumomab)*

are two FDA approved radiolabelled monoclonal antibodies (mAbs) used in the therapy of non Hodgkins lymphoma [32]. Both target the CD20 receptor which is expressed on normal and malignant B lymphocytes and have shown significant antitumour activity [31], [32]. However, CD20 receptors are also expressed on normal B-cells and the patient therefore becomes susceptible to infection as white cell count is diminished, despite this cells are replenished following termination of treatment [33].

1.2.2.2 Clinical [^{131}I]MIBG Therapy

Over 90% of neuroblastomas express high levels of the noradrenaline transporter (NAT), responsible for the active uptake of extracellular noradrenaline [34]. Metaiodobenzylguanidine (MIBG) is a structural analogue of noradrenaline (Figure 1.1) that was originally used as an aid to imaging and diagnostics in adrenomedullary medicine when conjugated to ^{123}I (used due to its shorter emission range). However, it was discovered that when conjugated to ^{131}I the β-emitting properties of ^{131}I had a cytotoxic effect on the cells into which it was internalised. This prompted an investigation into potential therapeutic applicability in neuroendocrine cancers [35]. [^{131}I]MIBG is readily taken up by an ATP dependent active uptake mechanism into tissues that express high levels of NAT [36]. However, [^{131}I]MIBG can also enter the cell by passive diffusion which is non-specific and less efficient, and thus plays only a minor role in the accumulation of [^{131}I]MIBG in tumour cells [37].

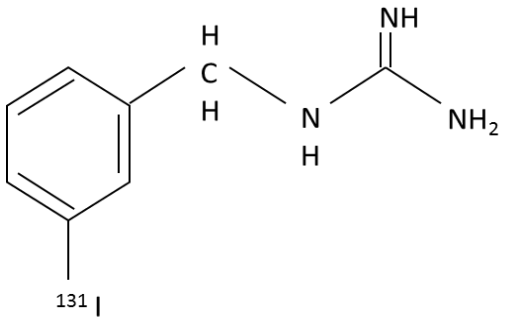

Figure 1.2 Structure of [^{131}I]Metaiodobenzylguanidine ([^{131}I]MIBG)

MIBG is structurally related to the noradrenergic neurone blocking drugs bretylium and guanethidine, and selectively accumulates in tissues that express the noradrenaline transporter (NAT) [71].

Initially, studies into the use of [^{131}I]MIBG as a therapeutic strategy were carried out in patients with phaeochromocytoma (a neuroendocrine tumour of the adrenal gland) and were soon expanded into those suffering from neuroblastoma (a neuroendocrine tumour originating in the neural crest and developing from the adrenal glands or nerve tissue in the chest, neck and abdomen) [35].

Clinical studies into [^{131}I]MIBG use as a monotherapy provided some promising results with one German study reporting that in 66% of patients a mean dose of 10.3mCi/kg (381.1MBq) of [^{131}I]MIBG displayed partial or full response to treatment [38]. However, another study in France reported that no patient had presented with an objective response to treatment in a study of 26 patients [35]. As a consequence of the differential success rates in monotherapy studies, combination studies utilising chemotherapeutic compounds, which exert radiosensitising properties in addition to [^{131}I]MIBG, were hypothesised to yield more favourable outcomes**.**

Work from our group (McCluskey *et al.,* (2005) demonstrated that [^{131}I]MIBG reduced the cell survival fraction of neuroblastoma cell lines both *in vitro* and *in vivo* but that its efficacy was increased by combining it with the topoisomerase inhibitor topotecan when the two were given simultaneously [36]. Further to this study the same researchers demonstrated that inhibition of PARP-1 using the inhibitor PJ34,

enhanced the efficacy of [^{131}I]MIBG therapy alone and also combined [^{131}I]MIBG/topotecan therapy [39]. [^{131}I]MIBG has been investigated as part of combination therapies with surgery, radiation, chemotherapy and external beam radiation [37] and the aforementioned study using PARP inhibitor PJ34 therefore provides preliminary evidence that [^{131}I]MIBG can also be combined with specific inhibitors to enhance the therapeutic effect.

Pilot studies on patients, using [^{131}I]MIBG in combination with cisplatin, a platinum based, DNA cross-linking compound with previous success in neuroblastoma treatment regimens and known radiosensitising properties, showed encouraging results with two complete responses and one partial response in four patients with recurrent disease [40]. The relative success of initial combination studies facilitated the expansion of the hypothesis to include other exisiting and novel radiosensitising agents. A pilot study by Mastrangelo *et al.,* (2001) assessed the therapeutic potential of the combination [^{131}I]MIBG-Cisplatin therapy (group 1) and [^{131}I]MIBG-Vincristine-Etoposide therapy (group 2) [41]. Partial response was observed in six out of nine patients in group 1 and six out of seven patients in group 2, with one patient presenting with a mixed response (group 1) and the final three displaying stable disease [41]. These results provided a promising rationale for further investigation into the use of radiosensitising agents in conjunction with [^{131}I]MIBG therapy [41].

Another preliminary phase 2 study investigated the development of treatment regimens utilising [^{131}I]MIBG in combination with carboplatin, etoposide, melphalan and stem cell replacement therapy [42]. The findings suggest that this combination had the potential to be an effective therapeutic option for patients with chemotherapy resistant disease provided they exhibited normal renal function to allow for efficient excretion of [^{131}I]MIBG and chemotherapeutic compounds [42]. Further to this phase 1 study, Yanik *et al.,* (2015) demonstrated in a recent phase 2 study that the combination therapy, although generally well-tolerated, failed to deliver significantly favourable patient responses in individuals with recurrent or refractory disease [43]. However, it was noted that improved response was observed in patients presenting, with partial response following induction therapy [43].

Another recent study, carried out by DuBois *et al.,* (2012), investigated the potential of combined administration of vincristine (microtubule disrupting agent), irinotecan (topoisomerase 1 inhibitor) and [^{131}I]MIBG [44]. This particular combination provided encouraging results, despite only 25% of patients showing an objective response. This was hypothesised to be due to the inclusion of patients suffering from bone marrow disease, which had previously been shown to be more refractory to [^{131}I]MIBG treatment [44]. As discussed, combination schedules with [^{131}I]MIBG and chemotherapeutic agents which interfere with DNA replication have provided encouraging results for cancer therapy, therefore combination of [^{131}I]MIBG with compounds that inhibit DNA repair, such as those investigated in this study, is hypothesised to produce equally promising results.

Although [^{131}I]MIBG combination therapy has produced remissions and palliation in patients with resistant disease, long term cure has not been achieved and therefore further investigation into the cellular response to [^{131}I]MIBG may provide important information on how to further improve the use of [^{131}I]MIBG as a therapeutic tool.

1.2.2.3 Radiation Induced Biological Bystander Effects (RIBBEs)

As mentioned in section 1.2.2, due to its path range ^{131}Iodine (^{131}I) can induce DNA damage not only in cells that uptake and retain ^{131}I but also neighbouring cells which are traversed by charged particles (radiation crossfire) [26]. In addition to this activity, the effect referred to as radiation induced biological bystander effects (RIBBEs), which is defined as the initiation of biological effects in cells that are not directly traversed by a charged particle but are in close proximity to cells that are [45] (Figure 1.3), also plays an important role in the biological efficacy of radionuclides. The mechanisms by which the RIBBEs occur is unclear; however, gap junctions are thought to be important in cell cultures of high confluency as direct communication can occur between irradiated and non-irradiated cells. However, cultures of low confluency also exhibit RIBBEs that are thought to be the result of the release of various signalling molecules from irradiated cells into the culture media that can then trigger responses in non-irradiated cells [45]. RIBBEs are already known to be

important in the tumouricidal activity of external beam radiation; however, Boyd *et al.,* (2006) also demonstrated that RIBBEs are important factors in the cytotoxicity of targeted radionuclides using a variety of classes of isotope.

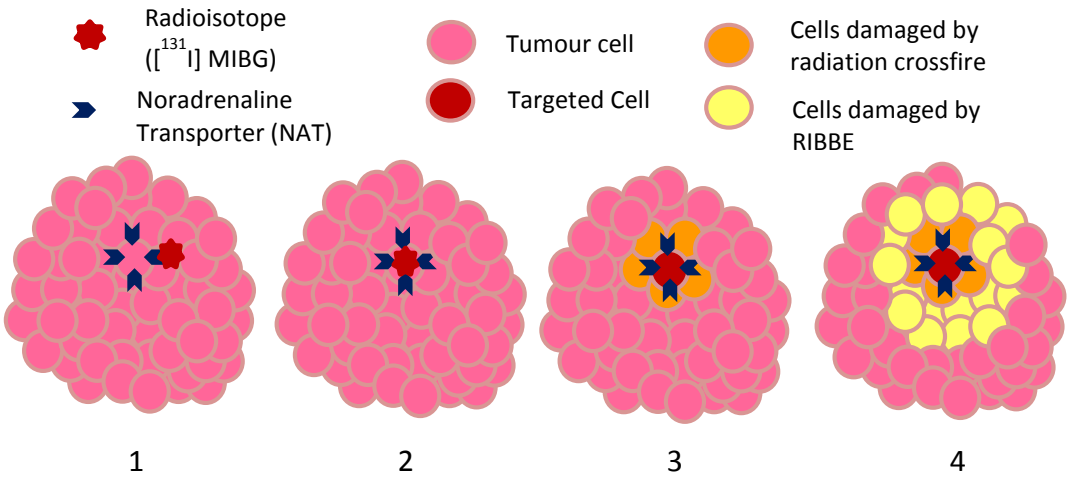

Figure 1.3 Radiation Induced Biological Bystander Effect (RIBBE)

1. The radioisotope is delivered to the tumour vicinity
2. NAT expressing cells uptake radioisotope
3. Radioisotope decay elicits damaging effects to the host cell and neighbouring cells that themselves do not express the targeting moiety for the radioisoptope (radiation crossfire).
4. Damaged cells then subsequently release signals which elicit damage to their adjacent cells (RIBBE).

As highlighted in section 1.2.2.1 combination therapies incorporating [^{131}I]MIBG have produced remission and palliation in some patients with resistant disease but long term cure has not been achieved. Therefore, new combination therapies are urgently saught to fully utilise the tumour-targeting properties of this conjugate. Over the last decade there has been an increase in the understanding of the biological pathways underlying cellular response to X-irradiation. This has led to a great increase interest in novel, molecular tumour targeted compounds, which through their inhibition of repair of radiation induced DNA damage are hypothesised to sensitise cells to radiation. Little however is known about the biological pathways underlying TRT. This

thesis focuses on the cellular response to X-irradiation and [^{131}I]MIBG induced DNA damage, and how these can be exploited for enhancement of radiation therapies.

1.3 Radiation induced DNA damage and repair

1.3.1 Radiation induced DNA double strand breaks and repair mechanisms

Upon traversing the cell, ionising radiation releases energy in the form of electrons that elicit damaging effects on the cell biomolecules, resulting in chemical and structural alterations [46]. The damage elicited by high LET radiation sources such as α particle emitters is often described as clustered, whereby a collection of two or more lesions form within close proximity to each other, due to their ability to release electrons over a short range [47]. Low LET radiation sources (X-rays and β-rays) on the other hand produce more sparsely distributed DSBs along the energy track with only 30% of the released energy creating clustered damage [47]. Radiation damages DNA directly by deposition of energy and also indirectly by ionisation of water molecules, which generates hydroxyl radicals that interact with the DNA. This concept is in contrast to more simple intrinsic lesions frequently generated either during DNA replication or, as a result of reactive oxygen species (ROS) production during metabolic processes, which tend to be more sequestered and evenly disseminated. The simpler damage created intrinsically is more easily repaired than complex DSBs, which are more serious to the cell resulting in greater levels of cell death [46].

In mammalian cells, radiation induced DNA double strand breaks are repaired primarily through non-homologous end joining (NHEJ) or homologous recombination (HR), with the former being cell cycle stage unspecific and is considered the major pathway for the repair of radiation induced breaks [46]. ATM and the MRN complex (section 1.4) are involved in the recognition of DNA DSBs and initiation of both NHEJ and HR however the substrates differ between the two repair pathways resulting in diverse repair kinetics.

1.3.1.1 Non-homologous end joining (NHEJ)

NHEJ coordinates the repair of ionising radiation induced DSB's as well as naturally occurring breaks and is primarily, but not exclusively, initiated in the G0 and G1 phases of the cell cycle [48]. Due to the lack of homologous DNA in G0 and G1 phases of the cell cycle, NHEJ is regarded as a more error prone form of repair due to its DNA sequence homology independent nature [48]. Accurate repair is often achieved for simple DNA breaks presenting with blunt ends. However, when more complex breaks occur the DNA sequence can be changed during repair, leading to loss of heterozygosity [49].

The Ku complex (a Ku70/80 heterodimer) is the predominant DNA binding component in mammalian cells initiating NHEJ [50]. Following DNA damage, the Ku heterodimer is localised to the DSB, which subsequently leads to the localisation of DNA-dependent protein kinase, catalytic subunit (DNA-PKcs) and Artemis. This complex can then create protein-protein interactions with DNA-PKcs molecules on the corresponding broken DNA ends to tether the two ends together facilitating ligation and break repair by DNA ligase IV and DNA polymerase respectively (Figure 1.4a) [50].

1.3.1.2 Homologous Recombination (HR)

In contrast to NHEJ, HR is active only in late S and G2/M phases of the cell cycle when homologous regions of DNA are abundant due to DNA replication [48]. The reliance of HR on regions of sequence homology makes this process significantly more precise and less likely to result in critical loss of genetic information [51].

The major components in HR differ to those necessary for NHEJ, reflecting their differing mechanistic properties. Following generation of DNA lesions, the initial event in the HR repair cascade is DNA strand resection, which produces regions of single stranded DNA (ssDNA) [48]. This ssDNA production is initiated by functionalisation of the MRN complex (see section 1.4.1) and its association with CtIP (CtBP-interacting protein), which ultimately leads to further recruitment of repair

modulators such as RPA and RAD51 [48]. RPA protects the exposed ssDNA from degradation by intracellular nucleases. However, this is subsequently unbound to allow formation of RAD51 filaments that catalyse DNA strand exchange and completion of the repair process (Figure 1.4b) [52].

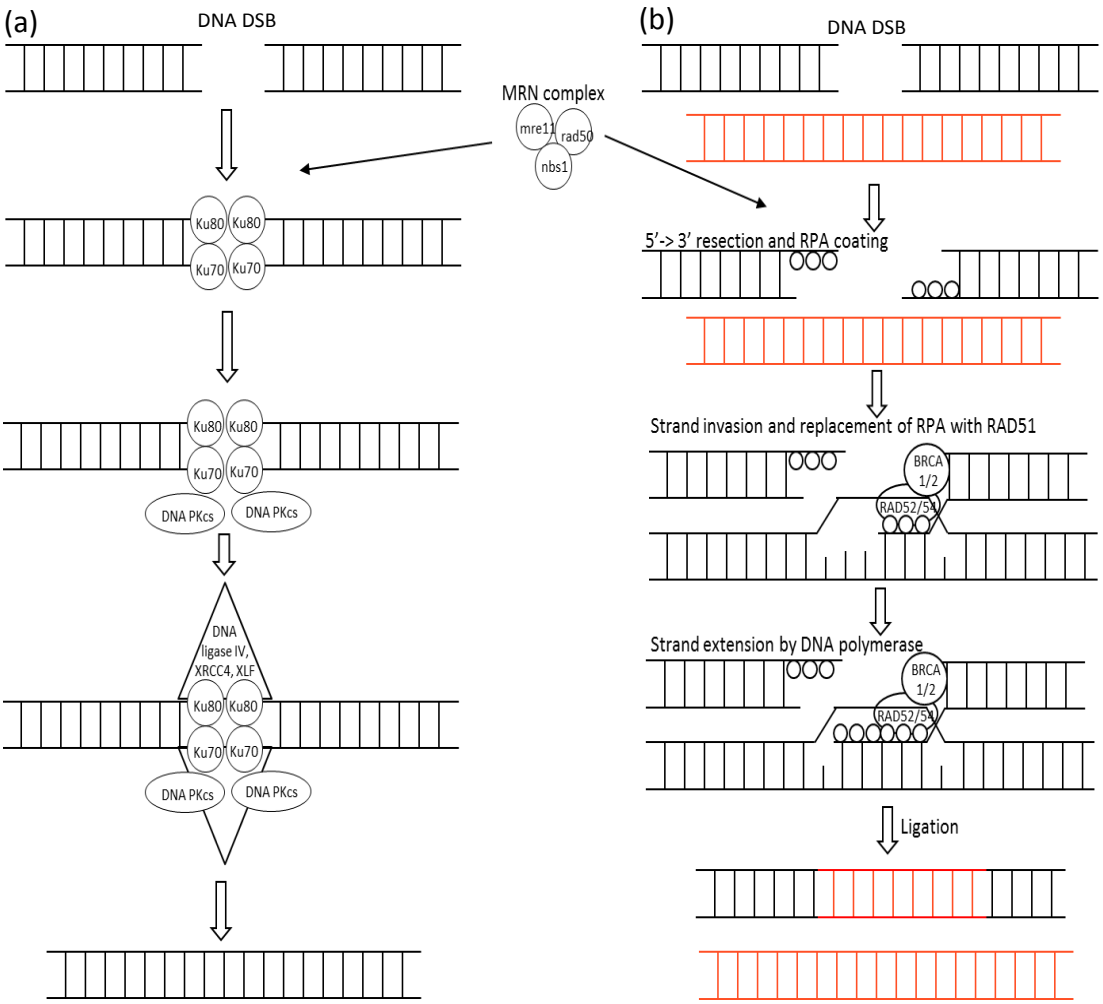

Figure 1.4 Schematic diagram of (a) NHEJ and (b) HR DNA repair pathways.

Adapted from Czornak *et al*., 2008 [137].

1.3.2 DNA Single Strand Break (SSB) repair mechanistics

In addition to the induction of DNA double strand breaks radiation also induces single strand breaks through damage of bases and cleavage of the DNA backbone. SSBs are also generated during normal cell proliferation processes and by production of

endogenous metabolic by-products with DNA damaging properties [53]. The primary DNA repair mechanism employed by the cell to detect and repair SSBs is base excision repair (BER), which involves cleavage of damaged bases in DNA and replacement of the section with correct bases produced during DNA synthesis [53], [54]. BER is used in cases where the base modification does not perturb the helical structure of the DNA. Modifications that do result in perturbation of the helix are repaired by nucleotide excision repair (NER), which is activated in a different manner to BER [55]. BER is initiated by DNA glycosylase, which liberates the variant base, allowing other proteins, including APE1 endonuclease and DNA polymerase β, to access the site and instigate a cascade of events, ultimately resulting in repair and ligation of the DNA strand [54], [56]. Poly-ADP Ribose Polymerase (PARP)-1 is a major constituent of the BER repair pathway and has a crucial role in the repair of SSBs. PARP-1 is recruited to sites of SSBs following the generation of SSB intermediates by the afore mentioned DNA glycosylase and APE1. The role of PARP-1 in DNA repair and cancer is further discussed in section 1.5. On the other hand, NER begins when a multi-protein complex comprised of RPA, XPA, XPC, TFIIH, XPG and XPF-ERCC1, cleaves a small section of the DNA surrounding the damaged base; as a result, the affected base is removed as part of an oligonucleotide allowing for synthesis of a new DNA strand to bridge the newly created gap in DNA structure, and ligation of the new DNA section to complete the sequence [55], [56].

It has been previously shown that abrogation of a cell's ability to recruit and activate DNA repair machinery leads to increased genetic instability and sensitivity to ionising radiation [3]. This is evidenced in patients suffering from severe combined immunodeficiency disorder (SCID) caused by lack of artemis activity, which is characterised by impaired NHEJ capability and therefore increased genetic instability and sensitivity to ionising radiation [57]. Likewise, Ataxia-Telengiectasia (A-T) is a condition characterised by increased cancer predisposition and chromosomal instability occurring as a consequence of impaired ATM kinase and therefore HR functionality. Targeting of this moiety with a chemotherapeutic compound is therefore hypothesised to produce a similar effect resulting in genetic instability and

thus cancer cell death [58]. Similar to DSB repair, SSB repair by BER is imperative for species fidelity as it has been shown, using mouse models, that knockdown of APE1 and DNA polymerase β activity is embryo toxic [59]. It has therefore been postulated that synthetic inhibition of major components within these pathways will result in enhancement of radiotherapies during cancer treatment via reduced DNA damage resolution.

1.3.3 [^{131}I]MIBG induced DNA repair processes

Little is known about the DNA repair kinetics associated with exposure of [^{131}I]MIBG. It is however hypothesised that due to the more chronic nature of this radiation type, DNA repair processes will be upregulated for a more extended duration than when cells are exposed to X-ray radiation over a significantly shorter time period. Previous studies investigating components of the DDR pathway have shown that following X-irradiation many components of the DDR pathway are elevated within minutes of initial exposure and are down-regulated again within 24 hours [60], [61]. This is however, not hypothesised to be the case with [^{131}I]MIBG as the more long term damaging effects associated with decay of ^{131}I suggests that DNA repair processes will be continually upregulated over the duration of retention of [^{131}I]MIBG.

1.4 Mirin and the MRN Complex

1.4.1 The MRN Complex

As previously described, the development of many radiosensitising compounds focuses on the inhibition of radiation induced DNA damage recognition and repair processes. DNA repair can be generally regarded as counter intuitive and undesirable in tumour cells undergoing radiation therapy that elicits toxicity through DNA damage. Targeting important components of DNA repair pathways, for example the MRN complex, and abrogating their function could be key to improving the therapeutic efficacy of DNA damaging agents including radiation.

The MRN complex is an essential component of both NHEJ and HR repair cascades which is recruited immediately following induction of double stranded breaks in DNA

including those generated by radiation. In this capacity it functions to sense DSBs, activate cell cycle checkpoint signalling pathways and initiate DNA repair through HR or NHEJ [62], [63]. The MRN complex is assembled through interactions between three proteins - Mre11, two subunits of Rad50, and a scaffold protein Nbs1 (Figure 1.5). The proteins arrange in the form of a globular head with two arm-like protrusions, with the globular head containing an Mre11 homodimer and the ABC-ATPase domain of Rad50 [62], [64]. It is via this domain that the complex binds DNA and allows Mre11, which also has important exo- and endo-nuclease functions, to excise fragmented ends of DNA during repair [64]. The coiled coil tautology of Rad50 domains form the arm-like structures which can adopt various orientations and function to tether the broken ends of DNA [62]. Finally, Nbs1 localizes the complex to the nucleus and mediates correct MRN complex formation at DSBs [65]. Nbs1 also binds to c-terminal binding protein interacting protein (CtIP) that has a vital role in DNA DSB resection during the process of HR and also induces the transcription of cell cycle inhibitory proteins including p21 [62], [66].

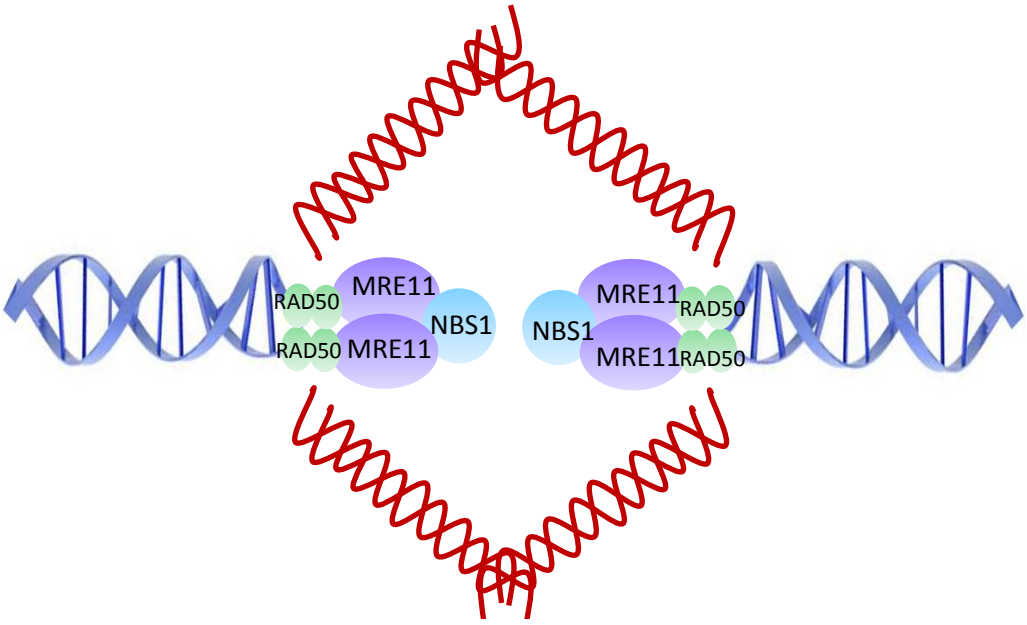

Figure 1.5 Schematic diagram of MRN complex assembly and interaction at DNA lesion.

The complex is shown interacting directly with DNA at the broken ends of DNA, with the coiled coil domains of RAD50 tethering the broken ends to facilitate repair and re-ligation. Adapted from Richard *et al*., 2010 [138]

1.4.2 ATM and ATR Kinases

Although the MRN complex is one of the first proteins to be recruited to the site of radiation induced DNA double strand breaks, it is via cross talk with Ataxia-telangiectasia mutated (ATM) and ATM-and Rad3-related (ATR) proteins that the repair processes become initiated [67]. The MRN complex identifies DNA breaks independently of ATM. However, initiation of ATM signalling is essential for induction of cell cycle arrest and DNA repair [68].

ATM and ATR protein kinases are phosphatidylinositol kinase-like kinases and are important structures in the process of stalling the cell cycle in order to allow DNA repair, or to initiate apoptosis in cells where repair mechanisms are exhausted [67]. The ATR kinase is responsible for surveying DNA replication and when an error occurs it will phosphorylate and activate checkpoint kinase 1 (Chk1); this halts G2/M stages of the cell cycle via inhibition of cdc25c and cyclin B1 [67]. ATR is recruited to the site of damage through ATM induced formation of RPA coated ssDNA [62]. ATM kinases exists within healthy cells as inactive dimers or multimers whose kinase domains are blocked by the FAT domain of another ATM molecule. Upon DNA damage by ionising radiation the ATM levels remain unchanged. However, each ATM molecule phosphorylates another at serine 1981 within the FRAP-ATM-TRRAP (FAT) domain, which thus releases it from inactive dimer status to form two active monomers [69]. As such, although there is no upregulation of ATM levels in the cell, there is a two to three fold increase in the kinase activity [68].

ATM activation is a complex phenomenon; however, MRN dependent activation has been hypothesised to occur as follows (Figure 1.6):

a. DNA binding of the MRN complex to DNA lesion.
b. Initiation of Mre11 exonuclease activity to process fragmented DNA ends.
c. ATM recruitment, autophosphorylation and acetylation (by TIP60 histone acetyltransferase).
d. ATM dependent phosphorylation of other DNA repair proteins.

ATM may subsequently be liberated from the lesion, allowing for phosphorylation of additional repair proteins, including the chromatin-bound histone H2AX and p53 (a

tumour suppressor protein) [48], [68]. Phosphorylation of the H2A histone protein (H2AX) occurs rapidly after initial DSB induction resulting in formation of γ-H2AX foci. Evidence suggests that this activation extends distally from the primary lesion, thereby amplifying the DSB repair response [60]. This amplification leads to a positive feedback loop and further recruitment of ATM and MRN complexes. MRN dependent activation of ATM therefore must occur promptly in response to DSB formation.

ATM also phosphorylates NBS1 in the MRN complex leading to activation of the S phase cell cycle checkpoint via chk2 [62]. Although ATM has also been proven to phosphorylate Mre11 and RAD50, this response is less biochemically important to the cell [62]. Mutations in ATM proteins are therefore strongly suggested to have a role in cancer development and, as a consequence, have become increasingly explored as a target for chemotherapy. It is well documented that repair processes involving ATM are upregulated in response to X-irradiation[62] however, very little is known about the role these processes have in response to [^{131}I]MIBG.

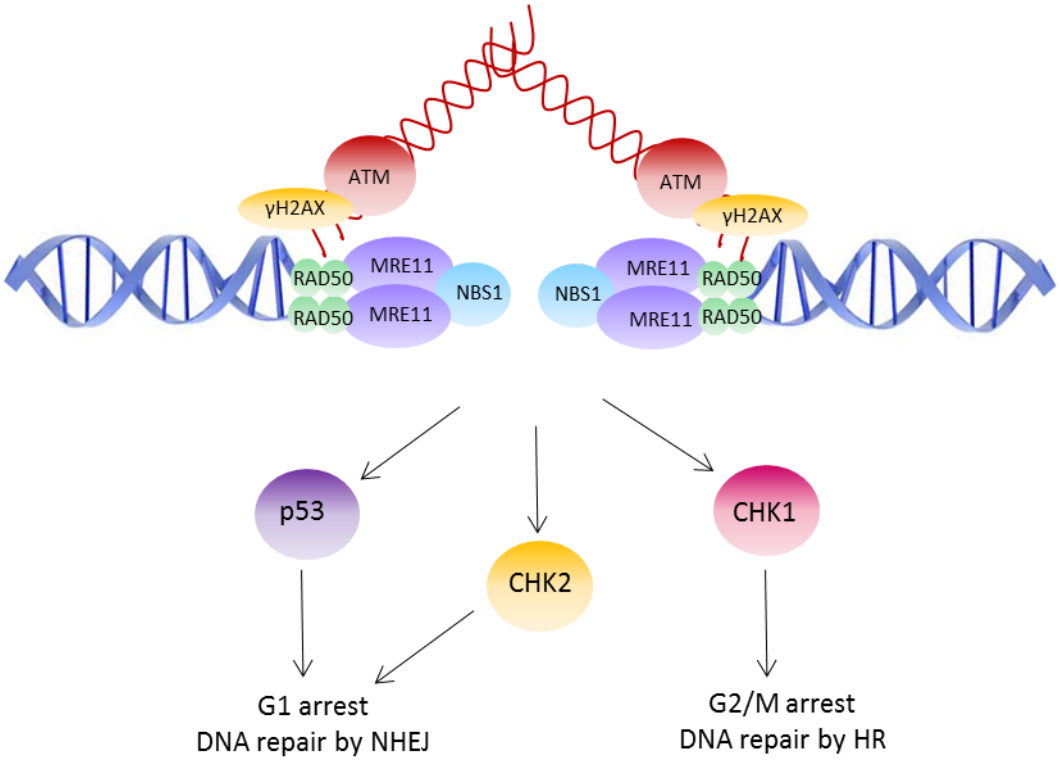

Figure 1.6 Schematic of the signalling and DNA repair pathway elicited by the MRN complex and ATM following DNA breakage

Adapted from Richard *et al*., 2010 [138] and Bolderson *et al*., 2009 [48]

1.4.3 Inhibition of radiation induced activation of the MRN complex

Small molecule inhibitors have been developed to target components of DNA damage response pathways. These include inhibitors of ATM, APE-1, PARP, MRE11 and many others, although many of these have not advanced to clinical trials. Mirin (**z**-5-(4-Hydroxybenzylidene)-2-imino-1,3-thiazolidin-4-one) is a thiazolidine based, small molecule inhibitor of MRE11 developed by Dupré *et al*., 2008. The specific mechanism of action of Mirin has eluded researchers for many years, however it has recently been suggested that it may act by obstructing the binding of DNA to the active site of the MRE11 [70]. Therefore, impeding DNA binding results in failure of the MRN complex to exert exonuclease activity, which has been suggested to occur as a result of MRE11 dependent opening of dsDNA, [70] and thus the activation of ATM dependent DNA repair cascades [71]. Studies investigating the effect of Mirin on radiation induced ATM activation have shown that Mirin does inhibit the MRN dependent activation of ATM kinase but not ATM kinase itself and this has also led to the observation that Mirin may abrogate the initiation of the G2/M checkpoint thus preventing repair of DSBs [72]. Taken together these studies suggest that Mirin would effectively sensitise cells to the effects of X-ray radiation and [^{131}I]MIBG.

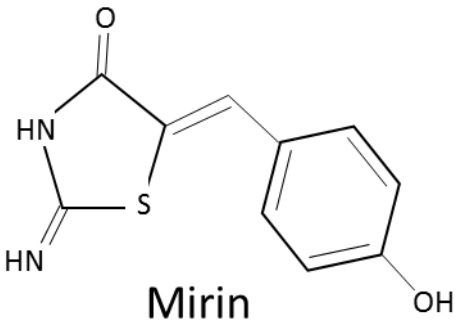

Mirin

Figure 1.7 Chemical structure of Mirin (Z-5-(4-Hydroxybenzylidene)-2-imino-1,3-thiazolidin-4-one).

Dupré *et al*., 2008 [71]

Evidence from siRNA knockdown studies suggest that disruption of the MRN complex sensitises cells to radiation. Zhang *et al.,* (2005), studied siRNA knockdown of the NBS gene which led to disruption of the function of the MRN complex and this resulted in increased radiosensitivity in lymphoblastoid cells [73]. Furthermore, Xu *et al.,* (2004) showed that using siRNA against MRE11 sensitised cells to radiation [74].
This thesis aims to further investigate the effect of MRE11 inhibition using the small molecule inhibitor Mirin on the sensitivity of cells to X-irradiation and [^{131}I]MIBG.

1.5 Poly (ADP-ribose) polymerase

Another potential target for inhibiting radiation induced DNA damage and repair pathways is through targeting poly (ADP-ribose) polymerase (PARP-1) using compounds such as Olaparib (Figure 1.8). PARP-1 is a protein located in the cell nucleus which detects DNA lesions induced by damaging factors including; oxidative stress, radiation and cytotoxic chemicals, triggering its own modification and that of other cellular proteins by ADP-ribosylation culminating in activation of repair processes such as base excision repair (BER), NHEJ and HR [75]. There are 18 members of the PARP family but PARP-1 is the most abundant and best characterised member which has multiple functions including transcriptional regulation, induction of necrosis, and apoptosis and protein removal as well as its repair function [75].
During DNA repair PARP-1 binds to the site of damage and only upon binding does it become activated and have the ability to induce repair processes [76]. Following binding to DNA (see Figure 1.9), PARP catalytically modifies itself by ADP-ribosylation utilising NAD+ as a substrate forming long and often branched polymers of ADP-ribose (an ester molecule). This post translational modification is however transient and is reversible by cleavage of the polymer using poly-ADP ribose glycohydrolases [77]. ADP-ribosylation results in the complex becoming negatively charged and as a consequence it becomes released from DNA, allowing DNA repair enzymes to access the lesion and initiate base excision repair (BER) [76].
PARP-1 has been most prominently associated with BER and SSB repair, however, it has also been suggested to have a role in an alternative form of NHEJ through its

association with DNA ligase III [78]. In this role PARP-1 binds to DNA lesions in direct competition with Ku70/80. However, in cells exposed to radiation, Ku70/80 has a greater affinity for DNA breaks and therefore PARP-1 becomes important only when constituents of the primary NHEJ pathway are null or inhibited [78].

PARP-1 has also been shown to contribute to HR through its interaction with DSB repair components including MRE11, NBS1 and ATM [79]. The co-operation between PARP-1 and ATM has been highlighted as of importance in the phosphorylation of downstream signalling molecules including p53 and H2AX, however this role is less well defined than that of PARP-1 in BER [79].

1.5.1 Olaparib

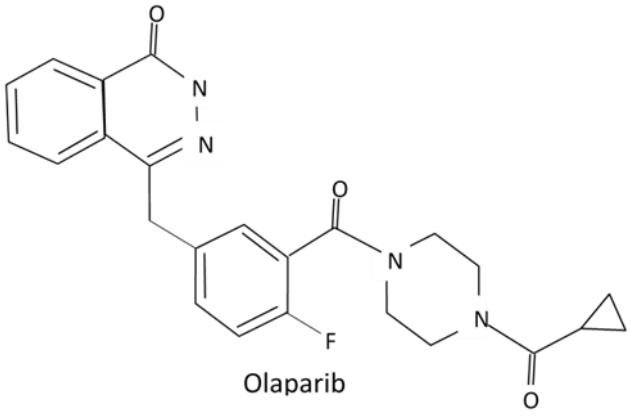

Figure 1.8 Chemical Structure of Olaparib

Olaparib is a pthalazinone molecule with high affinity for PARP-I and PARP-II and it is primarily inhibition of PARP-I by Olaparib that has shown potential radiosensitising effects [80]. However, much of the therapeutic interest has surrounded their use in cancer treatment regimens, in patients carrying a mutation in the breast cancer susceptibility gene (BRCA) [81]. BRCA1 is a tumour suppressor protein with essential roles in DNA damage signalling, repair and cell cycle checkpoint control, whilst BRCA2 binds to RAD51, facilitating its translocation to the nucleus to trigger repair cascades [80]. It is therefore widely recognised that loss of function in both BRCA1/2 alleles results in impaired DSB repair by HR, conferring genetic instability and a predisposition to cancer development (Figure 1.9) [80]. As previously described,

PARP-1 is an essential component of base excision repair (BER) and nucleotide excision repair (NER) DNA repair pathways. These pathways function in a compensatory manner in BRCA1/2 depleted cells due to their lack of HR capacity [75]. Loss of PARP-I activity via pharmaceutical inhibition in BRCA1/2 null cells can therefore mediate cell death by inhibiting SSB repair, thus resulting in the conversion of these SSBs to DSBs which cannot be repaired through a functional HR pathway. This forms the basis of the concept of synthetic lethality [81].

Synthetic lethality occurs when two functionally related genes or gene products are abrogated, in tandem, resulting in loss of fidelity and cell death [82]. It is important to note that the two mutations are non-lethal when they present individually [83]. This synthetic lethality has therefore been exploited in the treatment of cancers which have a natural deficit in BRCA1/2 activity, most notably those derived from breast and ovarian tissue [82].

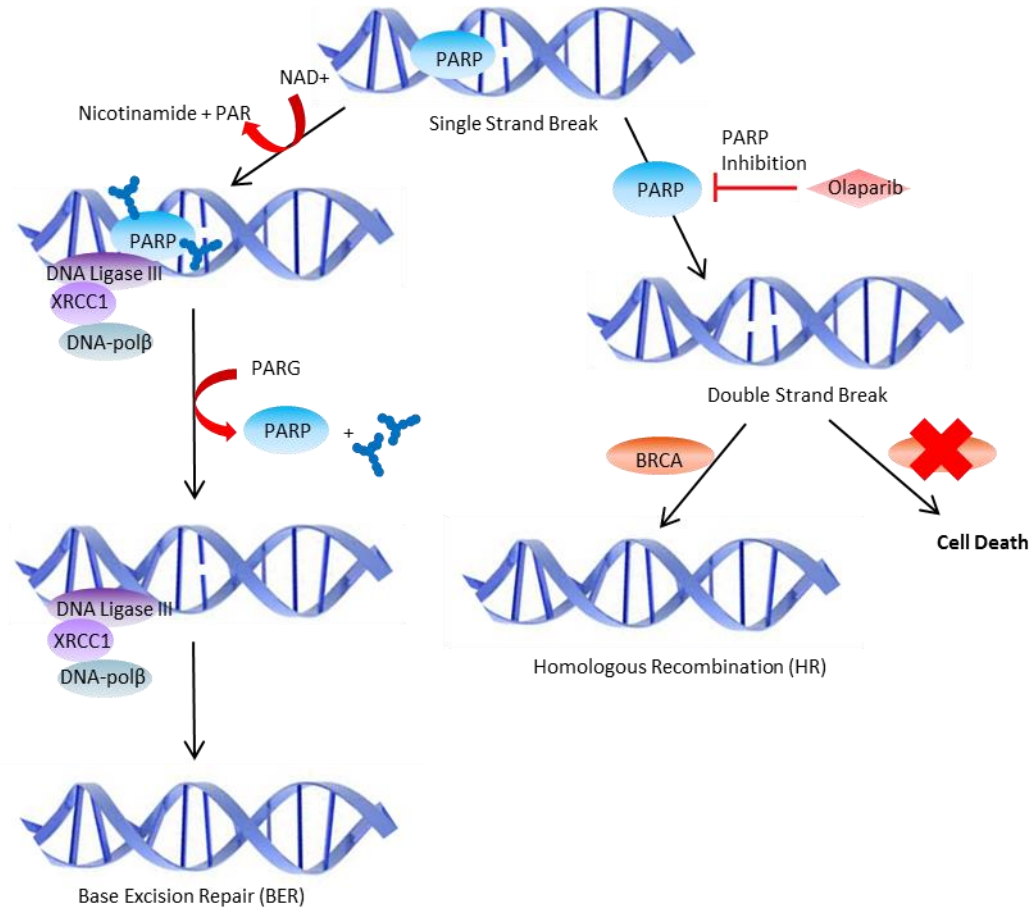

Figure 1.9 Consequences of PARP inhibition and BRCA inhibition on DNA repair processes

Pathway 1 on the left shows the cascade of events leading to normal DNA repair by BER. However, Pathway 2 on the right is the sequence of events following PARP inhibition of Pathway 1 by Olaparib. In BRCA functional cells, DNA can be repaired by HR. However, in BRCA compromised tumours DNA breaks are irreparable resulting in cell death. Adapted from Bryant *et al*., 2006 [84] and Helleday, 2011 [59].

1.5.1.1 Current status of Olaparib as a monotherapy

As stated above, Olaparib has been extensively studied for use in cancers that have a naturally occurring mutation in the BRCA1/2 genes resulting in a deficit in the cellular ability to repair DNA lesions by HR.

For example an *in vivo* study by Rottenberg *et al.,* (2008), indicated that inducing synthetic lethality in this manner might successfully treat BRCA1/2 deficient breast and ovarian cancer as they administered Olaparib to mice with BRCA1 null breast cancer tumours and demonstrated that these tumours display particular sensitivity to PARP inhibition, resulting in a reduction in tumour growth. This particular study also suggested that, by combining Olaparib with platinum compounds such as carboplatin and cisplatin, there was a substantial increase in animal survival and remission via tumour shrinkage [85], thus providing encouraging evidence towards its possible use as a combination therapy with other chemotherapeutic drugs.

Early Phase I clinical trials provided further evidence for the efficacy of Olaparib in BRCA1/2 deficient cancers. Fong *et al.,* (2009) began a study in 2005, enrolling 22 patients with BRCA1/2 mutations and one with a strong familial incidence of BRCA associated cancers. Of the 23 patients, 19 were suitable for inclusion in the study and 63% of the cohort presented advantageous clinical responses in particular, disease stabilisation following Olaparib treatment [86].

Subsequently, a Phase 2 trial in patients suffering from advanced ovarian or triple negative breast cancer also provided promising results using Olaparib as a monotherapy [87]. Of the 91 patients (65 ovarian and 26 with breast) 41% of the BRCA1/2 mutated ovarian patients showed objective responses (defined as tumour shrinkage) according to RECIST scoring. However, only 24% of ovarian patients lacking the BRCA1/2 mutation showed an objective response [87]. None of the breast cancer patients displayed significant responses; therefore it was concluded that Olaparib may be an option for patients presenting with BRCA1/2 mutated ovarian but not breast cancer [87]. A phase 3 clinical trial is currently being undertaken in women with advanced ovarian cancer caused by BRCA gene mutation.

1.5.1.2 Olaparib as a radiosensitising agent

Due to its known mode of action as a PARP-1 inhibitor Olaparib was assessed for its possible role as a radiosensitiser. A study carried out by Kotter *et al.,* (2014) investigated the use of Olaparib as a radiosensitiser in HR proficient cells (i.e. those

with proficient BRCA1/2 activity) and demonstrated that radiosensitivity was still elicited by Olaparib in these cells and that it was not significantly promoted by inhibition of DNA replication. Thus, in this case radiosensitivity is DNA replication-independent, meaning that it does not require the conversion of SSBs to DSBs by DNA replication in order to be effective. Another study by Tuli *et al.,* (2014) investigated the use of another PARP1/2 inhibitor ABT-888 (Veliparib) in combination with radiation treatment both *in vitro* and *in vivo* in pancreatic tumour models. This study reported significant enhancement of tumoricidal effect of radiation in cells treated with Veliparib both *in vitro* and *in vivo* and Veliparib is now subsequently undergoing Phase 1 clinical trial in combination with Gemcitabine and IMRT [88]. Olaparib has also been shown to sensitise non-small cell lung cancer cell lines to radiation both *in vitro* and *in vivo* [89]. Exposure of cells to Olaparib in combination with increasing doses of radiation (0-6Gy), resulted in a dose dependent decrease in cell survival compared to radiation alone [89]. *In vivo* tumour xenograft models were also investigated and Olaparib administration was shown to induce growth repression when combined with low dose radiation treatment. However, in contrast, the use of Olaparib alone had no effect on tumour development [89]. Taken together, all of the aforementioned studies provide a positive rationale for the expansion of the use of Olaparib into tumours not necessarily harbouring BRCA1/2 mutations as a radiosensitising agent.

1.6 Aim of this Study

Targeting of major DNA repair pathways within the cell has proven to be effective in the potentiation of radiation induced damage and DNA replication induced breaks in a wide range of tumour types. Thus, the aims of the present study were threefold:

(i) To assess the single agent toxicity of Mirin and Olaparib *in vitro* to elucidate non-toxic concentrations for further combination analyses.

(ii) To determine the radiosensitising potential of Olaparib and Mirin *in vitro,* using both X-ray irradiation and targeted radiotherapeutics with [^{131}I]MIBG.

(iii) To investigate whether the mechanisms underpinning cellular response to combination treatment differ with both radiation qualities.

Chapter 2

The effect of X-ray radiation and [^{131}I]MIBG on cancer cell survival and DNA damage repair pathways.

2.1 Introduction

External beam radiotherapy is utilised in more than 50% of cancer therapeutic regimens, however there are a plethora of normal tissue toxicities associated with this type of therapy, limiting the dose of radiation that can be safely delivered to the tumour tissue. The development of more targeted forms of radiotherapy have therefore been at the forefront of radiation research for many years with the best documented form of this type of treatment being that of ^{131}I, used in the treatment of thyroid cancer (see section 1.2.2) [21]. The focus of this study has been the use of both X-ray radiation and targeted radiotherapy in the form of [^{131}I]MIBG to determine the radiosensitising potential of DNA repair inhibiting compounds. Over the last decade the understanding of the biological pathways underlying the response to X-ray radiation has increased significantly. This has led to an exponential increase in the development of small molecule inhibitors targeting components of the DNA damage response pathway as a means of increasing the sensitivity of cancer cells to radiation. However, little is known about activation and kinetics of DDR response pathways in response to [^{131}I]MIBG. In this chapter we investigate the differing effects of the two radiation qualities on cell survival and the DNA damage response pathway.

2.2 Aims

The aims of the present study were to assess the clonogenic cell survival of SK-N-BE(2c), UVW/NAT and A375 cells following exposure to X-ray radiation and [^{131}I]MIBG, and to investigate the effect of X-ray radiation and [^{131}I]MIBG on the activation and kinetics of components of the DDR pathway.

2.3 Materials and Methods

2.3.1 Cell Lines and Culture conditions

Three human cancer cell lines were utilised throughout this study: UVW/NAT (glioblastoma cells transfected with bovine NAT (bNAT) cDNA) [90], A375 (melanoma cells) and SK-N-BE(2c) (neuroblastoma cells) obtained from ATCC (Middlesex, UK). UVW/NAT and A375 cells were maintained in either MEM medium (UVW/NAT) or DMEM (A375) supplemented with penicillin/streptomycin (100U/ml), fungizone (2µg/ml), L-glutamine (200mmol/L) and 10% foetal calf serum. SK-N-BE(2c) cells were maintained in DMEM supplemented with penicillin/streptomycin (100U/ml), fungizone (2µg/ml), L-glutamine (200mmol/L), sodium pyruvate, 1% (v/v) non-essential amino acids and 15% foetal calf serum.

All cells were incubated at 37^{o}C in a 5% CO_2 environment. In addition, 100µg/ml geneticin was added to UVW/NAT culture medium at each passage to maintain NAT transfection status.

MEM and DMEM media, penicillin/streptomycin, fungizone, sodium pyruvate, non-essential amino acids and L-glutamine were obtained from Invitrogen® (Paisley, United Kingdom) and foetal calf serum was obtained from Autogen Bioclear UK Ltd (Calne, United Kingdom).

Geneticin (Life Technologies Ltd, Paisley) was prepared by dissolving 1g of powdered Geneticin in 10ml of sterile distilled water followed by filtration using a syringe driven filter unit (Millipore, UK).

2.3.2 Treatment of cells with X-ray radiation and [^{131}I]MIBG

For X-ray radiation treatment studies, cell medium was removed and replaced with 5ml of fresh medium prior to X-ray radiation exposure using a Precision X-ray, X-RAD225 225KV X-ray cabinet (North Branford, CT, USA). Doses of 0-10Gy were delivered to cell samples with a dose rate of 2.3Gy/min. For [^{131}I]MIBG studies, medium was removed and replaced with 1ml of fresh medium before cells were incubated with no-carrier-added [^{131}I]MIBG for 2 hours, after which uptake is

maximal [91]. Medium was then removed and cells washed with PBS prior to re-addition of fresh medium. To examine the effect of dose, cells were treated within a dose range of 0-6MBq/ml. The no-carrier-added [^{131}I]MIBG was synthesised and provided by Dr. Sally Pimlott, NHS Greater Glasgow and Clyde.

2.3.3 Clonogenic (Colony Forming) Cell Survival Assay

Clonogenic assays were performed in order to determine whether UVW/NAT and A375 cells continue to form viable colonies of daughter cells following exposure to the radiation types investigated in this study.

UVW/NAT and A375 cell survival was determined using clonogenic cell survival assays, however, SK-N-BE(2c) cells did not form measurable colonies when plated in petri dishes and therefore their cell survival was determined using the soft agar cell survival assay (section 2.3.4). Monolayers of UVW/NAT and A375 cells were cultured in 25cm^2 flasks (Nunclon Plastics, Denmark) at a density of 1.5 x 10^5 cells per flask. Following a 48 hour incubation period once the cells had reached logarithmic growth phase (around 70-80% confluence), medium was removed and cells treated as described in section 2.3.2. Following 24 hour incubation post-treatment, medium was removed, the cells were washed with phosphate buffered saline (PBS) and detached from the flask by addition of 0.05% (v/v) trypsin-ethylenediaminetetracetic acid (Gibco, Paisley, UK). The detached cell solution was disaggregated to a single cell suspension by passage through a 21 gauge syringe and cells were counted using a haemocytometer. Cells were subsequently seeded in triplicate into 60mm petri dishes at a density of 250 cells per plate, with fresh medium and incubated at 37^{o}C in a 5% CO_2 environment until colonies of 50 cells or more were visible in the control plates (typically 7-10 days). Following 7-10 day incubation colonies were washed with PBS, fixed in 100% methanol and stained using 10% Giemsa stain. Cells were then washed with tap water and colonies counted manually. The survival fraction (SF) was calculated by dividing the number of colonies of the experimental treatment group by the number of colonies of the control plates where SF equals the number of colonies counted in each treatment group divided by the number of colonies formed

in the control group. Three independent experiments were performed in triplicate for each cell line.

2.3.4 Clonogenic (Soft Agar) Cell Survival Assay

The soft agar cell survival assay is based on the same principle as the colony forming clonogenic cell survival assay described in section 2.3.3. However, this method is used in cases when cell lines do not form discrete countable colonies in petri dishes. Therefore as SK-N-BE(2c) cells could not be assessed by colony-forming clonogenic assay, the soft agar clonogenic assay was used for this cell line. Briefly, SK-N-BE(2c) cells were seeded into 25cm^2 cell culture flasks at 3 x 10^5 cells per flask, and incubated for 48 hour at 37^{o}C, in a 5% CO_2 environment. Cells were treated as described above (section 2.3.2) and incubated for a further 24 hours. Cells were detached using Accutase (Sigma-Aldrich, Dorset, UK) and counted as described in section 2.3.3 and 2x10^4 cells were seeded into a suspension mixture of 0.03% low melting point agar (Sigma-Aldrich, Dorset, UK) with 2X DMEM media (Millipore, UK) supplemented as described in section 2.3.1. The cells were then distributed into 8 wells of a 96 well plate (2500 cells/well). To prevent cells from adhering to the bottom of the plate the plate was coated with a 0.5% agar solution in DMEM. Following 7 day incubation at 37^{o}C, in a 5% CO_2 environment, 100µl of 1x alamarBlue® reagent as 10% of the sample volume (diluted from 10x to 1x in cell growth media) (Invitrogen®, Paisley, UK) was added into each well. Plates were analysed for reduction of blue resazurin dye to fluorescent red resorufin 4 hours and 24 hours following addition of alamar blue using a fluorescence plate reader (excitation wavelength 560nm-590nm emission). Cell viability corresponds to the cells metabolic activity and is proportional to the level of fluorescence emitted. Data were collected using a SPECTRAmax Gemini XS fluorescent plate reader with SOFTmaxPro 4.3 drug discovery edition software (Molecular Devices, UK).

2.3.5 Cell Cycle Analysis

The progression of cells through the cell cycle was determined to assess if X-ray radiation and [^{131}I]MIBG caused an abrogation to the normal cycling of cells. Following treatment of cells as described in section 2.3.2, cell samples were collected 2, 6 and 24 hours post treatment. The time points were selected based on previous experiments which demonstrated the initiation of G2/M arrest from X-ray radiation exposure alone.

Cells were washed with PBS, detached using 0.05% trypsin EDTA or Accutase® (SK-N-BE(2c) cells only) and pelleted by centrifugation at 1200rpm for 5 minutes. The supernatant was then removed and the pellet re-suspended in PBS. The cells were then re-pelleted, the PBS was removed, and the cells were fixed by addition of ice cold 70% ethanol. Fixed samples were stored at -20^{o}C until analysis.

For analysis, fixed samples were pelleted at 2000rpm for 10 minutes before washing in PBS and re-pelleting. Samples were then incubated on ice, in the dark for a minimum of 1 hour in the presence of 10µg/ml propidium iodide (PI) (Sigma-Aldrich Company Ltd, Dorset, UK) to label DNA content and RNase A (50µg/ml) (Sigma-Aldrich Company Ltd, Dorset, UK) before Fluorescence Activated Cell Sorting (FACS) analysis. FACS analysis was carried out using the BD FACSCanto Analyser (Becton Dickinson Systems, Cowley, UK) and results were analysed using BD FACSDiva, v6.1.3 software. A minimum of 10000 cells per sample was analysed. Three independent experiments were performed for each cell line.

2.3.6 H2AX Foci Staining

γ-H2AX was used as a biochemical marker of the magnitude and resolution of DNA double stranded breaks in response to X-ray radiation and [^{131}I]MIBG.

Cells were seeded onto 13mm coverslips at a density of 1 x 10^4 cells/coverslip and cultured for 2 days to allow cells to enter the exponential growth phase. Cells were treated as described in section 2.3.2 and coverslips were removed from the dishes at various time points post treatment (2, 6 and 24 hours). Subsequently cells were washed in PBS and fixed in 4% paraformaldehyde at room temperature for 20

minutes. Cells were then washed in PBS and permeabilised in 0.5% triton X-100 for 20 minutes. Non-specific antibody binding was blocked by incubation in 0.5% BSA in PBS containing 0.15% triton X-100 for 20 minutes. The monoclonal anti-phospho-histone H2AX (ser 139) antibody (Millipore, UK) diluted 1:250 in 0.5% BSA in PBS containing 0.15% triton X-100 was added and cells incubated overnight at 4^{o}C. Cells were washed in PBS before incubation for 1.5 hours with a goat anti-mouse alexa-488 conjugated IgG antibody (Invitrogen®, (Paisley, UK)) at a 1:1500 dilution in 0.5% BSA in PBS containing 0.15% triton X-100 at room temperature. A final wash with PBS followed by distilled water was carried out before the coverslips were mounted on slides using Vectashield to prevent photobleaching (Vector Laboratories, Burlingame, CA) and storing at 4^{o}C in the dark. Confocal microscopy (Leica SP5 confocal) was used to capture z-stack images of approximately 50 cells per coverslip and foci in the DNA within the cell nuclei were subsequently counted using Volocity 3D Image Analysis Software (PerkinElmer, Waltham, MA) before plotting data using Microsoft Excel.

2.3.7 Fast activated cell-based ELISA Assay for pATM

ATM kinase is a phosphatidylinositol kinase-like kinase and has an important role in the process of stalling the cell cycle in order to allow DNA repair following induction of DNA damage [67]. To determine if X-ray radiation and [^{131}I]MIBG induced upregulation of pATM, a fast activated cell-based ELISA assay (FACE) was developed. Cells were seeded into 96-well plates at a density of 2x10^{3} cells per well in 200µl of medium and incubated for 48 hours at 37^{o}C, in a 5% CO_2 environment. Cells were treated with X-ray radiation or [^{131}I]MIBG in a volume of 200µl and fixed 2, 6 and 24 hours post treatment. Cells were washed twice with PBS containing 0.1% triton and incubated for 20 minutes in 4% paraformaldehyde. Endogenous peroxidase activity was quenched by incubating in 1%H_2O_2 and 0.1% sodium azide in PBS for 20 minutes and blocked for unspecific antibody binding by incubation in 5% marvel for 1 hour. Following blocking cells were incubated overnight at 4^{o}C with the monoclonal Anti-ATM Protein Kinase pS1981 Antibody, (Rockland Immunochemicals, PA) diluted 1:1000 in 5% marvel blocking buffer. Subsequently cells were washed and incubated

for 1 hour at room temperature with HRP-conjugated goat anti mouse IgG antibody (New England Biolabs, UK) (diluted 1:5000) avoiding light. The HRP substrate 3,3',5,5' - tetramethylbenzidine (TMB) was used to detect HRP activity, yielding a blue colour. To terminate this reaction 0.16M sulphuric acid was added (yielding a yellow colour) and the optical density read at 450nm. HRP-conjugated goat anti-mouse IgG without the primary antibody was used as a negative control. To obtain a measure of the total number of cells within each well the cells were washed in PBS and dH_2O before incubation in 1% crystal violet in ethanol (stains cell nuclei) for 30 minutes. Following a wash in dH_2O cells were lysed with 1% SDS solution and optical density read at wavelength 595nm. The absorbance measurements for pATM was normalised to the absorbance values obtained for crystal violet. This assay was validated by pATM foci staining using the protocol described in section 2.3.6.

2.3.8 Nuclear Protein Extraction

RAD51 is involved in homologous recombination of DNA and is recruited to radiation induced DNA double stranded breaks. To determine if X-ray radiation or [^{131}I]MIBG induced upregulation of RAD51, protein was initially extracted from the nucleus of the cells for subsequent assessment of RAD51 protein levels using an ELISA assay as described in section 2.3.10. Cells were seeded into 25cm^2 flasks and treated as described in section 2.3.3. Following incubation for varying times (2-24h) post-treatment, cells were scraped off the flask surface using cell scrapers into PBS and centrifuged at 13000rpm for 1 minute. The supernatant was subsequently removed and the pellet re-suspended in a lysis buffer containing 10mM hepes, 10mM KCl, 0.1mM EDTA, 0.1mM EGTA, 1mM DTT and protease inhibitors (pH 7.9). Samples were then incubated on ice for 15 minutes before addition of 10% triton X-100 and subsequent vortexing. Samples were re-pelleted at 13000 rpm and 50µl of supernatant was removed (cytoplasmic fraction). Protein was then extracted from the nuclear fraction by the addition of 50µl of a buffer containing 20mM hepes, 25% (v/v) glycerol, 0.4M NaCl, 1mM EDTA, 1mM EGTA, 1mM DTT and protease inhibitors (pH7.9) before vortexing and incubating on ice for 15 minutes. Finally, samples were

sonicated on ice for 2x30s and re-pelleted at 13000rpm for 15 minutes. Supernatants were transferred to fresh eppendorfs and stored at -20^{o}C. Protein content was assayed as described below in section 2.3.9.

2.3.9 BCA Assay

The BCA Assay (Pierce Biotechnology, Rockford, IL) was carried out as per the manufacturer's instructions to determine protein concentrations of samples for RAD51 ELISA and PARP assays. Briefly, 10µl of each sample plus albumin standard (0-2000µg) was pipetted into triplicate wells of a 96 well plate with 200µl of working reagent (50:1, Reagent A:B) and incubated at 37^{o}C for 30 minutes before measuring absorbance at 562nm using an absorbance plate reader. Absorbance was then plotted using Microsoft Excel and protein concentrations determined using the standard curve derived from data achieved from the albumin standards.

2.3.10 RAD51 ELISA

Sandwich ELISAs which are used to capture sample antigens on an antibody coated plate were used in order to determine nuclear RAD51 levels following exposure to X-ray radiation or [^{131}I]MIBG. The assessment of RAD51 levels was undertaken using a RAD51 ELISA kit according to the manufacturer's instructions (Uscn Life Science Inc., China). Briefly, 20ng nuclear protein of each sample or standard was pipetted into duplicate wells of a 96 well plate, pre-coated with a biotin conjugated antibody specific for RAD51 and incubated at 37^{o}C for 2 hours. All liquid was then removed from wells and cells incubated with HRP conjugated avidin (binds to biotin) for a further hour at 37^{o}C. After washing, the HRP substrate 3,3',5,5' -tetramethylbenzidine (TMB) was added for detection of HRP activity (30 minutes at 37^{o}C) and this reaction terminated by the addition of 0.16M sulphuric acid solution. The colour change was measured by optical density at a wavelength of 450nm. The concentration of RAD51 Homolog (RAD51) in the samples was determined by comparing the absorbance of the samples to the standard curve.

2.3.11 PARP Assay Protein Collection

PARP-1 is a protein located in the cell nucleus that detects DNA lesions triggering its own modification and that of other cellular proteins by ADP-ribosylation culminating in activation of repair processes such as BER, NHEJ and HR. To determine if X-ray radiation or [^{131}I]MIBG induced upregulation of PARP-1, protein was initially extracted from cells for subsequent assessment of PARP-1 protein levels using an ELISA assay as described in section 2.3.12. Cells were seeded into 25cm^2 flasks and treated as described in section 3.3.3. Following incubation for varying times (2, 6 and 24 hours) post-treatment, cells were scraped off the flask surface using cell scrapers into PBS and centrifuged at 2000rpm at 4^{o}C. The supernatant was subsequently removed and the pellet re-suspended in PARP assay lysis buffer (PARP assay lysis buffer contained 0.4mM Aprotinin (Sigma-Aldrich, Dorset), 1x protease and phosphatase inhibitors (Life Technologies, Paisley), 0.4M NaCl and 1% Triton X-100). Samples were then incubated on ice for 30 minutes (with periodic vortexing) before re-centrifuging at 13000xg for 10 minutes. The supernatant was then transferred to a fresh microcentrifuge tube and stored at -80^{o}C until BCA assay for assessment of protein concentration (Section 2.3.9).

2.3.12 PARP ELISA

The assessment of PARP activity was undertaken using a PARP assay kit which measures the incorporation of biotinylated poly(ADP-ribose) onto histoproteins according to the manufacturer's instructions (Trevigen, Gaithersburg, MD). Briefly 20µg of protein was prepared by dilution of previously collected samples (Section 3.3.6) in 1x PARP buffer and pipetted into histone coated wells in triplicate in a 96 well plate. Similarly PARP-HSA standards were serially diluted (0-2mg) in 1x PARP buffer and pipetted into triplicate wells of the 96 well plate. 1x PARP cocktail (containing 1x PARP cocktail, 1x Activated DNA and diluted in 1x PARP buffer) was then distributed into all wells using a multichannel pipette and the plate incubated at room temperature for 60 minutes. Plates were then washed 4 times in 1x PBS containing 0.1% Triton X-100 before incubating for 60 minutes with diluted HRP-

conjugated streptavidin (strep-HRP) which allows for detection in the form of colour change in the presence of developing substrate. Plates were then washed again as described before and incubated with TACS-Sapphire colorimetric substrate in the dark and monitored for blue colour development. The reaction was stopped using 0.2M HCl and the absorbance read at 450nm.

2.3.13 Statistical Analysis

All experiments were carried out 3 times and data presented as the mean±sd. Statistical analysis was carried out using GraphPad Prism version 6.05 (GraphPad Software Inc, San Diego). One-way ANOVA was used to determine statistical significance between treated and untreated control samples, p values <0.05 were reported as statistically significant.

2.4 Results

2.4.1 Determination of radiation toxicity

Clonogenic assays were performed in order to determine the cytotoxic effects of X-ray radiation and [^{131}I]MIBG as single agents on each cell line. The data collected in this series of investigations were then used to determine the radiation dose range to be utilised in further combination studies in subsequent chapters.

2.4.1.1 Clonogenic cell survival following exposure to X-ray radiation

SK-N-BE(2c) cells exhibited a dose dependent reduction in survival fraction following exposure to X-rays over the 1-10Gy dose range (Figure 2.1a), with a 25% (IC_{25}) reduction in clonogenicity observed at 2.11Gy, 50% (IC_{50}) reduction at 3.77Gy and a 75% (IC_{75}) reduction at 5.77Gy (Figure 2.1d). Similarly UVW/NAT cells exhibited a dose dependent reduction in survival fraction following exposure to X-rays over the 1-10Gy dose range (Figure 2.1b), from a 25% (IC_{25}) decrease in cell viability at 2.3Gy, 50% (IC_{50}) cell death at 3.51Gy and a 75% (IC_{75}) reduction at 4.91Gy (Figure 2.1d). Furthermore, A375 cells also exhibited a dose dependent reduction in colony survival with a 25% (IC_{25}) decrease in cell viability observed at 1.42Gy, a 50% (IC_{50}) reduction in cell survival at 3.18Gy and a 75% (IC_{75}) reduction at 5.75Gy (Figure 2.1d).
Based on the data presented in Figure 2.1d it can be concluded that SK-N-BE(2c) cells appeared to be the most radioresistant cell line requiring consistently higher doses of radiation compared to UVW/NAT and A375 cells to achieve the same level of cell death.
To assess the activation and kinetics of components of the DDR response pathway, X-ray radiation doses of 2, 4 and 6Gy were used as these doses covered a broad range of clonogenic cell kill ranging from below 25% to above 75% decrease in clonogenic cell kill.

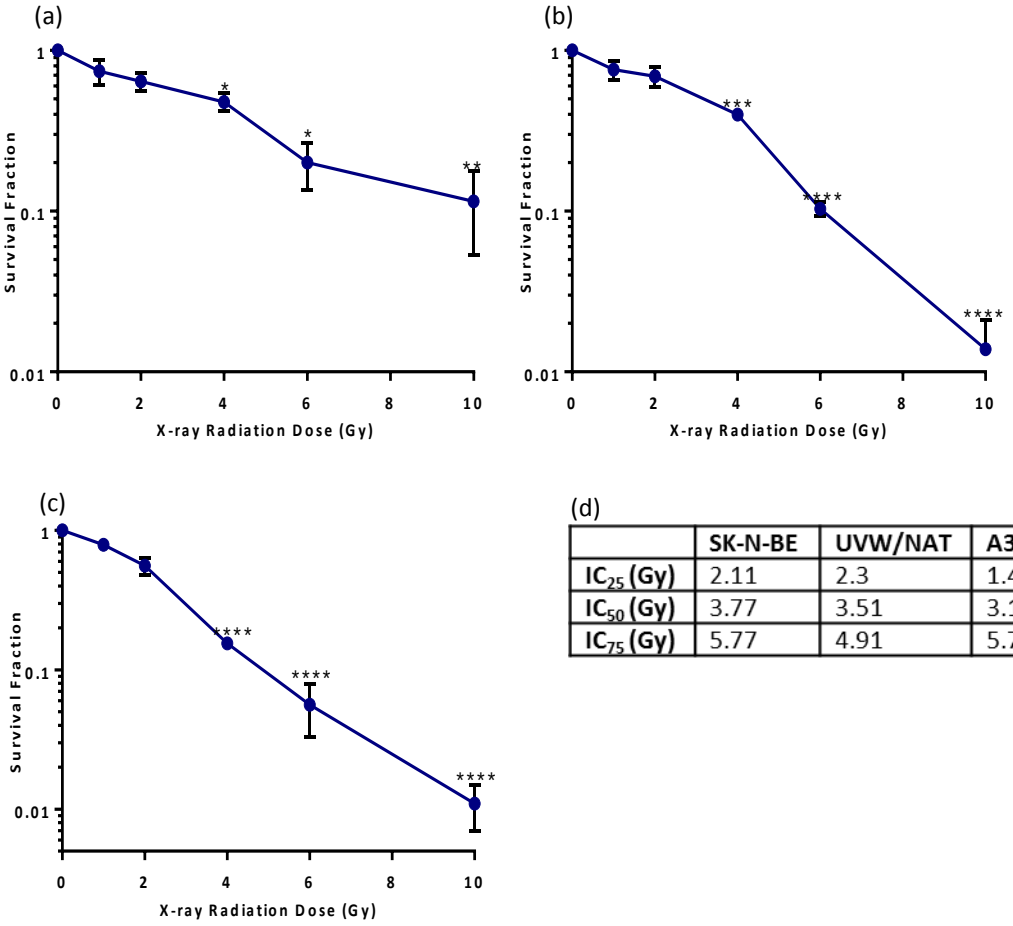

(d)

	SK-N-BE	UVW/NAT	A375
IC_{25} (Gy)	2.11	2.3	1.42
IC_{50} (Gy)	3.77	3.51	3.18
IC_{75} (Gy)	5.77	4.91	5.75

Figure 2.1 The toxicity of X-rays on clonogenic survival of (a) SK-N-BE(2c) (b) UVW/NAT (c) A375 cells.

The clonogenic capacity of all cells was assessed 24 hours after exposure to a range of X-ray doses. Clonogenic survival data for treated cells were normalised to untreated control cells. Results are presented as the average survival fraction of 3 independent experiments (mean±sd). One-way ANOVA was used to compare the means of X-ray treated cells to untreated control data for all cell lines. * denotes $p<0.05$, ** denotes $p<0.01$, *** denotes $p<0.001$, **** denotes $p<0.0001$

2.4.1.2 Clonogenic cell survival following treatment with [^{131}I]MIBG

Clonogenic survival data following treatment of cells with increasing doses of [^{131}I]MIBG are shown in Figure 2.2 for SK-N-BE(2c) and UVW/NAT cells. SK-N-BE(2c) cells exhibited a dose dependent reduction in survival fraction following treatment with [^{131}I]MIBG over the 1-6MBq dose range. As is shown in Figure 2.2c, a 25% (IC_{25}) reduction in cell viability was elicited after treatment with 1.53MBq, with a 50% reduction in colony survival (IC_{50}) occurring at 2.88MBq and 75% (IC_{75}) colony reduction at 4.54MBq. UVW/NAT cells also exhibited a dose dependent reduction in survival fraction following treatment with [^{131}I]MIBG over the 1-6MBq dose range. Survival fraction decreased by 25% (IC_{25}) at 1.24MBq, by 50% (IC_{50}) at 2.4MBq and 75% (IC_{75}) at 3.84MBq. Again, as with X-irradiation, SK-N-BE(2c) cells appeared to be more radio-resistant than UVW/NAT cells, requiring higher doses of [^{131}I]MIBG to achieve the same level of cell kill.

Based on these data, to assess the activation and kinetics of components of the DDR response pathway, [^{131}I]MIBG doses of 1, 2 and 6 MBq were used as these doses covered a broad range of clonogenic cell kill, ranging from below 25% to above 75% decrease in clonogenic viability.

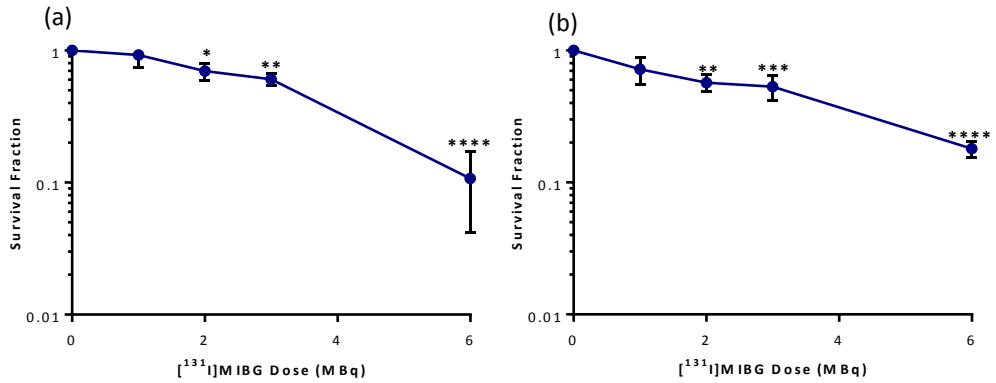

(c)

	SK-N-BE	UVW/NAT
IC_{25} (MBq)	1.53	1.24
IC_{50} (MBq)	2.88	2.4
IC_{75} (MBq)	4.54	3.84

Figure 2.2 The toxicity of [^{131}I]MIBG on clonogenic survival of (a) SK-N-BE(2c) (b) UVW/NAT cells.

The clonogenic capacity of all cells was assessed 24 hours after treatment with a range of [^{131}I]MIBG concentrations. The survival fraction of treated samples were normalised to untreated controls. Data are presented as the means of three independent experiments. One-way ANOVA was used to compare the means of [^{131}I]MIBG treated cells to untreated controls for both cell lines. * denotes $p<0.05$, ** denotes $p<0.01$, *** denotes $p<0.001$, **** denotes $p<0.0001$.

2.4.2 Activation of ATM in response to X-ray radiation and [^{131}I]MIBG treatment.

To determine whether the activation and kinetics of DDR pathway components vary upon exposure to different radiation qualities, we firstly interrogated the activation and kinetics of ATM in response to a range of doses of X-ray radiation and [^{131}I]MIBG. ATM kinase is one of the earliest kinases rapidly recruited to sites of DNA DSBs by the MRN complex and becomes activated upon phosphorylation [65]. Phosphorylation of ATM is central in the activation of downstream effector proteins to initiate cell cycle checkpoints that will ultimately allow DNA repair to occur. Investigation of its role in DNA repair over time, following radiation induced damage will allow us to rationalise possible therapeutic exploitation of ATM, or up and down stream targets of ATM, to potentiate the cytotoxic effects of X-ray radiation or [^{131}I]MIBG.

2.4.2.1 Characterisation of ATM kinase activity following exposure to X-ray radiation

Figure 2.3 shows the fold change (relative to untreated control cells) in phosphorylated ATM (pATM) levels in all cell lines investigated. pATM levels were investigated in response to increasing doses of X-ray radiation (2-6Gy) 2, 6 and 24 hours after exposure and compared to untreated control cells. A dose dependent increase in pATM levels was observed 2 hours post irradiation in SK-N-BE(2c) cells, however this trend was not mirrored at later time points where levels decreased, returning to almost basal levels 24 hours after initial irradiation (Figure 2.3a). Both UVW/NAT and A375 cells however exhibited a dose dependent increase in pATM levels across all time points (Figure 2.3c and e). In all examined cell lines, across all radiation doses, the levels of pATM were highest 2h post irradiation where pATM levels had increased by 44%±0.02, 50%±0.04 and 61%±0.05 respectively across the 2-6Gy dose range in SK-N-BE(2c) cells, 44%±0.2, 56%±0.3 and 71%±0.07 respectively in UVW/NAT cells and 54%±0.2, 63%±0.3 and 74%±0.3 respectively in A375 cells. The levels of pATM decreased between 2 and 6 hours post irradiation, and a further decrease in levels was observed between 6 and 24 hours. Between 2 and 24 hours post X-irradiation pATM levels decreased by 34%±0.01, 44%±0.05 and 66%±0.06 respectively across the dose range in SK-N-BE(2c) cells, 39%±0.2, 40%±0.01 and

42%±0.1 respectively in UVW/NAT cells and 40%±0.2, 40%±0.1 and 36%±0.1 respectively in A375 cells. Despite this decrease in pATM levels 24 hours after initial treatment, pATM levels remained elevated compared to untreated controls after exposure to 2 and 4Gy in SK-N-BE(2c) cells, 6Gy in UVW/NAT cells and 4 and 6Gy in A375 cells.

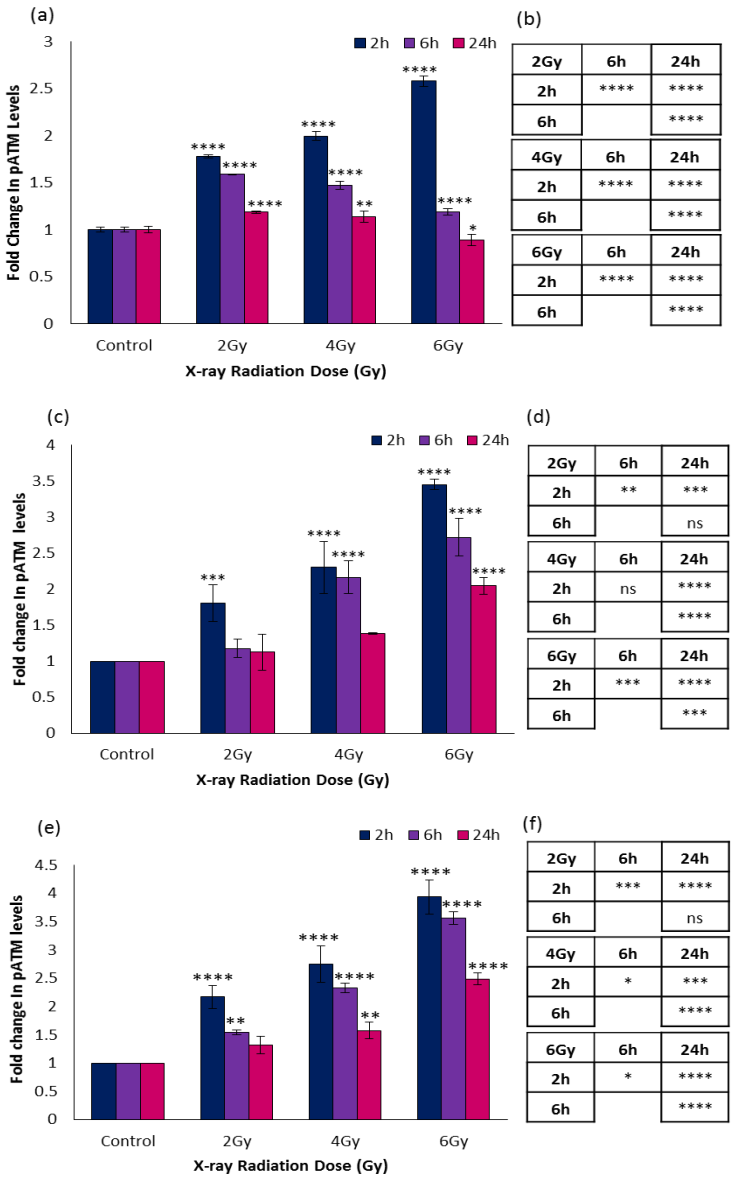

Figure 2.3 ATM kinase phosphorylation following exposure to X-ray radiation in (a) SK-N-BE(2c) (c) UVW/NAT and (e) A375 cells.

Fold change in pATM kinase levels following exposure to X-ray radiation was assessed in (a) SK-N-BE(2c) (c) UVW/NAT and (e) A375 cells over a 2-24 hour time course. The data was collected using a BioTek Epoch microplate spectrophotometer. Data are means ±SD; experiments were carried out three times in triplicate. Two-way ANOVA with Bonferroni post hoc test was used to statistically analyse means of treated samples to untreated controls (shown on graph) and the differences between time points (b,d,f) * denotes $p<0.05$ ** denotes $p<0.01$, *** denotes $p<0.001$, **** denotes $p<0.0001$

2.4.2.2 Characterisation of ATM kinase activity following treatment with [^{131}I]MIBG

Figure 2.4 shows the fold change in phosphorylated ATM (pATM) levels in SK-N-BE(2c) and UVW/NAT cells, 2, 6 and 24 hours after incubation with increasing doses of [^{131}I]MIBG (1-6MBq) compared to untreated control cells. A statistically significant dose dependent increase in pATM levels was observed at all doses and time points examined (Figure 2.4a and c). In both cell lines the highest pATM levels were observed 24 hours post initial [^{131}I]MIBG treatment, compared to untreated control cells. 2 hours post initial [^{131}I]MIBG treatment pATM increased by 62%±0.2, 68%±0.3 and 74%±0.1 and 56%±0.2, 62%±0.4 and 75%±0.5 in SK-N-BE(2c) ($p<0.0001$) and UVW/NAT ($p<0.0001$) cells across the dose range whilst 6 hours post initial treatment pATM had increased by 66%±0.3, 70%±0.2 and 83%±0.07 in SK-N-BE(2c) cells ($p<0.0001$) and 68%±0.1, 73%±0.1 and 82%±0.2 in UVW/NAT cells ($p<0.0001$) across the dose range compared to untreated controls. 24 hours after initial treatment a 69%±0.2, 78%±0.3 and 84%±0.2 increase was observed across the 2-6MBq dose range in SK-N-BE(2c) cells ($p<0.0001$) and a 76%±0.5, 80%±0.2 and 86%±0.06 increase across the dose range was observed in UVW/NAT cells ($p<0.0001$).

These data suggest that, although the DNA damage elicited by [^{131}I]MIBG appears to be accrued over a long time course, the cellular response to DNA damage is upregulated 2 hours after initial treatment. This is despite 2 hour treated cells exhibiting significantly less DNA damage than those treated with [^{131}I]MIBG for 24 hours. From the data obtained in these analyses it was hypothesised that γ-H2AX levels would also be elevated in a similar pattern to that observed here.

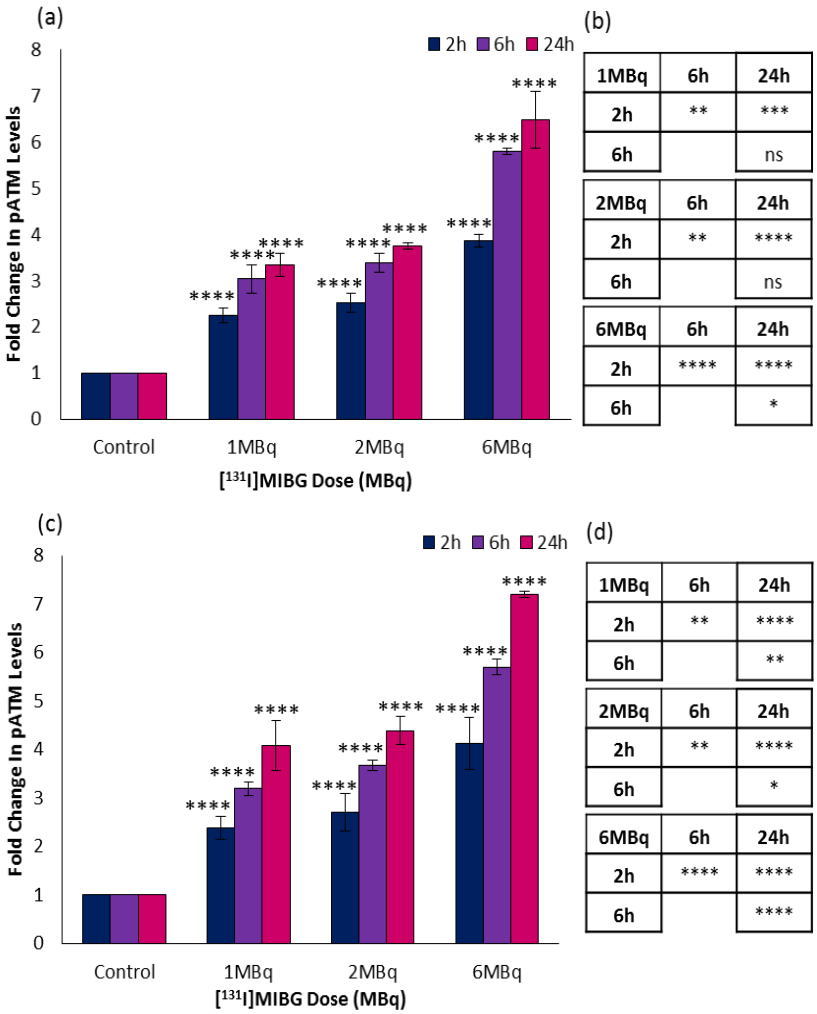

Figure 2.4 ATM kinase phosphorylation following exposure to [^{131}I]MIBG in (a) SK-N-BE(2c) and (b) UVW/NAT cells.

Fold change in pATM kinase levels following treatment with [^{131}I]MIBG was assessed in (a) SK-N-BE(2c) and (b) UVW/NAT cells over a 2-24 hour time period. Data are means ±SD of 3 independent experiments. Two-way ANOVA with Bonferroni post hoc test was used to statistically analyse means of treated samples to untreated controls (shown on graph) and the differences between time points (b,d) * denotes $p<0.05$ ** denotes $p<0.01$, *** denotes $p<0.001$, **** denotes $p<0.0001$

2.4.3 Investigation of γ-H2AX foci formation and resolution following X-ray radiation and [^{131}I]MIBG treatment

γ-H2AX foci form at DNA DSB sites following phosphorylation of H2AX. Although phosphatidylinositol 3 kinases, DNA-PK, ATM and ATR have all been implicated in H2AX phosphorylation ATM has been identified as major kinase involved in H2AX phosphorylation. In order to assess the kinetics of the DNA damage response pathway resulting from instantaneous and continual radiation exposure, we assessed γ-H2AX foci formation and resolution over a 24 hour time period.

2.4.3.1 Characterisation of γ-H2AX foci formation and resolution following X-ray radiation exposure

Fold changes in γ-H2AX levels compared to untreated control cells, following exposure to X-ray radiation (2, 4 and 6Gy) 2, 6 and 24 hours after irradiation in SK-N-BE(2c), UVW/NAT and A375 cells is shown in Figure 2.5. The highest levels of γ-H2AX foci were observed 2 hours following X-irradiation, whereupon a 86%±1.0, 89%±1.0 and 90%±0.9 increase across the 2-6Gy dose range was observed in SK-N-BE(2c) cells, an 88%±1.3, 90%±0.01 and 93±0.7 increase was observed in UVW/NAT cells and a 92%±0.2, 92%±0.2 and 93%± 0.1 increase was exhibited in A375 cells (Figure 2.5b,d,e). Additionally, 6 hours following exposure there was a significant reduction in γ-H2AX foci levels across the dose range, 46%±1.2, 65%±1.0, 60%±1.3 respectively in SK-N-BE(2c) cells, 45%±0.3, 55%±0.8, 60%±0.6 respectively in UVW/NAT cells and 76%±0.2, 80%±0.05, 83%±0.05 respectively in A375 cells. Furthermore, when compared to 2 hour samples ($p<0.001$ in all instances) with levels continuing to decline by 70%±0.7, 70%±0.3, 68%±0.3 in SK-N-BE(2c) cells, 79%±0.2, 80%±0.4, 73%±0.4 in UVW/NAT cells and 90%±0.3, 82%±1.0, 83%±1.1 in A375 cells at 24 hours (Figure 2.5). However in SK-N-BE cells levels of γ-H2AX foci remained above basal levels across the administered dose range whilst in UVW/NAT and A375 cells foci levels had returned to basal levels at lower administered doses of radiation (2 and 4Gy).

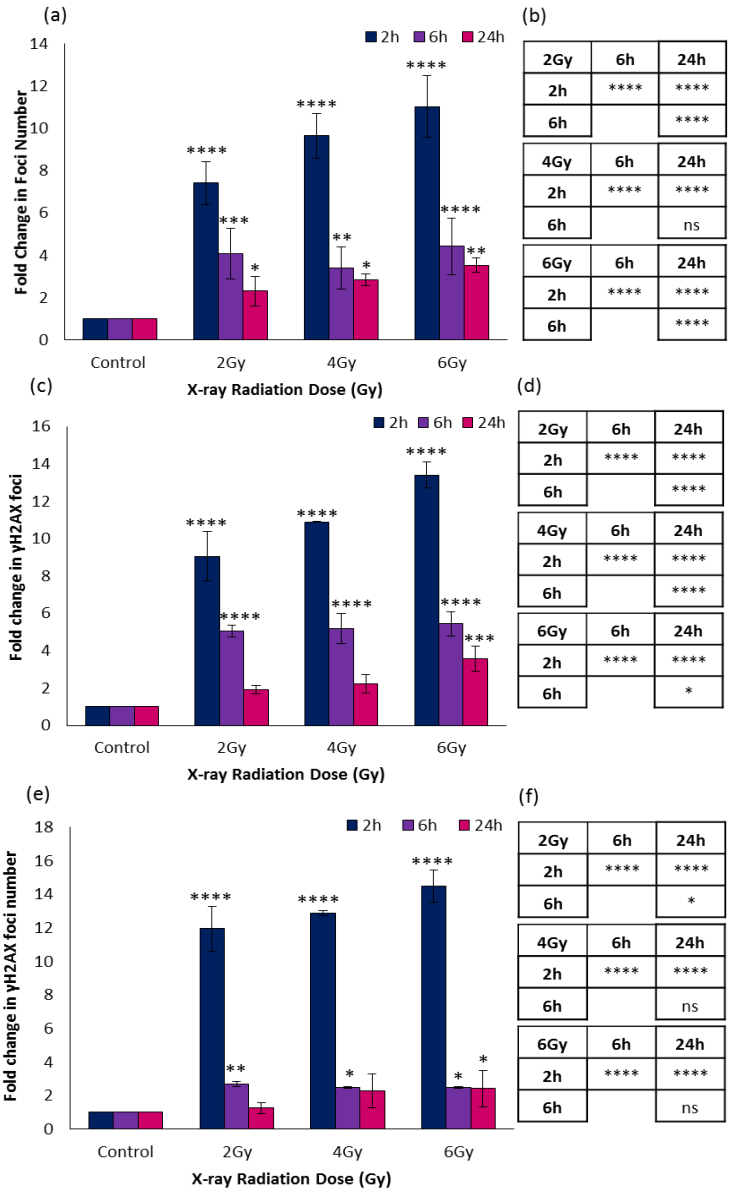

Figure 2.5 γ-H2AX foci formation and resolution following exposure to X-ray radiation in (a) SK-N-BE(2c) (c) UVW/NAT and (e) A375 cells.

Fold change in γ-H2AX foci formation following exposure to X-ray radiation was assessed in (a) SK-N-BE(2c) (c) UVW/NAT and (e) A375 cells over a 2-24 hour time course. Data are means ±SD; experiments were carried out three times in triplicate. Two-way ANOVA with Bonferroni post hoc test was used to statistically analyse means of treated samples to untreated controls (shown on graph) and the differences between time points (b,d,f) * denotes $p<0.05$ ** denotes $p<0.01$, *** denotes $p<0.001$, **** denotes $p<0.0001$

2.4.3.2 Characterisation of γ-H2AX foci formation and resolution following [^{131}I]MIBG treatment

Fold changes in γ-H2AX levels in UVW/NAT and SK-N-BE(2c) cells following incubation with [^{131}I]MIBG (1-6MBq) 2, 6 and 24 hours after initial treatment is shown in Figure 2.6. The data shows a significant dose dependent increase in γ-H2AX levels at all doses across the time period when compared to untreated control cells. 2 hours after initial treatment, increases in γ-H2AX foci levels were evident in all examined cell lines, with SK-N-BE(2c) cells demonstrating γ-H2AX foci levels that were 74%±0.4, 82%±0.2 and 79%±0.4 higher compared to untreated controls across the 1-6MBq dose range respectively, and UVW/NAT cells demonstrating 80%±0.5, 85%±0.7 and 90%±0.9 elevations 2 hours after initial treatment across the same dose range. After 6 hours γ-H2AX foci levels had increased further in both SK-N-BE(2c) and UVW/NAT cells and were now 83%±0.1, 86%±0.6 and 91%±0.2 higher in SK-N-BE(2c) cells and 86%±1.7, 89%±1.7 and 93%±2.0 higher in UVW/NAT cells compared to untreated control cells across the dose range. The highest levels of γ-H2AX foci were observed 24 hours following initial treatment with [^{131}I]MIBG at doses of 1, 2 and 6MBq whereupon SK-N-BE(2c) cells exhibited 84%±0.4, 87%±0.4 and 92%±0.2 increases respectively and UVW/NAT cells exhibited 92%±2.1, 93%±0.6 and 96%±3.5 increases respectively (Figure 2.6a and c). Additionally, across the 1-6MBq dose range there was a significant elevation in γ-H2AX foci levels between early and later time points (Figure 2.6b and d), with SK-N-BE(2c) cells showing 42%±0.5, 52%±0.2, and 62%±0.1 increases between 2 and 24 hour treatment groups, and UVW/NAT cells showing 60%±2.1, 53%±0.6 and 56%±3.5 increases between 2 and 24 hour treatment groups (Figure 2.6b).

These data suggest that, the DNA damage elicited by [^{131}I]MIBG is accrued over a long time course, as cells treated with [^{131}I]MIBG for 2 hours exhibited less DNA DSBs per cell than those incubated for the same time after X-ray radiation, however levels continually increased over the time course in [^{131}I]MIBG treated cells unlike X-irradiated samples which displayed a decrease from 6 hours. From the data obtained in these analyses it was hypothesised that nuclear RAD51 levels would also be

elevated in a similar pattern to that observed for γ-H2AX due to their co-localisation after DNA damage induction.

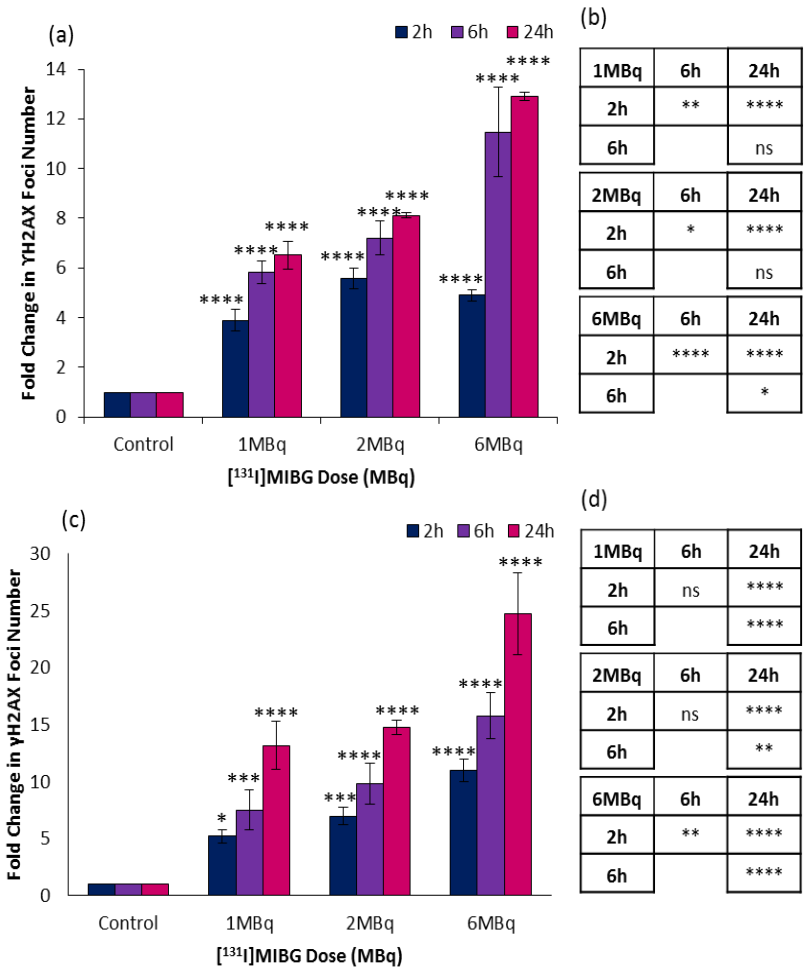

Figure 2.6 γ-H2AX foci formation and resolution following treatment with [^{131}I]MIBG in (a) SK-N-BE(2c) and (c) UVW/NAT cells.

Fold change in γ-H2AX foci formation following treatment with [^{131}I]MIBG was assessed in (a) SK-N-BE(2c) and (c) UVW/NAT cells over a 2-24 hour time course. Data are means ±SD; experiments were carried out three times in triplicate. Two-way ANOVA with Bonferroni post hoc test was used to statistically analyse means of treated samples to untreated controls (shown on graph) and the differences between time points (b,d) * denotes $p<0.05$ ** denotes $p<0.01$, *** denotes $p<0.001$, **** denotes $p<0.0001$

2.4.4. Characterisation of RAD51 nuclear expression following X-ray radiation and [^{131}I]MIBG treatment

RAD51 is a protein which is a key mediator of DNA repair by HR. Upon generation of DNA breaks, RAD51 forms nucleofilaments on the ssDNA ends. These nucleofilaments function to catalyse DNA strand exchange between the damaged DNA site and its complementary piece of DNA on a sister chromatid [92]. In order to determine the importance of HR in DNA repair following exposure to different radiation sources (X-rays and radioisotopes) we characterised the RAD51 nuclear protein expression profile over an experimental time course.

2.4.4.1 Characterisation of RAD51 nuclear expression following X-ray radiation exposure.

Fold changes in nuclear RAD51 protein levels in SK-N-BE(2c), UVW/NAT and A375 cells following exposure to X-ray radiation compared to untreated cells (2-6Gy) over a 2-24 hour time period is presented in Figure 2.7. There was a statistically significant, dose dependent increase in nuclear RAD51 levels across the dose range (2-6Gy) 2 hours post X-ray irradiation in all cell lines assessed. SK-N-BE(2c) cells exhibited 33%±0.1, 54%±0.09 and 57%±0.09 increases in nuclear RAD51 levels, UVW/NAT cells exhibited 37%±0.01, 44%±0.04 and 55%±0.01 increases and A375 cells exhibited 26%±0.07, 30%±0.3 and 41%±0.05 increases compared to untreated controls. Thereafter RAD51 levels decreased, and in SK-N-BE cells 24 hours post irradiation, levels decreased by 38%±0.16, 56%±0.2 and 48%±0.09 compared to 2 hour samples. In UVW/NAT cells nuclear RAD51 levels decreased by 25%±0.08, 23%±0.07 and 46%±0.04 between 2 and 24 hours post irradiation across the dose range and in A375 cells decreases of 23%±0.01, 13%±0.02 and 31%±0.002 were evident. However, despite the decline in nuclear RAD51 protein levels between 2 hours, and 6 and 24 hours, levels assessed after 6 and 24 hours remained significantly elevated in UVW/NAT and A375 cells compared to untreated controls, but in SK-N-BE(2c) cells, levels returned to basal levels 6 hours post irradiation at lower radiation doses (2 and 4Gy) and 24 hours post irradiation at 6Gy of radiation (Figure 3.27b).

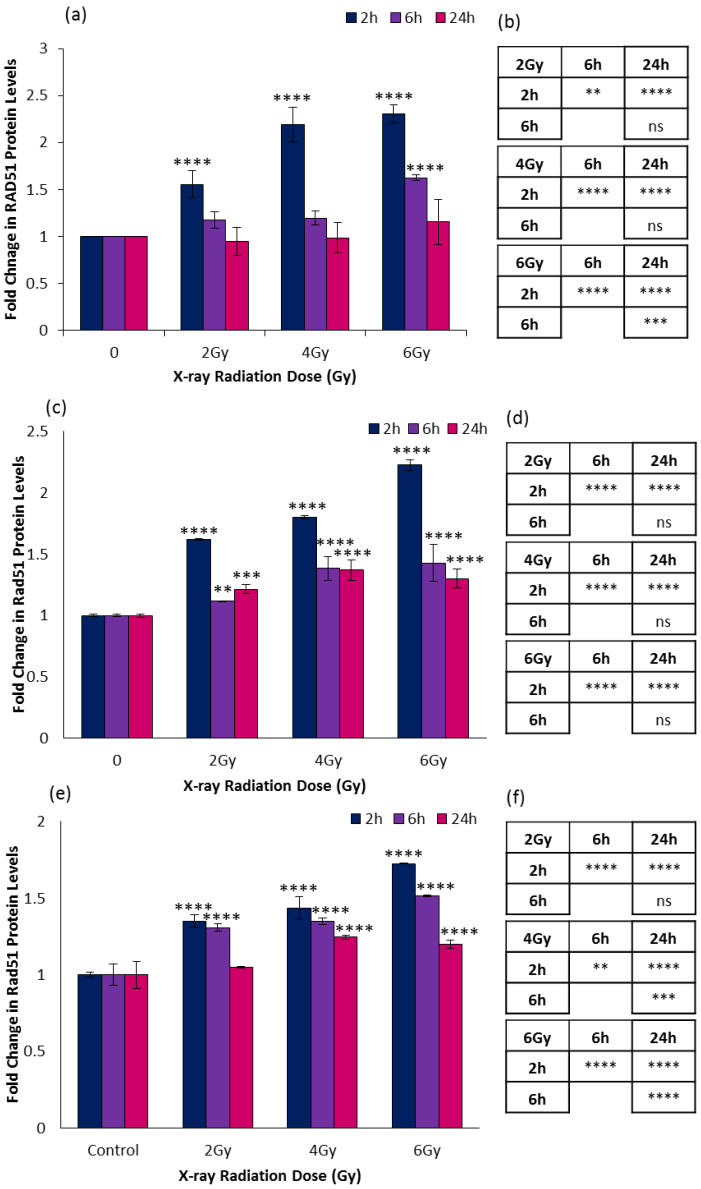

Figure 2. 7 The effect of X-ray radiation exposure on RAD51 activation in (a) SK-N-BE(2c) (b) UVW/NAT and (c) A375 cells.

Fold change relative to untreated controls in nuclear RAD51 protein levels following exposure to X-ray radiation was assessed in (a) SK-N-BE(2c) (b) UVW/NAT and (c) A375 cells over a 2-24 hour time course. Data are means ±SD; experiments were carried out three times in triplicate. Two-way ANOVA with Bonferroni post hoc test was used to statistically analyse means of treated samples to untreated controls (shown on graph) and the differences between time points (b,d,f) ** denotes $p<0.01$, *** denotes $p<0.001$, **** denotes $p<0.0001$

2.4.4.2 Characterisation of RAD51 nuclear expression following [^{131}I]MIBG treatment

Fold change in RAD51 protein levels relative to untreated controls, in SK-N-BE(2c) and UVW/NAT cells following incubation with [^{131}I]MIBG (1-6MBq) over a 2-24 hour time course is presented in Figure 2.8. There was a statistically significant, dose dependent increase in RAD51 levels across the administered dose range (1-6MBq) at all time points investigated. In SK-N-BE(2c) cells, RAD51 protein levels increased significantly 2 hours post initial treatment across the dose range administered (23%±0.008, 20%±0.004 and 28%±0.01 respectively). Nuclear RAD51 protein levels increased further 6 hours post initial treatment and were 33%±0.1, 38%±0.04 and 47%±0.03 higher respectively than in untreated control cells across the dose range. The highest levels of nuclear RAD51 were evident 24 hours after initial treatment, particularly at higher doses of [^{131}I]MIBG (2 and 6MBq) with levels increasing by 29%±0.07, 54%±0.01 and 67%±0.1 respectively across the 1-6MBq time course compared to untreated controls. In contrast, in UVW/NAT cells incubated with lower doses of [^{131}I]MIBG (1 and 2MBq), nuclear RAD51 protein levels did not increase significantly above basal levels until 24 hours after initial exposure. Percentage increases in nuclear RAD51 were 27%±0.1, 44%±0.05 and 40%±0.17 across the dose range 24 hours post initial [^{131}I]MIBG treatment. Additionally, a significant elevation in RAD51 protein levels between early and late time points is observed (Figure 2.8b and d), with SK-N-BE(2c) cells showing an 8%±0.07, 40%±0.01 and 54%±0.1 increase between 2 and 24 hour treatment groups at 1, 2 and 6MBq respectively, and UVW/NAT cells showing 22%±0.1, 30%±0.05 and 17%±0.2 increases between 2 and 24 hours across the dose range.

These data again suggest that, the DNA damage elicited by [^{131}I]MIBG is accrued over a long time course, as cells treated with [^{131}I]MIBG for 2 hours exhibited less nuclear RAD51 levels than those treated with X-ray radiation for the same time, however levels continually increased over the time course in [^{131}I]MIBG treated unlike X-irradiated samples which displayed a decrease from 6 hours.

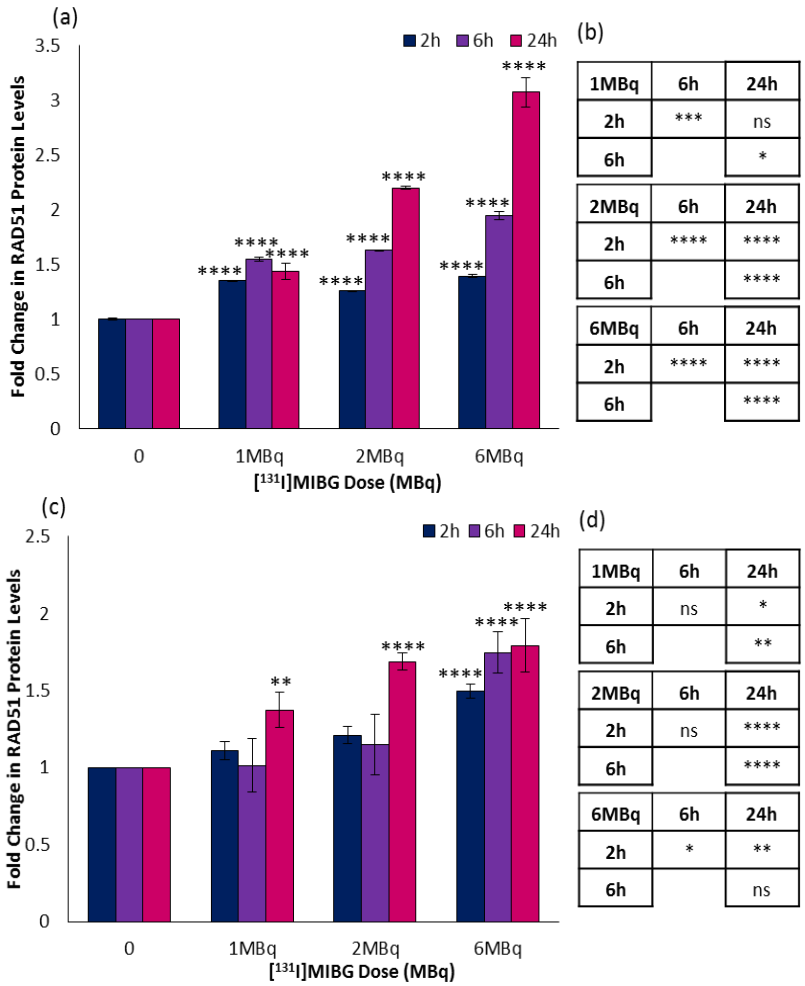

1MBq	6h	24h
2h	***	ns
6h		*

2MBq	6h	24h
2h	****	****
6h		****

6MBq	6h	24h
2h	****	****
6h		****

1MBq	6h	24h
2h	ns	*
6h		**

2MBq	6h	24h
2h	ns	****
6h		****

6MBq	6h	24h
2h	*	**
6h		ns

Figure 2.8 The effect of [^{131}I]MIBG treatment on RAD51 activation in (a) SK-N-BE(2c) and (b) UVW/NAT cells.

Fold change relative to untreated controls in nuclear RAD51 protein levels following treatment with [^{131}I]MIBG was assessed in (a) SK-N-BE(2c) and (b) UVW/NAT cells over a 2-24 hour time course. Data are means ±SD; experiments were carried out three times in triplicate. Two-way ANOVA with Bonferroni post hoc test was used to statistically analyse means of treated samples to untreated controls (shown on graph) and the differences between time points (b,d) * denotes $p<0.05$ ** denotes $p<0.01$, *** denotes $p<0.001$, **** denotes $p<0.0001$

2.4.5 Analysis of cell cycle progression following exposure to X-ray radiation and [^{131}I]MIBG.

To allow DNA repair to occur, cells are required to arrest within the cell cycle. Repair by homologous recombination has been shown to function only during late S and G2 phases of the cell cycle whilst NHEJ, although occurring mainly in G0 and G1 phase of the cell cycle, is functional in all phases of the cell cycle. It has previously been demonstrated that radiation induced DNA lesions require HR in order to repair efficiently [93], therefore we examined the effect of X-ray irradiation and [^{131}I]MIBG on cell cycle progression to determine if SK-N-BE(2c), UVW/NAT and A375 cells arrest in G2/M phase of the cell cycle.

2.4.5.1 Analysis of cell cycle progression following exposure to X-ray radiation in SK-N-BE(2c), UVW/NAT and A375 cells

Exposure of SK-N-BE(2c) cells to 2Gy and 4Gy of radiation resulted in a time dependent accumulation of cells in the G2/M phase of the cell cycle. Accumulation was evident 6 hours post irradiation in both 2Gy (52%±0.9, $p<0.0001$) and 4Gy (39.2%±1.1, $p<0.001$) irradiated samples compared to untreated control samples (21%±1.3). In 4Gy irradiated samples the percentage of cells in the G2/M phase of the cell cycle increased further from 6 hours to 24 hours with SK-N-BE(2c) cells demonstrating a 54%±1.1 ($p<0.01$) increase. The increase in the G2/M population of SK-N-BE(2c) cells was accompanied by a significant decrease in the proportion of cells in G1 and S phases of the cell cycle demonstrating that irradiated cells were unable to progress beyond G2 into the mitotic phase of the cell cycle (Figure 2.9a).

As was seen with SK-N-BE(2c) cells, UVW/NAT cells exhibited a time dependent accumulation of cells in the G2/M phase of the cell cycle from 2 to 24 hours post irradiation (Figure 2.9b). The accumulation of cells in G2/M phase 24 hours post exposure were 46.8%±7.1 and 58.65±5.6 in 2Gy and 4Gy samples respectively compared to untreated control samples (30.8%±0.3 and 30.5%±1.6 respectively)

($p<0.001$). The increase in the G2/M population of UVW/NAT cells at 24 hours was accompanied by a significant decrease in the proportion of cells in G1 and S phases of the cell cycle indicating that irradiated cells were unable to progress beyond G2 into the mitotic phase of the cell cycle (Figure 2.9b).

Similarly to SK-N-BE(2c) and UVW/NAT cells, A375 cells exhibited a time dependent accumulation of cells in the G2/M phase of the cell cycle (Figure 2.9c). The accumulation of cells in G2/M phase 24 hours post irradiation was 35.9%±8 in 2Gy treated samples ($p<0.001$) and 55.3%±5.6 in 4Gy irradiated samples ($p<0.0001$) compared to 24.9%±1.5 and 27.6%±5.7 respectively in untreated controls. The increase in the G2/M population of A375 cells exposed to 2Gy and 4Gy is accompanied by a significant decrease in the proportion of cells in G1 and S phases of the cell cycle indicating that irradiated cells were unable to progress beyond G2 into the mitotic phase of the cell cycle (Figure 2.9c).

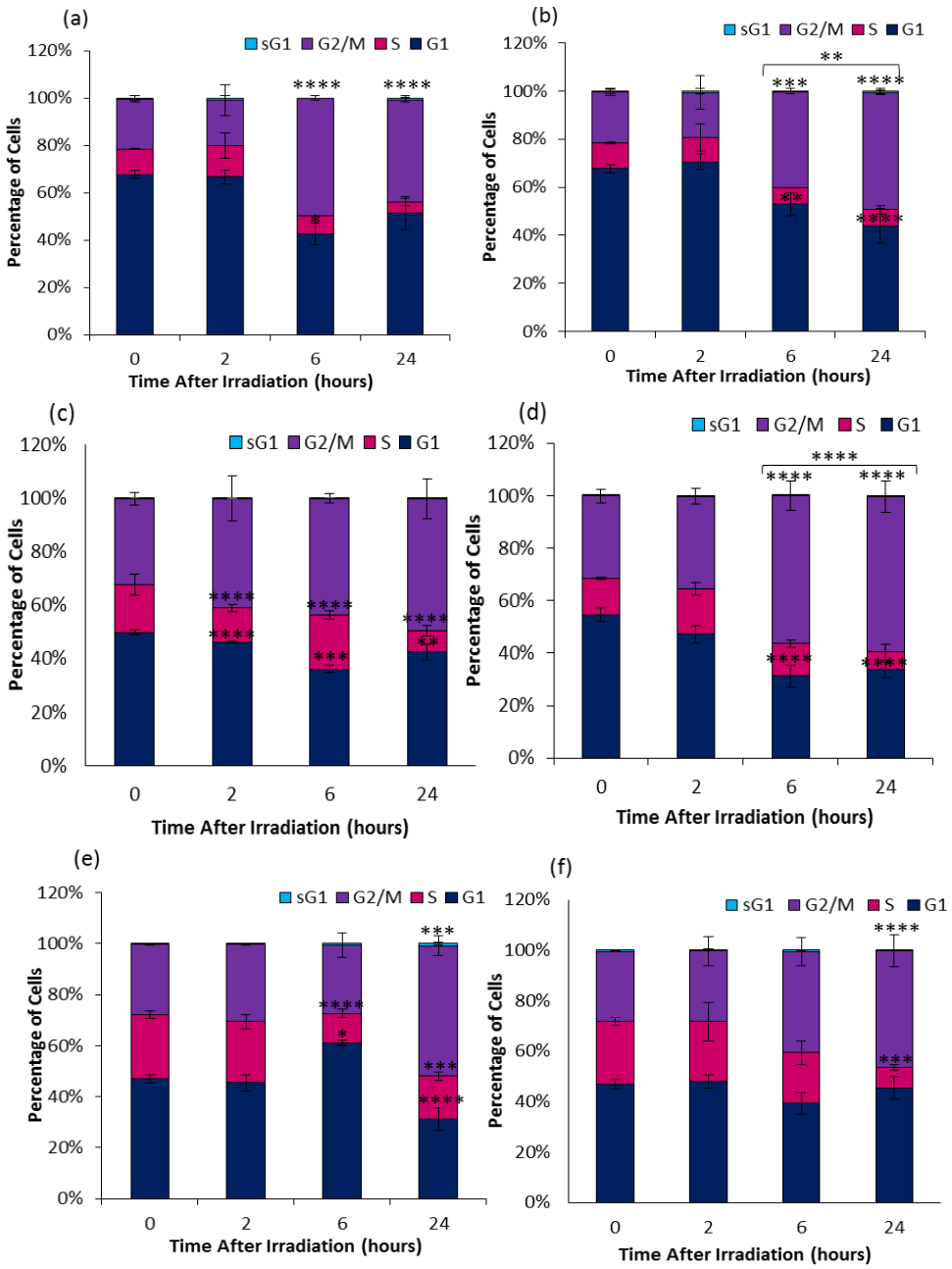

Figure 2.9 Cell cycle progression in (a and b) SK-N-BE(2c), (c and d) UVW/NAT and (e and f) A375 cells following exposure to X-ray radiation.

The effects of X-ray radiation (2Gy (a, c, e) and 4Gy (b, d, f)) were assessed in SK-N-BE(2c), UVW/NAT and A375 cells 2-24 hours post-irradiation. The data were analysed using FACSDiva software v6.1.3. Data are means ±SD of three independent experiments. Two-way ANOVA was used to compare the means of the sG1, G2/M, S and G1 fractions of X-irradiated cells to untreated control cells. * denotes $p<0.05$, ** denotes $p<0.01$, ***denotes $p<0.001$ **** denotes $p<0.0001$.

2.4.5.2 Analysis of cell cycle progression following treatment with [131I]MIBG in SK-N-BE(2c) and UVW/NAT

The percentage of cells in subG1, G1, S and G2/M phases of the cell cycle 2, 6 and 24 hours following incubation with [^{131}I]MIBG is shown in Figure 2.10. Treatment of SK-N-BE(2c) and UVW/NAT cells to [^{131}I]MIBG resulted in a time dependent accumulation of cells in the G2/M phase of the cell cycle (Figure 2.10a). In UVW/NAT cells significant accumulation of cells in the G2/M phase was evident 6 hours post [^{131}I]MIBG removal compared to untreated control cells ($p<0.01$) (Figure 2.10b). 24 hours post initial [^{131}I]MIBG treatment, the percentage of cells in the G2/M phase was 59.8%±5.8 compared to 38.9%±2 in UVW/NAT untreated control cells (Figure 2.10b). In SK-N-BE(2c) cells the percentage of cells in the G2/M phase was 54.4%±1.9 compared to 32.9%±7 in untreated control cells ($p<0.01$) (Figure 2.10b). The increase in the G2/M population of cells exposed to [^{131}I]MIBG was accompanied by a decrease in the proportion of cells in G1 and S phases of the cell cycle (Figure 2.10). This demonstrates that [^{131}I]MIBG treated cells were unable to progress beyond G2 into the mitotic phase of the cell cycle.

These data suggest that in all examined cell lines induction of DNA damage by exposure to both radiation sources resulted in G2/M arrest, and that this arrest was time dependent occurring 24 hours after initial exposure.

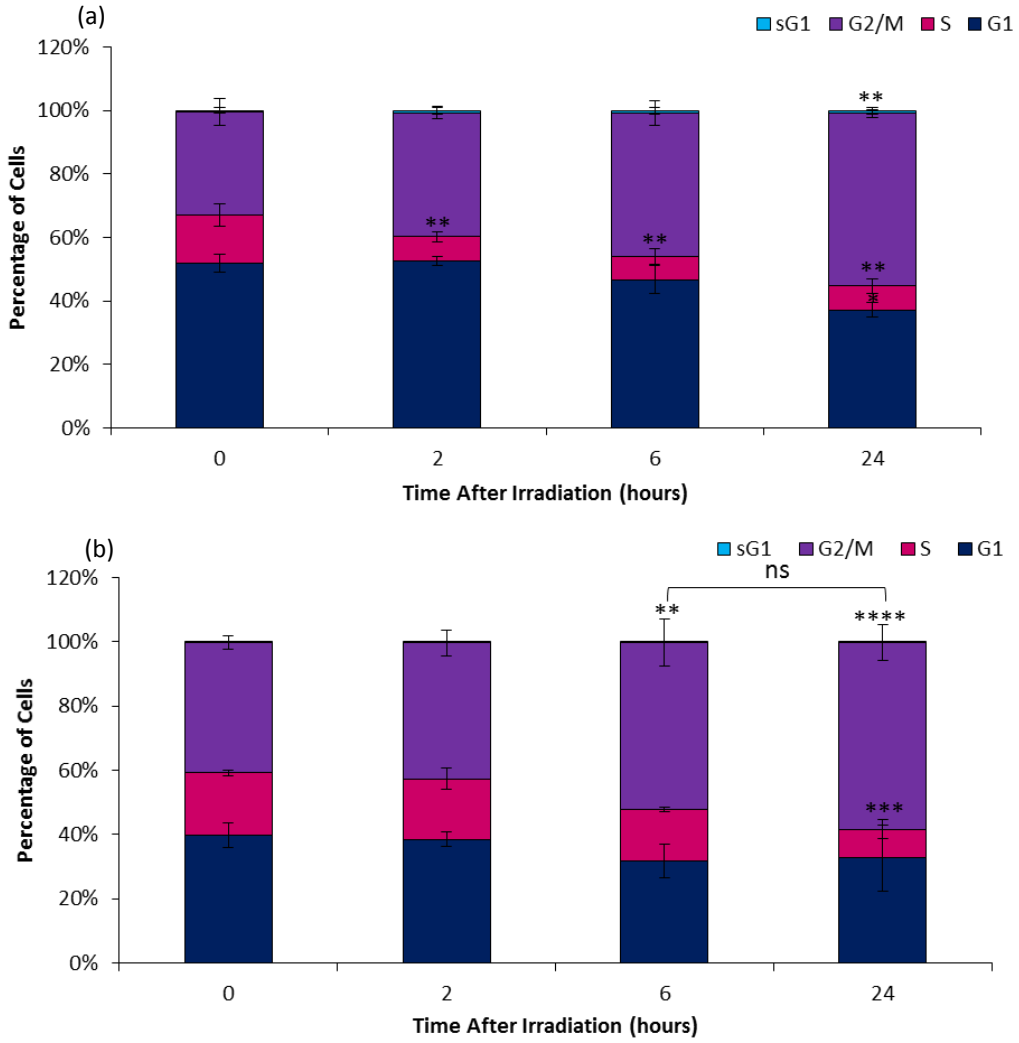

Figure 2.10 Cell cycle progression in (a) SK-N-BE(2c) and (b) UVW/NAT cells following treatment with [^{131}I]MIBG.

The effects of [^{131}I]MIBG were assessed in (a) SK-N-BE(2c) and (b) UVW/NAT cells 2-24 hours post [^{131}I]MIBG treatment. The data were analysed using BD FACSDiva software v6.1.3. Data are means ±SD of three independent experiments. Two-way ANOVA was used to compare the means of the sG1, G2/M, S and G1 fractions of combination treated cells to [^{131}I]MIBG treated controls * denotes $p<0.05$, ** denotes $p<0.01$, ***denotes $p<0.001$ **** denotes $p<0.0001$.

2.4.6 Characterisation of PARP-1 activity levels following X-ray radiation and [^{131}I]MIBG treatment.

PARP-1 is a key enzyme for BER and radiation-induced SSBs are primarily repaired by BER. However, PARP-1 has also been shown to contribute to HR through its interaction with DSB repair components including MRE11, NBS1 and ATM [79] and in the phosphorylation of downstream signalling molecules including p53 and H2AX [79]. To determine the importance of PARP-1 in repair of radiation induced DNA damage, the activation profile of PARP-1 following X-irradiation and [^{131}I]MIBG treatment was assessed.

2.4.6.1 Characterisation of PARP-1 activity levels following X-ray radiation exposure.

The effect of X-ray irradiation on PARP-1 activity in SK-N-BE(2c), UVW/NAT and A375 cells is shown in Figure 2.11. A dose dependent increase in PARP-1 activity occurred 2 hours and 6 hours after exposure to X-ray radiation in all three cell lines over the dose range (2-6Gy). SK-N-BE(2c) cells exhibited 33%±0.1, 50%±0.1 and 58%±0.2 increases at 2, 4 and 6Gy respectively 2 hours post exposure, UVW/NAT cells displayed 83%±0.5, 86%±0.9 and 93%±0.03 increases after 2 hours and A375 cells exhibited 23%±0.1, 33%±0.1 and 56%±0.3 increases in PARP-1 activity after 2 hours. Despite levels of PARP-1 remaining significantly elevated 6 hours post exposure, they decline relative to 2 hours samples with SK-N-BE(2c) cells showing 20%±0.2, 27%±0.2 and 28%±0.2 reductions in PARP-1 levels between 2 and 6 hours. UVW/NAT cells on the other hand show further increases in PARP-1 levels at 2Gy and 4Gy with a reduction only observed between 2 and 6 hours at 6Gy (14%±0.4). A375 cells exhibit 25%±0.006, 12%±0.01 and 16%±0.1 increases in PARP-1 between 2 and 6 hours at 2, 4 and 6Gy respectively. PARP-1 levels return to basal levels 24 hours after exposure with no significant elevations found when compared to untreated controls (except at the highest radiation dose (6Gy) in SK-N-BE(2c) cells. This may suggest that PARP-dependent radiation induced SSB repair was initiated rapidly in cells following X-ray radiation exposure and resolved within 24 hours.

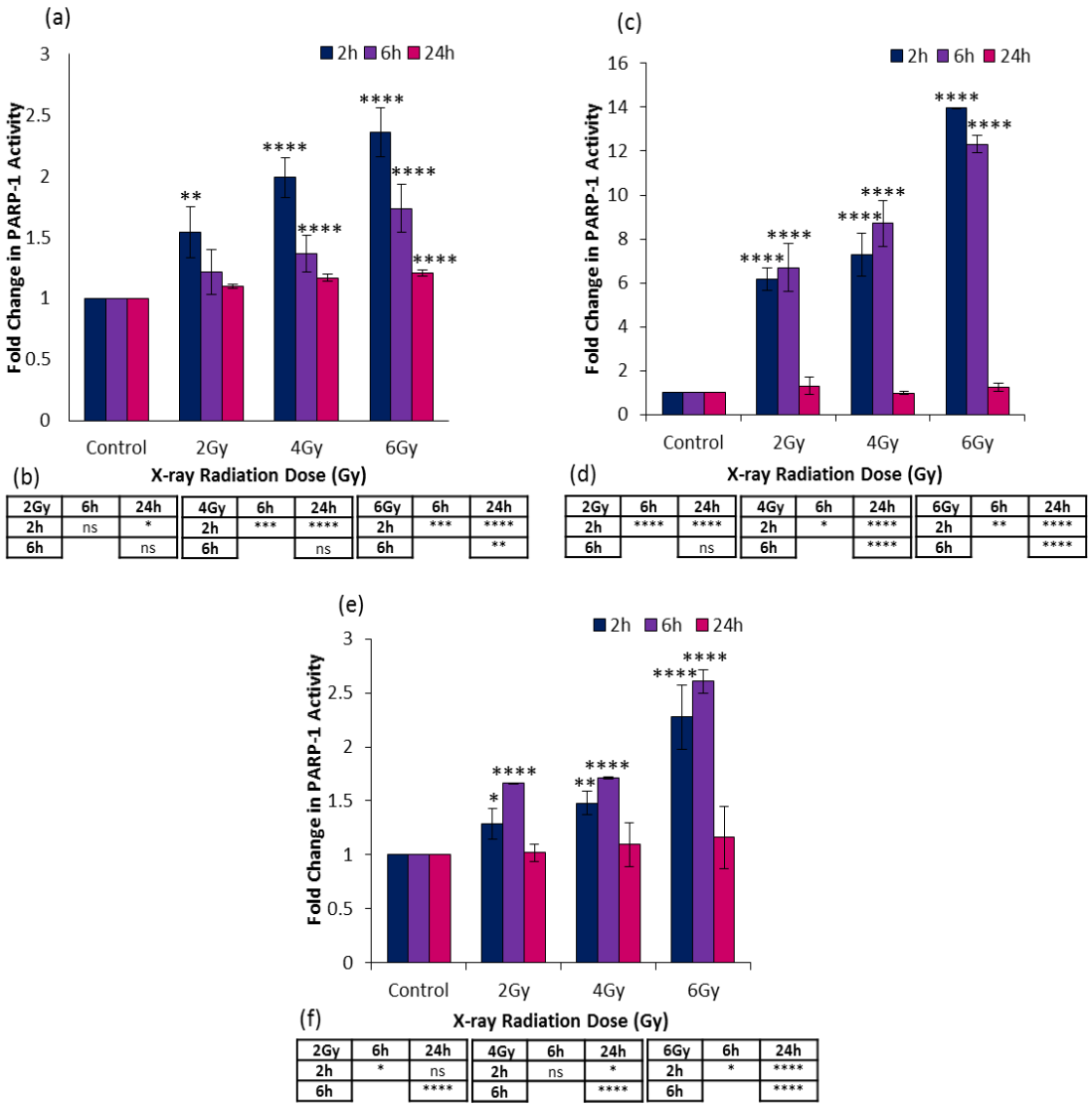

Figure 2.11 PARP-1 activity following exposure to X-ray radiation in (a) SK-N-BE(2c) (c) UVW/NAT (e) A375 cells.

Fold change in PARP-1 activity following exposure to X-ray radiation was assessed in (a) SK-N-BE(2c) (c) UVW/NAT and (e) A375 cells over a 2-24 hour time course. Data are means ±SD; experiments were carried out three times in triplicate. Two-way ANOVA with Bonferroni post hoc test was used to statistically analyse means of treated samples to untreated controls (shown on graph) and the differences between time points (b,d,f) * denotes p<0.05 ** denotes p<0.01, *** denotes p<0.001, **** denotes p<0.0001

2.4.6.2 Characterisation of PARP-1 activity levels following [^{131}I]MIBG treatment.

The effect of [^{131}I]MIBG administration on PARP-1 activity in SK-N-BE(2c) and UVW/NAT cells is shown in Figure 2.12. In contrast to X-ray radiation, PARP-1 activity was not significantly upregulated in SK-N-BE(2c) cells until 24 hours post initial treatment except for treatment of cells with 6MBq [^{131}I]MIBG where a 41%±0.2 increase in PARP-1 activity occurred 6 hours post initial treatment. 24 hours after incubation with [^{131}I]MIBG, SK-N-BE(2c) cells exhibited 33%±0.2, 47%±0.16 and 56%±0.19 increases in PARP-1 activity after administration with 1, 2 and 6MBq respectively. In contrast, UVW/NAT cells exhibited significant elevations in PARP-1 activity at only 2 and 6MBq 2, 6 and 24 hours post treatment, with 57%±0.1 and 76%±0.01 increases recorded 24 hours after initial treatment.

These data suggest that in both cell lines (but particularly in SK-N-BE(2c) cells), DNA damage is accrued over a long time course following treatment with [^{131}I]MIBG compared to X-ray irradiation. Alternatively, it is possible that PARP-1 was not recruited as an initial repair protein following early stage DNA damage with this radiation source.

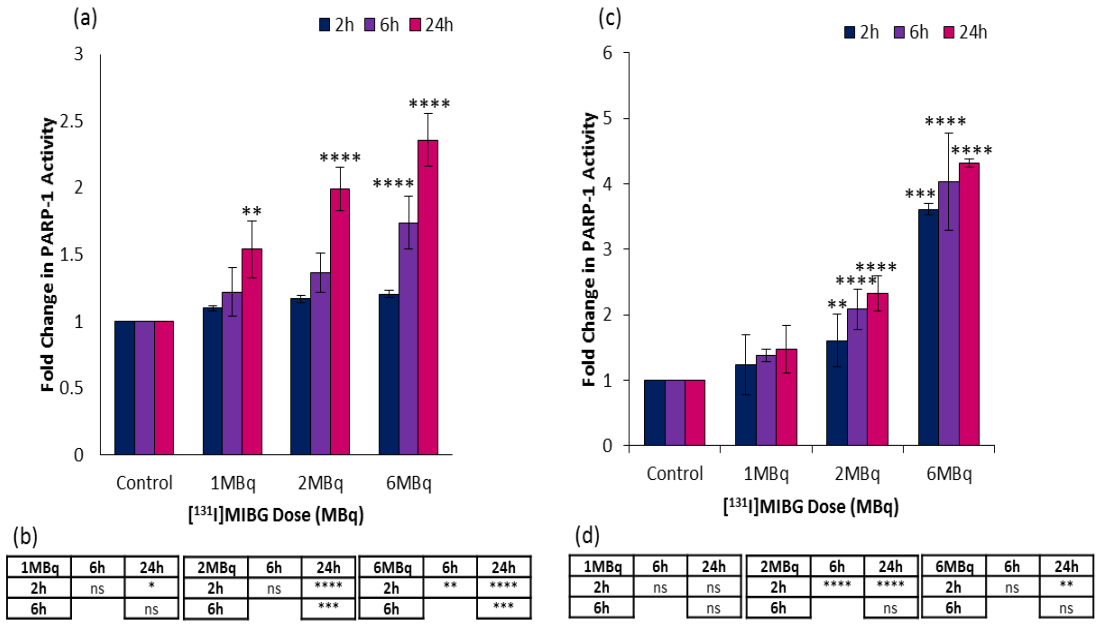

(b)

1MBq	6h	24h	2MBq	6h	24h	6MBq	6h	24h
2h	ns	*	2h	ns	****	2h	**	****
6h		ns	6h		***	6h		***

(d)

1MBq	6h	24h	2MBq	6h	24h	6MBq	6h	24h
2h	ns	ns	2h	****	****	2h	ns	**
6h		ns	6h		ns	6h		ns

Figure 2.12 PARP-1 activity following treatment with [^{131}I]MIBG in (a) SK-N-BE(2c) and (b) UVW/NAT cells.

Fold change in PARP-1 activity following treatment with [^{131}I]MIBG was assessed in (a) SK-N-BE(2c) and (b) UVW/NAT cells over a 2-24 hour time course. Data are means ±SD; experiments were carried out three times in triplicate. Two-way ANOVA with Bonferroni post hoc test was used to statistically analyse means of treated samples to untreated controls (shown on graph) and the differences between time points (b,d) * denotes $p<0.05$ ** denotes $p<0.01$, *** denotes $p<0.001$, **** denotes $p<0.0001$

2.5 Discussion

The aim of this chapter was to characterise the DDR pathway following treatment of cells with two radiation types, X-ray radiation and a radiopharmaceutical in the form of [^{131}I]MIBG. [^{131}I]MIBG is a radiopharmaceutical comprising the conjugation of the isotope ^{131}I to the noradrenaline analogue MIBG. ^{131}I is an isotope used in β-emitting forms of targeted radionuclide therapy that is internalised by cells expressing the noradrenaline transporter [36]. X-ray radiation induces instantaneous damage to the cell's DNA, for example in the present study 2Gy of X-ray radiation is administered at a high dose rate in 52 seconds. Whereas [^{131}I]MIBG is a low dose rate, low LET form of radiation with an 8 day half-life that following internalisation by cells emits damaging effects over an extended duration. For example, in the present study cells were treated with [^{131}I]MIBG for 2 hours before excess was washed off leaving only [^{131}I]MIBG retained within the cells to elicit damaging effects over a 24 hour time period. Both radiation types generate damage by direct traversal of the cell and the generation of ROS from the radiolysis of water molecules in the cell [94]. ROS once generated elicit damaging effects on cell biomolecules, in particular the DNA resulting in chemical and structural alterations. ^{131}I can also generate additional damage to neighbouring cells which may not express the appropriate transporter via radiation cross fire effects.

Therefore, conversely to X-ray radiation in this study which is delivered instantaneously at high dose rate, [^{131}I]MIBG is a continuous low dose rate delivery of radiation. This indicates that DNA damage with X-irradiation follows a pattern of instantaneous DNA damage and subsequent repair, whereas [^{131}I]MIBG is hypothesised to result in simultaneous damage and repair over an extended duration within the cell population [95].

As a result of the difference between the radiation qualities the aims of this study were to determine the cytotoxicity of X-ray radiation and [^{131}I]MIBG as single agents in SK-N-BE(2c), UVW/NAT and A375 cell lines. Additionally the phenotypic data was underpinned with mechanistic insight by undertaking analysis of how altering radiation quality affected the cell cycle and DNA repair pathway components. ATM

kinase, γ-H2AX, RAD51 and PARP-1 are markers of DNA damage therefore this study investigated whether the aforementioned difference in dose rate affects the upregulation and dynamics of the DDR pathway and if these components of the DDR pathway play as important a role in DNA repair following treatment with [^{131}I]MIBG as they have been shown to with X-irradiation [47], [96]. Additionally, due to the previously reported importance of these DDR pathway components in DNA repair following radiation induced damage it was subsequently hypothesised that targeting these components would sensitise cells to both radiation types.

Initial toxicity studies were undertaken in chosen cell lines to determine the levels of cytotoxicity elicited by both types of radiation over a broad dose range. X-ray irradiation induced a dose dependent reduction in survival fraction across the 0-10Gy dose range in all 3 cells lines, with over 90% cell kill achieved at the highest dose tested (10Gy). SK-N-BE(2c) cells appeared to be the most radio-resistant cell line requiring consistently higher doses of radiation compared to UVW/NAT and A375 cells to achieve the same level of cell death. This is a well-documented response with a plethora of studies demonstrating dose dependent reductions in cell survival across various dose ranges and cell lines [74], [97], [98]. Additionally, cell line dependent radiation sensitivity has previously been documented in studies such as that carried out by Banath *et al.,* (2004) which reported differences in radiosensitivity between six cervical cancer cell lines. [^{131}I]MIBG also produced a dose dependent reduction in survival fraction across the 0-6MBq administered dose range with over 80% cell kill achieved at the maximum administered dose of 6MBq. Again, this is a well-documented response with several studies demonstrating dose dependent reductions in cell survival across various dose ranges [16], [36], [37]. These data were utilised to determine a dose range which covers 25% to 75% cell kill for analysis of DDR pathway components.

One of the central co-ordinators of the DDR pathway is ATM. ATM is autophosphorylated and recruited to sites of DNA damage rapidly after initial exposure to radiation leading to the generation of γ-H2AX foci via phosphorylation of the histone H2A protein [99]. This process occurs rapidly after initial DSB generation

and foci levels increase in a linear fashion with DNA damage severity [89], [99]. In the present study upon increasing X-ray irradiation dose (thus increasing DNA damage severity) a dose dependent increase in phosphorylated ATM and γ-H2AX foci levels was observed. Both pATM and γ-H2AX foci levels peaked 2 hours following exposure to X-rays, thus highlighting the rapid induction of this process following damage. Furthermore, pATM and γ-H2AX foci levels were down regulated across later time points as DNA breaks are resolved. This has been previously reported in studies by An *et al.,* (2010) and Rainey *et al*., (2008) who exposed HeLa cells to ionising radiation and subsequently assessed γ-H2AX foci and pATM levels by Western blotting [100], [101]. These studies demonstrated that eliciting DNA damage via ionising radiation resulted in an increase in γ-H2AX foci and pATM levels in a time dependent manner with levels peaking rapidly after initial exposure [100], [101]. In the present study following treatment with [^{131}I]MIBG, DNA damage is evident as early as 2 hours post initial treatment, despite the low dose rate nature of this radiation source. This DNA damage is evidenced by the elevation of pATM and γ-H2AX foci levels, however the elevation in γ-H2AX foci levels demonstrated in response to [^{131}I]MIBG is lower than that produced in response to X-irradiation at the same time point. [^{131}I]MIBG treated samples showed up to 5 fold (2MBq) increases in γ-H2AX, whereas X-irradiated samples (2 and 4Gy) demonstrated 8 to 12 fold increases in γ-H2AX. This is further supported by Collis et al., (2004) who demonstrated that following exposure to low dose rate γ-rays there was significantly less activation of ATM and γ-H2AX foci formation compared to high dose rate γ-rays [95]. 24 hours after initial X-irradiation cells demonstrate resolution of DNA breaks, evidenced by the downregulation of γ-H2AX foci and pATM, however following [^{131}I]MIBG treatment there was a further increase in the number of DNA DSBs per cell. This is likely due to the longer cellular retention of [^{131}I]MIBG which elicits more continual damaging effects upon ^{131}I decay. This suggests that there is continued activation of DNA repair pathways which may be due to simultaneous DNA damage and repair occurring over the time course [102]. This has previously been speculated as a factor in the reduced γ-H2AX foci levels that have been associated with low dose radiotherapy [95].

Activation of RAD51 is a marker of HR DNA repair and following DNA DSB formation, RAD51 is recruited to the nucleus and forms long nucleofilaments that function to tether together the broken ends of DNA [92]. This recruitment is preceded by MRN complex dependent generation of regions of ssDNA at the 3' terminus of the DNA [92]. Therefore in order to determine the effects of different radiation qualities on the downstream signalling cascade, nuclear RAD51 levels following X-ray radiation and [^{131}I]MIBG treatment were assessed. The findings in this study indicate that nuclear RAD51 protein levels increased in a dose dependent manner in cells exposed to X-ray radiation. Furthermore, this elevation was also time dependent, with cells 2 hours post-irradiation showing the greatest elevation in nuclear RAD51 activity and activity decreasing significantly 24 hours after initial exposure. This has been previously reported in a study by Gildemeister *et al.,* (2009), who exposed cells to ionising radiation and subsequently assessed nuclear RAD51 levels by Western blotting [103]. Gildemeister *et al.,* (2009) demonstrated that eliciting DNA damage via ionising radiation resulted in an increase in nuclear RAD51 levels in a time dependent manner with levels peaking approximately 1-2 hours after initial exposure [103]. Again, as with pATM and γ-H2AX levels, in this study, RAD51 protein levels increase in a dose dependent manner when exposed to [^{131}I]MIBG, however this upregulation is much slower than that demonstrated by X-irradiated cells and levels reached their peak 24 hours after initial exposure. Additionally, SK-N-BE(2c) cells were shown to respond to [^{131}I]MIBG much more rapidly than UVW/NAT cells with RAD51 levels not reaching significant levels of elevation in UVW/NAT cells until 24 hours after initial treatment. This again suggests that the low dose rate nature of [^{131}I]MIBG is eliciting more cumulative damaging effects compared to the more instantaneous X-ray radiation effects. Furthermore, the slower upregulation of nuclear RAD51 with [^{131}I]MIBG may indicate that the accrual of DNA DSBs over time (as evidenced by γ-H2AX levels) initiates HR DNA repair processes only when the complexity of damage (possibly in the form of a greater volume of breaks) is increased.

Cell exposure to radiation commonly results in G2/M arrest due to the induction of DNA DSBs [56]. The results presented in this study also demonstrate that G2/M arrest occurs following radiation exposure and that despite utilising differing radiation qualities this effect is most noticeable 24 hours after initial exposure to both X-rays and [^{131}I]MIBG. This is consistent with previous studies, which report that exposure to ionising radiation from external sources resulted in G2/M arrest that is both dose and time dependent [93] and that treatment with [^{131}I]MIBG induces a dose and time dependent G2/M arrest when administered as a single agent [104]. This effect is likely due to the cells being at different stages of the cell cycle when first exposed to radiation and the long doubling time of cells, therefore significant effects on cell cycle progression are not apparent until all cells have undergone one full cycle.

This chapter also assessed the effects of X-irradiation and targeted radiotherapy on PARP-1 activity. PARP-1 has been resolutely associated with BER and SSB repair, however, it has also been suggested to have a role in an alternative form of NHEJ (alt-NHEJ) through its association with DNA ligase III [78]. The findings in the present study indicate that PARP-1 levels increased in a dose dependent manner in cells exposed to X-ray radiation and this elevation was also time dependent, with SK-N-BE(2c) and UVW/NAT samples analysed after a 2 hour incubation showing the greatest elevation in PARP-1 activity and A375 samples analysed after 6 hour incubation showing the greatest elevation in PARP-1 activity. Again, as with γ-H2AX, ATM kinase and RAD51 protein levels, a dose dependent increase in PARP-1 levels was observed when cells were treated with [^{131}I]MIBG, with levels peaking 24 hours after initial treatment. This again suggests that [^{131}I]MIBG is eliciting its damaging effects continually over a longer time frame compared to X-ray radiation, resulting in longer resolution times.

In addition to this, it was also hypothesised that X-irradiated cells would demonstrate rapid induction of DDR pathway components whereas [^{131}I]MIBG treated samples would exhibit a more gradual upregulation of these markers due to the more gradual accumulation of DNA damage. This study has confirmed that both X-ray radiation and [^{131}I]MIBG treatment result in a dose dependent cell death, and that cellular DDR

pathway components are upregulated for a much more extended duration upon [^{131}I]MIBG treatment compared to X-irradiation. As a consequence of the results obtained in these analyses, further studies have been carried out to investigate the radiosensitising potential of Mirin and Olaparib that both target individual components of the DDR pathway, inhibiting the resulting repair cascades, and are hypothesised to radiosensitise cells to both X-rays and [^{131}I]MIBG.

Chapter 3

The effect the MRE11 inhibitor Mirin on the sensitivity of cancer cells to X-ray radiation *in vitro*.

3.1 Introduction

The cytotoxic effects of ionising radiation are in a large part due to it's potential to generate either, directly or indirectly through ROS generation, DNA base damage leading to SSBs, DSBs and DNA crosslinking [96]. Combining X-ray radiation with an agent that prevents repair of these DNA lesions is therefore hypothesised to enhance the efficacy of X-ray radiation in cancer treatment.

Mirin is a novel compound which is a small molecule inhibitor of MRE11 exonuclease activity [71]. MRE11 is involved in the repair of DNA lesions through its exonuclease activity and co-localisation with NBS1 and RAD50 as part of the MRN complex which functions to signal to other damage repair components as discussed in section 1.4. Thus, MRE11 will be involved in the repair of radiation induced DNA lesions generated by X-irradiation [105]. As demonstrated in Chapter 2, exposure to X-ray radiation results in the rapid upregulation of several components of the DDR pathway. It was therefore hypothesised that Mirin will have radiosensitising properties when used in combination with X-ray radiation as a result of the abrogation of repair of radiation induced DNA damage. To date, the radiosensitising potential of Mirin on cell survival has not been reported although many studies have shown that MRE11 inhibition abrogates radiation induced upregulation of DNA repair processes [74]. Previous studies have utilised MRE11 siRNA in order to examine whether knockdown of this component of the MRN complex results in enhanced radiosensitivity of cells [74]. These studies have provided encouraging results with adenocarcinoma cells displaying increased sensitivity to X-ray radiation following 24 hour incubation with MRE11 siRNA, whereupon MRE11 protein levels were reduced by 60%.

3.2 Aims

The aims of the present study were to assess the clonogenic cell survival following exposure to Mirin as a single agent in SK-N-BE(2c), UVW/NAT and A375 cell lines, and the radiosensitising effects of Mirin in combination with X-rays in the above cell lines. Interrogation of the effect of Mirin (MRE11 inhibition) and radiation as single agents and in combination on upstream and downstream targets of MRE11 was also undertaken to elucidate the mechanistic basis for the results obtained in the earlier studies.

3.3 Materials and Methods

3.3.1 Cell Lines and Culture conditions

SK-N-BE(2c), UVW/NAT and A375 cells were cultured as described in section 2.3.1

3.3.2 Drug Preparation and Treatment of cells with Mirin and X-ray radiation

Mirin was purchased from Tocris (Bristol, UK). 100mM stock solutions were prepared by dissolving powdered Mirin (MW 220.25) in 100% dimethyl sulfoxide (DMSO) and stored at -80^{o}C. Working solutions of 10mM and 1mM were prepared by diluting the 100mM stock solution 1:10 and 1:100 respectively with 100% DMSO. Working solutions were stored at -20^{o}C.

For single agent treatment studies cell medium was replaced with 5ml of fresh medium prior to exposure in X-ray radiation studies or 1ml of fresh medium containing a range of concentrations of Mirin (0-50µM). For combination treatments cell medium was replaced with 1ml of fresh medium prior to incubation with Mirin for 2 hours before X-ray radiation exposure and further 24 hour incubation. Based on data obtained in Chapter 2, the effect of Mirin on X-ray radiation induced DDR response was assessed 2 and 24 hours post treatment.

3.3.3 Clonogenic Cell Survival Assay

Clonogenic assays were performed in UVW/NAT and A375 cells as described in section 2.3.3 in order to determine whether cultured cells continue to form viable colonies of daughter cells following exposure to Mirin and X-ray radiation as single agents and in combination.

3.3.4 Soft Agar Cell Survival Assay

Soft agar cell survival assays were performed as described in section 2.3.4 on SK-N-BE(2c) cells which fail to form discrete colonies in 2D cultures.

3.3.5 Assessing the efficacy of combination therapies

The linear-quadratic mathematical model used to assess whether the cytotoxicity of combinations of X-ray radiation and the DNA damage repair inhibiting compound Mirin was superior to each treatment type alone.

3.3.5.1 The linear-quadratic model

The linear quadratic model is used to assess the toxicity of radiation on cell survival and is based on the mathematical relationship between two components of cell killing, namely, radiation dose and cell survival [106], [107]. As the name suggests the linear-quadratic model is comprised of a linear component and a quadratic component. The linear component corresponds to the initial slope (α) of the survival curve and is thought to be representative of damage elicited to DNA by a single ionisation event at sub lethal radiation doses [106]. The quadratic component (β) is the latter portion of the curve that represents damage elicited at higher radiation doses and it thought to result from multiple ionisation events. This DNA damage is considered more severe and more complex to repair [106]. The linear quadratic equation can be used to assess the radiation enhancing properties of a radiosensitising compound more effectively. Following treatment with a radiosensitiser in addition to radiation, radiosensitisation would result in a leftward shift in the radiation survival curve. This leftward shift can be quantified and is described as the dose enhancement factor (DEF). DEF is the factor by which radiation dose can be reduced in the presence of a radiosensitising agent but still elicit the same level of cell kill as radiation alone.

3.3.5.2 Assessment of radio sensitisation using The Linear-Quadratic Model

3.3.5.2.1 The linear-quadratic equation

As described above the linear-quadratic model is a mathematical model describing the relationship between radiation dose and clonogenic cell survival.
The equation of the cell survival curve is:

$SF = \exp(-\alpha D - \beta D^2)$ Equation 1

Where SF is the fraction of viable cells following exposure to a dose (D) of radiation. The coefficient α represents the linear phase of the curve and is proportional to D whilst β is representative of the quadratic phase of the curve and is proportional to the square of D. GraphPadPrism version 6.05 was used to fit clonogenic survival data to the linear-quadratic model and to calculate α and β values.

3.3.5.2.2 Calculation of DEF

DEF is the factor by which the radiation dose can be reduced in the presence of a radiosensitising agent whilst still achieving the same level of clonogenic cell kill (x) as radiation alone. DEF is calculated using the equation:

DEF_x = IC_x radiation alone / IC_x of radiation in the presence of a drug Equation 2

The higher the DEF_x value, the smaller the dose of radiation required in combination with the drug in order to produce the same degree of cell kill as radiation alone.

3.3.6 Cell Cycle Analysis

The progression of cells through the cell cycle was investigated as described in section 2.3.5 to assess if Mirin and X-ray radiation alone and in combination caused an abrogation to the normal cycling of cells.

3.3.7 Fast activated cell-based ELISA Assay for pATM

To determine if Mirin inhibited radiation induced upregulation of pATM a fast activated cell-based ELISA assay (FACE) was developed and carried out as described in section 2.3.7.

3.3.8 H2AX Foci Staining

Although X-ray radiation leads to phosphorylation of H2AX which is mediated by all PIKK kinases, ATM, ATR and DNA-PK, ATM kinase is a major physiological mediator of H2AX phosphorylation. To determine if Mirin inhibited radiation induced upregulation of γ-H2AX, γ-H2AX foci staining was carried out as described in section 2.3.6.

3.3.9 RAD51 ELISA

Sandwich ELISAs were used in order to determine nuclear RAD51 levels following exposure to Mirin and X-ray radiation. RAD51 ELISAs were carried out as described in section 2.3.10.

3.3.10 Statistical Analysis

Statistical analysis was carried out using GraphPad Prism version 6.05 (GraphPad Software Inc, San Diego). One-way ANOVA was used to determine statistical significance in single agent dose response cell survival assays. Two-way ANOVA with Bonferroni post-hoc test was used to determine if results of the combination treatment (Mirin and X-ray radiation) were significantly different to that of radiation alone. In both cases p values <0.05 were reported as statistically significant.

3.4 Results

3.4.1 Determination of single agent toxicity

Initially clonogenic assays were performed to determine if there were any toxic effects of Mirin administered as a single agent on each cell line. The data collected in this series of investigations was then used to determine the drug concentrations to be utilised in further combination studies.

3.4.1.1 Clonogenic cell survival following exposure to Mirin

Mirin induced concentration dependent toxicity (1-50μM) in SK-N-BE(2c) cells following a 24 hour incubation (Figure 3.1a). Cell survival ranged from 95%±0.07 at 1μM to 72%±0.007 at 25μM. However at higher administered concentrations of Mirin, a significant reduction in cell survival was observed compared to untreated control cells ($p<0.01$) with cell survival decreasing 1.8 fold from 72%±0.007 to 40%±0.07 (IC_{60}) when the concentration of Mirin was increased from 25μM to 50μM ($p<0.01$). The concentration of Mirin that elicited a 50% decrease in survival fraction (IC_{50}) was 42μM (Figure 3.1a).

UVW/NAT cells exhibited minimal toxicity at low administered concentrations (1μM) of Mirin however toxicity increased with an increasing concentration of Mirin. Following treatment with 25μM (Figure 3.1b) survival fractions decreased from 88%±0.06 at 1μM to 81%±0.1 at 25μM. This decrease was not however statistically significant compared to untreated control cells ($p>0.05$). However, UVW/NAT cells displayed a significant reduction in survival fraction following the doubling of Mirin concentration from 25μM to 50μM, with survival fraction decreasing 1.76 fold from 81%±0.1 to 46%±0.1 ($p<0.01$). The concentration that elicited a 50% decrease in colony survival (IC_{50}) in UVW/NAT cells was 47μM (Figure 3.1b).

A375 cells also exhibited a similar sensitivity profile across the 1-50μM concentration range to both cell lines reported above (Figure 3.1c). Cell survival ranged from 91%±0.09 at 1μM to 75%±0.1 (IC_{25}) at 25μM with a subsequent 3.75 fold reduction in survival to 20%±0.06 (IC_{80}) upon increasing the concentration from 25μM to 50μM ($p<0.001$) compared to untreated control cells. The concentration of Mirin that

elicited a 50% decrease in colony survival (IC_{50}) was 36μM (Figure 3.1c), indicating that A375 cells were more sensitive to MRE11 inhibition.

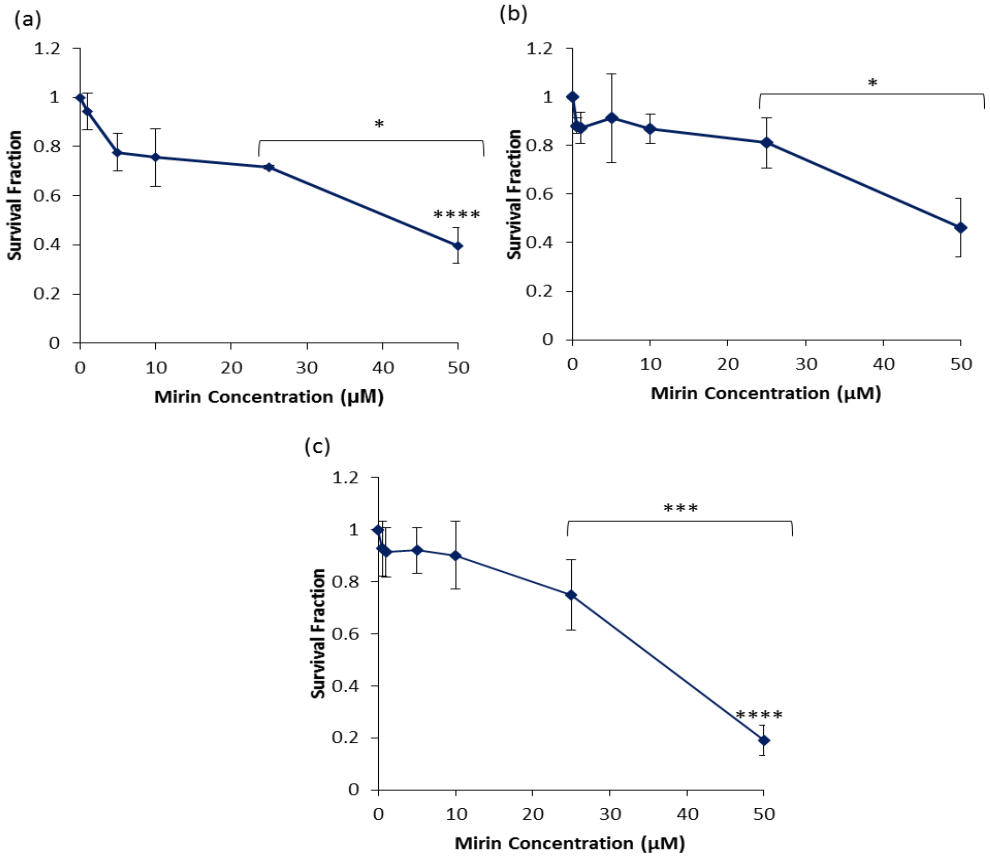

Figure 3.1 The effect of Mirin on clonogenic survival of (a) SK-N-BE(2c) (b) UVW/NAT (c) A375 cells.

The clonogenic capacity of all cell lines was assessed 24 hours after exposure to a range of Mirin concentrations (1-50µM). Data are presented as the mean survival fraction normalised to the survival fraction of untreated control ±SD; experiments were carried out three times in triplicate. One-way ANOVA was used to compare the survival fraction of Mirin treated cells to untreated control cells for all cell lines. * denotes $p<0.05$, *** denotes $p<0.001$, **** denotes

3.4.2 Clonogenic cell survival following exposure to the combination of Mirin and X-ray radiation.

Clonogenic survival assays were performed to determine the radiosensitising potential of Mirin. SK-N-BE(2c), UVW/NAT and A375 cells were incubated for 2 hours with Mirin (5 and 10μM) prior to irradiation with 1Gy, 2Gy or 4Gy of X-rays and incubated over a 24 hour period before plating out for a clonogenic assay. To evaluate if Mirin sensitised cells to X-ray radiation the data were fitted to the linear-quadratic mathematical model as described in section 3.3.5.2 and α, β, IC_{50} and DEF_{50} values determined.

Based on the effect of X-ray radiation on the clonogenic cell kill of each cell line determined in chapter 2, the dose range of 0-4Gy was used for subsequent combination studies as it allowed for decreases in survival fraction beyond that of radiation alone to be identified.

3.4.2.1 The effect of Mirin in combination with X-ray radiation on the clonogenic capacity of SK-N-BE(2c) cells, UVW/NAT and A375 cells.

Exposure of cells to combinations of Mirin and X-ray radiation suggested that Mirin did not sensitise any of the cell lines to radiation at any of the doses investigated (Figure 3.2a, 3.3a and 3.4a). In SK-N-BE(2c) cells the X-ray dose required to kill 50% of the cells (IC_{50} values) increased from 3.77Gy in cells exposed to X-rays alone to 4.28Gy, 4.05Gy in cells treated with X-rays and 5μM or 10μM Mirin respectively (Figure 3.2b). DEF_{50} values decreased for all administered concentrations of Mirin in combination with X-rays, from 1.00 in cells exposed to only X-rays to 0.88 and 0.93 in those exposed to 5μM and 10μM in combination with X-rays respectively (Figure 3.2b). Similarly, in UVW/NAT cells Mirin did not reduce the X-irradiation dose required to kill 50% of the cell population (IC_{50}). IC_{50} values were 3.39Gy, 3.44Gy and 3.33Gy in cells treated with radiation alone or in combination with 5μM or 10μM Mirin respectively (Figure 3.3b). Likewise, DEF_{50} values were unchanged when Mirin

was combined with X-ray radiation, compared to X-ray radiation alone (0.99 and 1.03 following X-rays plus 5μM and 10μM Mirin respectively).

In A375 cells IC_{50} values were 3.18Gy in radiation treated cells and 3.78Gy and 3.44Gy in cells treated with the combinations of radiation with either 5 or 10μM Mirin (Figure 3.4b). DEF_{50} values also remained relatively constant across the concentration range decreasing from 1.00 in X-ray irradiated cells to 0.84 (5μM) and 0.93 (10μM) in combination treated cells (Figure 3.4b).

To determine whether the clonogenic capacity of the cells following X-ray radiation was enhanced by addition of Mirin the data were analysed using Two-way ANOVA with Bonferroni post-hoc analysis. This analysis confirmed that compared to radiation alone combination treatment with Mirin did not significantly enhance the clonogenic capacity of the cells in any of the cell lines investigated as shown in statistics tables (Figure 3.2c, 4c, 5c).

This suggests that the MRE11 inhibitor Mirin did not enhance the sensitivity of SK-N-BE(2c), UVW/NAT or A375 cells to X-ray radiation.

(a)

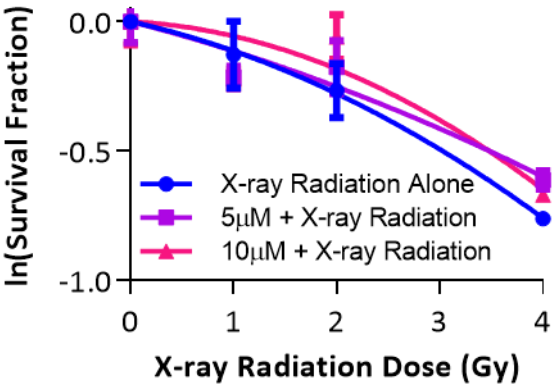

(b)

	Control	5μM	10μM
α	-0.0768	-0.02288	0.1073
β	-0.02834	-0.03251	-0.06864
IC_{50}	3.77	4.28	4.05
DEF_{50}	1.00	0.88	0.93

(c)

	1Gy		2Gy		4Gy
5μM+1Gy	ns	5μM+2Gy	ns	5μM+4Gy	ns
10μM+1Gy	ns	10μM+2Gy	ns	10μM+4Gy	ns

Figure 3.2 Clonogenic capacity of SK-N-BE(2c) cells exposed to Mirin in combination with radiation.

(a) Clonogenic capacity of SK-N-BE(2c) cells was determined 24 hours post exposure to X-ray radiation in the presence or absence of Mirin at a concentration of 5 or 10μM. Cells were incubated with Mirin for 2 hours prior to radiation exposure (1, 2 or 4Gy). (b) The data were fitted to the linear-quadratic equation using GraphPad Prism version 6.05 and α, β, IC_{50} and DEF_{50} calculated for all treatment groups. Data are presented as natural logarithms of the mean survival fraction normalised to untreated control (radiation alone) or drug treated controls (5μM or 10μM Mirin alone) ±SD; experiments were carried out three times in triplicate. (c)Two-way ANOVA with Bonferroni post-hoc test was used to compare the effect of combination treatments to that of cells exposed to radiation alone.

(a)

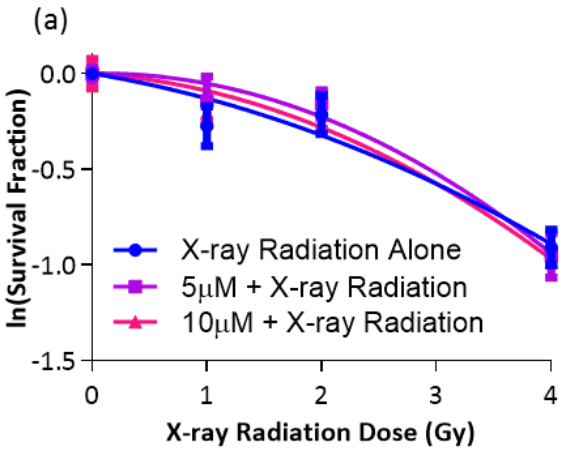

(b)

	Control	5μM	10μM
α	0.1003	-0.0075	0.04025
β	0.03063	0.06069	0.05053
IC_{50}	3.39	3.44	3.33
DEF_{50}	1.00	0.99	1.03

(c)

	1Gy		2Gy		4Gy
5μM+1Gy	ns	5μM+2Gy	ns	5μM+4Gy	ns
10μM+1Gy	ns	10μM+2Gy	ns	10μM+4Gy	ns

Figure 3.3 Clonogenic capacity of UVW/NAT cells exposed to Mirin in combination with radiation.

(a) Clonogenic capacity of UVW/NAT cells was determined 24 hours post exposure to X-ray radiation in the presence or absence of Mirin at a concentration of 5 or 10μM. Cells were incubated with Mirin for 2 hours prior to radiation exposure (1-4Gy). (b) The data were fitted to the linear-quadratic equation using GraphPad Prism version 6.05 and α, β, IC_{50} and DEF_{50} calculated for all treatment groups. Data are presented as natural logarithms of the mean survival fraction normalised to untreated control (radiation alone) or drug treated controls (5μM or 10μM Mirin alone) ±SD; experiments were carried out three times in triplicate. (c)Two-way ANOVA with Bonferroni post-hoc test was used to compare the effect of combination treatments to that of cells exposed to radiation alone.

(a)

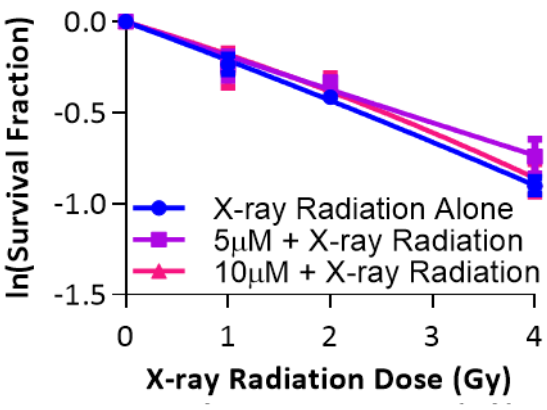

(b)

	Control	5μM	10μM
α	0.2074	0.1891	0.168
β	0.004331	-0.00138	0.01163
IC_{50}	3.18	3.77	3.35
DEF_{50}	1.00	0.83	0.94

(c)

	1Gy		2Gy		4Gy
5μM+1Gy	ns	5μM+2Gy	ns	5μM+4Gy	ns
10μM+1Gy	ns	10μM+2Gy	ns	10μM+4Gy	ns

Figure 3.4 Clonogenic capacity of A375 cells exposed to Mirin in combination with radiation.

(a) Clonogenic capacity of A375 cells was determined 24 hours post exposure to X-ray radiation in the presence or absence of Mirin at a concentration of 5 or 10μM. Cells were incubated with Mirin for 2 hours prior to radiation exposure (1-4Gy). (b) The data were fitted to the linear-quadratic equation using GraphPad Prism version 6.05 and α, β, IC_{50} and DEF_{50} calculated for all treatment groups. Data are presented as natural logarithms of the mean survival fraction normalised to untreated control (radiation alone) or drug treated controls (5μM or 10μM Mirin alone) ±SD; experiments were carried out three times in triplicate. (c)Two-way ANOVA with Bonferroni post-hoc test was used to compare the effect of combination treatments to that of cells exposed to radiation alone.

The results of the clonogenic assays demonstrated that, Mirin did not effectively sensitise SK-N-BE(2c), UVW/NAT and A375 cells to X-ray radiation. This could be due to inefficient targeting of the upstream and downstream targets of MRE11 by Mirin at the concentrations used in this study. As a consequence of these findings we further investigated the effect of Mirin on upstream (H2AX) and downstream (ATM and RAD51) targets in order to elucidate the lack of radiosensitisation that was originally hypothesised based on Mirin's mode of action. As has previously been demonstrated, Mirin efficiently inhibits ATM phosphorylation and MRE11 exonuclease activity [71]. It was therefore hypothesised that this study would also demonstrate inhibition of ATM phosphorylation in combination studies, in addition to reduced γ-H2AX foci formation and RAD51 activity.

3.4.3 Investigation of ATM phosphorylation following Mirin and X-ray radiation exposure

3.4.3.1 The effect of Mirin on radiation induced phosphorylation of ATM in SK-N-BE(2c), UVW/NAT and A375 cells.

The data presented in Figure 3.5 shows the effect of Mirin on radiation induced phosphorylation of ATM, 2 and 24 hours post exposure to 2Gy and 4Gy of X-ray radiation in SK-N-BE(2c), UVW/NAT and A375 cells. Mirin as a single agent at a concentration of 10μM resulted in no significant change in the phosphorylation of ATM either 2 or 24 hours after treatment in all investigated cell lines compared to untreated controls. However, exposure to 2Gy and 4Gy of X-ray radiation resulted in a significant increase in pATM levels in investigated cell lines with SK-N-BE(2c) cells exhibiting 41%±0.01 and 50%±0.04 elevations respectively ($p<0.0001$), UVW/NAT cells showing 44%±0.2 and 50%±0.2 increases respectively ($p<0.0001$) and A375 cells demonstrating the highest degree of elevation of 54%±0.02 and 62%±0.3 respectively ($p<0.0001$) compared to untreated control cells. Combination treated samples demonstrated a significant reduction (data shown in table) in radiation induced phosphorylation of ATM 2 hours post irradiation when compared to 2Gy and 4Gy

alone. In SK-N-BE(2c) cells radiation induced pATM levels were reduced by 48%±0.02 ($p<0.0001$) and 25%±0.01 ($p<0.0001$) in 2Gy and 4Gy exposed samples respectively (Figure 3.5a), UVW/NAT cells exhibited 34%±0.1 and 35%±0.1 reductions respectively (Figure 3.5b) and A375 pATM levels were abrogated by 28%±0.1 ($p<0.01$) and 26%±0.1 ($p<0.0001$) respectively when treated with Mirin (Figure 3.5c). However, this abrogation of pATM phosphorylation is not mirrored in samples incubated for 24 hours after initial combination treatment exposure in any of the investigated cell lines.

In X-ray irradiated samples (2Gy and 4Gy), there was a significant reduction in pATM levels 24 hours after initial exposure compared to 2 hour samples (bridges). SK-N-BE(2c) cells demonstrated 30%±0.01 and 45%±0.05 reductions in pATM levels respectively (Figure 3.5a), UVW/NAT cells were 39%±0.2 and 35%±0.04 ($p<0.0001$) less pATM laden respectively (Figure 3.5b) and A375 cells were 37%±0.1 and 49%±0.1 less pATM laden when compared to 2 hour X-irradiated samples (Figure 3.5c). SK-N-BE(2c) cells exposed to Mirin and 2Gy irradiation in combination, exhibited a significant increase in pATM levels ($p<0.01$) between 2 hour and 24 hour time points, whereas those exposed to the combination of Mirin and 4Gy irradiation showed no significant change in pATM levels. On the other hand, 24 hours after combination treatment exposure, UVW/NAT cells and A375 cells treated with Mirin in combination with 2Gy exhibited a significant decrease in pATM levels compared to the 2 hour samples (23%±0.2, $p<0.05$ and 32%±0.04, $p<0.0001$ respectively). Additionally, A375 cells also demonstrate a significant reduction in pATM levels 24 hours after exposure to combination treatment with 4Gy irradiation when compared to 2 hour samples (45%±0.02, $p<0.0001$).

These results suggest that DNA repair by HR is rapidly initiated following exposure to X-irradiation and that this repair mechanism is down regulated 24 hours after initial exposure. Additionally, results suggest that inhibition of MRE11 by Mirin results in partial abrogation of ATM phosphorylation. From these results it was hypothesised that a partial inhibition of γ-H2AX foci formation would also be observed due to the role ATM plays in H2AX phosphorylation.

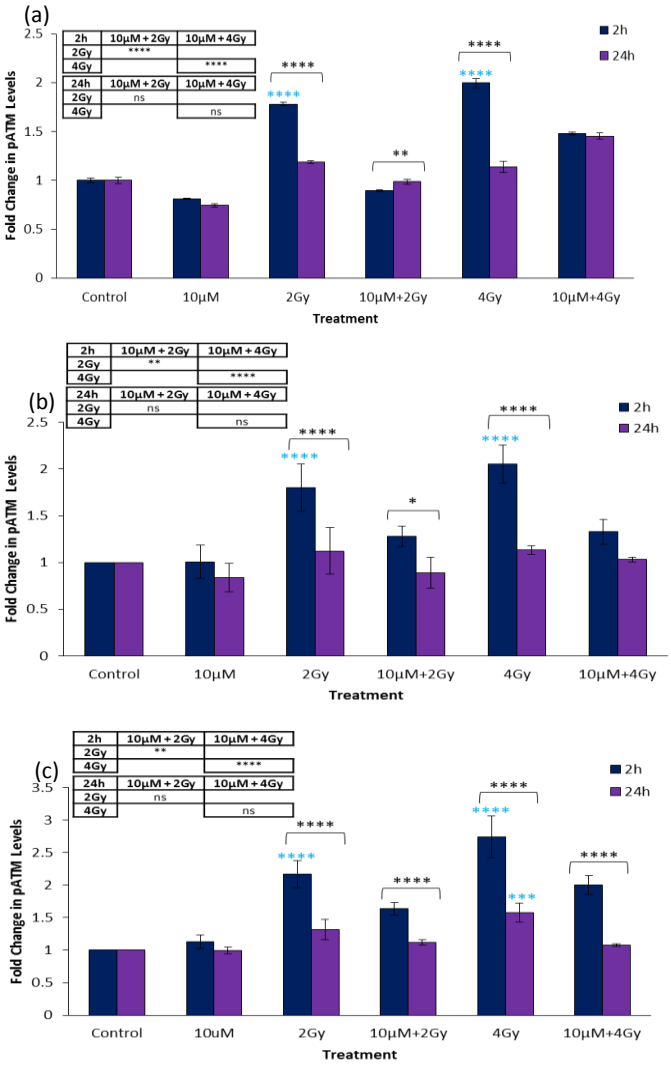

Figure 3.5 The effect of Mirin on radiation induced phosphorylation of ATM in (a) SK-N-BE(2c), (b) UVW/NAT and (c) A375 cells.

Fold change in levels of pATM following combination therapy to X-ray radiation and Mirin compared to untreated control cells was assessed in (a) SK-N-BE(2c) cells, (b) UVW/NAT and (c) A375 cells 2 hours and 24 hours post-irradiation. Cells were incubated with Mirin for 2h prior to irradiation. Data are means ±SD; experiments were carried out three times in triplicate. Two-way ANOVA with Bonferroni post-hoc test was used to compare the means of single agent treated samples to untreated controls (blue stars), the means of 2 hour samples compared to 24 hour samples (bridges) and the means of combination samples to radiation treated samples (table). * denotes $p<0.05$, ** denotes $p<0.01$, *** denotes $p<0.001$, **** denotes $p<0.0001$

3.4.4.1 The effect of Mirin on radiation induced γ-H2AX foci formation and resolution in SK-N-BE(2c), UVW/NAT and A375 cells.

Figure 3.6, 3.7 and 3.8 show the effect of Mirin on radiation induced γ-H2AX foci formation and resolution 2 and 24 hours post exposure to 2 and 4Gy of radiation in SK-N-BE(2c), UVW/NAT and A375 cells. In all three cell lines Mirin as a single agent at a concentration of 10μM had no effect on γ-H2AX foci levels compared to untreated control cells either 2 or 24 hours after treatment with the exception of A375 cells, where Mirin significantly increased γ-H2AX foci levels 2 hours post treatment. Exposure of all three cell lines to 2Gy and 4Gy of irradiation significantly elevated γ-H2AX foci levels compared to un-irradiated cells 2 hours post exposure. In SK-N-BE(2c) cells γ-H2AX foci levels increased by 89%±1.0 following exposure to 2Gy ($P<0.0001$) and 90%±1.0 following exposure to 4Gy ($p<0.001$) of radiation. In UVW/NAT cells γ-H2AX foci levels increased by 88%±1.3 ($p<0.001$) and 90%±0.01 ($p<0.0001$) and in A375 increases of 90%±1.3 ($p<0.001$) and 93%±0.9 ($p<0.001$) was observed 2 hours post exposure to 2 and 4Gy of radiation respectively. The addition of Mirin abrogated the observed radiation induced upregulation of γ-H2AX foci levels 2 hours post irradiation in all cell lines examined. For example, in SK-N-BE(2c) cells (Figure 3.6a) γ-H2AX foci levels were 56%±0.8 ($p<0.0001$) and 55%±0.9 ($p<0.0001$) lower when treated with Mirin compared to 2Gy and 4Gy irradiated samples, respectively. In UVW/NAT cells (Figure 3.7a) γ-H2AX foci levels decreased by 25%±0.3 and 30%±1.2 and in A375 cells (Figure 3.8a) levels were reduced by 25%±0.8 ($p<0.05$) and 36%±0.6 ($p<0.0001$) in combination treated samples compared to 2 and 4Gy irradiated samples, respectively.

These data indicate that the Mirin induced down regulation of pATM 2 hours post irradiation has a subsequent effect on ATM phosphorylation of H2AX.

In irradiated samples 24 hours after exposure, γ-H2AX foci levels decreased compared to 2 hours post exposure. In SK-N-BE(2c) cells levels decreased by 70%±0.2 ($p<0.0001$) and 69%±0.3 ($p<0.0001$) in 2Gy and 4Gy irradiated samples. In UVW/NAT cells levels decreased by 78%±0.2 ($p<0.0001$) and 72%±0.2 ($p<0.0001$) and in A375 γ-H2AX foci levels decreased by 80%±0.4 ($p<0.0001$) and 86%±0.2 ($p<0.0001$) 24 hours

post exposure to 2 and 4Gy of radiation, respectively. In SK-N-BE cells following 2 and 4Gy of exposure and in UVW/NAT cells only at 4Gy of exposure, γ-H2AX foci levels remained significantly elevated compared to unirradiated cells, suggesting that not all radiation induced DNA double stranded breaks had been resolved. In A375 cells however, γ-H2AX foci levels were similar to un-irradiated cells. At this time point, the addition of Mirin to cells irradiated with either 2 or 4Gy led to no change in the absolute levels of γ-H2AX foci compared to irradiated samples alone.

Taken together these results suggest that DNA repair mechanisms are rapidly initiated following X-irradiation and subsequently down regulated as the DNA double stranded breaks are resolved. Additionally results suggest that repair mechanisms are partially abrogated via MRE11 inhibition. As a result of the incomplete inhibition of γ-H2AX foci it was also hypothesised that levels of nuclear RAD51 would demonstrate a similar activation pattern in response to X-irradiation and MRE11 inhibition. RAD51 and γ-H2AX co-localise after induction of DNA damage with γ-H2AX being the driving factor in nuclear RAD51 focus formation.

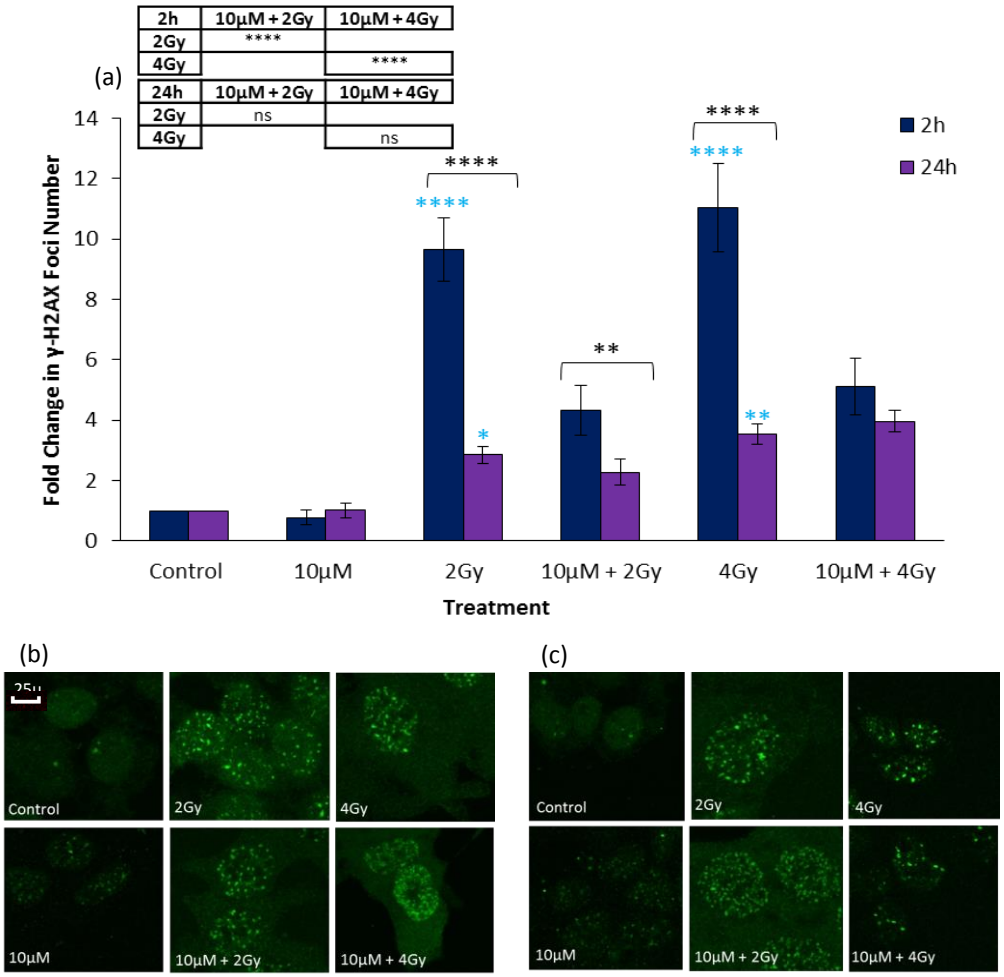

Figure 3.6 The effect of Mirin on radiation induced γ-H2AX foci formation and resolution in SK-N-BE(2c) cells.

(a) Formation and resolution of γ-H2AX foci following exposure to Mirin and X-ray radiation alone and in combination were assessed in SK-N-BE(2c) cells (b) 2 and (c) 24 hours following radiation exposure to 2 and 4Gy of radiation. The data was analysed using Volocity 3D Image Analysis Software and representative images from each treatment group is shown in b and c. Data are means ±SD; experiments were carried out three times and a minimum of 50 cells were counted for each treatment in each individual experiment. Two-way ANOVA with Bonferroni post-hoc test was used to compare: the means of single agent treated samples to untreated controls (blue stars), combination treated samples to 2Gy and 4Gy irradiated samples 2 and 24h post irradiation (table) and the effect of time (bridges). * denotes $p<0.05$, ** denotes $p<0.01$, **** denotes $p<0.0001$.

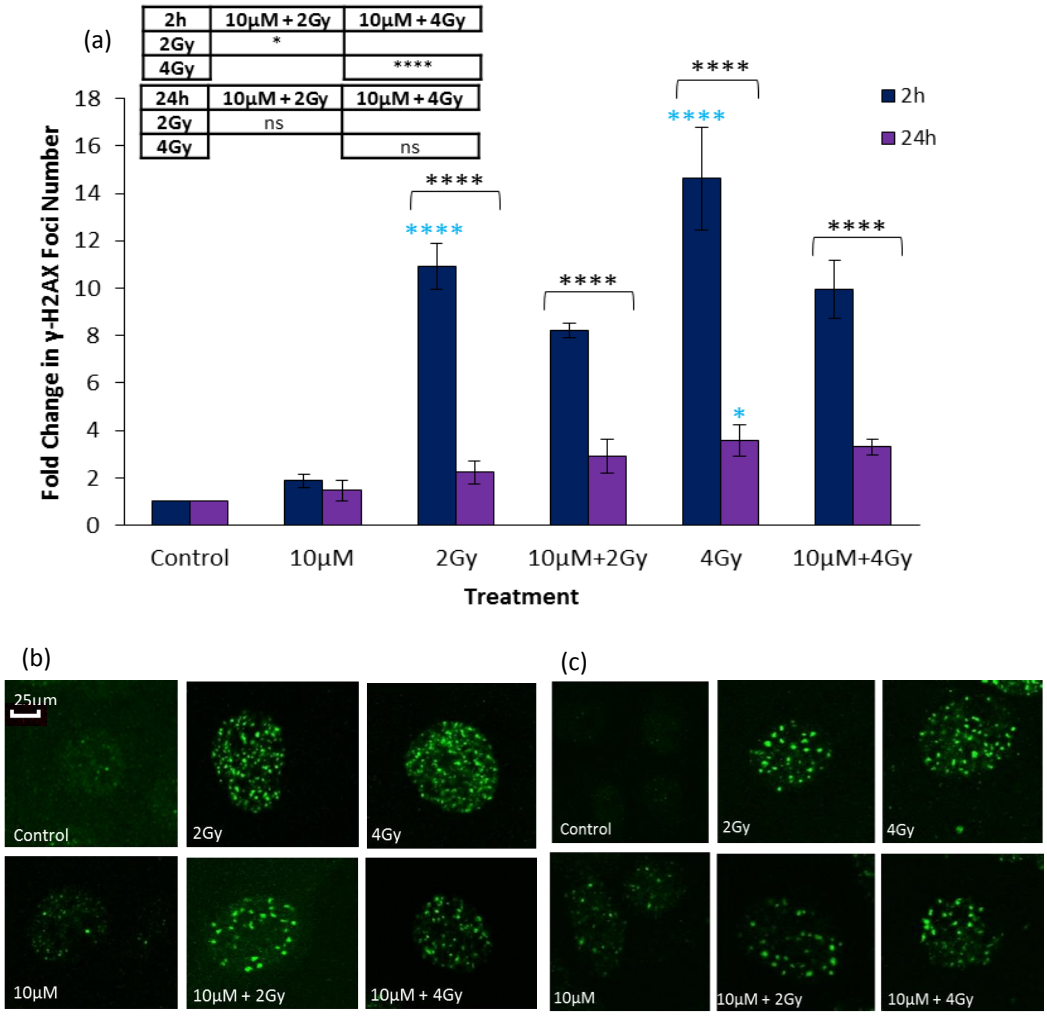

Figure 3.7 The effect of Mirin on radiation induced γ-H2AX foci formation and resolution in UVW/NAT cells.

(a) Formation and resolution of γ-H2AX foci following exposure to Mirin and X-ray radiation alone and in combination were assessed in UVW/NAT cells (b) 2 and (c) 24 hours following radiation exposure to 2 and 4Gy of radiation. The data was analysed using Volocity 3D Image Analysis Software and representative images from each treatment group is shown in b and c. Data are means ±SD; experiments were carried out three times and a minimum of 50 cells were counted for each treatment in each individual experiment. Two-way ANOVA with Bonferroni post-hoc test was used to compare the means of single agent treated samples to untreated controls (blue stars), combination treated samples to 2Gy and 4Gy irradiated samples 2 and 24h post irradiation (table) and means of 2h sample to 24h samples (bridges). * denotes $p<0.05$, **** denotes $p<0.0001$.

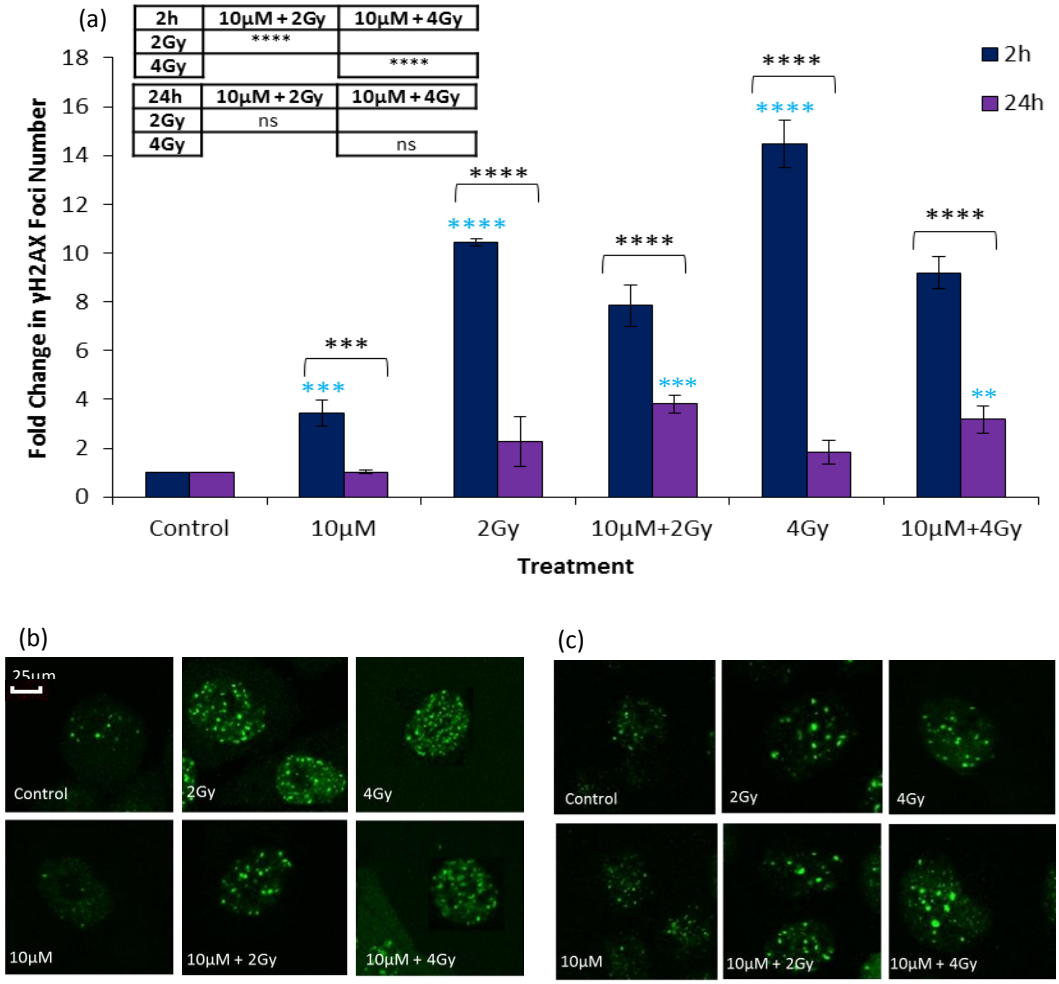

Figure 3.8 The effect of Mirin on radiation induced γ-H2AX foci formation and resolution in A375 cells.

(a) Formation and resolution of γ-H2AX foci following exposure to Mirin and X-ray radiation alone and in combination were assessed in A375 cells (b) 2 and (c) 24 hours following radiation exposure to 2 and 4Gy of radiation. The data was analysed using Volocity 3D Image Analysis Software and representative images from each treatment group is shown in b and c. Data are means ±SD; experiments were carried out three times and a minimum of 50 cells were counted for each treatment in each individual experiment. Two-way ANOVA with Bonferroni post-hoc test was used to compare the means of single agent treated samples to untreated controls (blue stars), combination treated samples to 2Gy and 4Gy irradiated samples 2 and 24h post irradiation (table) and means of 2h sample to 24h samples (bridges). ** denotes $p<0.01$, *** denotes $p<0.001$, **** denotes $p<0.0001$.

3.4.5 Investigation of nuclear RAD51 protein levels following Mirin and X-ray radiation exposure.

3.4.5.1 The effect of Mirin on radiation induced nuclear RAD51 protein levels in SK-N-BE(2c) cells.

Fold change in nuclear RAD51 protein levels in SK-N-BE(2c), UVW/NAT and A375 cells following exposure to combinations of Mirin and X-ray radiation 2 and 24 hours post irradiation is presented in Figure 3.9. In SK-N-BE cells Mirin as a single agent had no significant effect on nuclear RAD51 levels compared to untreated controls at any of the time points investigated (Figure 3.9a). However, UVW/NAT cells exposed to 10µM Mirin exhibited a small increase in RAD51 levels when compared to untreated controls ($p<0.01$) 2 hours, but not 24 hours after initial treatment (Figure 3.9b). A375 cells demonstrated a small but significant reduction in nuclear RAD51 levels compared to untreated controls ($p<0.05$) 2 hours, but not 24 hours after initial Mirin treatment (Figure 3.9c). Following exposure to X-ray radiation (2Gy and 4Gy), a significant elevation in nuclear RAD51 levels were observed in all investigated cell lines compared to untreated controls. SK-N-BE(2c) cells exhibited a 33%±0.1 (2Gy) and 54%±0.09 (4Gy) increase at 2 and 4Gy respectively ($p<0.0001$), UVW/NAT cells exhibited similar degrees of elevation to SK-N-BE(2c) cells (38%±0.01 and 44%±0.04 at 2 and 4Gy respectively ($p<0.0001$), however A375 cells exhibit a smaller degree of elevation at both 2Gy and 4Gy compared to the other two cell lines (26%±0.07 and 27%±0.003 respectively ($p<0.0001$).

Combination treated samples exhibited a significant reduction in RAD51 levels when compared to radiation treated samples in all cell lines investigated. SK-N-BE(2c) cells exposed to Mirin (10µM) and 2Gy displayed a 20%±0.1 ($p<0.05$) reduction in nuclear RAD51 levels when compared to 2Gy irradiated samples, and cells exposed to Mirin (10µM) and 4Gy exhibited a 32%±0.1 ($p<0.001$) decrease in nuclear RAD51 levels compared to 4Gy irradiated samples. Conversely, 24 hours following exposure to Mirin alone or combination treatments nuclear RAD51 levels returned to control levels in all treatment groups (Figure 3.9a). UVW/NAT cells exposed to combinations

of Mirin (10μM) and 2Gy or 4Gy X-irradiation displayed a 19%±0.008 and 23%±0.04 reduction in activity respectively when compared to 2Gy and 4Gy irradiated samples. Conversely, 24 hours following exposure to Mirin alone no significant elevation of RAD51 levels are observed (Figure 3.9b). A375 cells exposed to Mirin (10μM) and 2Gy or 4Gy X-irradiation displayed a 60%±0.01 and 30%±0.04 reduction in activity when compared to 2Gy and 4Gy irradiated samples respectively. Additionally, samples exposed to 10μM Mirin and 2Gy also demonstrated a significant abrogation of RAD51 activity when compared to untreated controls ($p<0.0001$, data not shown) (Figure 3.9c).

Significant reductions in nuclear RAD51 levels were observed between the 2 hour and 24 hour time points in both radiation treated samples and combination treated samples. SK-N-BE(2c) cells demonstrated 38%±0.2 and 56%±0.2 ($p<0.0001$) reductions between the 2 and 24 hour time points in radiation treated samples and 40%±0.001 ($p<0.001$) and 45%±0.02 ($p<0.0001$) decreases respectively between the 2 and 24 hour time points in combination treated samples. In UVW/NAT cells despite 24 hour RAD51 levels remaining elevated following 2Gy and 4Gy irradiation ($p<0.001$ and $p<0.0001$ respectively), nuclear RAD51 levels had declined significantly at 24 hours compared to 2 hour samples (25%±0.08 and 23%±0.07 respectively, $p<0.0001$) (Figure 3.9a). UVW/NAT combination treated samples also displayed a significant reduction in nuclear RAD51 levels between 2 hours and 24 hours (15%±0.02, $p<0.01$ and 22%±0.04, $p<0.0001$ respectively), however cells exposed to Mirin (10μM) and 4Gy showed a further significant reduction in RAD51 levels 24 hours after initial treatment when compared to 4Gy alone irradiated samples ($p<0.0001$) (Figure 3.9b). In A375 cells, RAD51 levels declined significantly 24 hours after initial treatment in both radiation treated cells (23%±0.01 (2Gy) and 14%±0.02 (4Gy), $p<0.0001$) and combination treated cells exposed to 4Gy and 10μM Mirin (17%±0.004, $p<0.0001$) when compared to 2 hour samples. However, A375 cells exposed to 10μM Mirin and 2Gy irradiation for 24 hours exhibit a significant increase in nuclear RAD51 levels compared to 2 hour samples ($p<0.05$) (Figure 3.9c). Despite this, taken together these

results suggest that the DNA repair proteins in all investigated cell lines are down regulated 24 hours after exposure to radiation induced DNA damage.

RAD51 is an important factor in the initiation of DNA repair by HR in G2/M phase of the cell cycle. It was therefore hypothesised that abrogation of RAD51 activity would result in a an accumulation of cells in G2/M phase of the cell cycle due to the inability of cells to repair DNA by HR and thus transition through the cell cycle.

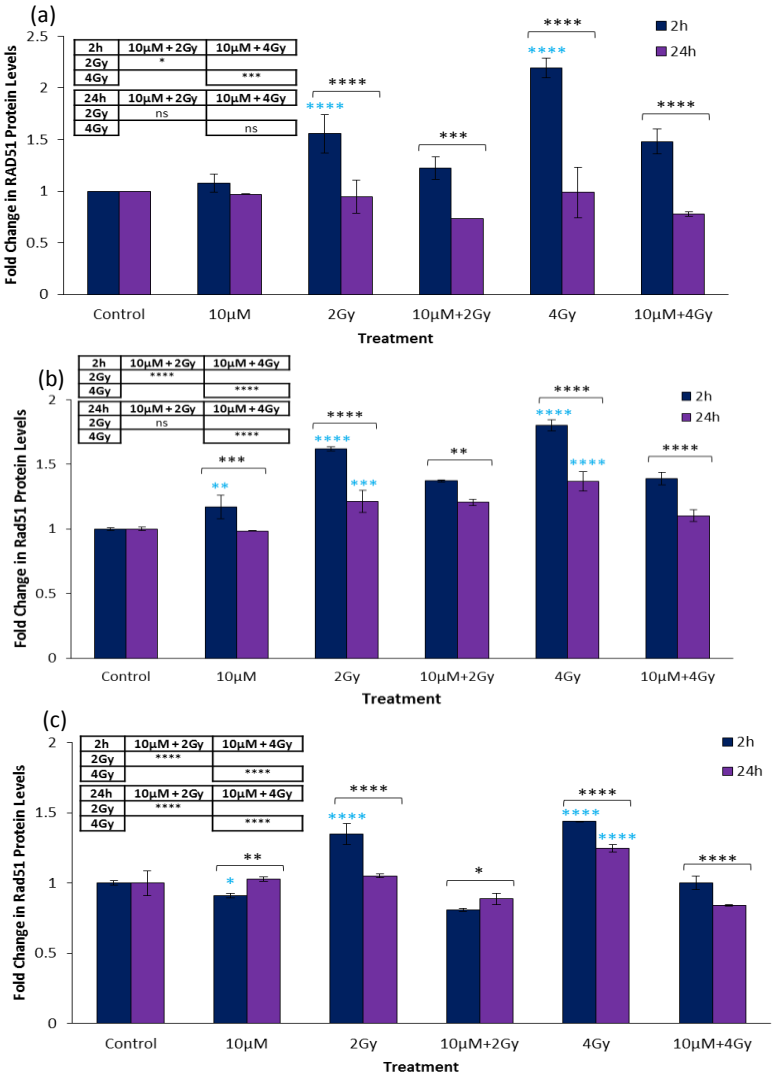

Figure 3.9 The effect of Mirin on radiation induced nuclear RAD51 protein levels in (a) SK-N-BE(2c), (b) UVW/NAT and (c) A375 cells.

Nuclear RAD51 protein levels were assessed following exposure to Mirin and X-ray radiation in (a) SK-N-BE(2c), (b) UVW/NAT and (c) A375 cells 2 and 24 hours post irradiation. Nuclear RAD51 protein levels were determined by ELISA. Data are means ±SD; experiments were carried out three times in duplicate. Two-way ANOVA with Bonferroni post-hoc test was used to compare the means of single agent treated samples to untreated controls (blue stars), combination treated samples to X-ray irradiated samples (bridges) and means of 2h samples to 24h samples (shown in table). * denotes $p<0.05$, ** denotes $p<0.01$, *** denotes $p<0.001$, **** denotes $p<0.0001$.

3.4.6 Analysis of cell cycle progression following exposure to Mirin and X-ray radiation

ATM is a known modulator of G2/M checkpoint activation therefore cell cycle analysis was carried out to determine if disruption of ATM signalling via MRN complex inhibition using Mirin resulted in abrogation of G2/M checkpoint initiation and thus continual cycling of cells.

3.4.6.1 Analysis of cell cycle progression following exposure to combinations of Mirin and X-ray radiation in SK-N-BE(2c) cells

The effect of combined Mirin and X-ray radiation treatment on SK-N-BE(2c), UVW/NAT and A375 cell cycle distribution 24 hours post irradiation is presented in Figure 3.10. Mirin as a single agent has no statistically significant effect on the proportion of cells in each phase of the cell cycle, however exposure to X-rays (2Gy and 4Gy) resulted in a significant accumulation of cells in G2/M phase of the cell cycle (55%±3.0 (2Gy) and 63%±5.0 (4Gy) in SK-N-BE(2c) cells, 46.8%±7.1 and 58.65±5.6 in UVW/NAT cells and 35.9%±8 and 55.3%±5.6 in A375 cells respectively), with a concomitant decrease in cells present in the G1 and S phases of the cell cycle across all investigated cell lines. However, no statistically significant increase in the proportion of cells in G2/M phase of the cell cycle was observed when Mirin (10µM) was combined with 2Gy and 4Gy of X-ray radiation when compared to X-ray radiation alone in any of the assessed cell lines. This suggests that inhibition of MRE11 had no effect on radiation-induced G2/M arrest, which is consistent with the observed reduction in RAD51, indicating reduced capacity for DNA repair by HR and therefore no progression of the cell cycle.

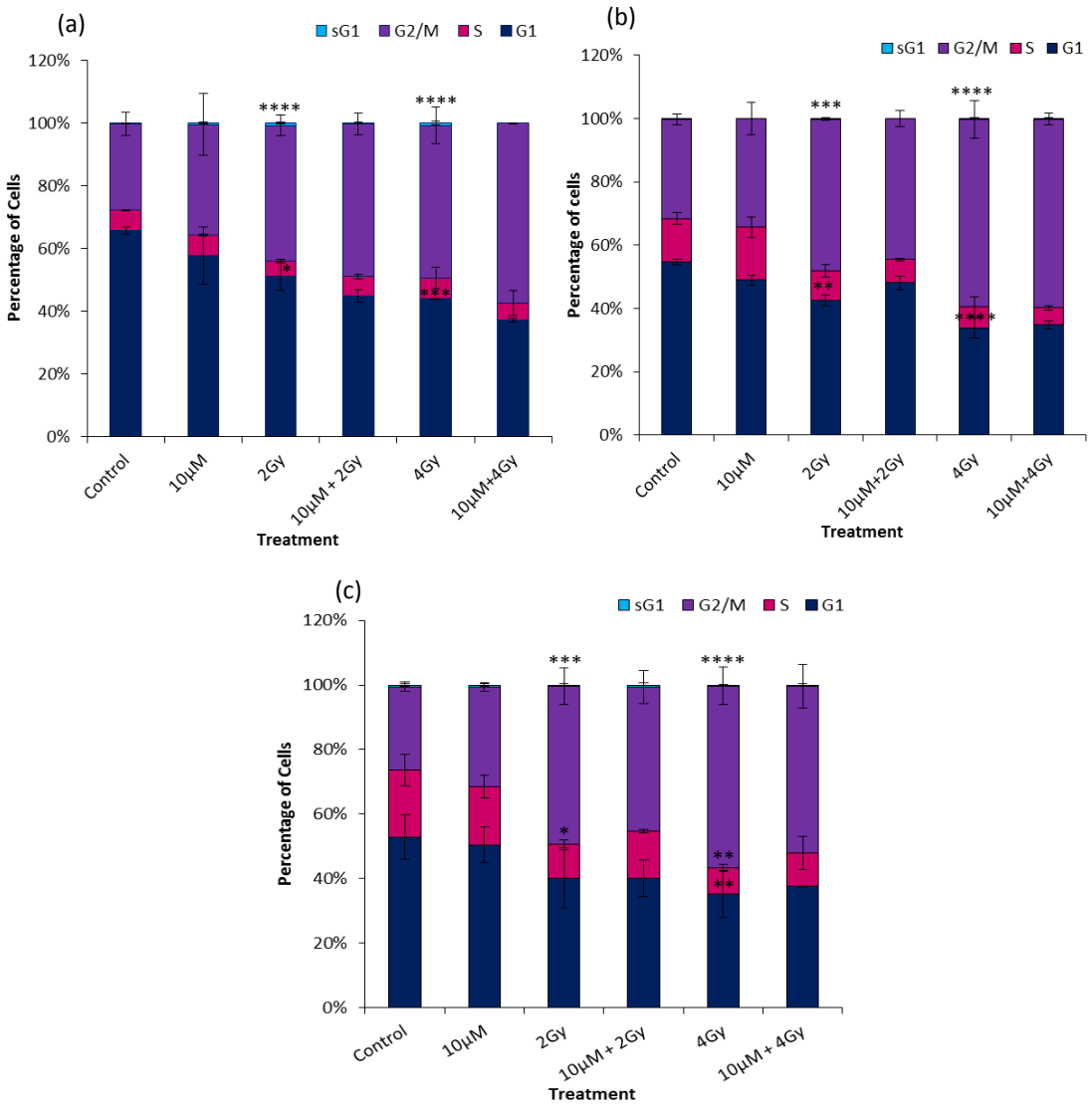

Figure 3.10 Cell cycle progression in (a) SK-N-BE(2c), (b) UVW/NAT and (c) A375 cells following exposure to Mirin and X-ray radiation both as single agents and in combination.

The effects of X-ray radiation and Mirin alone and in combination were assessed in (a) SK-N-BE(2c), (b) UVW/NAT and (c) A375 cells 24 hours post-irradiation. Cells were pre-treated with Mirin (10µM) for 2 hours prior to radiation exposure. The data were analysed using BD FACSDiva software. Data are means ±SD; experiments were carried out three times. Two-way ANOVA was used to compare the means of single agent treated samples to untreated controls (stars) and means of the G2/M fraction of combination treated cells to X-ray radiation treated controls * denotes $p<0.05$, ** denotes $p<0.01$, *** denotes $p<0.001$, ****denotes $p<0.0001$

3.5 Discussion

A well-documented disadvantage associated with X-ray radiation treatment in patients is the high level of toxicity elicited to normal tissues traversed by the radiation beam during therapy. The development of combination therapies which have the potential to specifically sensitise tumour cells enabling cell kill using lower radiation doses, whilst minimising damage to normal tissue, would therefore be of great benefit in cancer treatment schedules. However, due to the dose limiting toxicities to healthy tissues associated with some drug based cancer treatments it is also an advantage to select a drug for use in combination therapies, produces little to no toxicity to cells when used as a single agent, yet provides radio-enhancement (ideally specifically in tumour cells) when combined with radiation. This chapter aimed to determine the cytotoxicity of Mirin as a single agent and in combination with X-ray radiation on SK-N-BE(2c), UVW/NAT and A375 cells. Additionally the phenotypic data was underpinned with mechanistic insight by undertaking analysis of how the combinations affected the cell cycle and DDR pathway components in the MRE11 signalling pathway.

In the present study it was hypothesised that inhibition of MRE11 nuclease activity using Mirin would result in radiosensitisation of cells exposed to X-ray irradiation. As discussed previously in section 1.4.2 inhibition of MRE11 nuclease activity leads to a downregulated ability for the cell to activate DNA repair cascades through, for example, ATM kinase activation. Yuan *et al.,* (2012), demonstrated that over-expression of MRE11 in breast cancer patients resulted in more aggressive tumour behaviour and further suggested that targeting MRE11 would be an effective therapeutic tool in breast cancer therapy [108].

Firstly, toxicity studies were undertaken in all chosen cell lines in order to determine the levels of cytotoxicity elicited by Mirin alone across the concentration range 0-50µM. This was carried out in order to determine the optimal drug concentrations to utilise in further combination studies. The dose dependent Mirin toxicity observed in this study is consistent with previous studies, that demonstrated a similar toxicity pattern across a range of cancer cell lines [71], [109]. Based on the data presented

here and in Chapter 2, and as a result of the aforementioned problems with normal tissue toxicity often encountered in cancer therapy, the subsequent combination studies were undertaken using non-toxic Mirin concentrations (5μM and 10μM) and X-ray irradiation doses of 1Gy, 2Gy and 4Gy. From these combination studies it was demonstrated that contrary to the original hypothesis, where Mirin was expected to sensitise cells to X-irradiation, Mirin did not act as an efficacious radiosensitising agent when combined with X-ray radiation at the drug concentrations and X-ray doses investigated with respect to reducing clonogenic capacity. Currently there are no studies, to which I am aware, that have investigated the effects of Mirin and X-irradiation on cell survival. However, previous studies demonstrate that abrogation of MRE11 activity using siRNA [74] or oncolytic adenoviruses [105] resulted in significant enhancement of radiation cytotoxicity. More specifically, using human adenocarcinoma cells as the target population, Xu *et al.,* (2004), demonstrated that 24 hour incubation of cells with MRE11 siRNA and subsequent exposure to X-ray irradiation at 2Gy and 4Gy, resulted in a significant sensitisation of cells to X-ray radiation [74]. In addition, Rajecki *et al.,* (2009) achieved synergy between ionising radiation and MRE11 inhibition by oncolytic viruses where infection of a host cell with oncolytic adenoviruses results in adenoviral proteins abrogating MRE11 binding to the MRN complex and initiating MRN complex degradation thus preventing DNA DSB repair [105]. The authors demonstrated that infection of prostate (DU145 and PC-3) and lung cancer cells (A549) with the viruses 24 hours after exposure to radiation (4Gy and 15Gy) achieved a statistically significant reduction in tumour volume *in vivo* in both subcutaneous and orthotopic models.

Mirin has previously been shown to inhibit the exonuclease activity of MRE11 [71], however it has been reported that it does not abrogate MRN complex association or DNA binding [71] unlike siRNA to MRE11 and oncolytic adenoviruses. This suggests that disruption of MRN complex association, achieved by both siRNA and oncolytic adenoviruses, may be required in order to sensitise cells to radiation. Additionally different scheduling of Mirin administration may lead to increased efficacy because

as highlighted above, MRE11 inhibition after X-irradiation induced tumour volume reduction.

As was discussed previously, Mirin did not elicit radiosensitising effects in combination with X-irradiation. Therefore to establish whether the lack of sensitisation was as a result of insufficient inhibition of key components of the MRN-ATM signalling pathway by Mirin further investigation of the upstream and downstream substrates of MRE11 following inhibition with Mirin was carried out. These included ATM kinase (which is activated at least in part by MRE11, and is one of the first proteins recruited and activated to the site of DSB), γ-H2AX foci formation (occurs as a result of ATM kinase phosphorylation of the H2A histone protein), and nuclear RAD51 protein (an integral factor of DNA repair by HR) were assessed. The results from these analyses suggested that although exposure to Mirin did not produce any radiation enhancement in terms of reducing the clonogenic capacity of SK-N-BE(2c), UVW/NAT and A375 cells, Mirin treatment significantly abrogated, but did not completely abolish, the activation of upstream and downstream targets of DNA repair pathways derived from MRE11 and the MRN complex. This effect on cell signalling has previously been highlighted in a study by Dupre *et al*., (2008) where Mirin alone at a concentration of 100μM was shown to inhibit MRN dependent ATM kinase activation, however had no effect on MRN-independent ATM kinase activation. Dupre *et al.,* (2008) also demonstrated that Mirin at a concentration of 25μM resulted in depleted cellular capacity for HR, by measuring the presence of the DR-GFP reporter (a marker of DSB induced HR) [71].

One of the primary responses in cells following exposure to DNA damaging agents is the generation of γ-H2AX foci via phosphorylation of the histone H2A protein [99]. Recruitment and phosphorylation of ATM occurs rapidly after radiation induced DNA damage, and it is this process which leads to H2AX phosphorylation. γ-H2AX foci levels increase in a linear fashion with DNA damage severity [89], [99]. As previously shown in section 2.5, upon increasing X-ray irradiation dose, a dose dependent increase in γ-H2AX foci levels was observed in all cell lines used in this study, with γ-H2AX foci levels peaking 1 to 2 hours following exposure to X-rays. Literature suggests

that γ-H2AX foci continue to form in cells deficient in MRE11 [110], however, deficiencies in ATM (using AT cells naturally deficient for ATM) results in a depletion in γ-H2AX foci formation [111]. Mirin has previously been shown to inhibit the MRN dependent activation of ATM kinase with Dupre *et al.,* (2008) reporting an IC_{50} for ATM inhibition of 12μM [71] therefore it was subsequently hypothesised that incubation of cells with Mirin prior to radiation exposure would result in a reduction in the cell capacity to activate ATM kinase and form γ-H2AX foci. In this study it was found that Mirin significantly reduced radiation induced ATM kinase activity in all examined cell lines therefore the present study supports the previous reports that Mirin inhibited the MRN dependent ATM kinase activation. Furthermore, γ-H2AX foci formation has been demonstrated to be partially dependent on ATM kinase and in this study γ-H2AX foci levels in all cell lines examined were reduced by between 25 and 55% across the cell lines 2 hours post initial treatment, however this was not reflected in 24 hour treated samples which show significant resolution of DSBs, evidenced by downregulation of γ-H2AX foci. This supports the hypothesis that inhibition of MRN dependent activation of ATM kinase elicits secondary inhibitory effects on γ-H2AX foci formation. Previous studies carried out using fibroblasts from ATM knockout mice have shown that γ-H2AX foci levels were reduced to almost control levels despite being exposed to X-ray radiation (10Gy) [112]. Furthermore, Cariveau *et al.,* (2007), demonstrated that inhibition of another component of the MRN complex, NBS1 with NBS1 targeting peptides also resulted in complete abrogation of γ-H2AX foci formation in HeLa cells following exposure to X-ray irradiation [113]. However, despite Mirin inhibiting radiation induced γ-H2AX foci formation in this study, residual foci formation was observed, suggesting there is less recognition of radiation induced DSBs, but despite this no effect on cell survival is reported. This could be due to incomplete MRE11 inhibition with Mirin, resulting in incomplete inhibition of MRN dependent ATM kinase activity and therefore residual γ-H2AX foci formation. Additionally, mechanisms such as DNA-PK and ATR also contribute to γ-H2AX foci formation [60]. It has been shown that DNA-PK and ATM operate with functional redundancy [60] therefore it is highly possible that upon

inhibition of ATM kinase activation by Mirin, DNA-PK is able to continue providing adequate levels of H2AX activation to enable cells to repair DNA damage and thus avoid cell death [114]. In future studies this could be tested by assessment of Mirin in DNA-PK knockout cells. Furthermore, as Mirin is only responsible for inhibiting the MRN dependent activation of ATM, it is also possible that ATM autophosphorylation contributes to residual activity. This study is therefore in agreement with previous studies which have shown that inhibition of MRN dependent activation of ATM via MRE11 degradation by adenoviruses or NBS siRNA resulted in impairment of ATM functionality, however did not knock it down entirely [115].

As has been previously discussed (section 1.4), Mirin targets components of the HR DNA repair pathway. RAD51 is an important contributing factor to the HR DNA repair pathway and following DNA DSB formation, RAD51 is recruited and forms long nucleofilaments which function to tether together the broken ends of DNA [92]. This recruitment is preceded by MRN complex dependent generation of regions of ssDNA at the 3' terminus of the DNA [92], therefore in order to determine whether Mirin treatment also targets this downstream signalling cascade RAD51 levels following Mirin and X-ray radiation treatment were assessed.

This study demonstrated that Mirin alone had no significant effect on nuclear RAD51 protein levels however, when used in combination with X-ray irradiation Mirin produced a significant (26-54% increase following 2Gy and 4Gy irradiation) reduction in nuclear RAD51 protein levels 2 hours after initial exposure, compared to X-irradiation alone. These findings suggest that Mirin is acting to abrogate activation of RAD51 following X-ray radiation exposure, although residual RAD51 activity still remains. As suggested before this may be due to incomplete inhibition of MRE11 and therefore incomplete inhibition of the upstream and downstream signalling molecules associated with this pathway including RAD51. It is also possible that RAD51 is activated by other signalling molecules out with the MRN dependent activation of the HR DNA repair cascade. In support of this hypothesis, Cousineau *et al.,* (2005) reported that RAD51 is activated by both BRCA1 and BRCA2 in response to chromosomal damage. BRCA 2 exists as a dimer and binds two RAD51 molecules in

opposing orientations leading to activation and modulation of RAD51 nucleofilament formation as well as cellular localisation [116]. BRCA1 however interacts with the MRN complex, in particular to regulate MRE11 induced ssDNA generation [117]. Since ssDNA acts as a substrate for RAD51, it is therefore possible that incomplete inhibition of radiation induced nuclear RAD51 protein levels by Mirin is due to activation of RAD51 by BRCA1, which would subsequently result in DNA repair activity leading to cell rescue and reduced cell kill.

In early studies interrogating the MRN-ATM pathway, Mirin was hypothesised to elicit abolition of the G2/M checkpoint, via inhibition of ATM kinase activation [118], the outcome of such a G2/M checkpoint inhibition would be the continual cycling of cells and prevention of DNA repair, ultimately leading to the accumulation of damage and ultimate apoptotic cell death. However, previous studies have reported that administration of Mirin at a concentration of 10µM had no significant effect on cell cycle progression [71] and this observation is consistent with the data reported in this study. The combination treatments investigated in this study further substantiated the characterisation studies carried out on Mirin whereby addition of Mirin 2 hours prior to radiation exposure did not elicit the G2/M checkpoint abolishing effect that was initially projected therefore cells proceeded to accumulate in G2/M phase of the cell cycle.

It is hypothesised here that the potential clinical usefulness of Mirin in combination with X-ray irradiation is limited by the continued residual functionality of DNA repair processes in the cell, including ATR dependent signalling and p53 directed DNA repair. Tomimatsu *et al.,* (2009) postulated that ATR kinase can function independently of ATM and MRE11 to phosphorylate and activate modulators of DNA repair including p53 [119]. However, targeting the ATM signalling pathway by other means has already shown potential, such as direct ATM kinase inhibition, which has previously been shown to result in much greater, more complete inhibition of ATM kinase and its substrates including p53 and γ-H2AX [120]. For example, Rainey *et al.,* (2008) demonstrated that transient inhibition of ATM kinase using a small molecule kinase inhibitor in HeLa cells resulted in an increased cellular sensitivity to ionising

radiation and thus a reduced cell survival fraction [101]. Previous studies have also investigated the effects of NBS1 inhibition on radiosensitivity utilising NBS1 inhibitory peptides [113]. For example Cariveau *et al.,* (2007), demonstrated that inhibition of NBS1 with NBS1 inhibitory peptides resulted in a significant reduction in clonogenic cell survival in HeLa cells following exposure to X-ray radiation and a cellular inability to form γ-H2AX foci. These findings therefore provide promising evidence that direct targeting of ATM kinase has the potential to be an effective means of generating radiosensitivity, however, the indirect targeting of this pathway is susceptible to compensatory DNA repair processes.

In this study Mirin, a small molecule inhibitor of MRE11, did not increase radiosensitivity when combined with X-ray irradiation in SK-N-BE(2c), UVW/NAT and A375 cell lines. This was despite Mirin producing inhibitory effects on the DNA repair pathway to which ATM kinase is ultimately the linchpin. It is possible therefore, that as a result residual ATM kinase activity this DNA repair pathway retains sufficient activity to prevent cell death, in addition alternative components of the DDR including DNA-PK and ATR may upregulate to compensate for the partial loss of activity induced by Mirin. Further investigation should be carried out into the development of a more potent MRE11 targeting compound, with the potential to knockdown MRN complex association, in order to produce greater inhibitory effects on the MRN-ATM signalling pathway. The development of co-inhibitory schedules utilising Mirin in combination with drugs which target for example DNA-PK, therefore knocking down the alternative DNA repair pathways that may currently function to compensate for MRE11 abrogation, could also produce more successful radiosensitisation with X-irradiation.

Chapter 4

The effect of MRE11 inhibition using the small molecule inhibitor Mirin on the sensitivity of cancer cells to [^{131}I]MIBG targeted radiation.

4.1 Introduction

As discussed in section 1.1.2, [^{131}I]MIBG is a radiopharmaceutical, which contains a β-emitting radionuclide conjugated to a noradrenaline analogue to enable it to be targeted to tumour cells expressing the NAT [90]. ^{131}I elicits its cytotoxic effects via release of electrons that directly interact with DNA via generation of highly reactive oxidising species in the tumour creating pockets of DNA damage [26]. Combining [^{131}I]MIBG with an agent that exacerbates these DNA lesions through repair prevention is therefore hypothesised to enhance the efficacy of [^{131}I]MIBG in neuroblastoma treatment. As demonstrated in Chapter 3, X-irradiation results in a rapid upregulation of DDR pathway components however this is not translated to enhancement of cell kill. The uptake and retention of [^{131}I]MIBG results in a more continuous DNA damaging effect of low dose rate compared to the high dose rate, short term exposure time of X-ray radiation which produces a more instantaneous damaging effect. This difference may therefore be reflected in the how the cell responds to DNA repair inhibition using Mirin.

Mirin is a novel compound which is reported to be an inhibitor of MRE11 exonuclease activity [71] which in turn modulates MRN complex activity resulting in a reduced capacity to repair DNA lesions by HR and NHEJ. As previously shown in this study, incubation of cells with [^{131}I]MIBG resulted in an increase in the levels of specific proteins (pATM, RAD51 and γ-H2AX) regulated by the MRN complex, it is therefore hypothesised that inhibition of this MRN dependent regulation of protein activity by Mirin will have radiation enhancing properties. Thus far, the use of radiopharmaceuticals in combination with radiosensitisers is not well understood and no investigation of MRE11 inhibitors in combination with targeted radiopharmaceuticals have been reported. However, as mentioned in section 3.1,

previous studies have utilised MRE11 siRNA in order to examine whether knockdown of MRE11 results in enhancement of cell sensitivity to the more conventional forms of external beam radiation [74]. These studies have provided encouraging results, with cells displaying increased sensitivity to X-ray radiation, however this study has not shown the same effect when using a small molecule inhibitor of MRE11. It was therefore considered that using a radiation type with differing damage inducing characteristics may result in more successful radiosensitisation.

4.2 Aims

The aims of the present study were to assess the clonogenic cell survival following exposure to Mirin as a single agent in SK-N-BE(2c) and UVW/NAT cell lines, and the radiosensitising effects of Mirin in combination with [^{131}I]MIBG in the above cell lines. Interrogation of the effect of MRE11 inhibition using the small molecule inhibitor Mirin on [^{131}I]MIBG induced DDR pathway was also undertaken to elucidate the mechanistic basis for the results obtained in the earlier studies.

4.3 Materials and Methods

4.3.1 Cell Lines and Culture conditions

The human NAT transfected glioblastoma cell line (UVW/NAT) and the NAT expressing human neuroblastoma cell line SK-N-BE(2c) were employed in this study. Cells were maintained as described in section 3.3.1.

4.3.2 Drug Preparation and Treatment

Mirin was prepared as described in section 3.3.2.

Cells were treated with 0-50μM of Mirin and incubated for 24 hours for single agent studies before being seeded out for clonogenic assay. When carrying out combination studies, cells were treated with Mirin (5 and 10μM) 2 hours prior to incubation with [^{131}I]MIBG. Following a further 2 hour incubation with [^{131}I]MIBG, cells were washed 3 times with PBS to remove any excess non uptaken [^{131}I]MIBG, fresh media containing Mirin was added and cells were subsequently incubated for 24 hours before seeding for clonogenic cell survival assays. Based on data obtained in Chapter 2, the effect of Mirin on [^{131}I]MIBG induced DDR response was assessed 2 and 24 hours post treatment.

4.3.3 Clonogenic Cell Survival Assay

Clonogenic assays were performed as described in section 3.3.3 to determine whether cultured cells continue to form viable colonies of daughter cells following treatment with Mirin and [^{131}I]MIBG either as single agents or in combination [36].

4.3.4 Soft Agar Cell Survival Assay

Soft agar cell survival assays were performed as described in section 2.3.4 on SK-N-BE(2c) cells which fail to form discrete colonies in 2D cultures.

4.3.5 Cell Cycle Analysis

Cells were plated as described in section 3.3.3 and treated as described in section 4.3.2. 24 hours after treatment cells were collected and analysed for cell cycle distribution as described in section 2.3.5.

4.3.6 FACE Assay

Cells were prepared and analysed as described in section 3.3.6 and treated as described in section 4.3.2

4.3.7 H2AX Foci Staining

Cells were treated as described in section 4.3.2 and collected for H2AX foci staining as described in section 3.3.7

4.3.8 RAD51 ELISA

Following nuclear protein extraction (section 2.3.8), protein content of samples was quantified by BCA assay (section 2.3.8) and nuclear RAD51 protein levels were analysed 2 and 24 hours after by sandwich ELISA as described in section 3.3.8

4.3.9 Assessment of radio sensitisation using The Linear-Quadratic Model

The linear-quadratic mathematical model was employed as described in section 3.3.5.2 to assess radiosensitisation in Mirin, [^{131}I]MIBG combination treated cells.

4.3.9.1 Calculation of DEF

DEF was calculated as described in section 3.3.5.2.2

4.3.10 Statistical Analysis

Statistical analysis was carried out using GraphPad Prism version 6.05 (GraphPad Software Inc, San Diego). One-way ANOVA was used to determine statistical significance in single agent dose response cell survival assays. Two-way ANOVA with Bonferroni post-hoc test was used to determine statistically significant differences between combination treated cells and [^{131}I]MIBG only treated cells. In both cases p values <0.05 were reported as statistically significant.

4.4 Results

4.4.1 Clonogenic cell survival following treatment with the combination of Mirin and [^{131}I]MIBG.

Clonogenic survival assays were performed to determine the radiosensitising potential of Mirin on cells incubated for 24 hours with [^{131}I]MIBG. SK-N-BE(2c) and UVW/NAT cells were treated for 2 hours with Mirin (5 and 10μM) prior to a 2 hour incubation with 1-3MBq of [^{131}I]MIBG and a further 24 hour incubation after removal of excess [^{131}I]MIBG. To evaluate if Mirin sensitised cells to [^{131}I]MIBG the data were fitted to the linear-quadratic mathematical model and α, β, IC_{50} and DEF_{50} values determined.

4.4.1.1 The effect of Mirin in combination with [^{131}I]MIBG on the clonogenic capacity of SK-N-BE(2c) and UVW/NAT cells

Treatment of cells with combinations of Mirin and [^{131}I]MIBG suggested that Mirin induced a radiosensitising effect in SK-N-BE(2c) cells (Figure 4.1a and 4.2a). In SK-N-BE(2c) cells the [^{131}I]MIBG dose required to kill 50% of the cells (IC_{50} values) decreased from 2.88MBq in control samples treated with [^{131}I]MIBG alone to 2.25MBq and 1.64MBq in cells treated with 5μM and 10μM respectively (Figure 4.1b). DEF_{50} values increased for all administered concentrations of Mirin, from 1.00 in radiation controls to 1.28 and 1.76 in those exposed to 5μM and 10μM in combination with [^{131}I]MIBG respectively (Figure 4.1b). Similarly, UVW/NAT cells also exhibited a reduction in the [^{131}I]MIBG dose required to kill 50% of the cell population as IC_{50} values decreased from 2.9MBq in [^{131}I]MIBG treated control samples to 1.89MBq and 1.72MBq in 5μM and 10μM treated samples respectively (Figure 4.2b). Likewise, DEF_{50} values were increased across the concentration range from 1.00 in [^{131}I]MIBG treated controls to 1.27 and 1.39 in 5μM and 10μM treated samples respectively (Figure 4.2b).

To determine whether the clonogenic capacity of the cells following [^{131}I]MIBG treatment was enhanced by addition of Mirin the data were analysed using Two-way ANOVA with Bonferroni post-hoc analysis. This analysis confirmed that the most

significant radiosensitisation was observed following addition of 5 and 10μM of Mirin with 2MBq of [^{131}I]MIBG, with samples exposed to 1MBq and 3MBq only showing significant enhancement with a 10μM concentration of Mirin. This suggests that low doses of both Mirin and [^{131}I]MIBG produce the most successful enhancement of the sensitivity of SK-N-BE(2c) and UVW/NAT cells to [^{131}I]MIBG.

(a)

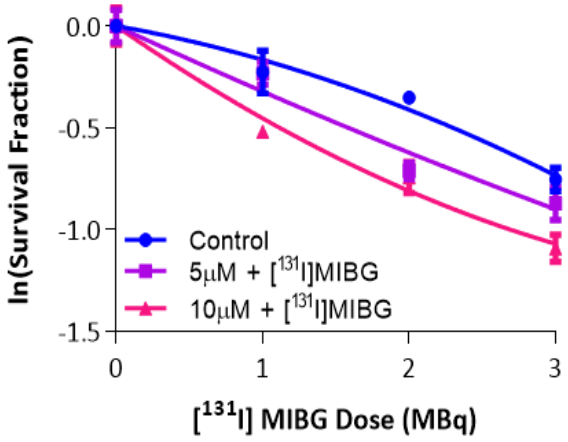

(b)

	Control	5μM	10μM
α	-0.1277	-0.3329	-0.502
β	-0.03905	0.01091	0.04844
IC_{50}	2.88	2.25	1.64
DEF_{50}	1.00	1.28	1.76

(c)

	1MBq		2MBq		3MBq
5μM+1MBq	ns	5μM+2MBq	****	5μM+3MBq	ns
10μM+1MBq	****	10μM+2MBq	****	10μM+3MBq	**

Figure 4.1 Clonogenic capacity of SK-N-BE(2c) cells treatment with Mirin in combination with [^{131}I]MIBG.

(a) Clonogenic capacity of SK-N-BE(2c) cells was determined 24 hours post treatment with [^{131}I]MIBG in the presence or absence of increasing Mirin at concentrations of 5 or 10μM. Cells were incubated with Mirin for 2 hours prior to radiation exposure (1-3MBq). (b) The data were fitted to the linear-quadratic equation using GraphPad Prism version 6.05 and α, β, IC_{50} and DEF_{50} calculated for all treatment groups. Data are presented as natural logarithms of the mean survival fraction normalised to untreated control (radiation alone) or drug treated controls (5μM or 10μM Mirin alone) ±SD; experiments were carried out three times in triplicate. Two-way ANOVA with Bonferroni post-hoc test was used to compare (c) the effect of combination treatments to that of cells exposed to radiation alone. ** denotes $p<0.01$, **** denotes $p<0.0001$

(a)

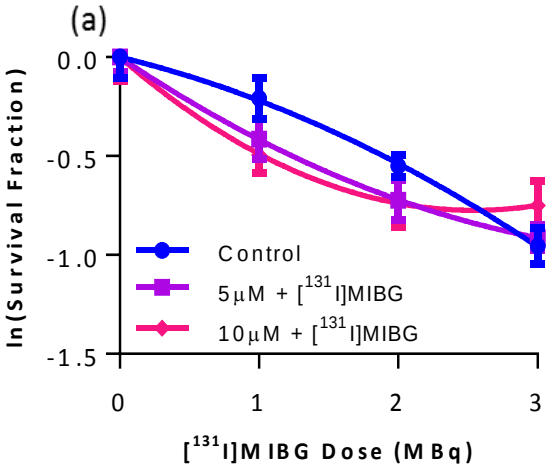

(b)

	Control	5μM	10μM
α	-0.1693	-0.4731	-0.6087
β	-0.04994	0.05625	0.1197
IC_{50}	2.40	1.89	1.72
DEF_{50}	1.00	1.27	1.39

(c)

	1MBq		2MBq		3MBq
5μM+1MBq	ns	5μM+2MBq	ns	5μM+3MBq	ns
10μM+1MBq	ns	10μM+2MBq	**	10μM+3MBq	ns

Figure 4.2 Clonogenic capacity of UVW/NAT cells treatment with Mirin in combination with [131I]MIBG.

(a) Clonogenic capacity of UVW/NAT cells was determined 24 hours post treatment with [131I]MIBG in the presence or absence of increasing Mirin concentrations (5 or 10μM). Cells were incubated with Mirin for 2 hours prior to radiation exposure (1-3MBq). (b) The data were fitted to the linear-quadratic equation using GraphPad Prism version 6.05 and α, β, IC_{50} and DEF_{50} calculated across all treatment groups. Data are presented as natural logarithms of the mean survival fraction normalised to untreated control (radiation alone) or drug treated controls (5μM or 10μM Mirin alone) ±SD; experiments were carried out three times in triplicate. Two-way ANOVA with Bonferroni post-hoc test was used to compare (c) the effect of combination treatments to that of cells exposed to radiation alone. ** denotes $p<0.01$

As demonstrated by clonogenic assay, Mirin effectively sensitises SK-N-BE(2c) and UVW/NAT cells to [^{131}I]MIBG in a dose dependent manner. The successful radiosensitisation demonstrated upon incubation with [^{131}I]MIBG could be due to the continuous damage elicited by this radiation type compared to the short term damaging effects elicited by X-ray radiation. As a consequence of these findings we further investigated the effect of Mirin on upstream (H2AX) and downstream (ATM and RAD51) targets of MRE11 to determine a rationale for radiosensitivity using [^{131}I]MIBG. As has previously been demonstrated, Mirin efficiently inhibits ATM phosphorylation and MRE11 exonuclease activity. It was therefore hypothesised that this study would also demonstrate inhibition of ATM phosphorylation in combination studies, in addition to reduced γ-H2AX foci formation and RAD51 activity.

4.4.2 Investigation of ATM phosphorylation following Mirin and [^{131}I]MIBG treatment

4.4.2.1 The effect of Mirin on [^{131}I]MIBG induced phosphorylation of ATM in SK-N-BE(2c) and UVW/NAT cells.

The data presented in Figure 4.3 shows the effect of the addition of Mirin on [^{131}I]MIBG induced phosphorylation of ATM in SK-N-BE(2c) and UVW/NAT cells. Mirin as a single agent at a concentration of 10μM induced no significant change in pATM kinase levels either 2 hours or 24 hours after treatment in both cell lines. Conversely, both cell lines exhibited a significant elevation in pATM levels following incubation with 2MBq of [^{131}I]MIBG both 2 and 24 hours post initial treatment. In SK-N-BE(2c) cells a 60%±0.2 increase in pATM kinase levels was observed 2 hours post initial treatment ($p<0.0001$) and a 73%±0.06 increase was observed 24 hours post initial treatment ($p<0.0001$) compared to untreated control cells. Similarly, UVW/NAT cells exhibited an increase in pATM levels 2 and 24 hours after [^{131}I]MIBG administration (62%±0.3 ($p<0.0001$) and 77%±0.2 ($p<0.0001$), respectively) compared to untreated control cells. In addition, both SK-N-BE(2c) and UVW/NAT samples incubated with [^{131}I]MIBG for 24 hours are significantly more pATM laden than those incubated for

2 hours, with 24 hour samples showing a 34%±0.006 (SK-N-BE(2c) ($p<0.0001$) and 40%±0.2 (UVW/NAT) ($p<0.0001$) increase respectively compared to 2 hour samples. The addition of Mirin caused a decrease in [^{131}I]MIBG induced phosphorylation of ATM in both SK-N-BE(2c) and UVW/NAT cells. Specifically in SK-N-BE(2c) pATM levels were reduced by 40%±0.07 2 hours ($p<0.0001$) and 43%±0.2 24 hours ($p<0.0001$) post initial treatment compared to [^{131}]MIBG alone treated samples. Similarly, UVW/NAT pATM levels were reduced by 38%±0.3 2 hours ($p<0.0001$) and 59%±0.01 24 hours ($p<0.0001$) post initial treatment when compared to [^{131}I]MIBG treated alone samples. Despite the observed reduction in pATM levels induced by addition of Mirin, Mirin did not completely abolish [^{131}I]MIBG induced phosphorylation of ATM. pATM levels remained significantly elevated compared to untreated control samples at both of the time points investigated (33%±0.07 (2 hours), $p<0.01$ and 53%±0.2 (24 hours), $p<0.0001$ higher respectively in SK-N-BE(2c) cells and 44%±0.3 (2 hours), $p<0.01$ and 45%±0.1 (24 hours), $p<0.01$ higher respectively in UVW/NAT cells. These results suggest that DNA repair is rapidly initiated following incubation with [^{131}I]MIBG and that this repair mechanism is upregulated 24 hours after initial treatment, indicating a more chronic DNA damaging effect is elicited by [^{131}I]MIBG compared to X-irradiation. Additionally, results suggest that inhibition of MRE11 by Mirin results in partial abrogation of ATM phosphorylation. Due to the decrease in ATM phosphorylation it was hypothesised that γ-H2AX would also be downregulated in a similar manner.

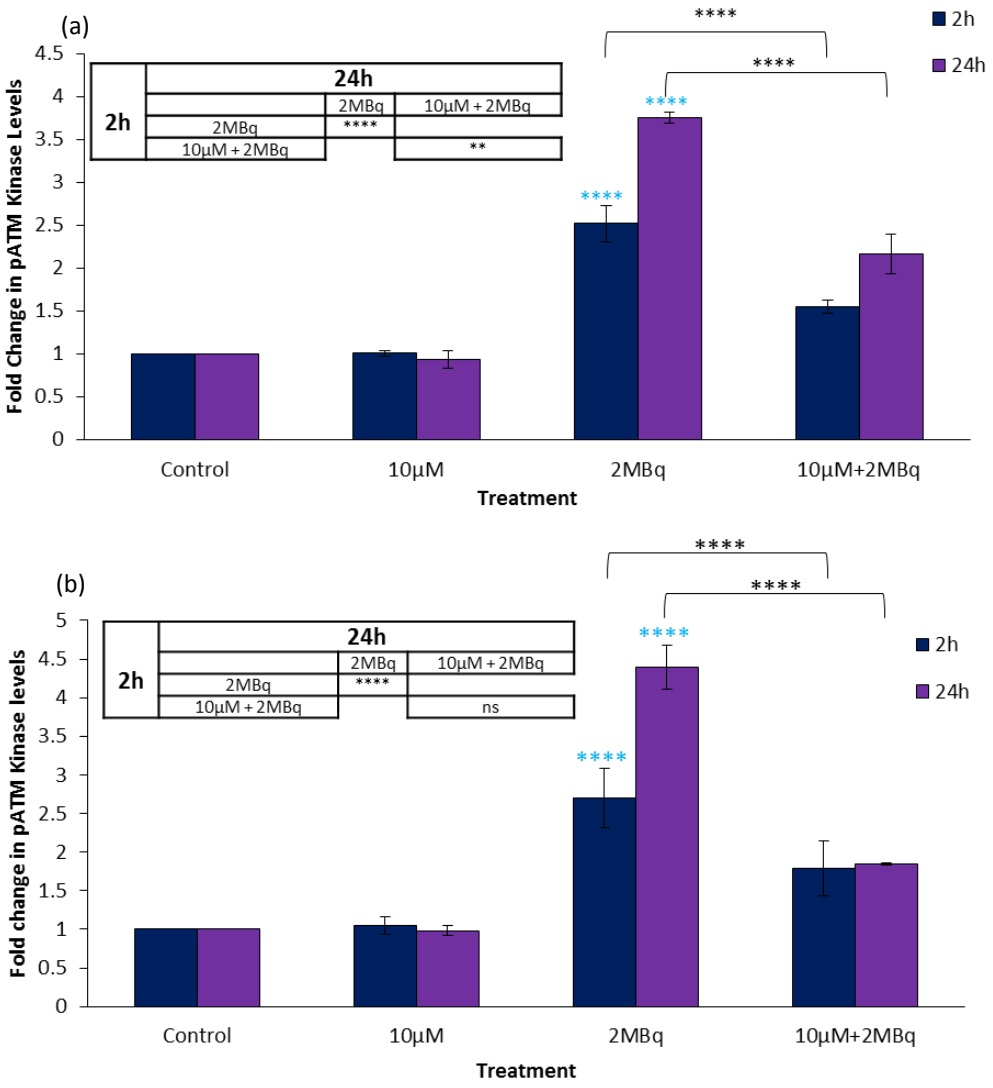

Figure 4.3 The effect of Mirin on [^{131}I]MIBG induced phosphorylation of ATM in (a) SK-N-BE(2c) and (b) UVW/NAT cells.

Fold change in levels of pATM following combination treatment with Mirin and [^{131}I]MIBG in (a) SK-N-BE(2c) and (b) UVW/NAT cells was assessed 2 hours and 24 hours post-initial [^{131}I]MIBG treatment . Cells were incubated with Mirin for 2 hours prior to irradiation. Data are means ±SD; experiments were carried out three times in triplicate. Two-way ANOVA with Bonferroni post-hoc test was used to compare the means of single agent treated samples to untreated controls (blue stars), the means of 2 hour samples compared to 24 hour samples (table) and the means of combination treated samples to 2MBq irradiated samples (bridges). ** denotes $p<0.01$, **** denotes $p<0.0001$

4.4.3 Investigation of γ-H2AX foci levels following Mirin and [^{131}I]MIBG treatment

4.4.3.1 The effect of Mirin on [^{131}I]MIBG induced γ-H2AX foci levels in SK-N-BE(2c) and UVW/NAT cells.

Treatment of SK-N-BE(2c) and UVW/NAT cells to Mirin (10μM) and [^{131}I]MIBG (2MBq) alone and in combination on γ-H2AX foci levels is shown in Figures 4.4 and 4.5. In both cell lines Mirin as a single agent at a concentration of 10μM resulted in no significant change in γ-H2AX foci levels at either of the time points investigated compared to untreated control cells. However, incubation with 2MBq of [^{131}I]MIBG resulted in a significant elevation of γ-H2AX levels compared to untreated control cells 2 hours and 24 hours after initial treatment in both SK-N-BE(2c) (84%±0.4 (2 hours), $p<0.0001$ and 87%±0.1 (24 hours), $p<0.0001$ respectively) and UVW/NAT cells (85%±0.7 (2 hours), $p<0.0001$ and 93%±0.6 (24 hours), $p<0.0001$ respectively). The addition of Mirin abrogated the observed [^{131}I]MIBG induced upregulation of γ-H2AX foci levels 2 and 24 hours post initial treatment. Specifically in SK-N-BE(2c) cells (Figure 4.4) Mirin decreased [^{131}I]MIBG induced upregulation of γ-H2AX foci by 30%±0.8 ($p<0.0001$) 2 hours post initial treatment and 31%±0.2 ($p<0.001$) 24 hours post initial treatment, however levels remained significantly elevated compared to untreated control samples ($p<0.0001$). Likewise in UVW/NAT cells, Mirin decreased [^{131}I]MIBG induced upregulation of γ-H2AX foci by 37%±0.2 ($p<0.01$) 2 hours post initial treatment and 37%±1.2 ($p<0.001$) 24 hours post initial [^{131}I]MIBG treatment. Despite this, and similarly to SK-N-BE(2c) cells, Mirin did not completely abolish γ-H2AX foci formation following incubation with [^{131}I]MIBG as γ-H2AX foci remained significantly elevated compared to untreated control samples.

These data indicate that the Mirin induced down regulation of pATM 2 and 24 hours post incubation with [^{131}I]MIBG has a subsequent effect on ATM phosphorylation of H2AX.

In cells incubated with [^{131}I]MIBG for 24 hours, γ-H2AX foci levels increased compared to 2 hours post treatment. In SK-N-BE(2c) cells levels increased by 28%±0.1 ($p<0.0001$) between 2 and 24 hours in 2MBq exposed samples and in UVW/NAT cells

levels increased by 30%±0.6 ($p<0.0001$) between 2 and 24 hours in 2MBq exposed samples suggesting that [^{131}I]MIBG induced DNA double stranded breaks had not been resolved.

Taken together these results suggest that DNA repair mechanisms are rapidly initiated following [^{131}I]MIBG treatment and remain continually elevated as the isotope decays creating more complex DNA double stranded breaks over the 24 hour time period assessed. Additionally results suggest that repair mechanisms are partially abrogated via MRE11 inhibition. As a result of γ-H2AX foci formation abrogation it was also hypothesised that levels of nuclear RAD51 would decline in response to MRE11 inhibition. RAD51 and γ-H2AX co-localise after induction of DNA damage with γ-H2AX being the driving factor in nuclear RAD51 focus formation.

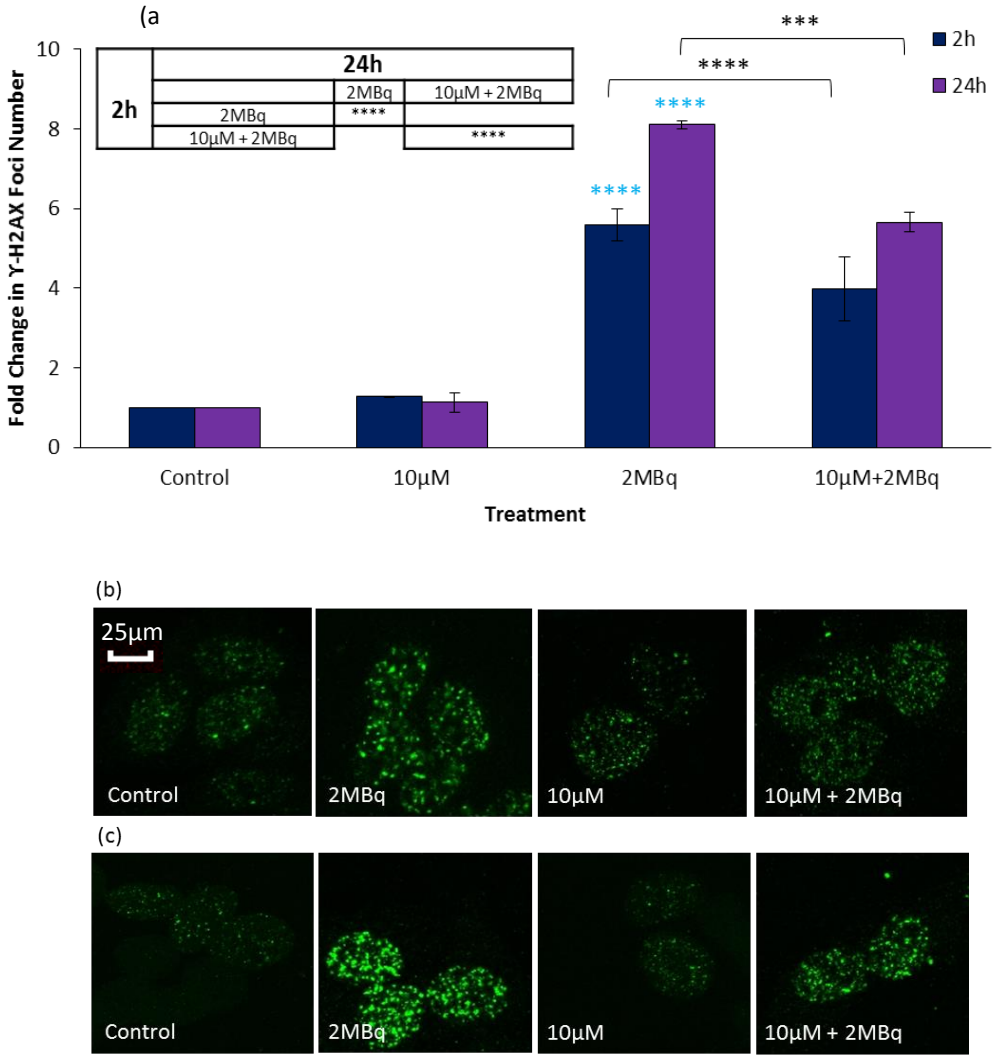

Figure 4.4 The effect of Mirin on [^{131}I]MIBG induced γ-H2AX foci levels in SK-N-BE(2c) cells.

(a) Fold change in γ-H2AX foci levels following treatment with Mirin and [^{131}I]MIBG alone and in combination were assessed in SK-N-BE(2c) cells (b) 2 and (c) 24 hours following exposure to 2MBq of [^{131}I]MIBG. The data was analysed using Volocity 3D Image Analysis Software (b and c). Data are means ±SD; experiments were carried out three times and a minimum of 50 cells were counted for each treatment in each individual experiment. Two-way ANOVA with Bonferroni post-hoc test was used to compare the means of single agent treated samples to untreated controls (blue stars), combination treated samples to 2MBq irradiated samples 2 and 24h post irradiation (table) and means of 2h sample to 24h samples (bridges). *** denotes $p<0.001$, **** denotes $p<0.0001$

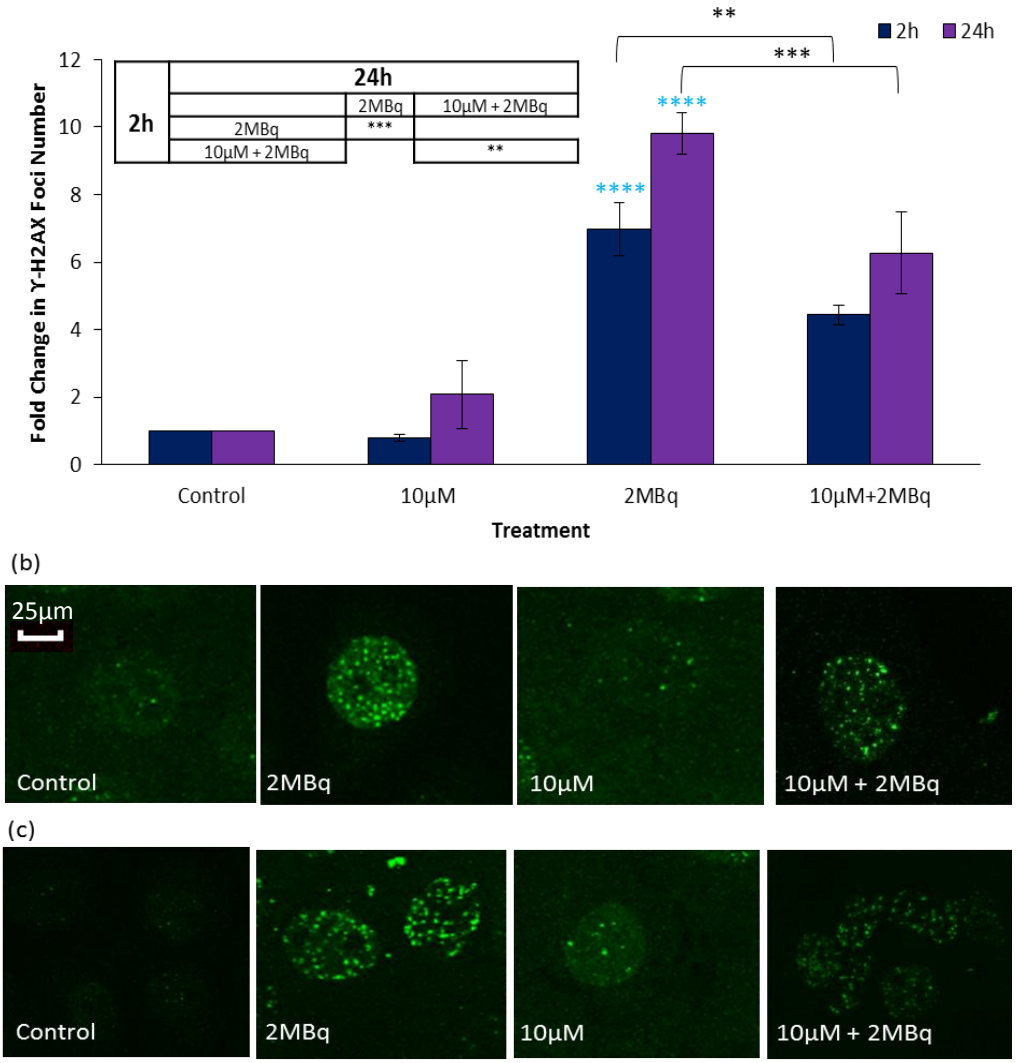

Figure 4.5 The effect of Mirin on [^{131}I]MIBG induced γ-H2AX foci levels in UVW/NAT cells.

(a) Fold change in γ-H2AX foci levels following treatment with Mirin and [^{131}I]MIBG alone and in combination were assessed in UVW/NAT cells (b) 2 and (c) 24 hours following radiation exposure to 2 MBq of [^{131}I]MIBG. The data was analysed using Volocity 3D Image Analysis Software (b and c). Data are means ±SD; experiments were carried out three times and a minimum of 50 cells were counted for each treatment in each individual experiment. Two-way ANOVA with Bonferroni post-hoc test was used to compare the means of single agent treated samples to untreated controls, (blue stars) combination treated samples to 2MBq irradiated samples 2 and 24h post irradiation (table) and means of 2h sample to 24h samples (bridges). ** denotes $p<0.01$, *** denotes $p<0.001$, **** denotes $p<0.0001$

4.4.4 Investigation of RAD51 activity following Mirin and [^{131}I]MIBG treatment.

RAD51 is an important contributing factor to the HR DNA repair pathway and following DNA DSB formation, RAD51 is recruited and forms long nucleofilaments which function to tether together the broken ends of DNA [92]. This recruitment is preceded by MRN complex dependent generation of regions of ssDNA at the 3' terminus of the DNA [92], therefore in order to determine whether Mirin treatment also targets this downstream signalling cascade RAD51 levels following Mirin [^{131}I]MIBG treatment were assessed.

4.4.4.1 The effect of Mirin on [^{131}I]MIBG induced RAD51 activation in SK-N-BE(2c) and UVW/NAT cells.

Fold change in nuclear RAD51 protein levels in SK-N-BE(2c) and UVW/NAT cells following incubation with Mirin and 2MBq of [^{131}I]MIBG 2 and 24 hours post initial [^{131}I]MIBG treatment is presented in Figure 4.6. Exposure of cells to Mirin as a single agent at a concentration of 10μM resulted in no significant change in RAD51 levels both 2 and 24 hours after initial [^{131}I]MIBG treatment compared to untreated control cells in either cell line. Treatment of SK-N-BE(2c) cells to 2MBq of [^{131}I]MIBG significantly increased nuclear RAD51 protein levels both 2 hours (15%±0.004) and 24 hours (54%±0.01) post initial treatment compared to untreated control, although levels were 43%±0.01 higher 24 hours after initial treatment compared to 2 hours post initial treatment ($p<0.0001$). Conversely, treatment of UVW/NAT cells to 2MBq of [^{131}I]MIBG had no effect on nuclear RAD51 protein levels 2 hours post initial treatment compared to untreated control cells, however a significant increase in nuclear RAD51 (37%±0.05) was observed 24 hours post initial treatment compared to untreated control cells ($p<0.0001$), with 24 hour samples exhibiting a 25%±0.05 elevation compared to 2 hours samples ($p<0.0001$).

Mirin reduced the [^{131}I]MIBG induced upregulation of nuclear RAD51 protein by 27%±0.009 ($p<0.0001$) in SK-N-BE(2c) cells and 23%±0.06 ($p<0.001$) in UVW/NAT cells 24 hours post initial treatment, however 2 hours after initial [^{131}I]MIBG treatment no

significant difference in nuclear RAD51 protein levels was observed in either cell line exposed to the combination treatment. Despite this reduction in nuclear RAD51, Mirin did not completely abolish [^{131}I]MIBG induced upregulation of nuclear RAD51 protein levels, with levels remaining significantly elevated compared to untreated control samples at both of the time points investigated in SK-N-BE(2c) cells (38%±0.006 (2 hours), $p<0.0001$ and 26%±0.009 (24 hours), $p<0.0001$ higher respectively) and at 24 hours only in UVW/NAT cells (24%±0.06, $p<0.01$ higher).

These results further suggest that DNA repair by HR (as measure by nuclear RAD51 levels) is rapidly initiated following incubation of cells with [^{131}I]MIBG and that this repair mechanism remains upregulated 24 hours after initial treatment, indicating a more chronic DNA damaging effect is elicited by [^{131}I]MIBG compared to X-irradiation, where we saw in Chapter 3 that RAD51 levels has declined significantly 24 hours after initial treatment. Additionally, results suggest that inhibition of MRE11 by Mirin results in partial abrogation of RAD51 nuclear translocation 24 hours after treatment. RAD51 is an important factor in the initiation of DNA repair by HR in G2/M phase of the cell cycle. It was therefore hypothesised that cells would accumulate in G2/M phase of the cell cycle due to the inability of cells to repair DNA by HR and thus transition through the cell cycle.

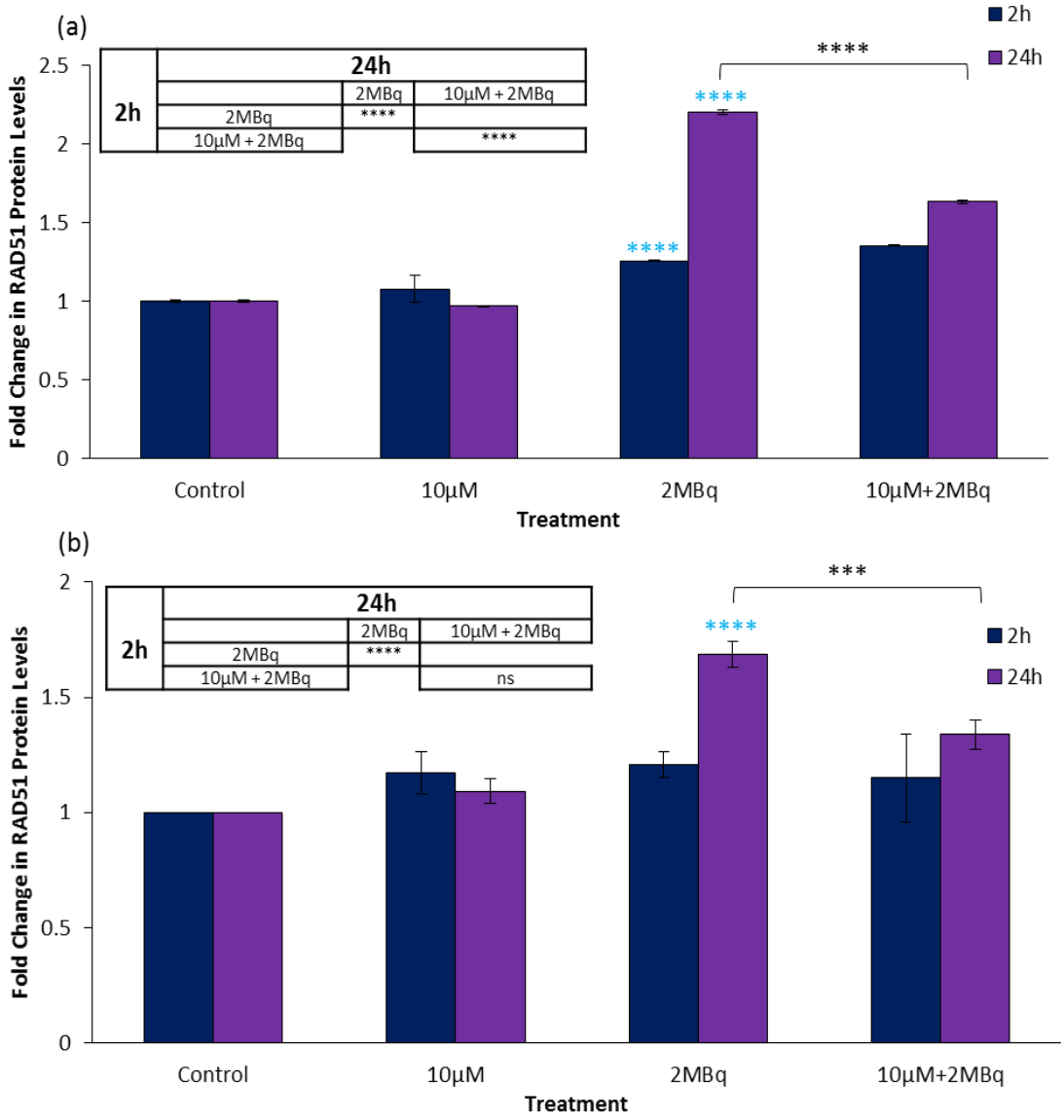

Figure 4.6 The effect of Mirin on [^{131}I]MIBG induced nuclear RAD51 protein levels in (a) SK-N-BE(2c) and (b) UVW/NAT cells

RAD51 protein levels were assessed following treatment with Mirin and [^{131}I]MIBG in (a) SK-N-BE(2c) and (b) UVW/NAT cells 2 and 24 hours post initial [^{131}I]MIBG treatment. Data are means ±SD; experiments were carried out three times in duplicate. Two-way ANOVA with Bonferroni post-hoc test was used to compare the means of single agent treated samples to untreated controls (blue stars), the means of 2 hour samples compared to 24 hour samples (table) and the means of combination treated samples to 2MBq irradiated samples (bridges). *** denotes $p<0.001$, **** denotes $p<0.0001$

4.4.5 Analysis of cell cycle progression following incubation with Mirin and [^{131}I]MIBG.

4.4.5.1 Analysis of cell cycle progression following incubation with combinations of Mirin and [^{131}I]MIBG in SK-N-BE(2c) and UVW/NAT cells

The effect of Mirin and [^{131}I]MIBG as single agents and in combination on SK-N-BE(2c) and UVW/NAT cell cycle distribution following 24 hour incubation is presented in Figure 4.7. Treatment of SK-N-BE(2c) and UVW/NAT cells with 2MBq of [^{131}I]MIBG resulted in a statistically significant increase (38%±1.7, $p<0.01$ and 52%±1.9, $p<0.0001$ respectively) in the proportion of cells in G2/M phase of the cell cycle, with concomitant 31.5%±2.1 ($p<0.05$) and 39%±2.0 ($p<0.001$) reductions respectively in the proportion of cells in G1 phase 24 hours after initial treatment. Treatment with Mirin significantly increased the [^{131}I]MIBG induced G2/M cell cycle arrest with combination samples demonstrating an 8%±1.7 increase in the proportion of SK-N-BE(2c) cells in G2/M phase ($p<0.05$) and a 10%±1.9 increase in the proportion of UVW/NAT cells in G2/M phase ($p<0.05$).

This suggests that inhibition of MRE11 in UVW/NAT cells prevents the transition of cells into the mitotic phases of the cell cycle following DNA damage elicited by [^{131}I]MIBG. This is consistent with the observed reduction in RAD51, indicating reduced capacity for DNA repair by HR and therefore no progression of the cell cycle.

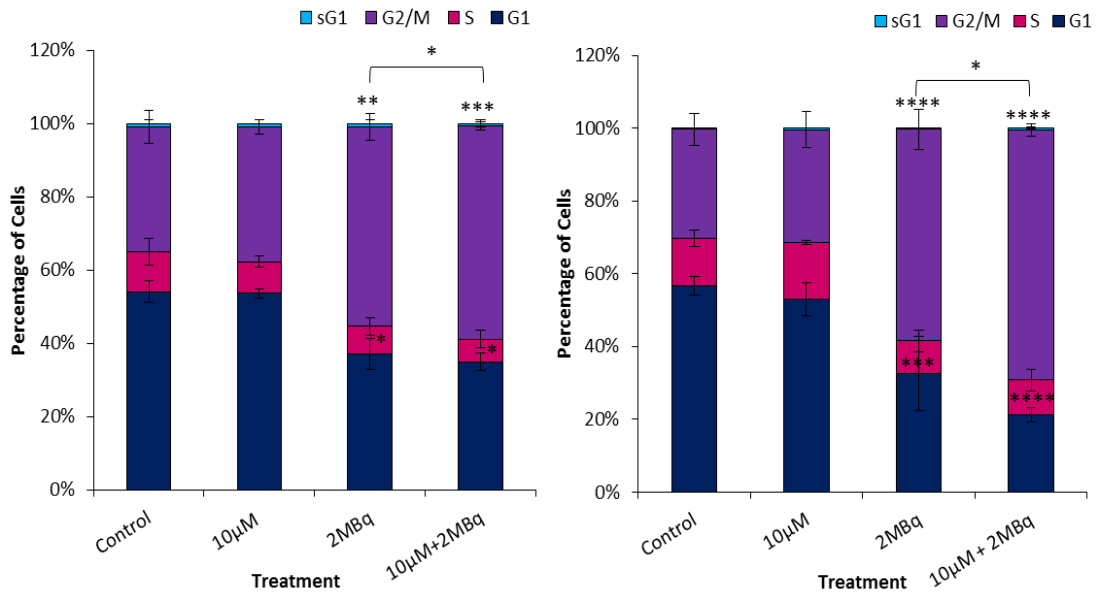

Figure 4.7 (a) SK-N-BE(2c) and (b) UVW/NAT cell cycle progression following treatment with Mirin and [^{131}I]MIBG both as single agents and in combination.

The effects of [^{131}I]MIBG and Mirin both alone and in combination were assessed in SK-N-BE(2c) cells 24 hours post-irradiation. SK-N-BE(2c) cells were pre-treated with Mirin (10μM) for 2 hours prior to [^{131}I]MIBG exposure. The data were analysed using BD FACSDiva software. Data are means ±SD; experiments were carried out three times. Two-way ANOVA was used to compare the means of the G2/M fraction of combination treated cells to [^{131}I]MIBG treated controls * denotes $p<0.05$, ** denotes $p<0.01$, ***denotes $p<0.001$, **** denotes $p<0.0001$.

4.5 Discussion

There are a plethora of well-documented and undesirable toxicities associated with X-ray radiation treatment in patients, therefore development of more targeted forms of radiation therapy are at the fore front of cancer research. This study interrogated the utilisation of [^{131}I]MIBG, which has a proven efficacy in delivering radiation to tumour sites via exploitation of specific uptake mechanisms [44], [121], and combined this with non-toxic concentrations of Mirin to enhance the DNA damaging effects associated with ^{131}I decay whilst avoiding additional drug based toxicities. Based on the findings discussed in section 2.4.2, where a dose dependent increase in ATM phosphorylation was observed over a 24 hour time course in response to [^{131}I]MIBG, suggesting that ATM is also involved in the recognition of DNA DSBs with low dose rate radiation sources. It was therefore hypothesised that inhibition of [^{131}I]MIBG induced ATM phosphorylation should lead to inhibition of DNA damage recognition and repair resulting in in enhanced radiation cell kill. This chapter therefore aimed to determine the cytotoxicity of Mirin and [^{131}I]MIBG in combination on SK-N-BE(2c), and UVW/NAT cell lines. Following this, analysis of the mechanistic processes underpinning the initial phenotypic results was undertaken through interrogation of how the combinations affected cell cycle, and up and downstream targets of MRE11, including ATM kinase, γ-H2AX and RAD51, after incubation with each single agent and in combination.

As was previously outlined in section 3.4.1, non-toxic concentrations of Mirin (5μM and 10μM) were selected for further investigation in combination studies. These subsequent combination studies demonstrated that Mirin exhibited a significant radiosensitising effect on [^{131}I]MIBG induced cell kill. SK-N-BE(2c) cells demonstrated a greater sensitivity to Mirin in combination with [^{131}I]MIBG at the highest Mirin concentration (10μM) investigated here, however, this effect was shown to be irrespective of increasing Mirin or [^{131}I]MIBG dose in UVW/NAT cells, with SK-N-BE(2c) cells demonstrating DEF_{50} values of 1.28 and 1.76. This is in contrast to a DEF_{50} value of 1.27 and 1.39 demonstrated by UVW/NAT cells. This suggests that UVW/NAT cells are less sensitive to combination treatment with [^{131}I]MIBG, however SK-N-

BE(2c) cells respond better, despite the initial radio-resistance observed when treated with [^{131}I]MIBG alone. There are no previous studies to demonstrate the efficacy of inhibiting components of the MRN-ATM signalling pathway when combined with [^{131}I]MIBG or indeed any other radiopharmaceuticals, all previous studies have been with external beam radiation sources. However, in previous studies by McCluskey *et al.,* (2012), the cytotoxic effects of [^{131}I]MIBG have been shown to be enhanced by addition of topotecan, a topoisomerase-1 inhibitor that acts to increase DNA strand breaks, by preventing DNA re-ligation following breakage during the replication process [36]. These findings provided a rationale for the use of other compounds which potentiate the production of breaks in the DNA helix in combination with [^{131}I]MIBG.

As discussed previously (section 1.4.2) abrogation of MRE11 activity using siRNA [74] or oncolytic adenoviruses [105] results in significant enhancement of X-ray radiation cytotoxicity. In this study, MRE11 nuclease activity was inhibited using the small molecule inhibitor Mirin in combination with X-ray irradiation and despite downregulation of X-ray induced upregulation of ATM kinase phosphorylation, γ-H2AX foci formation and levels of nuclear RAD51, no radiosensitisation with respect to cell kill was found in this study when using X-rays. As discussed in the previous chapter, this suggests that X-irradiation may initiate a compensatory DNA repair process, allowing radiation induced DNA DSBs to be repaired. Subsequently, to substantiate the hypothesis that Mirin abrogates important components of the MRN-ATM signalling pathway that ultimately culminates in G2/M checkpoint activation and to understand the mechanism by which it exerts sensitisation with [^{131}I]MIBG, further investigation of the upstream and downstream signalling effects of MRE11 were assessed in combination with [^{131}I]MIBG. As discussed in section 2.5, γ-H2AX foci levels were upregulated 2 hours after initial treatment with [^{131}I]MIBG however, contrary to the pattern shown upon exposure to X-rays levels continued to escalate 24 hours following incubation with 2MBq [^{131}I]MIBG, indicating that the number of DNA DSBs continues to increase. However γ-H2AX foci numbers per cell observed 2 hours after initial treatment with [^{131}I]MIBG were significantly lower than that

observed following X-irradiation, indicating that the rate at which foci form is different between X-rays and [^{131}I]MIBG, which is likely due to [^{131}I]MIBG being low dose, low dose rate irradiation and X-rays being high dose, high dose rate irradiation. Mirin has previously been shown to inhibit the MRN dependent activation of ATM kinase [71] therefore it was subsequently hypothesised that incubation of cells with Mirin prior to [^{131}I]MIBG treatment would result in a reduced cellular capacity to activate ATM kinase and form γ-H2AX foci. Cellular deficiencies in ATM results in a depletion in γ-H2AX foci formation as shown by Burma *et al.,* (2001) whereupon ATM null mouse fibroblast cells demonstrated no γ-H2AX foci formation following exposure to X-irradiation [112]. This study demonstrated that this was indeed the case, where a significant reduction (38-40%) in phosphorylated ATM kinase (pATM) levels in cells pre-treated for 2 hours with Mirin before subsequent [^{131}I]MIBG treatment was evident. Subsequently, γ-H2AX foci levels were investigated and in both cell lines following 2 hour pre-treatment with Mirin γ-H2AX foci levels were also depleted (by 30-37%), further supporting the hypothesis that inhibition of MRN dependent activation of ATM kinase would elicit secondary inhibitory effects on γ-H2AX foci formation.

As has been previously discussed (section 1.4) Mirin also targets components of the HR DNA repair pathway. RAD51 is also an important contributing factor to the HR DNA repair pathway and following DNA DSB formation RAD51 is recruited and forms long nucleofilaments which function to tether the broken ends of DNA [92]. This recruitment is preceded by MRN complex dependent generation of regions of ssDNA at the 3' terminus of DNA [92] therefore in order to determine whether Mirin treatment also targets this downstream signalling cascade, nuclear RAD51 levels following Mirin and [^{131}I]MIBG treatment were assessed. Initially it was demonstrated that Mirin alone had no significant effect on nuclear RAD51 levels however, when used in combination with [^{131}I]MIBG it elicited significant abrogation of [^{131}I]MIBG induced RAD51 activity 24 hours following initial treatment. Following 2 hour incubation with [^{131}I]MIBG there was no significant elevation of nuclear RAD51 levels. This was in contrast to X-irradiation where nuclear levels of RAD51

were increased 2 hours post-irradiation. This is likely due to the reduced induction of DNA DSBs at this time point, as indicated by less γ-H2AX foci number in cells, in response to [^{131}I]MIBG treatment compared to X-irradiation. However with continuous and prolonged treatment with [^{131}I]MIBG DNA repair by HR is triggered, as evidenced by an elevation in nuclear RAD51 levels 24 hours after initial treatment. Again, this is supported by the increase in γ-H2AX foci number in cells at this time point, indicating the presence of more DSBs.

Mirin was hypothesised to elicit abolition of the [^{131}I]MIBG induced G2/M checkpoint, via inhibition of ATM kinase activation [118], and thus result in the continual cycling of cells and prevention of DNA repair. However, in all three cell lines tested in this study Mirin did not abrogate [^{131}I]MIBG induced G2/M cell cycle arrest. In previous studies by others Mirin at a concentration of 10μM had no significant effect on cell cycle progression [71] which is consistent with the data reported in this study. Combination studies across all three cell lines however highlighted that addition of Mirin 2 hours prior to [^{131}I]MIBG treatment again, as with X-ray radiation and Mirin treatment, did not elicit the G2/M checkpoint abolishing effect that was initially projected. Therefore cells proceeded to accumulate in G2/M phase of the cell cycle. This suggests that Mirin at a concentration of 10μM is not inhibiting activation of the G2/M checkpoint. Additionally, despite the hypothesis that Mirin would abolish G2/M checkpoint activation, Dupre *et al.,* (2008) also showed that Mirin did not abolish the G2/M checkpoint at a concentration of 50μM until cells were progressing synchronously through the cell cycle, which cells in tumours do not.

As this study has shown, in all the cell lines tested, Mirin did not induce radiosensitivity when combined with X-ray radiation, however a significant radiosensitising effect was found when Mirin was combined with [^{131}I]MIBG. Inhibitory effects on the DNA repair pathway to which ATM kinase is ultimately the linchpin are elicited in both cases however, [^{131}I]MIBG appears to be exerting a much more continuous and long term damaging effect resulting in extended activation of DNA repair proteins. Further investigation should be carried out into the differences between X-ray radiation induced damage and [^{131}I]MIBG induced damage which may

highlight differences in the nature, severity or quantity of the DNA breaks and subsequently the mechanism involved in the repair of DSBs, thus giving an insight into the radiation quality dependent radiosensitising success of Mirin.

Taken together the findings from both investigations may suggest that due to the high dose rate nature of X-ray radiation and the low dose rate nature of [^{131}I]MIBG it is possible that cells initiate a compensatory DNA repair cascade following X-irradiation, which does not appear to be activated in SK-N-BE(2c) cells in response to [^{131}I]MIBG. UVW/NAT cells on the other hand exhibit a plateau in radiation induced cell kill following treatment with 3MBq of [^{131}I]MIBG indicating that this compensatory mechanism may initiate after higher dosage. In addition, the level of damage elicited by [^{131}I]MIBG most likely slowly accumulates over an extended time period therefore cells do not initiate this compensatory mechanism, either at all or until much later, in order to cope with the damage levels. Consequently this accumulation of damage would result in more high risk of cell death.

Mirin has demonstrated a potential clinical usefulness as a radiosensitiser when combined with [^{131}I]MIBG, however more work is necessary in order to determine whether the *in vitro* effects demonstrated in this study will translate to more robust tumour masses. Investigation of combination treatment in spheroids may be indicative of whether or not Mirin and [^{131}I]MIBG treatment has the potential to be further analysed in mouse models, which are necessary before patient studies can arise.

Chapter 5

The effect of PARP-1 inhibition using the small molecule inhibitor Olaparib on the sensitivity of cancer cells to X-ray radiation *in vitro.*

5.1 Introduction

Olaparib and other PARP-1 inhibitors have previously been shown to exert radiation enhancing properties when used with ionising radiation, in both non-human cell lines and human cancer derived cell lines of various origin [122]–[124]. *In vivo* studies have also demonstrated radiopotentiation by Olaparib in the form of significant tumour growth delay in both studies [89], [98]. As demonstrated in Chapter 2, exposure to X-ray radiation results in the rapid upregulation of several components of the DDR pathway including PARP-1. The radiosensitising effects of Olaparib are thought to be, in part, as a result of the abrogation of the radiation induced SSB repair pathway resulting in the generation of more lethal DSBs via collapsed replication forks [89], therefore it is hypothesised that this will translate into reduced clonogenic capacity of cells.

To date, Olaparib has proved to be successful as a radiosensitiser in multiple cell lines including pancreatic [124], glioblastoma [125] and NSCLC [89]. Within this study Olaparib was investigated as a candidate for combination radio-chemotherapy therapy in neuroblastoma, glioblastoma and melanoma cell lines. In order to assess the potential radiation enhancing effects of Olaparib in combination with X-ray radiation it was first necessary to examine the cytotoxic effect of each individual agent by application of clonogenic survival assays.

5.2 Aims

The aims of the present study were to assess clonogenic cell survival following exposure to X-ray radiation and Olaparib as single agents in SK-N-BE(2c), UVW/NAT and A375 cell lines, and the radiosensitising effects of Olaparib in combination with X-rays on the clonogenic cell survival in the above cell lines. Furthermore the mechanistic basis for the results obtained in the aforementioned investigations were interrogated by assessment of ATM kinase activity, γ-H2AX foci formation, RAD51 activity and cell cycle progression.

5.3 Materials and Methods

5.3.1 Cell Lines and Culture conditions

SK-N-BE(2c), UVW/NAT and A375 cells were cultured as described in section 2.3.1

5.3.2 Drug Preparation and Treatment of cells with Olaparib and X-ray radiation

Olaparib was kindly provided by AstraZeneca (Macclesfield, UK). 100mM stock solutions were prepared by dissolving powdered Olaparib (MW 434.46) in 100% dimethyl sulfoxide (DMSO) and stored at -80^{o}C. Working solutions of 10mM and 1mM were prepared by diluting the 100mM stock solution 1:10 and 1:100 respectively with 100% DMSO. Working solutions were stored at -20^{o}C.

For single agent treatment studies cell medium was replaced with 5ml of fresh medium prior to exposure in X-ray radiation studies or 1ml of fresh medium containing a range of concentrations of Olaparib (0-50µM). For combination treatments cell medium was replaced with 1ml of fresh medium prior to incubation with Olaparib for 2 hours before X-ray radiation exposure and further 24 hour incubation.

5.3.3 Clonogenic Cell Survival Assay

Clonogenic assays were performed as described in section 2.3.3 to determine the effect of Olaparib and X-ray radiation as single agents and in combination on the clonogenic capacity of UVW/NAT and A375 cells.

5.3.4 Soft Agar Cell Survival Assay

Soft agar cell survival assays were performed as described in section 2.3.4 on SK-N-BE(2c) cells which fail to form discrete colonies in 2D cultures.

5.3.5 Assessing the efficacy of combination therapies

To assess whether the cytotoxicity of combinations of X-ray radiation and the DNA damage repair inhibiting compound Olaparib was superior to each treatment type alone, clonogenic survival data were analysed using the linear-quadratic mathematical model as described in section 3.3.5.2. DEF values were calculated as described in section 3.3.5.2.2.

5.3.6 PARP Assay

The assessment of PARP activity was undertaken as described in section 2.3.8 using a standard PARP assay kit according to the manufacturer's instructions (Trevigen, Gaithersburg, MD).

5.3.7 Cell Cycle Analysis

The progression of cells through the cell cycle was investigated as described in section 2.3.5 to assess if Olaparib and X-ray radiation alone and in combination caused an abrogation to the normal cycling of cells.

5.3.8 H2AX Foci Staining

γ -H2AX was used as a biochemical marker of the magnitude and resolution of DNA double stranded breaks in response to Olaparib and X-ray radiation. γ-H2AX foci staining and quantification was carried out as described in section 2.3.6.

5.3.9 Statistical Analysis

Statistical analysis was carried out using GraphPad Prism version 6.05 (GraphPad Software Inc, San Diego). One-way ANOVA was used to determine statistical significance in single agent dose response cell survival assays. Two-way ANOVA with Bonferroni post-hoc test was used to determine if combination treated samples were significantly different compared to radiation treated samples. In both cases p values <0.05 were reported as statistically significant.

5.4 Results

5.4.1 Determination of single agent toxicity

Clonogenic assays were performed to determine the toxic effects of Olaparib and X-ray radiation as single agents on each cell line. The data collected in this series of investigations were then used to determine the radiation dose range and drug concentrations to be utilised in further combination studies.

5.4.1.1 Clonogenic cell survival following exposure to Olaparib

SK-N-BE(2c) cells exhibited relatively minimal toxicity following 24 hour exposure to Olaparib over the 1-50μM concentration range. Cell survival decreased from 94%±0.02 at 1μM to 66% survival at 50μM±0.1 (Figure 5.1a). The concentration of Olaparib which elicited a 50% decrease in colony survival (IC_{50}) in SK-N-BE(2c) cells could not be determined as the IC_{50} value was not reached with the drug concentration used.

UVW/NAT cells also showed mild toxic effects following 24 hour exposure to Olaparib over the 1-10μM concentration range, from 90%±0.07 (IC_{10}) cell survival at 1μM to 74%±0.1 survival at 10μM. A sharp reduction in survival fraction was observed between 10μM and 50μM with only 33%±0.06 cell viability at the highest concentration tested (50μM). The concentration of Olaparib which elicited a 50% decrease in colony survival (IC_{50}) in UVW/NAT cells was 28μM (Figure 5.1b)

A375 cells exhibited greater sensitivity than SK-N-BE(2c) and UVW/NAT cells to increasing concentrations of Olaparib following 24 hour exposure. Cell survival decreased from 83%±0.02 at 1μM to 72%±0.1 survival at 5μM. Over the 10μM to 50μM concentration range cell viability declines sharply from 60%±0.1 (IC_{40}) to 23%±0.06 respectively. The concentration of Olaparib which elicited a 50% decrease in colony survival (IC_{50}) in A375 cells was 16μM (Figure 5.1c).

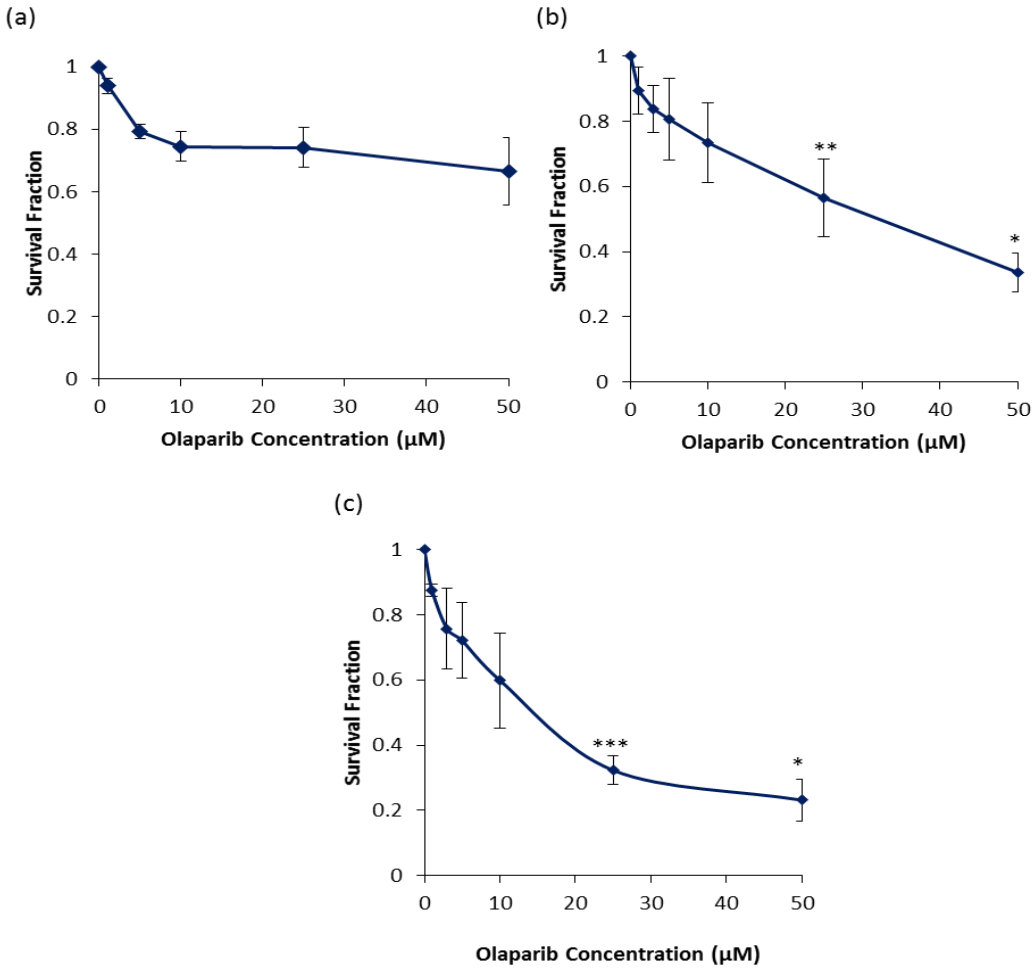

Figure 5.1 The toxicity of Olaparib on clonogenic survival of (a) SK-N-BE(2c) (b) UVW/NAT (c) A375 cells.

The clonogenic capacity of all cells was assessed 24 hours after treatment with a range of Olaparib concentrations (0-50µM). Data are presented as the mean survival fraction of treated cells normalised to untreated control cells ±SD; experiments were carried out three times in triplicate. One-way ANOVA was used to compare the means of Olaparib treated cells to untreated control data for all cell lines. * denotes $p<0.05$, ** denotes $p<0.01$ *** denotes $p<0.001$.

5.4.2 Clonogenic cell survival following exposure to the combination of Olaparib and X-ray radiation.

Clonogenic survival assays were performed to determine the radiosensitising potential of Olaparib. SK-N-BE(2c), UVW/NAT and A375 cells were treated for 2 hours with a range of Olaparib concentrations (1-25μM) prior to irradiation with 1Gy, 2Gy or 4Gy of X-rays and incubated for a further 24 hour period. To evaluate if Olaparib sensitised cells to X-ray radiation the experimental data were fitted to the linear-quadratic mathematical model and α, β, IC_{50} and DEF_{50} values determined.

5.4.2.1 The effect of Olaparib in combination with X-ray radiation on the clonogenic capacity of SK-N-BE(2c), UVW/NAT and A375 cells.

Exposure of cells to combinations of Olaparib and radiation suggested that Olaparib induced a radiosensitising effect in SK-N-BE(2c), UVW/NAT and A375 cells exposed to low doses of X-ray irradiation (Figure 5.2a, 5.3a and 5.4a). In SK-N-BE(2c) cells IC_{50} values decreased from 3.54Gy in control samples treated with X-rays alone to 2.14Gy and 1.70Gy in cells treated with 1μM and 5μM of Olaparib respectively (Figure 5.2b). However in cells treated with 25μM Olaparib there was a less pronounced reduction in IC_{50} value (3.54Gy in control, to 3.02Gy in combination treated sample) indicating that administration of a higher drug concentration did not induce a reduction in surviving fraction compared to radiation treatment alone (Figure 5.2b). DEF_{50} values for all administered Olaparib concentrations were greater than 1.00 (1.65, 2.09 and 1.17 for 1, 5 and 25μM respectively) indicating that Olaparib is exerting radiosensitising properties to varying extents depending on dose, with the greatest DEF_{50} achieved in combination with 5μM of Olaparib (Figure 5.2b). In UVW/NAT cells, IC_{50} values decreased from 3.34Gy in control samples treated with X-rays alone to 2.50Gy, 2.56Gy and 2.27Gy in cells treated with 1-25μM of Olaparib respectively (Figure 5.3b). Similarly to SK-N-BE(2c) cells, DEF_{50} values for all Olaparib concentrations are greater than 1.00 (1.33, 1.30 and 1.47 for 1, 5 and 25μM

respectively) indicating that Olaparib is enhancing the toxicity of X-ray radiation. In addition, there is minimal variation in DEF_{50} values in UVW/NAT cells between Olaparib concentrations suggesting that radiation enhancement is not significantly enhanced by increasing Olaparib concentration in this cell line (Figure 5.3b). In A375 cells IC_{50} values decreased from 2.06Gy in control samples treated with X-rays alone to 1.54Gy, 0.89Gy and 1.34Gy in cells treated with 1-25μM of Olaparib respectively (Figure 5.4b). Again as with SK-N-BE(2c) cells and UVW/NAT cells, DEF_{50} values in A375 cells for all Olaparib concentrations were greater than 1.00 (1.34, 2.32 and 1.54 respectively) indicating that Olaparib is enhancing the radiation toxicity. As was the case with SK-N-BE(2c) cells, the greatest DEF_{50} was observed with 5μM of Olaparib (Figure 5.4b). In SK-N-BE(2c) and A375 cells, low concentrations of Olaparib (1 and 5μM) demonstrate the greatest sensitising effect (greater DEF_{50} values). However, in UVW/NAT cells despite effective sensitisation at low concentrations, 25μM elicits the highest degree of sensitisation.

To determine whether the clonogenic capacity of the cells following X-ray radiation was enhanced by addition of Olaparib the data were analysed using Two-way ANOVA with Bonferroni post-hoc analysis. This analysis confirmed that in SK-N-BE(2c) and A375 cells the most significant radiosensitising effects were observed at low drug concentrations (1-5μM) and low radiation doses (1-2Gy) with samples exposed to combinations of Olaparib and 4Gy irradiation exhibiting no significant enhancement when compared to 4Gy irradiated samples (Figure 5.2c and 5.3c). However, UVW/NAT cells were sensitised to all radiation doses, across all drug concentrations investigated (excluding 1μM combined with 1Gy) (Figure 5.3c).

(a)

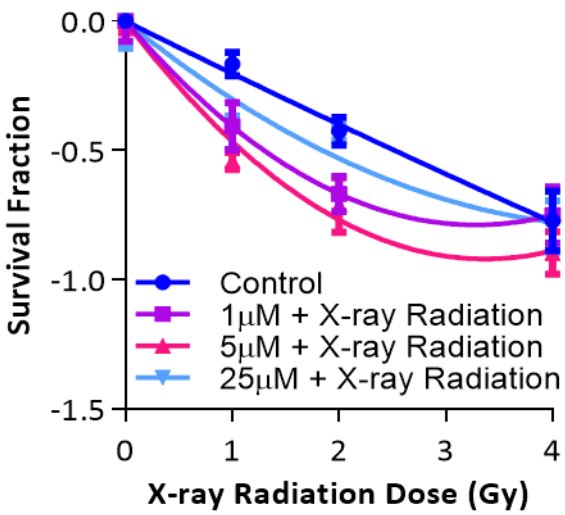

(b)

	Control	1μM	5μM	25μM
α	-0.2051	-0.4803	-0.5463	-0.3367
β	0.002645	0.07317	0.08105	0.03555
IC_{50}	3.54	2.14	1.70	3.02
DEF_{50}	1.00	1.65	2.09	1.17

(c)

	1Gy
1μM+1Gy	*
5μM+1Gy	***
25μM+1Gy	***

	2Gy
1μM+2Gy	ns
5μM+2Gy	*
25μM+2Gy	ns

	4Gy
1μM+4Gy	ns
5μM+4Gy	ns
25μM+4Gy	ns

Figure 5.2 Clonogenic capacity of SK-N-BE(2c) cells exposed to Olaparib and X-ray radiation.

(a) Clonogenic capacity of SK-N-BE(2c) cells was determined 24 hours post exposure to X-ray radiation in the presence or absence of increasing Olaparib concentrations (1-25μM). Cells were incubated with Olaparib for 2 hours prior to radiation exposure and a further 24 hours post-irradiation. (b) The data were fitted to the linear-quadratic equation using GraphPad Prism version 6.05 and α, β, IC_{50} and DEF_{50} calculated across all treatment groups. Data are presented as natural logarithms of the survival fraction of combination treated samples normalised to the mean survival fraction of Olaparib only samples ±SD; experiments were carried out three times in triplicate. (c) Two-way ANOVA was used to compare means of combination treatments to those of cells exposed to radiation alone * denotes $p<0.05$, *** denotes $p<0.001$

(a)

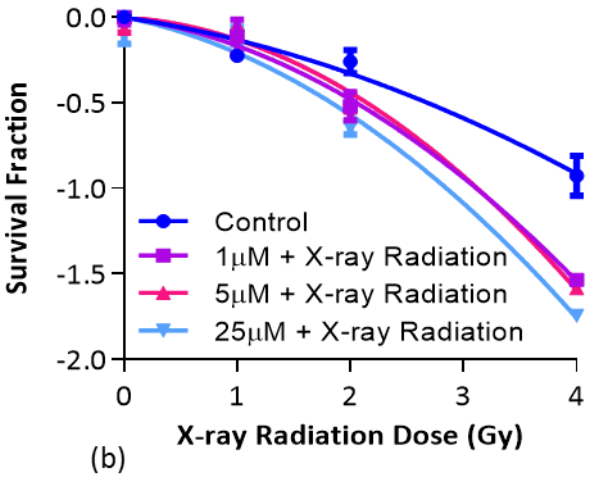

(b)

	Control	1μM	5μM	25μM
α	-0.1003	-0.09467	-0.04155	-0.1320
β	-0.03211	-0.07268	-0.08926	-0.07683
IC_{50}	3.34	2.50	2.56	2.27
DEF_{50}	1.00	1.33	1.30	1.47

(c)

	1Gy		2Gy		4Gy
1μM+1Gy	ns	1μM+2Gy	**	1μM+4Gy	***
5μM+1Gy	**	5μM+2Gy	***	5μM+4Gy	****
25μM+1Gy	****	25μM+2Gy	****	25μM+4Gy	****

Figure 5.3 Clonogenic capacity of UVW/NAT cells exposed to Olaparib and X-ray radiation.

(a) Clonogenic capacity of UVW/NAT cells was determined 24 hours post exposure to X-ray radiation in the presence or absence of increasing Olaparib concentrations (1-25μM). Cells were incubated with Olaparib for 2 hours prior to radiation exposure and a further 24 hours post irradiation. (b) The data were fitted to the linear-quadratic equation using GraphPad Prism version 6.05 and α, β, IC_{50} and DEF_{50} calculated across all treatment groups. Data are presented as natural logarithms of the survival fraction of combination treated samples normalised to the mean survival fraction of Olaparib only samples ±SD; experiments were carried out three times in triplicate. (c)Two-way ANOVA was used to compare the means of combination treatments to those of cells exposed to radiation alone for all cell lines ** denotes p<0.01, *** denoted p<0.001, **** denotes p<0.0001

(a)

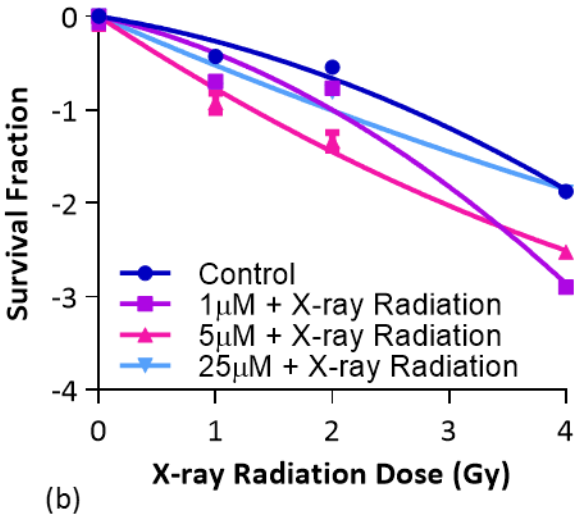

(b)

	Control	1μM	5μM	25μM
α	-0.2006	-0.2856	-0.8224	-0.5437
β	-0.06576	-0.1072	0.04901	0.02023
IC_{50}	2.06	1.54	0.89	1.34
DEF_{50}	1.00	1.34	2.32	1.54

(c)

	1Gy		2Gy		4Gy
1μM+1Gy	**	1μM+2Gy	ns	1μM+4Gy	ns
5μM+1Gy	****	5μM+2Gy	****	5μM+4Gy	ns
25μM+1Gy	****	25μM+2Gy	****	25μM+4Gy	ns

Figure 5.4 Clonogenic capacity of A375 cells exposed to Olaparib and X-ray radiation.

(a) Clonogenic capacity of A375 cells was determined 24 hours post exposure to X-ray radiation in the presence or absence of increasing Olaparib concentrations (1-25μM). Cells were incubated with Olaparib for 2 hours prior to radiation exposure and a further 24 hours post irradiation. (b) The data were fitted to the linear-quadratic equation using GraphPad Prism version 6.05 and α, β, IC_{50} and DEF_{50} calculated across all treatment groups. Data are presented as natural logarithms of the survival fraction of combination treated samples normalised to the mean survival fraction of Olaparib only samples ±SD; experiments were carried out three times in triplicate. (c)Two-way ANOVA was used to compare the means of combination treatments to those of cells exposed to radiation alone for all cell lines ** denotes $p<0.01$, **** denotes $p<0.0001$

5.4.3 Investigation of PARP-1 activity levels following Olaparib and X-ray radiation exposure

PARP-1 is a key enzyme for BER and radiation-induced SSBs are primarily repaired by BER, therefore the radiosensitising effect of PARP inhibitors is hypothesised to occur through inhibition of this BER pathway, leading to an increase in the number of collapsed replication forks generating DSBs, which are more complex than SSBs and potentially lethal to the cell.

5.4.3.1 The effect of Olaparib on PARP-1 activity in X-ray radiation exposed SK-N-BE(2c), UVW/NAT and A375 cells.

The data presented in Figure 5.5 shows the effect of Olaparib on PARP-1 activity 2 and 24 hours post exposure to 2Gy of X-ray radiation in SK-N-BE(2c) cells. Olaparib as a single agent at concentrations of 5 and 25µM resulted in a significant reduction in PARP-1 activity 2 hours after treatment in all three cell lines. SK-N-BE(2c) cells exhibited 33%±0.06 ($p<0.05$) and 56%±0.01 ($p<0.0001$) reductions respectively following treatment with 5µM and 25µM concentrations of Olaparib. UVW/NAT and A375 cells exhibited similar levels of PARP-1 abrogation to SK-N-BE(2c) cells with activity decreasing by 31%±0.1 ($p<0.01$) and 41%±0.008 ($p<0.0001$) respectively in UVW/NAT cells and 33%±0.06 and 47%±0.1 in A375 cells exposed to 5 and 25µM Olaparib. X-ray radiation exposure resulted in a 41%±0.03 ($p<0.0001$) increase in SK-N-BE(2c) PARP-1 activity, a 28%±0.1 ($p<0.0001$) increase in UVW/NAT PARP-1 activity and a 37%±0.3 increase in A375 PARP-1 activity 2 hours post-irradiation. However, cells exposed to 2Gy X-ray radiation in combination with 5 and 25µM Olaparib exhibited a significant reduction in radiation induced PARP-1 activation 2 hours post irradiation when compared to 2Gy alone. SK-N-BE(2c) PARP-1 activity levels were reduced by 30%±0.2 ($p<0.0001$) and 24%±0.2 ($p<0.01$) respectively when treated with 5µM and 25µM Olaparib in combination with X-irradiation, UVW/NAT PARP-1 activity levels were reduced by 50%±0.1 ($p<0.0001$) and 27%±0.04 ($p<0.001$) respectively and A375 PARP-1 activity levels were reduced by 58%±0.07 ($p<0.0001$)

and 47%±0.09 ($p<0.0001$) respectively. Following 24 hour incubation with 5 and 25µM of Olaparib, SK-N-BE(2c) and A375 cells exhibited a significant increase in PARP-1 activity compared to 2 hour samples therefore no significant reduction in PARP-1 activity was observed compared to untreated controls. Despite this, both SK-N-BE(2c) and A375 combination treated samples exhibited a reduction in PARP-1 activity compared to radiation treated samples alone 24 hours after initial treatment 35%±0.2 ($p<0.01$) and 31%±0.1 ($p<0.0001$) respectively in SK-N-BE(2c) cells and 25%±0.07 ($p<0.05$) and 28%±0.05 ($p<0.01$) respectively in A375 cells. UVW/NAT cells on the other hand remain significantly PARP-1 inhibited 24 hours after initial treatment with 5µM and 25µM Olaparib and as a result demonstrate a much greater level of PARP-1 abrogation 24 hours after initial combination treatment (46%±0.06 ($p<0.0001$) and 37%±0.07 ($p<0.0001$) respectively). Due to the role PARP-1 plays in repair of SSBs and DSBs it was hypothesised that inhibition of PARP-1 activation would result in an increase in γ-H2AX foci formation through exacerbation of DNA breaks.

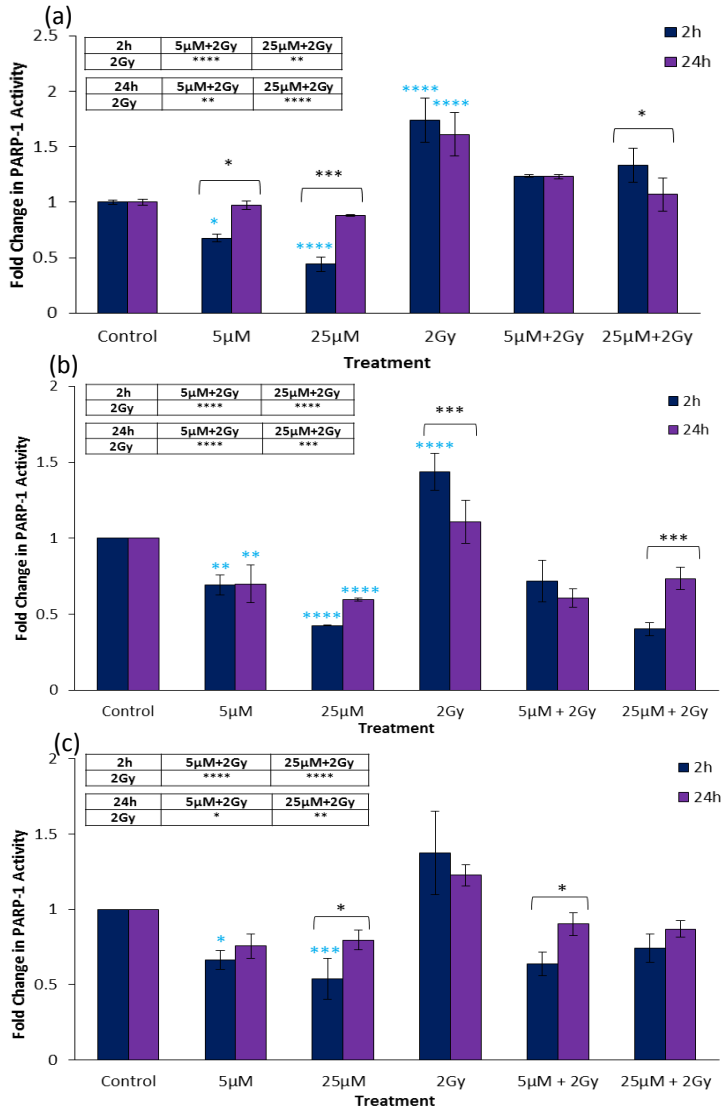

Figure 5.5 PARP-1 activity following exposure to combinations of Olaparib and X-ray radiation in (a) SK-N-BE(2c), (b) UVW/NAT and (c) A375 cells.

The effects of X-ray radiation and Olaparib as single agents and in combination were assessed in (a) SK-N-BE(2c), (b) UVW/NAT and (c) A375 cells 2 hours and 24 hours post-irradiation. Cells were incubated with Olaparib for 2 hours prior to irradiation. Data are means ±SD; experiments were carried out three times in triplicate. Two-way ANOVA with Bonferroni post-hoc test was used to compare: the means of single agent treated samples to untreated controls (blue stars), combination treated samples to 2Gy irradiated samples 2 and 24 hours post irradiation (table) and the effect of time (bridges). * denotes p<00.05, ** denotes p<0.01, *** denotes p<0.001, **** denotes p<0.0001

5.4.4 Investigation of γ-H2AX foci formation and resolution following Olaparib and X-ray radiation exposure.

It is well known that PARP-1 inhibition compromises the repair of DNA SSBs and consequently increased DSBs following treatment of cells with radiation. To determine if Olaparib in combination with X-ray radiation increased DSBs in this study γ-H2AX foci levels were assessed.

5.4.4.1 The effect of Olaparib on radiation induced γ-H2AX foci formation and resolution in SK-N-BE(2c), UVW/NAT and A375 cells.

The effect of Olaparib in combination with X-ray radiation on γ-H2AX foci levels 2 and 24 hours post irradiation in SK-N-BE(2c), UVW/NAT and A375 cells is shown in Figures 5.6, 5.7 and 5.8. Olaparib at concentrations of 5 and 25μM increased γ-H2AX foci levels compared to untreated controls in all cell lines assessed. SK-N-BE(2c) demonstrated 54%±0.5 (ns) and 77%±0.3 ($p<0.0001$) elevations respectively 2 hours post irradiation and 66%±0.7 ($p<0.001$) and 78%±0.5 ($p<0.0001$) elevations respectively 24 hours post irradiation (Figure 5.6). Likewise, UVW/NAT cells demonstrated 78%±0.9 ($p<0.0001$) and 75%± 0.5 ($p<0.0001$) increases respectively 2 hours post initial treatment and 61%± 0.4 ($p<0.05$) and 68%±0.008 ($p<0.0001$) increases 24 hours post initial treatment (Figure 5.7). A375 cells also demonstrated 84%±0.7 ($p<0.0001$) and 82%±0.2 ($p<0.0001$) elevations respectively after 2 hour incubation and 73%±0.7 ($p<0.001$) and 79%±0.9 ($p<0.0001$) increases after 24 hour incubation (Figure 5.8).

X-ray irradiation also increased γ-H2AX levels in all three cell lines with SK-N-BE(2c), UVW/NAT and A375 cells exhibiting 86%±0.9 ($p<0.0001$), 90%±0.9 ($p<0.0001$) and 90%±0.1 ($p<0.0001$) elevations respectively 2 hours post irradiation compared to untreated control cells. Subsequently, 24 hours post irradiation γ-H2AX foci levels decreased by 64%±0.1 ($p<0.0001$), 80%±0.5 ($p<0.0001$) and 75%±1.0 ($p<0.0001$) compared to 2 hours post irradiation in SK-N-BE(2c), UVW/NAT and A375 cells respectively. The addition of Olaparib (5μM and 25μM) enhanced the radiation

induced upregulation of γ-H2AX foci levels with SK-N-BE(2c) cells exposed to combination treatment demonstrating a 24%±0.4 ($p<0.0001$) and 20%±0.7 ($p<0.01$) increase in γ-H2AX foci levels respectively when compared to 2Gy alone 2 hours post irradiation (Figure 5.6). Conversely, UVW/NAT cells exposed to 5μM Olaparib and 2Gy irradiation, exhibit a significant decrease (14%±0.8) in γ-H2AX foci levels when compared to 2Gy irradiation alone 2 hours after initial treatment. However this decrease was not reflected in samples exposed to 25μM Olaparib in combination with 2Gy irradiation (Figure 5.7). Similarly to SK-N-BE(2c) cells, A375 cells demonstrate a significant increase (17%±0.4) in γ-H2AX foci levels in cells exposed to 25μM Olaparib in combination with 2Gy, when compared to 2Gy alone 2 hours post treatment ($p<0.05$). However, this effect was not reflected in cells exposed to 5μM Olaparib in combination with 2Gy irradiation with no significant difference in γ-H2AX foci levels observed (Figure 5.8). 24 hours post treatment, in all three cell lines exposed to combination treatment, γ-H2AX foci levels had decreased compared to 2 hour treated samples. SK-N-BE(2c) cells exhibited a 63%±0.4 and 34%±0.02 reduction, UVW/NAT cells decreased by 80%±0.5 ($p<0.0001$) and 57%±0.2 ($p<0.0001$) and A375 cells decreased by 41%±1.0 ($p<0.0001$) and 46%±0.7 ($p<0.001$) respectively at 5μM and 25μM in combination with 2Gy irradiation respectively.

However as Olaparib as a single agent increased γ-H2AX foci levels, to determine if the effect of combination treatment on γ-H2AX foci levels was additive, statistical analysis was also performed on combination data normalised to Olaparib alone. This demonstrated that the effect of combination treatment was additive in all cell lines, with cells exhibiting no further increase in γ-H2AX foci levels compared to the increase exerted by each single agent alone. This suggests that despite PARP-1 inhibition by Olaparib possibly acting to increase the conversion of SSBs into DSBs in non-irradiated samples, X-irradiation may directly induce a greater volume of DSBs than SSBs, therefore Olaparib is demonstrating no additional exacerbation of radiation induced damage.

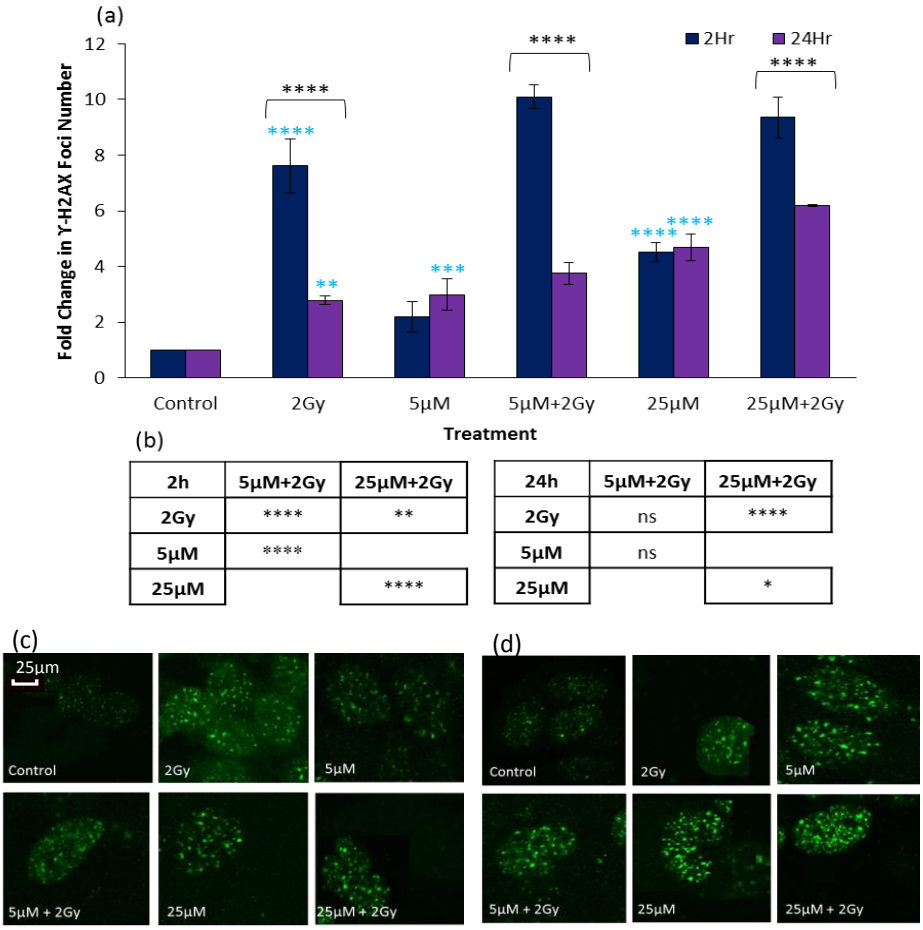

2h	5μM+2Gy	25μM+2Gy
2Gy	****	**
5μM	****	
25μM		****

24h	5μM+2Gy	25μM+2Gy
2Gy	ns	****
5μM	ns	
25μM		*

Figure 5.6 The effect of Olaparib on radiation induced γ-H2AX foci formation and resolution in SK-N-BE(2c) cells.

(a) Formation and resolution of γ-H2AX foci following exposure to Olaparib and X-ray radiation alone and in combination were assessed in SK-N-BE(2c) cells (c) 2 and (d) 24 hours following radiation exposure to 2Gy of X-ray radiation. The data was analysed using Volocity 3D Image Analysis Software (b and c). Data are means ±SD; experiments were carried out three times and a minimum of 50 cells were counted for each treatment in each individual experiment. Two-way ANOVA with Bonferroni post-hoc test was used to compare the means of single agent treated samples to untreated controls, combination treated samples to 2Gy irradiated samples 2 and 24h post irradiation (table) and means of 2h sample to 24h samples (bridges). * denotes $p<0.05$, ** denotes $p<0.01$, *** denotes $p<0.001$, **** denotes $p<0.0001$

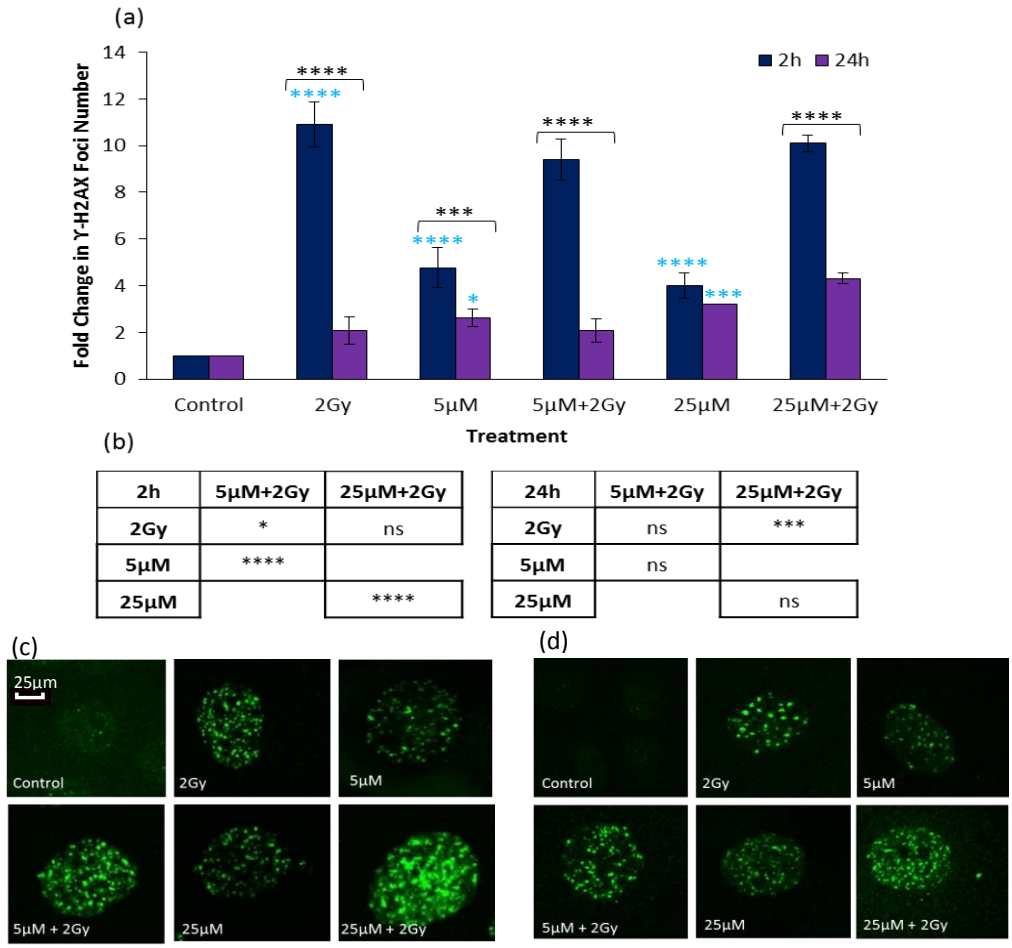

2h	5μM+2Gy	25μM+2Gy
2Gy	*	ns
5μM	****	
25μM		****

24h	5μM+2Gy	25μM+2Gy
2Gy	ns	***
5μM	ns	
25μM		ns

Figure 5.7 The effect of Olaparib on radiation induced γ-H2AX foci formation and resolution in UVW/NAT cells.

(a) Formation and resolution of γ-H2AX foci following exposure to Olaparib and X-ray radiation alone and in combination were assessed in UVW/NAT cells (c) 2 and (d) 24 hours following radiation exposure to 2Gy of X-ray radiation. The data was analysed using Volocity 3D Image Analysis Software and representative images for all treatment groups are shown in c and d. Data are means ±SD; experiments were carried out three times and a minimum of 50 cells were counted for each treatment in each individual experiment. Two-way ANOVA with Bonferroni post-hoc test was used to compare the means of single agent treated samples to untreated controls (blue stars), combination treated samples to 2Gy irradiated or Olaparib treated cells alone (table) and means of 2h sample to 24h samples (bridges). * denotes $p<0.05$, *** denotes $p<0.001$, **** denotes $p<0.0001$

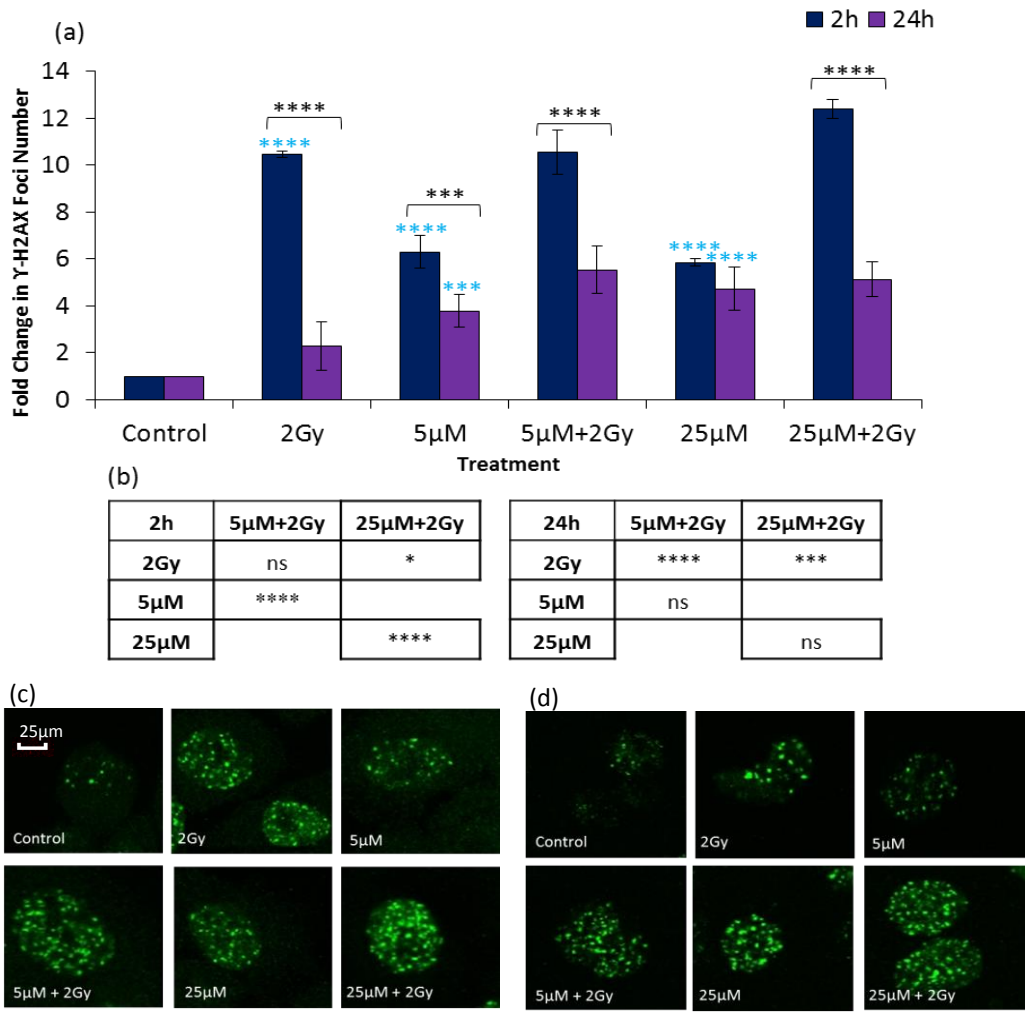

2h	5μM+2Gy	25μM+2Gy
2Gy	ns	*
5μM	****	
25μM		****

24h	5μM+2Gy	25μM+2Gy
2Gy	****	***
5μM	ns	
25μM		ns

Figure 5.8 The effect of Olaparib on radiation induced γ-H2AX foci formation and resolution in A375 cells.

(a) Formation and resolution of γ-H2AX foci following exposure to Olaparib and X-ray radiation alone and in combination were assessed in A375 cells (c) 2 and (d) 24 hours following radiation exposure to 2Gy of X-ray radiation. The data was analysed using Volocity 3D Image Analysis Software and representative images for all treatment groups are shown in c and d. Data are means ±SD; experiments were carried out three times and a minimum of 50 cells were counted for each treatment in each individual experiment. Two-way ANOVA with Bonferroni post-hoc test was used to compare the means of single agent treated samples to untreated controls (blue stars), combination treated samples to 2Gy irradiated or Olaparib treated cells alone (table) and means of 2h sample to 24h samples (bridges). * denotes $p<0.05$, *** denotes $p<0.001$, **** denotes $p<0.0001$

5.4.5 Analysis of cell cycle progression following exposure to Olaparib and X-ray radiation

5.4.5.1 Analysis of cell cycle progression following exposure to combinations of Olaparib and X-ray radiation in SK-N-BE(2c), UVW/NAT and A375 cells

The effect of combined Olaparib and X-ray radiation treatment on cell cycle distribution following 24 hour incubation in SK-N-BE(2c), UVW/NAT and A375 cells is presented in Figure 5.9. Olaparib had no significant effect on the progression of cells through the cell cycle in all cell lines investigated. However, X-ray radiation exposure induced an increase in the proportion of cells in the G2/M phase of the cell cycle compared to untreated control cells (40% increase ($p<0.0001$) in SK-N-BE(2c) cells, 34% increase ($p<0.05$) in UVW/NAT cells and a 24% increase ($p<0.001$) in A375 cells). Combination treatment increased the proportion of cells in the G2/M phase further in the presence of both 5 and 25μM Olaparib (23%, $p<0.01$ in both cases) compared to radiation alone in SK-N-BE(2c) cells and by 33% ($p<0.01$) and 34% ($p<0.01$) in UVW/NAT cells. This however was not the case in combination treated A375 cells, as despite a visible shift into G2/M phase, this was not significant compared to radiation exposed samples in this cell line. Taken together these results suggest that inhibition of PARP-1 may prevent the transition of cells into the mitotic phase of the cell cycle. However in A375 cells the radiosensitisation elicited by Olaparib may not be primarily induced via interference with G2/M checkpoint signalling.

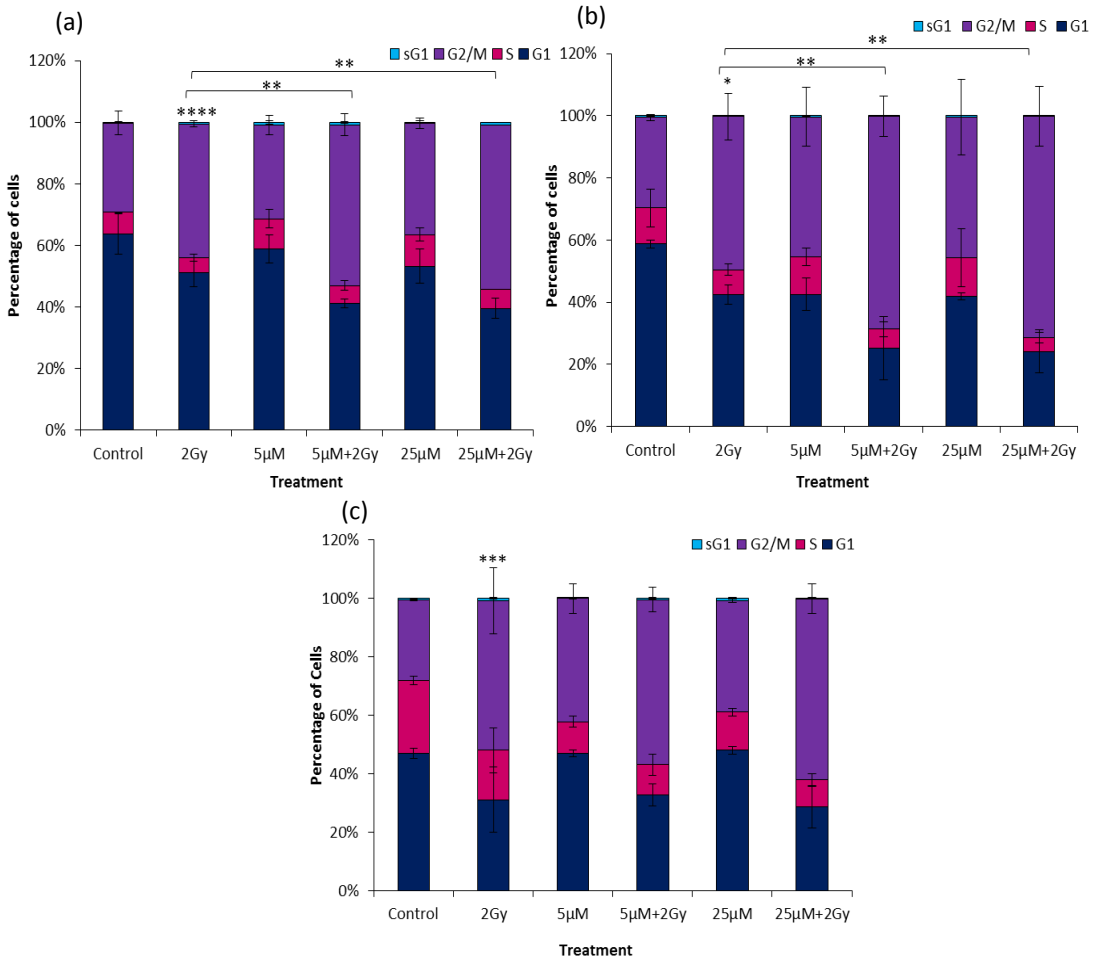

Figure 5.9 Cell cycle progression in (a) SK-N-BE(2c), (b) UVW/NAT and (c) A375 cells following exposure to Olaparib and X-ray radiation both as single agents and in combination.

The effects of X-ray radiation and Olaparib both alone and in combination were assessed in (a) SK-N-BE(2c), (b) UVW/NAT and (c) A375 cells 24 hours post-irradiation. Cells were pre-treated with Olaparib (5μM and 25μM) for 2 hours prior to radiation exposure. The data were analysed using BD FACSDiva Pro software. Data are means ±SD; experiments were carried out three times. Two-way ANOVA was used to compare the means of each cell cycle fraction in combination treated cells to radiation treated controls * denotes $p<0.05$, **denotes $p<0.01$, *** denotes $p<0.001$, **** denotes $p<0.0001$

5.5 Discussion

As previously discussed (section 1.1), a well-documented disadvantage associated with X-ray radiation treatment in patients is the high level of toxicity elicited to normal tissue that is traversed by the radiation beam during therapy. Therefore, the development of combination therapies that have the potential to promote tumour volume reduction without the need for increased radiation exposure would be of great benefit in cancer treatment schedules. In addition, due to the dose limiting toxicities associated with drug based cancer treatments it is also an advantage to select a drug concentration that produces little or no toxicity to cells when used as a single agent, yet provides radio-enhancement when combined with radiation. This creates a scenario with the potential to minimise any additional drug induced toxicities that may also produce undesirable side effects.

Olaparib is a previously approved drug initially designed for the treatment of BRCA1/2 deficient cancers [87]. It has EU approval for the treatment of platinum-sensitive relapsed BRCA-mutated (germline and/or somatic) high-grade serous epithelial ovarian, fallopian tube or primary peritoneal cancer and US approval as a fourth line therapy for the treatment of patients with germline BRCA-mutated advanced ovarian cancer [126]. However, more recently there has been increased interest in its potential use as a radiosensitising agent that may allow for the expansion of its use into a more diverse range of cancer types. Several of these studies have provided encouraging results demonstrating that Olaparib acts as a radiosensitiser both in BRCA1/2 deficient cells [81] but also in BRCA1/2 functional cells [89], [125], [127].

This chapter aimed to determine the cytotoxicity of Olaparib as a single agent and in combination with X-irradiation in SK-N-BE(2c), UVW/NAT and A375 cell lines. Additionally, the phenotypic data was underpinned with mechanistic insight by undertaking analysis of how combinations affected the cell cycle and components of SSB and DSB repair pathways, including γ-H2AX and PARP-1.

It was initially hypothesised that Olaparib would sensitise cancer cells to X-irradiation through reduction in the cellular capacity to repair radiation induced DNA breaks.

Early studies were undertaken to determine the single agent toxicity exerted by Olaparib for selection of optimal concentrations (1-25μM) for further combination studies. SK-N-BE(2c) cells exhibited little sensitivity to Olaparib as a single agent across the concentration range 0-50μM. Whereas UVW/NAT and A375 cells showed greater sensitivity to higher concentrations of Olaparib. This may suggest A375 and to a slightly lesser extent UVW/NAT cells have natural deficits in DSB repair making them more sensitive to inhibitors of SSB repair. Additionally it has previously been shown that cells with faster doubling times show increased sensitivity to Olaparib treatment [122], and studies within our group have highlighted that A375 cells have significantly shorter doubling times than UVW/NAT and SK-N-BE(2c) cells. As demonstrated in section 2.4.1, all cell lines displayed sensitivity to X-ray radiation in a dose dependent manner, albeit to different extents with SK-N-BE(2c) and UVW/NAT cells having a similar profile, however A375 exhibited a much lower IC_{50} value suggesting increased radiosensitivity.

Based on these data and the data presented in section 2.4.1, combination studies were carried out using a smaller range of Olaparib doses (0-25μM) and a lower more clinically relevant radiation dose (2Gy). It was demonstrated that Olaparib exerted radiosensitising properties in all cell lines, as indicated by the increase in DEF_{50} values compared to radiation controls (Figure 5.3 to 5.5). Furthermore, this effect is most successfully achieved using lower radiation doses, which is consistent with a study by Chalmers *et al.,* (2004) who demonstrate radiosensitising effects using low dose radiation with PARP-1 inhibitors in a range of human tumour and mouse fibroblast cell lines [122]. Olaparib has been previously shown to exert radiosensitising effects in other paediatric tumour cells such as ependymoma cells, medulloblastoma cells and glioblastoma cells. Van Vuurden *et al.,* (2011) studied 2 hour pre-treatment with low concentrations of Olaparib (1μM-8μM) in cell lines derived from the aforementioned cancers and observed a concentration dependent reduction in cell viability following radiation exposure (0-6Gy) in all cell lines. However, as is the case in this study, each cell line displayed variable degrees of sensitivity to the combination therapy [125]. In addition to this, Lee *et al.,* (2013) investigated the

effects of PARP-1 inhibition by Olaparib in two Ewing sarcoma cell lines and again showing that Olaparib treatment increased the sensitivity of these cell lines to radiation. However within the same study they also demonstrated that two non-Ewing sarcoma cell lines did not show enhanced radiosensitivity when treated with Olaparib and radiation [127]. Again this highlights the cell line-specific nature of treatment efficacy. The radiosensitising effect of Olaparib is thought to be due to the conversion of SSBs generated via inhibition of BER into DSBs which exhibit much greater levels of cytotoxicity and thus higher cell killing capacity [128].

PARP-1 binds rapidly and directly to both SSBs and DSBs to initiate DNA repair processes including BER and NHEJ. Therefore in order to further interrogate the signalling mechanisms by which Olaparib exerts its radiosensitising effect when combined with X-ray radiation, studies were carried out on PARP-1 activity levels. This study demonstrates that Olaparib as a single agent transiently inhibited PARP-1 activity in a dose dependent manner across all cell lines. Conversely, as shown in section 2.4.6 exposure to increasing doses of radiation resulted in a transient dose dependent increase in PARP-1 activity. Subsequently it was hypothesised that 2 hour pre-treatment with Olaparib would result in abrogation of radiation induced PARP-1 activity. Combination studies were therefore carried out and from the data presented in this chapter it was demonstrated that Olaparib pre-treatment did indeed result in abrogation of radiation induced PARP-1 activation, and that despite Olaparib alone having transient inhibitory effects, PARP-1 levels remained downregulated 24 hours after initial exposure to radiation. Senra *et al.,* (2011) utilised western blotting in order to demonstrate the inhibitory effect elicited by Olaparib on PARP-1 activity both in samples incubated with Olaparib alone and in samples exposed to radiation in addition to Olaparib in A549 lung cancer cells [89]. The sensitisation of cells to radiation elicited by Olaparib, coupled with the abrogation of radiation induced PARP-1 activity suggests that Olaparib is acting to inhibit DNA repair, possibly by BER, due to its fundamental role in SSB repair. γ-H2AX foci formation was therefore assessed to determine if Olaparib induced PARP-1 deficiency may result in an increase in as a result of SSB exacerbation resulting in DSB formation.

γ-H2AX foci are surrogate markers of DNA DSBs therefore allowing for further insight into whether Olaparib was generating DSBs in SK-N-BE(2c), UVW/NAT and A375 cell lines. γ-H2AX foci formation is one of the primary responses in cells following exposure to DNA damaging agents occurring rapidly after initial DSB generation [99]. Foci levels have previously been shown to increase in a linear fashion with DNA damage severity [89], [99] and this is in agreement with the data produced in this study which showed that upon increasing X-ray radiation dose, dose dependent increases in γ-H2AX foci levels were observed. In addition to this, γ-H2AX foci levels also peaked 1 to 2 hours following exposure to X-rays therefore also highlighting that this process occurred rapidly following damage and was down regulated across later time points as DNA DSBs were resolved. It was also demonstrated that incubation of cells with Olaparib alone resulted in an increase in γ-H2AX foci levels when compared to control levels both 2 hours and 24 hours following initial exposure, which is again in agreement with previous studies carried out where Olaparib was shown to increase foci levels as a single agent [89]. More specifically, Senra et al., (2011) demonstrate that Olaparib at a concentration of 1μM and 5μM resulted in a significant increase in γ-H2AX foci levels. Additionally, upon exposure to X-rays (1-4Gy) Olaparib further potentiated the radiation induced γ-H2AX foci formation. Bourton *et al.,* (2013) also demonstrated that lymphoblastoid cells also showed potentiation of foci formation upon incubation with Olaparib and γ-radiation over a 24 hour time period [81]. Taken together, the effect of Olaparib on PARP-1 activity and γ-H2AX foci formation suggests that Olaparib as a single agent could be acting to convert SSBs which are generated naturally within the cell during cell cycle progression into DSBs upon replication. Furthermore, Olaparib may be acting to increase the volume of radiation induced DSBs via conversion of radiation induced SSBs into DSBs.

To further analyse the basis for the radiosensitising effects of Olaparib in SK-N-BE(2c), UVW/NAT and A375 cells the effects of Olaparib and X-ray radiation were studied on cell cycle distribution. The data collected during this study demonstrated that no statistically significant changes in SK-N-BE(2c) cell cycle distribution occurred across

a 24 hour time course following exposure to Olaparib, however a small (but non-significant) increase in cells in G2/M phase was observed at the later time point. Olaparib also resulted in a decrease in the proportion of UVW/NAT and A375 cells in G1 and S phases of the cell cycle and again, no statistically significant increase in the proportion of G2/M phase cells was observed, but this was not statistically significant. This is consistent with a study carried out by Jelinic *et al.,* (2014) which showed that Olaparib treatment resulted in a reduction in S-phase cells and an increase in G2/M phase cells [129]. Additionally, as has been demonstrated in previous studies exposure of cells to radiation sources results in an accumulation of cells in G2/M phase of the cell cycle [93]. This is due to the generation of double strand breaks following ionisation of the DNA strands and the subsequent activation of cellular repair mechanisms, thus preventing the transition of cells into the mitotic phase of the cell cycle [130]. Based on the initial single agent studies it was hypothesised that combination studies, where cells were incubated with Olaparib for 2 hours prior to radiation exposure, would result in a significant accumulation of cells in G2/M phase of the cell cycle with a subsequent reduction in G1 and S phase portions. The data collected in this study, largely confirm this hypothesis with both SK-N-BE(2c) and UVW/NAT cells displaying a significantly higher G2/M phase portion than radiation treated cells. In contrast, A375 cells exhibited a marginal increase in G2/M phase cell number, but this was not statistically significant compared to radiation controls. The responses observed in SK-N-BE(2c) and UVW/NAT cells are similar to the results documented in a study by Karnak *et al.,* (2014) who reported an increase in G2 phase cells following exposure to Olaparib and X-ray radiation with a subsequent decrease in the G1 portion [128]. This suggests that, in SK-N-BE(2c) and UVW/NAT cells Olaparib may be functioning to inhibit SSB repair, resulting in conversion of these breaks to DSBs thus requiring HR repair processes to progress into the mitotic phase of the cell cycle which occur only at the G2/M checkpoint in the cell cycle when regions of homologous DNA are present [131].

Following combination treatment with Olaparib and X-irradiation, SK-N-BE(2c) and UVW/NAT cells demonstrate radiosensitisation via a reduction in clonogenic capacity

and an increase in the proportion of cells in G2/M phase of the cell cycle. A375 cells exhibit the highest degree of radiosensitivity, however they do not show an accumulation of cells in G2/M phase. This may suggest that the increased radiosensitivity apparent in A375 cells is as a result of cells transitioning into mitotic phases of the cell cycle whilst harbouring existing DNA damage leading to enhanced likelihood of mitotic catastrophe. Additionally, in all three cell lines examined, there is a prolonged reduction in radiation induced PARP-1 activity with a concomitant increase in γ-H2AX foci formation across the same 24 hour duration. This may also suggest that Olaparib acts as a radiosensitiser via a mechanism that is largely dependent on the generation of DSBs possibly via conversion of SSBs through inhibition of SSB repair by PARP-1.

Olaparib has demonstrated a strong potential clinical usefulness as a radiosensitiser when combined with X-ray radiation, however more work is necessary in order to determine whether the in vitro effects demonstrated in this study will translate to more robust tumour masses. Investigation of combination treatment in spheroids may be indicative of whether or not Olaparib and X-ray radiation treatment has the potential to be further analysed in mouse models, which are necessary before patient studies can arise.

This chapter investigated the potential radiosensitising effects of Olaparib in combination with external beam radiation. However, these results are not indicative of the potential effects of Olaparib on the efficacy of targeted radionuclides, due to differences in the toxicity profiles of different radiation types. This will be investigated further in the next chapter.

Chapter 6

The effect of PARP-1 inhibition using the small molecule inhibitor Olaparib on the sensitivity of cancer cells to [^{131}I]MIBG *in vitro.*

6.1 Introduction

As has been previously demonstrated in Chapter 5, Olaparib acts as an effective radiosensitiser in combination with X-ray radiation. However, the development of more targeted forms of radiation is at the forefront of cancer research, especially for the treatment of tumours expressing specific natural targeting moieties or those originating in complex areas of the body such as the brain and spinal cord. Previous studies have investigated the PARP-1 inhibitor PJ34 in combination with [^{131}I]MIBG and topotecan, and have demonstrated successful sensitisation of SK-N-BE(2c) and UVW/NAT cells [39].

The potential radiosensitising properties of Olaparib in combination with [^{131}I]MIBG were therefore investigated in neuroblastoma (which naturally over express the NAT) and glioma (a tumour of the brain and spine) cell lines. In order to assess the potential radiation enhancing effects of Olaparib in combination with [^{131}I]MIBG it was first necessary to examine the cytotoxic effect of each individual agent by application of clonogenic survival assays.

6.2 Aims

The aims of this study were to assess clonogenic cell survival following treatment with [^{131}I]MIBG and Olaparib as single agents in SK-N-BE(2c) and UVW/NAT cell lines, and the radiosensitising effects of Olaparib in combination with [^{131}I]MIBG in the above cell lines. The mechanistic effects of combination therapy were also interrogated by assessment of cell cycle progression and DNA damage repair kinetics including ATM kinase activity, γ-H2AX foci formation and RAD51 activity.

6.3 Materials and Methods

6.3.1 Cell Lines and Culture conditions

SK-N-BE(2c) and UVW/NAT cells were cultured as described in section 2.3.1

6.3.2 Drug Preparation and Treatment of cells with Olaparib and [^{131}I]MIBG

Olaparib was kindly provided by AstraZeneca (Macclesfield, UK) and prepared and stored as described in Section 5.3.2.

For single agent treatment studies cell medium was replaced with 1ml of fresh medium prior to treatment with [^{131}I]MIBG or 1ml of fresh medium containing a range of concentrations of Olaparib (0-25μM). For combination treatments cell medium was replaced with 1ml of fresh medium prior to incubation with Olaparib for 2 hours before [^{131}I]MIBG exposure for 2 hours. Cells were then washed 3 times with PBS before re-addition of Olaparib and further 24 hour incubation.

6.3.3 Clonogenic Cell Survival Assay

Clonogenic assays were performed as described in section 2.3.3 to determine the effect of Olaparib and [^{131}I]MIBG as single agents and in combination on the clonogenic capacity of UVW/NAT cells.

6.3.4 Soft Agar Cell Survival Assay

Soft agar cell survival assays were performed as described in section 2.3.4 on SK-N-BE(2c) cells which fail to form discrete colonies in 2D cultures.

6.3.5 Assessing the efficacy of combination therapies

To assess whether the cytotoxicity of combinations of X-ray radiation and the DNA damage repair inhibiting compound Olaparib was superior to each treatment type alone, clonogenic survival data were analysed using the linear-quadratic

mathematical model as described in section 3.3.5.2. DEF values were calculated as described in section 3.3.5.2.2.

6.3.6 PARP Assay

The assessment of PARP activity was undertaken as described in section 2.3.8 using a standard PARP assay kit according to the manufacturer's instructions (Trevigen, Gaithersburg, MD).

6.3.7 Cell Cycle Analysis

The progression of cells through the cell cycle was investigated as described in section 2.3.5 to assess if Olaparib and X-ray radiation alone and in combination caused an abrogation to the normal cycling of cells.

6.3.8 H2AX Foci Staining

γ-H2AX was used as a biochemical marker of the magnitude and resolution of DNA double stranded breaks in response to Olaparib and X-ray radiation. H2AX foci staining and quantification was carried out as described in section 2.3.6.

6.3.9 Statistical Analysis

Statistical analysis was carried out using GraphPad Prism version 6.05 (GraphPad Software Inc, San Diego). One-way ANOVA was used to determine statistical significance in single agent dose response cell survival assays. Two-way ANOVA with Bonferroni post-hoc test was used to determine if combination treated samples were significantly different compared to radiation treated samples. In both cases p values <0.05 were reported as statistically significant.

6.4 Results

The data collected from clonogenic assays performed in section 2.4.1were used to determine the toxic effects of Olaparib and [^{131}I]MIBG as single agents on SK-N-BE(2c) and UVW/NAT cell lines. The results from this series of investigations was then used to determine the radiation dose range and drug concentrations to be utilised in further combination studies.

6.4.1 Clonogenic cell survival following treatment with the combination of Olaparib and [^{131}I]MIBG.

Clonogenic survival assays were performed to determine the radiosensitising potential of Olaparib on cells exposed for 24 hours to [^{131}I]MIBG. SK-N-BE(2c) and UVW/NAT cells were treated for 2 hours with a range of Olaparib concentrations (1-25μM) prior to irradiation with 1MBq, 2MBq or 3MBq of [^{131}I]MIBG and incubated over a 24 hour period. To evaluate if Olaparib sensitised cells to [^{131}I]MIBG the resultant data were fitted to the linear-quadratic mathematical model and α, β, IC_{50} and DEF_{50} values determined.

6.4.1.1 The effect of Olaparib in combination with [^{131}I]MIBG on the clonogenic capacity of SK-N-BE(2c) and UVW/NAT cells.

Treatment of cells with combinations of Olaparib and [^{131}I]MIBG suggested that Olaparib induced a radiosensitising effect in SK-N-BE(2c) and UVW/NAT cells (Figure 6.1a). In SK-N-BE(2c) cells, IC_{50} values decreased from 2.73MBq in control samples treated with [^{131}I]MIBG alone to 1.86MBq, 1.53MBq and 1.30MBq in cells treated with 1μM, 5μM and 25μM of Olaparib respectively (Figure 6.1b). DEF_{50} values increased in a dose dependent manner across the Olaparib concentration range (1-25μM) from 1.00 in [^{131}I]MIBG control samples to 1.47, 1.78 and 2.10 upon addition of Olaparib, with the greatest DEF_{50} achieved in combination with 25μM of Olaparib. Likewise in UVW/NAT cells, IC_{50} values decreased from 1.99MBq in control samples

treated with [^{131}I]MIBG alone to 1.25MBq and 0.75MBq in cells treated with 5µM and 25µM of Olaparib respectively (Figure 6.2b). However, cells treated with 1µM of Olaparib in combination with [^{131}I]MIBG showed no change in IC_{50} value, suggesting that the lowest concentration of Olaparib did not act in a radiopotentiating manner. As is expected based on the aforementioned IC_{50} values, DEF_{50} values for combinations utilising the lowest Olaparib concentration also remained unchanged, however upon increasing Olaparib concentration DEF_{50} values increased from 1.00 in radiation control samples to 1.60 and 2.71 in 5µM and 25µM samples respectively.

To determine whether the clonogenic capacity of the cells following [^{131}I]MIBG treatment was enhanced by addition of Olaparib the data were analysed using Two-way ANOVA with Bonferroni post-hoc analysis (Figure 6.1c and 6.2c). This analysis confirmed that significant radiosensitising effects were observed at all Olaparib concentrations and [^{131}I]MIBG doses in SK-N-BE(2c) cells, indicating that Olaparib is exerting radiosensitising properties at all administered concentrations (Figure 6.1b), however in UVW/NAT cells significant radiosensitisation was only observed following addition of 5 and 25µM concentrations of Olaparib across the 1-3MBq [^{131}I]MIBG dose range. This suggests that despite Olaparib inducing a radiosensitising effect in UVW/NAT cells, unlike SK-N-BE(2c) cells this radiosensitisation was dependent on drug concentration and [^{131}I]MIBG dose.

.

(a)

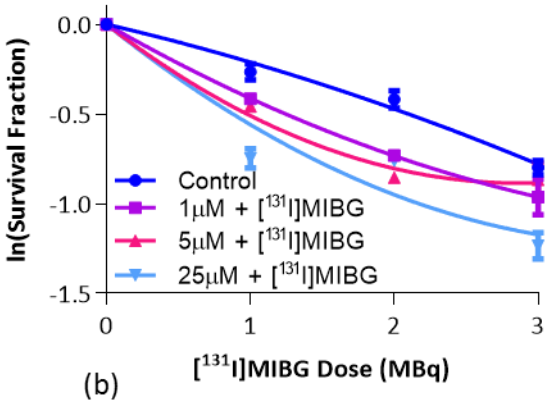

(b)

	Control	1μM	5μM	25μM
α	0.1871	0.4583	0.6163	0.6425
β	0.02428	-0.04588	-0.1073	-0.084
IC_{50}	2.73	1.86	1.53	1.30
DEF_{50}	1.00	1.47	1.78	2.10

(c)

	1MBq		2MBq		3MBq
1μM+1MBq	**	1μM+2MBq	***	1μM+3MBq	***
5μM+1MBq	***	5μM+2MBq	****	5μM+3MBq	**
25μM+1MBq	****	25μM+2MBq	***	25μM+3MBq	****

Figure 6.1 Clonogenic capacity of SK-N-BE(2c) cells treated with Olaparib and [131I]MIBG.

(a) Clonogenic capacity of SK-N-BE(2c) cells was determined 24 hours post treatment with [131I]MIBG in the presence or absence of increasing Olaparib concentrations (1-25μM). Cells were incubated with Olaparib for 2 hours prior to [131I]MIBG exposure. (b) The data were fitted to the linear-quadratic equation using GraphPad Prism version 6.05 and α, β, IC_{50} and DEF_{50} calculated across all treatment groups. Data are presented as natural logarithms of survival fraction means normalised the mean survival fraction of Olaparib only treated cells ±SD; experiments were carried out three times in triplicate. (c) Two-way ANOVA was used to compare the means of combination treatments to those of cells exposed to [131I]MIBG alone. ** denotes $p<0.01$, *** denotes $p<0.001$, **** denotes $p<0.0001$

(a)

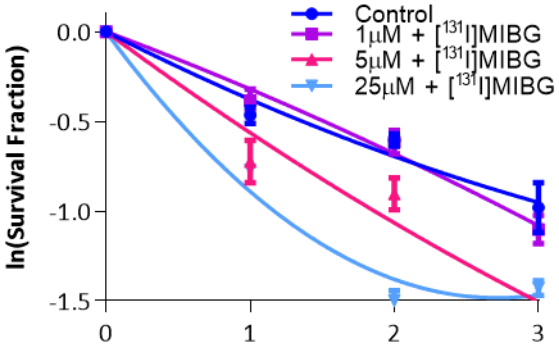

(b) [^{131}I]MIBG Dose (MBq)

	Control	1μM	5μM	25μM
α	-0.408	-0.3002	-0.5936	-1.09
β	0.03034	-0.01998	-0.03067	0.2004
IC_{50}	1.99	2.03	1.25	0.74
DEF_{50}	1.00	0.98	1.60	2.71

(c)

	1MBq		2MBq		3MBq
1μM+1MBq	ns	1μM+2MBq	ns	1μM+3MBq	ns
5μM+1MBq	*	5μM+2MBq	*	5μM+3MBq	ns
25μM+1MBq	****	25μM+2MBq	***	25μM+3MBq	**

Figure 6.2 Clonogenic capacity of UVW/NAT cells treated with Olaparib and [^{131}I]MIBG.

(a) Clonogenic capacity of UVW/NAT cells was determined 24 hours post treatment with [^{131}I]MIBG in the presence or absence of increasing Olaparib concentrations (1-25μM). Cells were incubated with Olaparib for 2 hours prior to [^{131}I]MIBG exposure. (b) The data were fitted to the linear-quadratic equation using GraphPad Prism version 6.05 and α, β, IC_{50} and DEF_{50} calculated across all treatment groups. Data are presented as natural logarithms of survival fraction means normalised the mean survival fraction of Olaparib only treated cells ±SD; experiments were carried out three times in triplicate. (c) Two-way ANOVA was used to compare the means of combination treatments to those of cells exposed to [^{131}I]MIBG alone. * denotes $p<0.05$, ** denotes $p<0.01$, *** denotes $p<0.001$, ****denotes $p<0.0001$

6.4.2 Analysis of PARP-1 activity levels following treatment with Olaparib and [131I]MIBG

6.4.2.1 Analysis of PARP-1 activity levels following treatment with combinations of Olaparib and [^{131}I]MIBG in SK-N-BE(2c) and UVW/NAT cells

PARP-1 activity levels following treatment with Olaparib followed by subsequent treatment with 2MBq of [^{131}I]MIBG is shown in Figure 6.3. Olaparib as a single agent at concentrations of 5 and 25µM resulted in a significant reduction in PARP-1 activity 2 hours after treatment in both cell lines (33%±0.06 ($p<0.05$) and 56%±0.01 ($p<0.0001$) in SK-N-BE(2c) cells and 31%±0.06 and ±30%±0.1 ($p<0.01$) in UVW/NAT cells respectively). UVW/NAT cells also exhibit a significant reduction in PARP-1 activity 24 hours after Olaparib treatment with 5µM and 25µM concentrations (58%±0.1 and 40%±0.008 ($p<0.0001$) respectively), however this is not the case in SK-N-BE(2c) cells. Treatment with 2MBq of [^{131}I]MIBG resulted in no significant change in PARP-1 activity 2 hours post-treatment in SK-N-BE(2c) cells, however UVW/NAT cells demonstrate a 63%±0.4 increase in PARP-1 activity 2 hours post-treatment. SK-N-BE(2c) cells treated with 2MBq in combination with 5 and 25µM Olaparib also exhibited no significant change in PARP-1 activity levels 2 hours post treatment in SK-N-BE(2c) cells when compared to 2MBq alone. However, UVW/NAT cells treated with 2MBq in combination with 5 and 25µM Olaparib exhibited a significant reduction (44%±0.04 ($p<0.001$) and 50%±0.1 ($p<0.0001$) respectively) in PARP-1 activity levels 2 hours post treatment when compared to 2MBq alone. Conversely, 24 hours after initial treatment with 2MBq of [^{131}I]MIBG a 53%±0.2 increase ($p<0.0001$) in PARP-1 activity levels was observed in SK-N-BE(2c) cells (39%±0.2 higher than 2 hour samples) and a 57%±0.3 increase ($p<0.0001$) in PARP-1 activity levels was observed in UVW/NAT cells compared to untreated controls (31%±0.2 higher than samples exposed for 2 hours).

Despite Olaparib showing no significant effect on PARP-1 activity 24 hours after initial treatment in SK-N-BE(2c) cells, combination treated samples remained PARP-1

abrogated by 58%±0.2 ($p<0.0001$) and 70%±0.1 ($p<0.0001$) compared to [^{131}I]MIBG treated samples alone. UVW/NAT combination treated samples also remained PARP-1 abrogated by 24 hours after initial treatment compared to 2MBq treated samples (49%±0.1 and 42%±0.07 respectively, $p<0.0001$ in both cases), however despite this samples exposed to 25µM Olaparib in combination with 2MBq for 24 hours had significantly higher (41%±0.07) PARP-1 activity levels than those exposed for 2 hours ($p<0.01$).

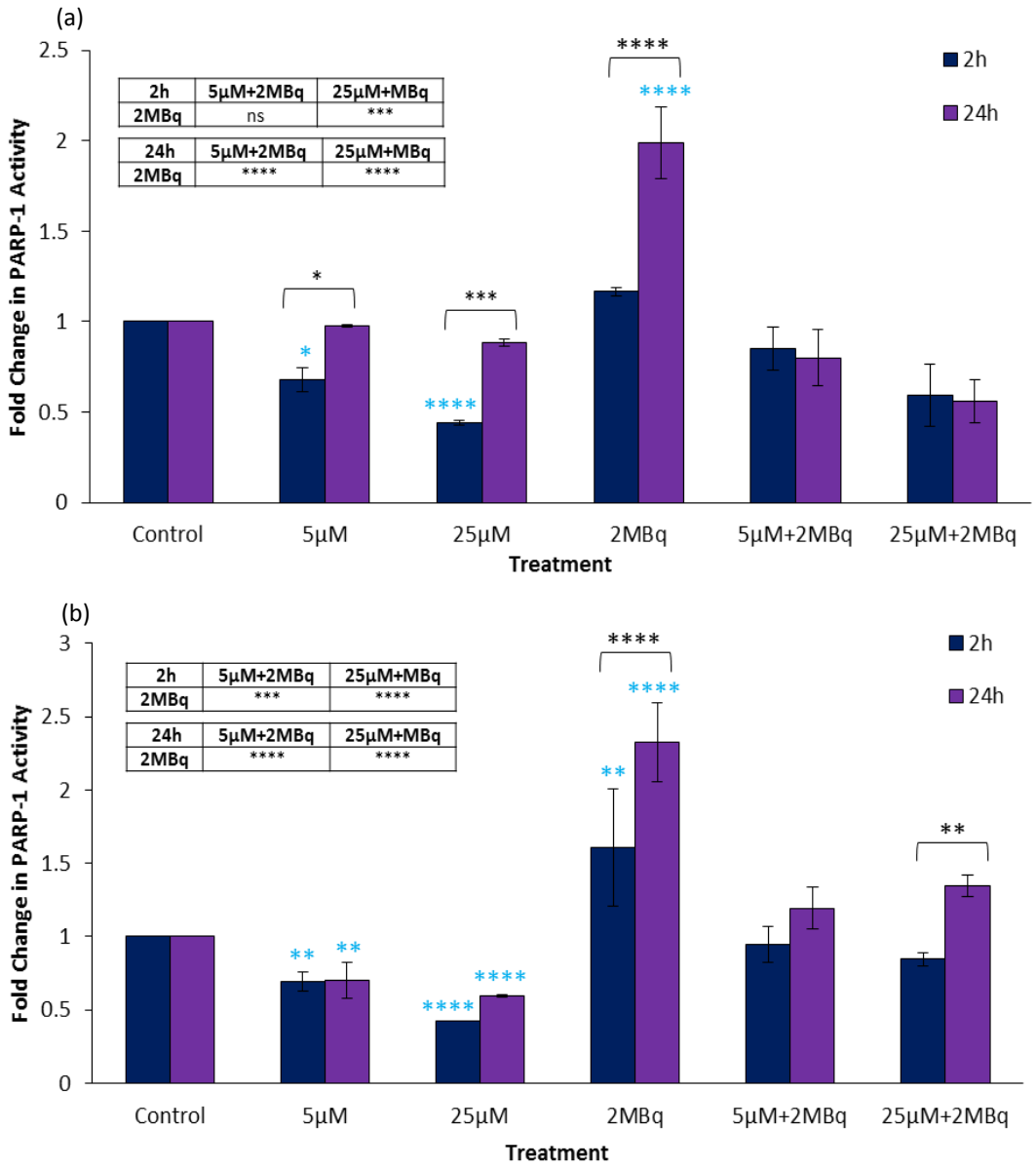

Figure 6.3 PARP-1 activity following treatment with combinations of Olaparib and [^{131}I]MIBG in (a) SK-N-BE(2c) and (b) UVW/NAT cells.

The effects of combination therapy utilising [^{131}I]MIBG and Olaparib were assessed in (a) SK-N-BE(2c) and (b) UVW/NAT cells at 2 hours and 24 hours post-irradiation. Cells were incubated with Olaparib for 2 hours prior to irradiation. Data are means ±SD; experiments were carried out three times in triplicate. Two-way ANOVA with Bonferroni post-hoc test was used to compare the means of single agent treated samples to untreated controls (blue stars), combination samples to radiation treated samples (data shown in table) and means of samples at both time points (shown on graph). ** denotes p<0.01, *** denotes p<0.001, **** denotes p<0.0001

6.4.3 Investigation of γ-H2AX foci formation following Olaparib and [^{131}I]MIBG treatment.

It is well known that PARP 1 inhibition compromises the repair of DNA SSBs and consequently increased DSBs following treatment of cells with radiation. To determine if Olaparib in combination with [^{131}I]MIBG increased DSBs in this study γ-H2AX foci levels were assessed.

6.4.3.1 The effect of Olaparib on [^{131}I]MIBG induced γ-H2AX foci levels in SK-N-BE(2c) and UVW/NAT cells.

The effect of Olaparib in combination with [^{131}I]MIBG on γ-H2AX foci levels in SK-N-BE(2c) and UVW/NAT cells 2 and 24 hours post irradiation is shown in Figures 6.4 and 6.5. Olaparib at concentrations of 5 and 25μM increased γ-H2AX foci levels by 44%±0.4 (ns) and 69%±0.1 ($p<0.0001$) respectively 2 hours post treatment and 69%±0.3 ($p<0.001$) and 70%±0.3 ($p<0.0001$) respectively 24 hours post treatment in SK-N-BE(2c) cells. Similarly, in UVW/NAT cells, at concentrations of 5 and 25μM γ-H2AX foci levels increased by 69%±0.4 ($p<0.0001$) and 62%±0.4 ($p<0.0001$) respectively 2 hours post initial treatment and 84%±1.0 ($p<0.05$) and 87%±0.5 ($p<0.0001$) 24 hours post initial treatment compared to untreated controls.

Treatment with 2MBq of [^{131}I]MIBG resulted in a significant elevation of γ-H2AX levels both 2 hours and 24 hours post treatment in both cell lines, with SK-N-BE(2c) cells demonstrating 85%±0.8 ($p<0.0001$) and 87%±0.4 ($p<0.0001$) increases at 2 and 24 hours respectively and UVW/NAT cells showing 85%±0.7 ($p<0.0001$) and 93%±0.6 ($p<0.0001$) increases respectively. In combination treated samples γ-H2AX foci levels remained unchanged compared to 2MBq treated samples 2 hours post treatment in both cell lines, however 24 hours after initial incubation with combination treatment γ-H2AX foci levels increased by 12%±0.08 ($p<0.05$) and 20%±0.6 ($p<0.001$) respectively in SK-N-BE(2c) cells and 20%±1.6 and 20%±3.0 ($p<0.05$) respectively in UVW/NAT cells when compared to 2MBq treated samples. However as Olaparib as a single agent increased γ-H2AX foci levels, to determine if the effect of combination treatment on γ-H2AX foci levels was additive, statistical analysis was also performed

on combination data normalised to Olaparib alone. This demonstrated that the effect of combination treatment was additive, with cells exhibiting no significant further increase in γ-H2AX foci levels compared to the increase exerted by each single agent alone. This suggests that despite PARP-1 inhibition by Olaparib possibly acting to increase the conversion of SSBs into DSBs in non-irradiated samples, [^{131}I]MIBG may directly induce DSBs and therefore Olaparib is demonstrating no additional exacerbation of these.

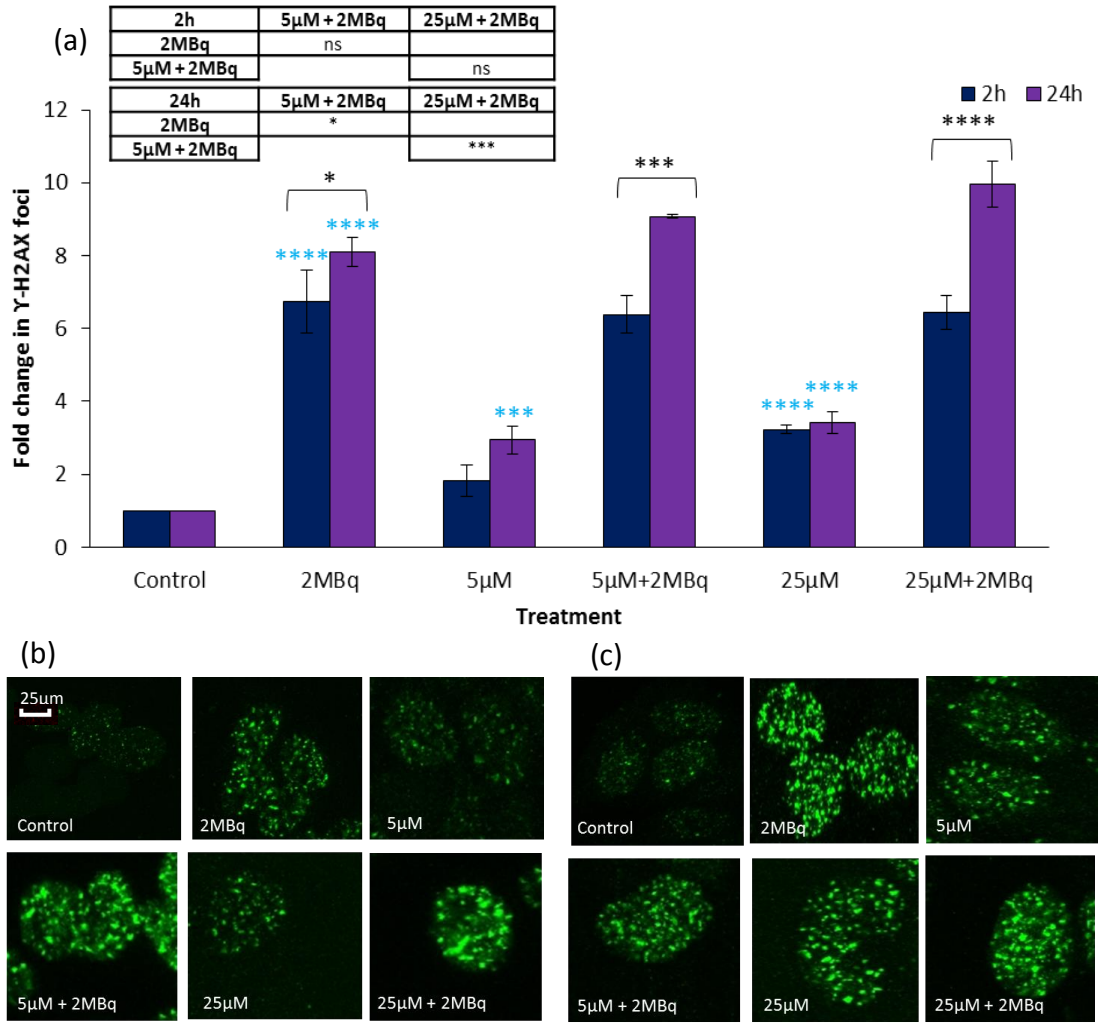

Figure 6.4 The effect of Olaparib on [^{131}I]MIBG induced γ-H2AX foci formation and resolution in SK-N-BE(2c) cells.

(a) Formation and resolution of γ-H2AX foci following treatment with Olaparib and [^{131}I]MIBG alone and in combination were assessed in SK-N-BE(2c) cells (b) 2 and (c) 24 hours following radiation exposure to 2MBq of [^{131}I]MIBG. The data was analysed using Volocity 3D Image Analysis Software (b and c). Data are means ±SD; experiments were carried out three times and a minimum of 50 cells were counted for each treatment in each individual experiment. Two-way ANOVA with Bonferroni post-hoc test was used to compare the means of single agent treated samples to untreated controls (blue stars), combination treated samples to 2MBq irradiated samples 2 and 24h post irradiation (table) and means of 2h sample to 24h samples (bridges). * denotes $p<0.05$, *** denotes $p<0.001$, **** denotes $p<0.0001$

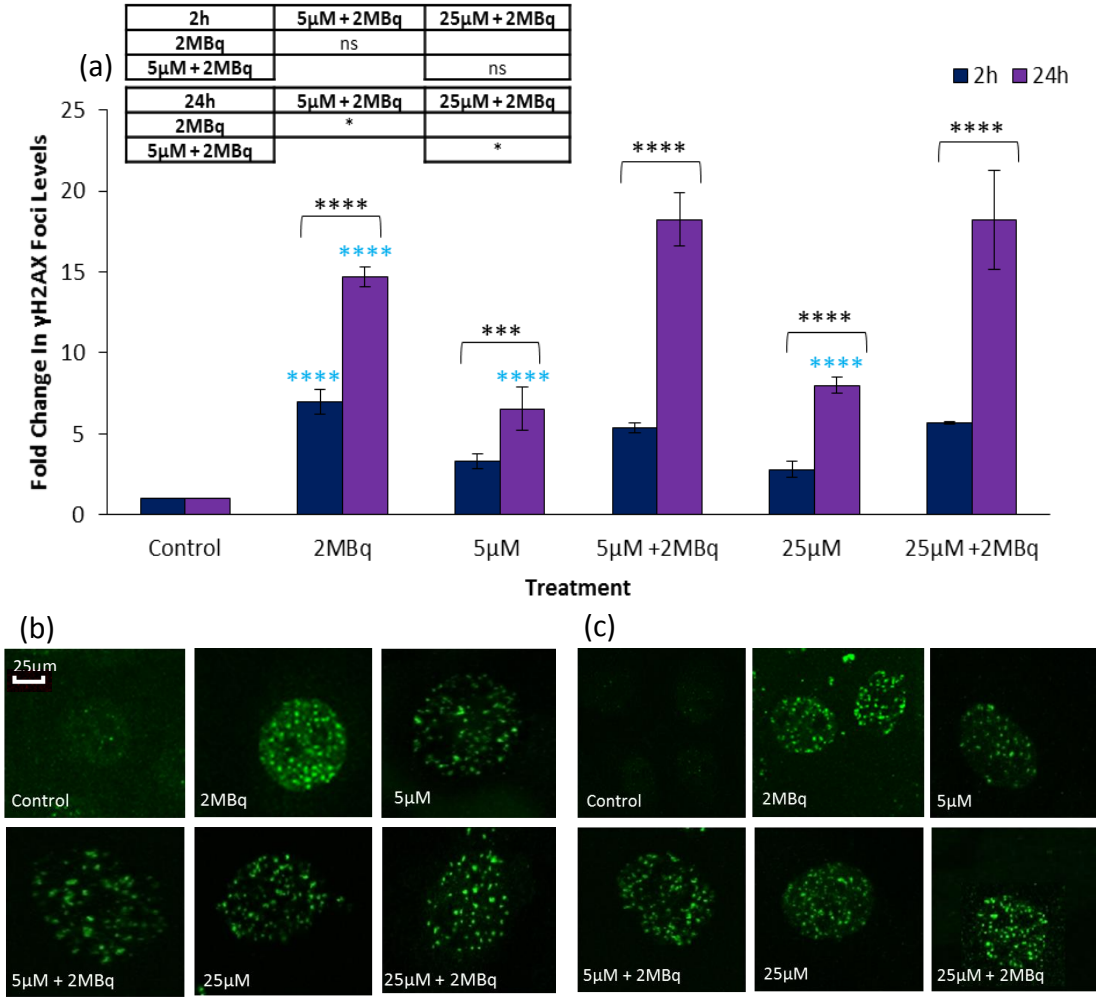

Figure 6.5 The effect of Olaparib on [^{131}I]MIBG induced γ-H2AX foci formation and resolution in UVW/NAT cells.

(a) Formation and resolution of γ-H2AX foci following treatment with Olaparib and [^{131}I]MIBG alone and in combination were assessed in UVW/NAT cells (b) 2 and (c) 24 hours following radiation exposure to 2MBq of [^{131}I]MIBG. The data was analysed using Volocity 3D Image Analysis Software (b and c). Data are means ±SD; experiments were carried out three times and a minimum of 50 cells were counted for each treatment in each individual experiment. Two-way ANOVA with Bonferroni post-hoc test was used to compare the means of single agent treated samples to untreated controls (blue stars), combination treated samples to 2MBq irradiated samples 2 and 24h post irradiation (table) and means of 2h sample to 24h samples (bridges). * denotes $p<0.05$, *** denotes $p<0.001$, **** denotes $p<0.0001$

6.4.4.1 Analysis of cell cycle progression following treatment with combinations of Olaparib and [^{131}I]MIBG in SK-N-BE(2c) cells

The effect of combined Olaparib and [^{131}I]MIBG treatment on cell cycle distribution following 24 hour incubation in SK-N-BE(2c) cells is presented in Figure 6.6. Olaparib had no significant effect on the progression of cells through the cell cycle in all cell lines investigated. However, a statistically significant increase in the proportion of cells in G2/M phase of the cell cycle is observed following treatment with 2MBq of [^{131}I]MIBG in both SK-N-BE(2c) (31% increase, $p<0.01$) and UVW/NAT cells (35% increase, $p<0.0001$).

Combination treatment increased the proportion of cells in the G2/M phase further in the presence of both 5 and 25µM Olaparib (5%, $p<0.01$ and 23 %, $p<0.0001$) compared to [^{131}I]MIBG alone in SK-N-BE(2c) cells and by 19% ($p<0.0001$) and 16% ($p<0.0001$) in UVW/NAT cells. Taken together these results suggest that inhibition of PARP-1 may prevent the transition of cells into the mitotic phase of the cell cycle.

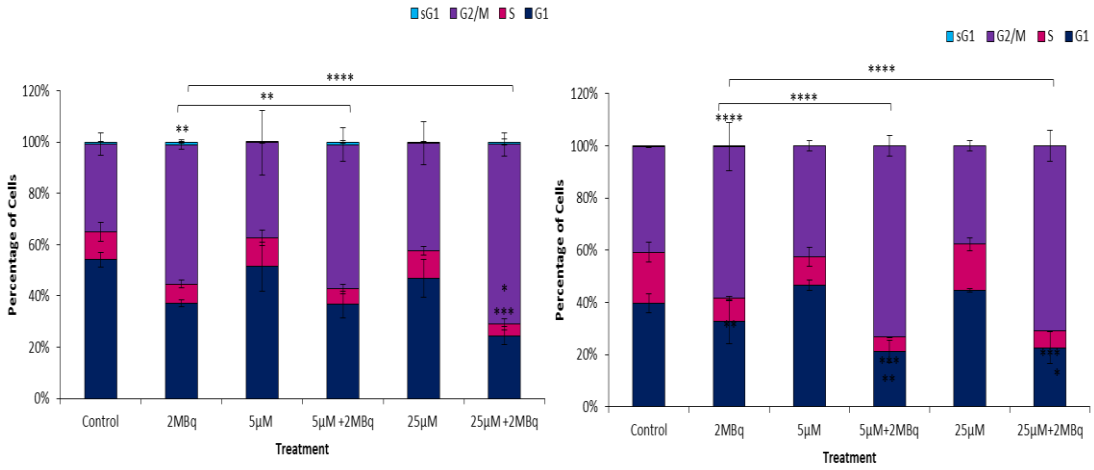

Figure 6.6 SK-N-BE(2c) cell cycle progression following treatment with Olaparib in combination with [^{131}I]MIBG.

Cell cycle progression in SK-N-BE(2c) cells was assessed 24 hours post incubation with Olaparib and [^{131}I]MIBG. SK-N-BE(2c) cells were pre-treated with Olaparib (5µM and 25µM) for 2 hours prior to radiation exposure. The data were analysed using BD FACSDiva. Data are means ±SD; experiments were carried out three times. Two-way ANOVA was used to compare the means of the G2/M fraction of combination treated cells to X-ray radiation treated controls **denotes $p<0.01$, **** denotes $p<0.0001$

6.5 Discussion

As discussed previously (section 1.1), there is extensive evidence supporting the problems associated with the off target toxicities of X-ray radiation treatment in patients. As a result, the development of more specific and targeted forms of radiation therapy have been at the fore front of cancer research for many years. This study interrogates the possibility of using [^{131}I]MIBG, which has a proven efficacy in delivering radiation to tumour sites via exploitation of specific uptake mechanisms [44], [121], in combination with Olaparib to elicit radio-potentiating effects. In turn this is hypothesised to promote tumour volume reduction without the need for increased radiation exposure and would therefore be of great benefit in cancer treatment schedules.

As discussed in section 5.1, Olaparib was originally designed for the treatment of BRCA1/2 deficient cancers [87]. However, many studies have now been conducted using this compound in combination with X-rays and other forms of ionising radiation, several of which have provided encouraging results demonstrating that Olaparib acts as a radiosensitiser both in BRCA1/2 deficient cells [81] and in BRCA1/2 functional cells [89], [125], [127]. This therefore provided a positive basis for the investigation of Olaparib in combination with [^{131}I]MIBG to determine if the efficacy already established both in the present study and others of exposure to Olaparib and X-ray radiation translates to more targeted forms of radiation.

Within this chapter, the aims of the study were to determine the cytotoxicity of Olaparib and [^{131}I]MIBG in combination on SK-N-BE(2c) and UVW/NAT cell lines. Additionally, the phenotypic data was underpinned with mechanistic insight by undertaking analysis of how combinations affected the cell cycle and components of SSB and DSB repair pathways, including γ-H2AX and PARP-1.

It was initially hypothesised that Olaparib would sensitise cancer cells to both X-irradiation and [^{131}I]MIBG through reduction in the cell capacity to repair DNA breaks. Initial studies were carried out in sections 2.4.1.2 and 5.4.1.1 to determine single agent toxicity of [^{131}I]MIBG and Olaparib respectively for determination of appropriate concentrations for future studies.

After determination of initial toxicity levels associated with Olaparib and [^{131}I]MIBG, appropriate concentration ranges were established for combination studies, which seek to reduce the exposure of normal tissue to the damaging effects associated with chemo-radiotherapy. These subsequent combination studies were carried out using a smaller range of Olaparib concentrations (1-25μM) and low [^{131}I]MIBG doses (1-3MBq). These results demonstrate that Olaparib exhibited a significant radiosensitising effect when combined with [^{131}I]MIBG and that this effect was shown to be further enhanced upon increasing [^{131}I]MIBG dose, however radiosensitisation was irrespective of increasing Olaparib concentration. Currently there are no other studies providing evidence to directly support the findings presented here, however a study carried out by McCluskey *et al.,* (2012) demonstrated that PARP-1 inhibition using another inhibitor, PJ34, resulted in the enhancement of [^{131}I]MIBG/topotecan cytotoxicity in both SK-N-BE(2c) and UVW/NAT cells, with supradditive toxicity demonstrated. In addition, Chalmers *et al.,* (2004) investigated PARP-1 inhibition using very low doses of chemical inhibition in combination with low dose radiation. This study demonstrated that mouse fibroblast and human tumour cells show increased sensitivity to low dose radiation when treated with PARP-1 inhibitors and that this effect may be enhanced by faster cell doubling times [122]. Therefore to further analyse the basis for the radiosensitising effects of Olaparib in SK-N-BE(2c) and UVW/NAT cells the effects of Olaparib and [^{131}I]MIBG were studied on PARP-1 activity, γ-H2AX foci levels and cell cycle distribution.

PARP-1 binds rapidly and directly to both SSBs and DSBs to initiate DNA repair processes including BER and NHEJ [132]. Therefore in order to further interrogate the signalling mechanisms by which Olaparib exerts its radiosensitising effect when combined with X-ray radiation, studies were carried out on PARP-1 activity levels.

As previously discussed (section 5.4.1), Olaparib as a single agent transiently inhibited PARP-1 activity in a dose dependent manner across all cell lines and conversely treatment with increasing doses of [^{131}I]MIBG resulted in a dose and time dependent increase in PARP-1 activity. Subsequently it was hypothesised that 2 hour pre-treatment with Olaparib would result in abrogation of PARP-1 activity following

treatment with [^{131}I]MIBG. As was hypothesised, exposure of cells to combinations of Olaparib and [^{131}I]MIBG resulted in significant abrogation of [^{131}I]MIBG induced PARP-1 activation both 2 hours and 24 hours following initial treatment, however PARP-1 levels were more significantly reduced 24 hours after initial treatment with [^{131}I]MIBG. As with Olaparib and X-irradiation this may suggest that Olaparib induced PARP-1 deficiency results in an increase in DSBs as a result of SSB exacerbation resulting in DSB formation. McCluskey *et al.,* (2012) assessed PARP-1 activity following treatment with PJ34 (PARP-1 inhibitor) and [^{131}I]MIBG/topotecan, and demonstrated that there was a reduction in PARP-1 activity in both UVW/NAT and SK-N-BE(2c) cells 24 hours after initial treatment, however, in UVW/NAT cells this effect was dependent on scheduling of PJ34. The concentrations of PJ34 utilised in this study (29-31.97μM) were slightly higher than those in the current study, however, it does support the findings in the current study which also demonstrate reduced PARP-1 activity 24 hours after initial combination treatment and may indicative that Olaparib is a more potent PARP-1 inhibitor than PJ34.

To further interrogate the signalling mechanisms by which Olaparib exerts its radiosensitising effect when combined with [^{131}I]MIBG, studies were carried out on γ-H2AX foci levels. γ-H2AX foci are surrogate markers of DNA DSBs therefore allowing for further insight into whether Olaparib was generating DSBs in SK-N-BE(2c) and UVW/NAT cell lines. γ-H2AX foci formation is one of the primary responses in cells following exposure to DNA damaging agents occurring rapidly after initial DSB generation [99]. Foci levels have previously been shown to increase in a linear fashion with DNA damage severity [89], [99] and this is in agreement with the data produced in the present study, which showed that upon increasing [^{131}I]MIBG dose, dose dependent increases in γ-H2AX foci levels were observed. It was therefore hypothesised that an increase in γ-H2AX foci levels would be observed in combination treatment groups which had been subjected to impaired SSB repair by Olaparib.

In this study, γ-H2AX foci levels peaked 24 hours following treatment with [^{131}I]MIBG indicating that although this process occurs rapidly following damage by the more conventional X-rays and is down regulated across later time points as DNA repair

processes are activated, [^{131}I]MIBG is likely to be eliciting a constant stream of damaging effects upon ^{131}I decay resulting in continued upregulation of DNA repair pathways. It was also demonstrated that incubation of cells with Olaparib alone resulted in an increase in γ-H2AX foci levels when compared to control levels both 2 hours and 24 hours following initial treatment, which is again in agreement with previous studies carried out whereupon Olaparib is shown to increase foci levels both as a single agent and in combination with radiation [89]. This again therefore suggests that Olaparib is acting to convert SSBs, which are generated naturally within the cell during cell cycle progression into DSBs that require more extensive and precise repair generally initiated by γ-H2AX foci formation. Furthermore, combination studies demonstrated that treatment of cells with Olaparib in combination with [^{131}I]MIBG resulted in an increase in γ-H2AX foci formation, however when compared to [^{131}I]MIBG treated samples alone only samples exposed to the combination for 24 hours displayed significantly higher γ-H2AX foci levels. This is further indicative of an increase in the generation of DSBs in the DNA following extended incubation times.

Taken together, the effect of Olaparib on PARP-1 activity and γ-H2AX foci formation suggests that Olaparib as a single agent could be acting to convert SSBs, which are generated naturally within the cell during cell cycle progression into DSBs upon replication. Furthermore, Olaparib may be acting to increase the volume of radiation induced DSBs via conversion of radiation induced SSBs into DSBs.

To further analyse the basis for the radiosensitising effects of Olaparib in SK-N-BE(2c) and UVW/NAT cells the effects of Olaparib and X-ray radiation were studied on cell cycle distribution. No statistically significant changes in SK-N-BE(2c) cell cycle distribution occur across a 24 hour time course following exposure to Olaparib. An increase in the proportion of SK-N-BE(2c) cells in G2/M phase was observed at the later time point, but this was not statistically significant. Olaparib also induced a decrease in the proportion of UVW/NAT cells in G1 and S phases of the cell cycle and a concurrent increase in the G2/M phase population. This is consistent with a study carried out by Jelinic *et al.,* (2014) which shows that Olaparib treatment resulted in a reduction in S-phase cells and an increase in G2/M phase in osteosarcoma cells and

non-small cell lung cancer cells [129]. Treatment of cells with [^{131}I]MIBG alone resulted in a significant G2/M arrest 24 hours post treatment which is in agreement with a previous study by McCluskey *et al.,* (2008) which also demonstrates that treatment with [^{131}I]MIBG induced G2/M arrest when administered as a single agent [104]. Subsequent combination studies were carried out in order to determine whether treatment with combinations of Olaparib and [^{131}I]MIBG resulted in an increase in G2/M arrest. Upon analysis of both SK-N-BE(2c) and UVW/NAT cells it was noted that a significant shift in the proportion of cells in G2/M phase of the cell cycle following exposure to combination treatment was observed when compared to [^{131}I]MIBG treated cells alone. This is consistent with the previously discussed cell cycle data which indicates that cells are arresting in G2 phase of the cell cycle 24 hours post exposure to combination treatment. Taken together this suggests that inhibition of SSB repair by Olaparib may be resulting in the concomitant generation of DSBs possibly via collapsed replication forks. Thus, cells are unable to progress into mitotic stages of the cell cycle.

Taken together the results reported in this chapter demonstrate that SK-N-BE(2c) and UVW/NAT cells are sensitised to [^{131}I]MIBG by Olaparib evidenced by a reduction in clonogenic capacity and an increase in the proportion of cells in G2/M phase of the cell cycle. Additionally, in both cell lines examined, there is a prolonged reduction in radiation induced PARP-1 activity with a concomitant increase in γ-H2AX foci formation across the same 24 hour duration. This may also suggest that Olaparib acts as a sensitiser to [^{131}I]MIBG via a mechanism that is largely dependent on the generation of DSBs possibly via conversion of SSBs through inhibition of SSB repair by PARP-1.

Olaparib has demonstrated a strong potential clinical usefulness as a radiosensitiser when combined with [^{131}I]MIBG, however more work is necessary in order to determine whether the in vitro effects demonstrated in this study will translate to more robust tumour masses. Investigation of combination treatment in spheroids may be indicative of whether or not Olaparib and [^{131}I]MIBG treatment has the

potential to be further analysed in mouse models, which are necessary before patient studies can arise.

6.6 Final Conclusions and Future Work

In this study novel approaches to cancer therapy using different radiation qualities and radiosensitising compounds were investigated. MRE11 has previously been demonstrated to be a promising target to sensitise cells to radiation. For example Yuan *et al.,* (2012), reported that over-expression of MRE11 in breast cancer patients resulted in more aggressive tumour behaviour and further suggested that targeting MRE11 would be an effective therapeutic tool in breast cancer therapy [108]. In addition, abrogation of MRE11 activity using siRNA [74] or oncolytic adenoviruses [105] resulted in significant enhancement of radiation cytotoxicity. More specifically, Xu *et al.,* (2004), demonstrated that 24 hour incubation of human adenocarcinoma cells with MRE11 siRNA and subsequent exposure to X-ray irradiation at 2Gy and 4Gy, resulted in a significant sensitisation of cells to X-ray radiation [74]. Rajecki *et al.,* (2009) also achieved synergy between ionising radiation and MRE11 inhibition by infection of a host cell with oncolytic adenoviruses resulting in adenoviral proteins abrogating MRE11 binding to the MRN complex and initiating MRN complex degradation thus preventing DNA DSB repair [105].

In this study, for the first time, Mirin, a small molecule inhibitor of MRE11 nuclease activity was employed as a radiosensitiser with both X-irradiation and the targeted radiopharmaceutical [^{131}I]MIBG. It was demonstrated here that despite the initial hypothesis that radiosensitisation would be observed in cells treated with Mirin and subsequently exposed to X-rays, this was not the outcome achieved. In all cell lines exposed to this combination, there was no sensitisation elicited with respect to clonogenic capacity reduction. However, further analysis of the upstream and downstream components of the MRE11 signalling pathway revealed that although no effect is observed on clonogenic capacity, a significant abrogation of the MRE11 signalling cascade and stalling of cells in G2/M phase of the cell cycle is observed after initial treatment. These data therefore suggested that despite the apparent inhibition of the MRE11 related DDR pathway, the lack of radiosensitisation elicited to cells following exposure to X-ray radiation may be due to incomplete MRE11 inhibition with Mirin, and as a consequence insufficient inhibition of ATM kinase. As a result,

residual γ-H2AX foci formation and DDR activation may occur. It is also possible that additional components of the DDR pathway such as DNA-PK and ATR which also contribute to γ-H2AX foci formation, compensate for the inhibition of the ATM directed pathway [60].

Conversely, this study found that treatment of cells with [^{131}I]MIBG in combination with Mirin resulted in significant radiosensitisation. This is, to my knowledge, the first report which highlights the possibility of radiation type dependency associated with MRE11 inhibition using Mirin. Again, further analysis of the upstream and downstream substrates of MRE11 showed that Mirin induced a significant reduction in ATM kinase phosphorylation, which consequently lead to reduced γ-H2AX foci formation and nuclear RAD51 activity. Contrary to the rapid induction of DDR components in the MRN-ATM pathway with X-rays, it was observed that [^{131}I]MIBG induced a much more gradual accrual of DNA damage, whereupon although an increase in ATM kinase and γ-H2AX foci formation are observed 2 hours post initial treatment with [^{131}I]MIBG, this increase in γ-H2AX foci formation is much less significant than that observed in X-irradiated cells. These findings were further supported by a lack of nuclear RAD51 elevation 2 hours after initial treatment with [^{131}I]MIBG. RAD51 is a marker of DNA repair by HR, where it acts to catalyse DNA strand exchange [133] therefore these findings may suggest that DNA repair by HR was not upregulated at the earliest time point after initial [^{131}I]MIBG treatment. Following 24 hour incubation post initial treatment with [^{131}I]MIBG all components of the MRN-ATM DDR pathway were significantly elevated and furthermore cells stalled in G2/M phase of the cell cycle, indicating that sufficient DNA damage had occurred to trigger repair, most likely by HR owing to the concomitant elevation of nuclear RAD51 levels. Finally, the [^{131}I]MIBG induced elevation of DDR components, ATM kinase, γ-H2AX and RAD51 24 hours after initial treatment with [^{131}I]MIBG was significantly reduced by Mirin in combination studies, which again indicates that Mirin effectively targets ATM kinase, γ-H2AX and RAD51 components of DNA repair. However, as radiosensitisation is elicited with [^{131}I]MIBG it is possible that damage is accrued more gradually across the time course suggesting compensatory

mechanisms such as repair processes initiated by ATR, DNA-PK and p53 may occur in X-irradiated cells but not in those treated with [^{131}I]MIBG until significantly more damage has accrued. These findings therefore suggest that irradiation elicited by radiopharmaceuticals, which is chronic low dose and low dose rate radiation, may elicit damaging effects over a much longer duration. Therefore DNA repair by HR may only be induced after damage has accrued more slowly over, in this case, a 24 hour time period. More specifically, the present study demonstrated that following X-irradiation ATM kinase, γ-H2AX and RAD51 activity were upregulated rapidly within 2 hours. However, upon treatment with [^{131}I]MIBG, levels of the same proteins despite being upregulated 2 hours after initial treatment, continue to increase over the 24 hour time course. This therefore suggests for the first time that there is a difference in the kinetics of components of the MRN-ATM signalling pathway. Future studies should therefore further interrogate the kinetics of other DDR pathway components in order to determine if targeting specific proteins may provide greater success with one specific radiation type or whether scheduling of drug administration may differ between radiation types.

Olaparib, developed originally by KuDOS Pharmaceuticals and later by AstraZeneca, for the treatment of BRCA1/2 deficient cancers (section 1.5.1) was also employed as a radiosensitiser in this study with both X-irradiation and [^{131}I]MIBG. Olaparib has been previously shown to exert radiosensitising effects using X-rays in other paediatric tumour cells such as ependymoma cells, medulloblastoma cells and glioblastoma cells. Van Vuurden *et al.,* (2011) studied 2 hour pre-treatment with low concentrations of Olaparib (1μM-8μM) in cell lines derived from the aforementioned cancers and observed a concentration dependent reduction in cell viability following radiation exposure (0-6Gy) in all cell lines [125]. In addition to this, Lee *et al.,* (2013) investigated the effects of PARP-1 inhibition by Olaparib in two Ewing sarcoma cell lines and again showed that Olaparib treatment increased the sensitivity of these cell lines to radiation[127].

It was demonstrated here that in agreement with the initial hypothesis, Olaparib effectively radiosensitised cells to X-rays in all cell lines investigated, albeit to

different extents with SK-N-BE(2c) and UVW/NAT cells having a similar profile, however A375 exhibited a much greater radiosensitivity demonstrating consistently lower IC50 values that SK-N-BE(2c) and UVW/NAT cells (Figure 5.2-5.4). In order to further interrogate the signalling mechanisms by which Olaparib exerts its radiosensitising effect when combined with X-ray radiation, studies were carried out on PARP-1 activity levels following treatment with 5 and 25μM Olaparib and 2Gy X-irradiation. It was demonstrated that PARP-1 levels were elevated in response to X-irradiation 2 hours post initial X-ray exposure however these levels declined after 24 hours. Pre-treatment of cells with Olaparib for 2 hours abrogated this radiation induced upregulation of PARP-1 which may indicate that SSBs are converted to DSBs in cells with depleted PARP-1 activity. To determine if an increase in DSB production could underlie the radiosensitisation observed γ-H2AX foci levels were assessed. Olaparib as a single agent resulted in an increase in γ-H2AX foci formation which was further increased by the addition of X-irradiation, indicating an increase in the number of DSBs.

The findings in the present study are supported by previous studies carried out where Olaparib was shown to increase foci levels both as a single agent and in combination with X-ray radiation [89]. More specifically, Senra et al., (2011) demonstrate that Olaparib at a concentration of 1μM and 5μM resulted in a significant increase in γ-H2AX foci levels. Additionally, upon exposure to X-rays (1-4Gy) Olaparib further potentiated the radiation induced γ-H2AX foci formation. Bourton *et al.,* (2013) also demonstrated that lymphoblastoid cells also showed potentiation of foci formation upon incubation with Olaparib and γ-radiation over a 24 hour time period [81]. Taken together these results suggest that PARP-1 inhibition by Olaparib may contribute to the conversion of SSBs to DSBs upon cell replication, thus resulting in an increase in γ-H2AX foci formation.

To determine if the increase in DSB formation exerted by Olaparib and X-irradiation translated to effects on the cell cycle, both SK-N-BE(2c) and UVW/NAT cells were analysed for progression through the stages of the cell cycle 2 hour pre-treatment with 5μM and 25μM Olaparib and subsequent X-irradiation with 2Gy. Olaparib as a

single agent was demonstrated to have no effect on cell cycle progression, however, combination treatment with Olaparib increased the proportion of cells in the G2/M phase compared to radiation alone treated samples in both SK-N-BE(2c) and UVW/NAT cells. This however was not the case in combination treated A375 cells, as despite a visible shift into G2/M phase, this was not statistically significant compared to radiation alone exposed samples in this cell line. Taken together these results suggest that inhibition of PARP-1 may prevent the transition of cells into the mitotic phase of the cell cycle. However in A375 cells the radiosensitisation elicited by Olaparib may not be primarily induced via interference with G2/M checkpoint signalling. Future work should interrogate markers of cell cycle checkpoints such as CDK4/6 for G1 and the cdc2/cyclin-B complex for G2/M to determine if the pattern of upregulation of these proteins differs between cell lines [56], [134].

Whilst there is a lot of previous studies utilising PARP-1 inhibition with external beam radiation, little is known about the potential benefit of combining PARP-1 inhibition with [^{131}I]MIBG or other radiopharmaceuticals. McCluskey *et al.,* (2012) demonstrated that PARP-1 inhibition using another inhibitor, PJ34, resulted in the enhancement of [^{131}I]MIBG/topotecan cytotoxicity in both SK-N-BE(2c) and UVW/NAT cells, with cells demonstrating supra-additive toxicity [39]. Again, as was hypothesised Olaparib sensitised cells to [^{131}I]MIBG in an [^{131}I]MIBG dose dependent manner to a similar extent to that observed with X-irradiation. In order to further interrogate the signalling mechanisms by which Olaparib exerts its radiosensitising effect when combined with [^{131}I]MIBG, studies were carried out on PARP-1 activity levels following [^{131}I]MIBG single agent treatment and combination treatment. As was hypothesised, exposure of cells to combinations of Olaparib and [^{131}I]MIBG resulted in significant abrogation of [^{131}I]MIBG induced PARP-1 activation both 2 hours and 24 hours following initial treatment, however PARP-1 levels were more significantly reduced 24 hours after initial treatment with [^{131}I]MIBG. Again since inhibition of PARP-1 activity is predicted to result in conversion of SSBs to DSBs (due to a reduction in cellular capacity for DNA SSB repair by BER) further analysis of observed γ-H2AX foci levels was performed. Incubation of cells with Olaparib alone

resulted in an increase in γ-H2AX foci levels when compared to control levels both 2 hours and 24 hours following initial exposure, which is again in support of previous studies carried out by McCluskey *et al.,* (2012) where Olaparib is shown to increase foci levels both as a single agent and in combination with [^{131}I]MIBG/topotecan treated cells [39]. Furthermore this increase was further enhanced by addition of [^{131}I]MIBG, suggesting that conversion of SSBs to DSBs may be a driving factor for the radiosensitising effect of Olaparib. Although specific examination of SSBs and DSBs specifically was out with the scope of this project, future work should be carried out for example, by comet assay to assess DNA breaks or by assessing 53BP-1, a specific marker of DNA DSBs [135], to determine if an increase in DNA DSBs is observed following treatment of cells with Olaparib and X-irradiation.

To determine if the increase in DSB formation exerted by Olaparib and [^{131}I]MIBG translated to abrogation of cell cycle progression both SK-N-BE(2c) and UVW/NAT cells were analysed for progression through the stages of the cell cycle. It was noted that a statistically significant shift in the proportion of cells in the G2/M phase of the cell cycle following exposure to combination treatment was observed when compared to [^{131}I]MIBG treated cells alone. This is consistent with the previously discussed cell cycle data (section 6.4.4.1) which indicates that cells were arresting in G2 phase of the cell cycle 24 hours post exposure to combination treatment. Taken together these results suggest that inhibition of SSB repair by Olaparib may be resulting in the concomitant generation of DSBs possibly via collapsed replication forks. Thus, cells are unable to progress into mitotic stages of the cell cycle.

Despite the lack of efficacy exhibited by Mirin in combination with X-ray radiation, a potential clinical use for MRE11 inhibition has been demonstrated in the present study when used in combination with [^{131}I]MIBG. Additionally, Olaparib demonstrated significant potential for clinical use as a radiosensitiser when combined with both X-ray radiation and [^{131}I]MIBG, reducing clonogenic survival significantly in both cases. Olaparib and [^{131}I]MIBG have previously undergone *in vivo*, and clinical studies for use in the treatment of cancers such as, Ovarian cancer and Neuroblastoma respectively, and X-rays are routinely used in cancers originating

from almost any tissue. As a result of this, the translation of the Olaparib and radiation combinations investigated in this study into clinical use has the potential to be much more rapid than for treatments which have never undergone such investigation before.

However, more work is necessary in order to determine whether the *in vitro* effects demonstrated in studies utilising Mirin will translate into tumour control in more representative tumour models. For example, investigation of combination treatment in spheroids may be indicative of whether chemo-radiotherapy using Mirin has the potential to be further analysed in mouse models, before suggestions of patient studies can arise. Previous studies by Boyd *et al.,* (2002) have demonstrated that transfectant mosaic spheroids (spheroids composed of a mixture of NAT expressing and non-NAT expressing cells) are effective models for determination of the response conferred by cells in a 3D presentation to [^{131}I]MIBG in combination with gene therapy [20], [136]. In particular the use of transfectant spheroids is of benefit as this mimics the heterogeneity of *in vivo* tumours. This principle can therefore be applied to the investigation of combination treatments using Mirin with both X-irradiation and [^{131}I]MIBG to determine a more accurate representation of how an *in vivo* tumour may respond. Further to these studies assessment of combination treatment should be undertaken *in vivo*, providing more physiologically relevant insight with respect to toxicity and scheduling. Despite the efficacy of radiosensitisation demonstrated by Mirin in combination with [^{131}I]MIBG, further drug discovery programmes to elucidate a more potent and effective MRE11 inhibitor with different modes of action may result in increased efficacy with X-ray radiation as well. Since the present study began no other MRE11 inhibitor has been developed. Despite Mirin having been previously shown to inhibit MRE11 and its downstream targets [71], it has been established that Mirin only prevents MRE11 nuclease activity and not the association of the MRN complex [71]. On the other hand, MRE11 siRNA downregulated MRN complex formation, which may indicate that an inhibitor with the capacity to abrogate MRN complex formation may provide more successful radiosensitisation with X-rays [74]. Owing to the lack of efficacy observed with X-

irradiation with Mirin, further interrogation of potential compensatory repair pathways may highlight a potential target for co-inhibition of other DDR pathway components, such as DNA-PK, to enhance the efficacy of MRE11 inhibition.

References

[1] Porter, A., Aref, A., Chodounsky, Z., Elzawawy, A., Manatrakul, N., Ngoma, T., Orton, C.,Van't Hooft, E and Sikora, K., (1999) A global strategy for radiotherapy: a WHO consultation. *Clinical Oncology,* 11, 368–370.

[2] Tribius, S and Bergelt, C., (2011) Intensity-modulated radiotherapy versus conventional and 3D conformal radiotherapy in patients with head and neck cancer: is there a worthwhile quality of life gain? *Cancer Treatment Review*, 37, 511–9.

[3] Lees-Miller, S.P and Meek, K., (2003) Repair of DNA double strand breaks by non-homologous end joining. *Biochimie*, 85, 1161–1173.

[4] Chial, B.H., (2008) Proto-oncogenes to oncogenes to cancer. *Nature Education,* 1, 1-5.

[5] Chial, B.H., (2008) Tumor suppressor (TS) genes and the two-hit hypothesis. *Nature Education* 1, 1-5.

[6] He, M., Rosen, J., Mangiameli, D and Libutti, S.K., (2007) Cancer Development and Progression. *Advances in Experimental and Medical Biology*, 593,117–133.

[7] Willis R.A., (1960) Pathology of Tumours. 3rd editon, Washington D.C: Butterworth.

[8] Weinberg, R.A., (2007) The Biology of Cancer. New York: Garland Science.

[9] Rontgen, W.C., (1896) On a New Kind of Rays. *Science.*, 3, 227–231.

[10] Slater, J.M., (2012) Ion Beam Therapy: Fundamentals, Technology, Clinical Applications. *Springer*, 320, 3-17.

[11] Franiel, T., Lüdemann, L., Taupitz, M., Böhmer, D., and Beyersdorff, D., (2009) MRI before and after external beam intensity-modulated radiotherapy of patients with prostate cancer: the feasibility of monitoring of radiation-induced tissue changes using a dynamic contrast-enhanced inversion-prepared dual-contrast gradient echo sequence. *Radiotherapy and Oncology.*, 93, 241–5.

[12] Gupta, T., Agarwal, J., Jain, S., Phurailatpam, R., Kannan, S., Ghosh-Laskar, S., Murthy, V., Budrukkar, A., Dinshaw, K., Prabhash, K., Chaturvedi, P., and D'Cruz, A., (2012) Three-dimensional conformal radiotherapy (3D-CRT) versus intensity modulated radiation therapy (IMRT) in squamous cell carcinoma of the head and neck: a randomized controlled trial. *Radiotherapy and Oncology.*, 104, 343–8.

[13] Leibel, S.A., Fuks, Z., Zelefsky, M.J., Wolden, S.L., Rosenzweig, K.E., Alektiar, K.M., Hunt, M.A., Yorke, E.D., Hong, L.X., Amols, H.I., Burman, C.M., (2002) Intensity-Modulated Radiotherapy. The *Cancer Journal*, 8, 164–176.

[14] Sharp, G.C., Jiang, S.B., Shimizu, S., and Shirato, H., (2004) Prediction of respiratory tumour motion for real-time image-guided radiotherapy. *Physics in Medicine and Biology,* 49, 425–440.

[15] Dawson, L.A and Sharpe, M.B., (2006) Image-guided radiotherapy : rationale, benefits, and limitations. *Lancet Oncology*, 7, 848-858.

[16] Boyd, M., Mairs, R.J., Wilson, L., Carlin, S., and Wheldon, T.E., (2001) A gene therapy / targeted radiotherapy strategy for radiation cell kill by [131 I] meta- iodobenzylguanidine. *The Journal of Gene Medicine,* 3, 165–172.

[17] Hamoudeh, M., Kamleh, M.A., Diab, R., and Fessi, H., (2008) Radionuclides delivery systems for nuclear imaging and radiotherapy of cancer. *Advanced Drug Delivery Reviews*, 60, 1329–1346.

[18] Gaze, M.N., Mairs, R.J., Boyack, S.M., Wheldon, T.E., and Barrett, A., (1992) 131I-meta-iodobenzylguanidine therapy in neuroblastoma spheroids of different sizes. *British Journal of Cancer*, 66, 1048–1052.

[19] Carter, P., (2001) Improving the efficacy of antibody-based cancer therapies. *Nature Reviews,* 1, 118–129.

[20] Boyd, M., Mairs, S.C., Stevenson, K., Livingstone, A., Clark, A.M., Ross, S.C and Mairs, R.J., (2002) Transfectant mosaic spheroids: A new model for evaluation of tumour cell killing in targeted radiotherapy and experimental gene therapy. *Journal of Gene Medicine*, 4, 567–576.

[21] Ersahin, D., Doddamane, I., and Cheng, D., (2011) Targeted Radionuclide Therapy. *Cancers*, 3, 3838–3855.

[22] Couturier, O., Supiot, S., Degraef-Mougin, M., Faivre-Chauvet, A., Carlier, T., Chatal, J.F., Davodeau, F and Cherel, M., (2005) Cancer radioimmunotherapy with alpha-emitting nuclides, *European Journal of Nuclear Medicine and Molecular Imaging*, 32, 601–614.

[23] Sartor, O., Maalouf, B.N., Hauck, C.R., Macklis, R.M., Clinic, C and College, L., (2012) Targeted use of Alpha Particles : Current Status in Cancer Therapeutics," *Journal of Nuclear Medicine and Radiation Therapy*, 3.

[24] Nestor, M.V., (2010) Targeted radionuclide therapy in head and neck cancer. *Head Neck*, 32, 666–678.

[25] Kassis, A.I., (2011) Molecular and cellular radiobiological effects of Auger emitting radionuclides. *Radiation Protection Dosimetry*, 143, 241–247.

[26] Boyd, M., Ross, S.C., Dorrens, J., Fullerton, N.E., Tan, K.W., Zalutsky, M.R and Mairs, R.J., (2006) Radiation-induced biologic bystander effect elicited in vitro

by targeted radiopharmaceuticals labeled with alpha-, beta-, and auger electron-emitting radionuclides. *Journal of Nuclear Medicine*, 47, 1007–1015.

[27] Neshasteh-Riz, A., Mairs, R.J., Angerson, W.J., Stanton, P.D., Reeves, J.R., Rampling, R., Owens, J., and Wheldon, T.E., (1998) Differential cytotoxicity of [^{123}I]IUdR, [^{125}I]IUdR and [^{131}I]IUdR to human glioma cells in monolayer or spheroid culture: effect of proliferative heterogeneity and radiation cross-fire. *British Journal of Cancer*, 77, 385–390.

[28] Chung, J.K., (2002) Sodium iodide symporter: its role in nuclear medicine. *Journal of Nuclear Medicine*, 43, 1188–1200.

[29] Kogai, T., Taki, K., and Brent, G.A., (2006) Enhancement of sodium/iodide symporter expression in thyroid and breast cancer. *Endocrine Related Cancer*, 13, 797–826.

[30] Zweit, J., (1996) Radionuclides and carrier molecules for therapy. *Physics in Medicine and Biology*, 41, 1905–1914.

[31] Goldenberg, D.M., (2003) Advancing role of radiolabeled antibodies in the therapy of cancer. *Cancer Immunology and Immunotherapy*, 52, 281–96.

[32] Durrant, L.G and Scholefield, J. H., (2009) Principles of cancer treatment by immunotherapy, *Surgery*, 27, 161–164.

[33] Witzig, T.E., (2002) Randomized Controlled Trial of Yttrium-90-Labeled Ibritumomab Tiuxetan Radioimmunotherapy Versus Rituximab Immunotherapy for Patients With Relapsed or Refractory Low-Grade, Follicular, or Transformed B-Cell Non-Hodgkin's Lymphoma. *Journal of Clinical Oncology*, 20, 2453–2463.

[34] Polishchuk, A. L., Dubois, S. G., Haas-Kogan, D., Hawkins, R., and Matthay, K. K., (2011) Response, survival, and toxicity after iodine-131-

metaiodobenzylguanidine therapy for neuroblastoma in preadolescents, adolescents, and adults. *Cancer*, 117, 4286–4293.

[35] Kayano, D and Kinuya, S., (2014) Iodine-131 Metaiodobenzylguanidine Therapy for Neuroblastoma : Reports So Far and Future Perspective, *The Scientific World Journal,* 2015.

[36] McCluskey, A.G., Boyd, M., Ross, S.C., Cosimo, E., Clark, A.M., Angerson, W.J., Gaze, M.N., and Mairs, R.J., (2005) [^{131}I] meta -Iodobenzylguanidine and Topotecan Combination Treatment of Tumors Expressing the Noradrenaline Transporter reatment of Tumors Expressing the Noradrenaline Transporter, *Clinical Cancer Research,* 11, 929-7937.

[37] Mairs R.J and Boyd, M., (2008) Optimizing MIBG therapy of neuroendocrine tumors: preclinical evidence of dose maximization and synergy. *Nuclear Medicine and Biology*, 35, 9-20.

[38] Klingebiel T., Feine U., Treuner J., Reuland P and N. D., (1991) Treatment of neuroblastoma with [^{131}I]metaiodobenzylguanidine: long-term results in 25 patients, *Journal of Nuclear Biology and Medicine*, 35, 216–219.

[39] McCluskey, A. G., Mairs, R. J., Tesson, M., Pimlott, S. L., Babich, J. W., Gaze, M. N., Champion, S., and Boyd, M., (2012) Inhibition of poly(ADP-Ribose) polymerase enhances the toxicity of 131I-metaiodobenzylguanidine/topotecan combination therapy to cells and xenografts that express the noradrenaline transporter. *Journal of Nuclear Medicine*, 53, 1146–54.

[40] Mastrangelo, R., Tornesello, A., Riccardi, R., Lasorella, A., Mastrangelo, S., Mancini, A., Rufini, V and Troncone, L., (1995) A new approach in the treatment of stage IV neuroblastoma using a combination of [^{131}I]meta-iodobenzylguanidine (MIBG) and cisplatin. *European Journal of Cancer*, 31A, 606–611.

[41] Mastrangelo, S., Tornesello, A., Diociaiuti, L., Pession, A., Prete, A., Rufini, V., Troncone, L and Mastrangelo, R., (2001) Treatment of advanced neuroblastoma : feasibility and therapeutic potential of a novel approach combining 131-I-MIBG and multiple drug chemotherapy, *British Journal of Cancer*, 84, 460–464.

[42] Matthay, K.K., Tan, J. C., Villablanca, J. G., Yanik, G. A., Veatch, J., Franc, B., Twomey, E., Horn, B., Reynolds, C. P., Groshen, S., Seeger, R. C and Maris, J. M., (2006) Phase I dose escalation of iodine-131-metaiodobenzylguanidine with myeloablative chemotherapy and autologous stem-cell transplantation in refractory neuroblastoma: A new approaches to neuroblastoma therapy consortium study. *Journal of Clinical Oncology,* 24, 500–506.

[43] Yanik, G.A., Villablanca, J. G., Maris, J. M., Weiss, B., Groshen, S., Marachelian, A., Park, J. R., Tsao-Wei, D., Hawkins, R., Shulkin, B. L., Jackson, H., Goodarzian, F., Shimada, H., Courtier, J., Hutchinson, R., Haas-Koga, D., Hasenauer, C. B., Czarnecki, S., Katzenstein, H. M and Matthay, K. K., (2015) 131I-Metaiodobenzylguanidine with Intensive Chemotherapy and Autologous Stem Cell Transplantation for High-Risk Neuroblastoma. A New Approaches to Neuroblastoma Therapy (NANT) Phase II Study. *Biology of Blood Marrow Transplant*, 21, 673–681.

[44] DuBois, S. G., Chesler, L., Groshen, S., Hawkins, R., Goodarzian, F., Shimada, H., Yanik, G., Tagen, M., Stewart, C., Mosse, Y. P., Maris, J. M., Tsao-Wei, D., Marachelian, A., Villablanca, J. G and Matthay, K. K., (2012) Phase I study of vincristine, irinotecan, and 131I- metaiodobenzylguanidine for patients with relapsed or refractory neuroblastoma: A new approaches to neuroblastoma therapy trial, *Clinical Cancer Research*, 18, 2679–2686.

[45] Hei, T.K., Zhou, H., Chai, Y., Ponnaiya, B and Ivanov, V.N., (2011) Radiation induced non-targeted response: mechanism and potential clinical implications, *Current Molecular Pharmacology*, 4, 96–105.

[46] Lomax, M.E., Folkes, L.K and O'Neill, P., (2013) Biological consequences of radiation-induced DNA damage: Relevance to radiotherapy. *Clinical Oncology*, 25, 578–585.

[47] Mognato, M., Grifalconi, M., Canova, S., Girardi, C and Celotti, L., (2011) The DNA-damage response to ionizing radiation in human lymphocytes. *Selected Topics in DNA repair*, 3-28

[48] Bolderson, E., Richard, D. J., Zhou, B.-B. S and Khanna, K. K., (2009) Recent advances in cancer therapy targeting proteins involved in DNA double-strand break repair. *Clinical Cancer Research.*, 15, 6314–20.

[49] Helleday, T., Lo, J., van Gent, D.C and Engelward, B.P., (2007) DNA double-strand break repair: From mechanistic understanding to cancer treatment. *DNA Repair*, 6, 923–935.

[50] Hefferin M.L and Tomkinson, A.E., (2005) Mechanism of DNA double-strand break repair by non-homologous end joining. *DNA Repair*, 4, 639–48.

[51] Jasin, M and Rothstein, R., (2013) Repair of strand breaks by homologous recombination. *Perspectives in Biology*, 5, 1–20.

[52] Li, X and Heyer, W.D., (2008) Homologous recombination in DNA repair and DNA damage tolerance. *Cell Research.*, 18, 99–113.

[53] Wallace, S.S., (2014) Base excision repair: A critical player in many games. *DNA Repair*, 19, 14–26.

[54] Frosina, G., Fortini, P., Rossi, O., Carrozzino, F., Raspaglio, G., Cox, L.S., Lane, D.P., Abbondandolo, A and Dogliotti, A., (1996) Two pathways for base excision repair in mammalian cells. *Journal of Biological Chemistry*, 271, 9573–8.

[55] Krokan, H.E., Nilsen, H., Skorpen, F., Otterlei, M and Slupphaug, G., (2000) Base excision repair of DNA in mammalian cells. *FEBS Letters*, 476, 73–7

[56] Sancar, A., Lindsey-Boltz, L.A., Unsal-Kaçmaz, K and Linn, S., (2004) Molecular mechanisms of mammalian DNA repair and the DNA damage checkpoints. *Annual Review of Biochemistry*, 73, 39–85.

[57] Burma, S., Chen, B.P.C and Chen, D.J., (2006) Role of non-homologous end joining (NHEJ) in maintaining genomic integrity. *DNA Repair*, 5, 1042–1048.

[58] Barlow, C., Hirotsune, S., Paylor, R., Liyanage, M., Eckhaus, M., Collins, F., Shiloh, Y., Crawley, Z.N., Ried, T., Tagle, D and Wynshaw-Boris, A., (1996) Atm-deficient mice: A paradigm of ataxia telangiectasia. *Cell*, 86, 159–171.

[59] Helleday, T., (2011) The underlying mechanism for the PARP and BRCA synthetic lethality: clearing up the misunderstandings. *Molecular Oncology*, 5, 387–93.

[60] Muslimovic, A., Johansson, P and Hammarsten, O., (2012) Measurement of H2AX Phosphorylation as a Marker of Ionizing Radiation Induced Cell Damage. *Current Topics in Ionising Radiation Research,* InTech.

[61] Stiff, T., O'Driscoll, M., Rief, N., Iwabuchi, K., Löbrich, M and Jeggo, P.A., (2004) ATM and DNA-PK Function Redundantly to Phosphorylate H2AX after Exposure to Ionizing Radiation. *Cancer Research*, 64, 2390–2396.

[62] Bhatti, S., Kozlov, S., Farooqi, A.A., Naqi, A., Lavin, M and Khanna, K.K., (2011) ATM protein kinase: The linchpin of cellular defenses to stress. *Cellular and Molecular Life Sciences*, 68, 2977–3006.

[63] Lamarche, B.J., Orazio, N.I and Weitzman, M.D., (2010) The MRN complex in double-strand break repair and telomere maintenance. *FEBS Letters,* 584, 3682–3695.

[64] Stivers, J., (2008) Small moleule versus DNA repair nanomachine. *Nature Chemical Biology,* 4, 86–88.

[65] Uziel, T., Lerenthal, y., Moyal, l., Andegeko, y., Mittelman, l and Shiloh, Y., (2003) Requirement of the MRN complex for ATM activation by DNA damage. *EMBO Journal*, 22, 5612–5621.

[66] You, Z and Bailis, J.M., (2010) DNA damage and decisions : CtIP coordinates DNA repair and cell cycle checkpoints. *Trends in Cell Biology*, 20, 402–409.

[67] Myers, J.S and Cortez, D., (2006) Rapid activation of ATR by ionizing radiation requires ATM and Mre11. *Journal of Biological Chemistry*, 281, 9346–9350.

[68] Kurz, E.U and Lees-Miller, S.P., (2004) DNA damage-induced activation of ATM and ATM-dependent signaling pathways. *DNA Repair*, 3, 889–900.

[69] Aguilar-Quesada, R., Muñoz-Gámez, J.A., Martín-Oliva, D., Peralta, A., Valenzuela, M.T., Matínez-Romero, R., Quiles-Pérez, R., Menissier-de Murcia, J., de Murcia, G., Ruiz de Almodóvar, M and Oliver, F.J., (2007) Interaction between ATM and PARP-1 in response to DNA damage and sensitization of ATM deficient cells through PARP inhibition. *BMC Molecular Biology*, 8, 29.

[70] Shibata, A., Moiani, D., Arvai, A.S., Perry, J., Harding, S.M., Genois, M.M., Maity, R., van Rossum-Fikkert, S., Kertokalio, A., Romoli, F., Ismail, A., Ismalaj, E., Petricci, E., Neale, M.J., Bristow, R.G., Masson, J.Y., Wyman, C., Jeggo, P.A and Tainer, J.A., (2014) DNA Double-Strand Break Repair Pathway Choice Is Directed by Distinct MRE11 Nuclease Activities. *Molecular Cell*, 53, 7–18.

[71] Dupré, A., Boyer-Chatenet, L., Sattler, R.M., Modi, A.P., Lee, J.H., Nicolette, L., Kopelovich, L., Jasin, M., Baer, R., Paull, T.T and Gautier, J., (2008) A forward chemical genetic screen reveals an inhibitor of the Mre11-Rad50-Nbs1 complex., *Nature Chemical Biology*, 4, 119–125.

[72] Rass, E., Grabarz, A., Plo, I., Gautier, J., Bertrand, P and Lopez, B.S., (2009) Role of Mre11 in chromosomal nonhomologous end joining in mammalian cells. *Nature Structural and Molecular Biology*, 16, 819–824.

[73] Zhang, Y., Lim, C.U.K., Williams, E.S., Zhou, J., Zhang, Q., Fox, M.H., Bailey, S.M and Liber, H.L., (2005) NBS1 knockdown by small interfering RNA increases ionizing radiation mutagenesis and telomere association in human cells. *Cancer Research*, 65, 5544–53.

[74] Xu, M., Myerson, R.J., Hunt, C., Kumar, S., Moros, E.G., Straube, W.L and Roti Roti, R.L., (2004) Transfection of human tumour cells with Mre11 siRNA and the increase in radiation sensitivity and the reduction in heat-induced radiosensitization. *International Journal of Hyperthermia*, 20, 157–162.

[75] Sodhi, R.K., Singh, N and Jaggi, A.S., (2010) Poly(ADP-ribose) polymerase-1 (PARP-1) and its therapeutic implications. *Vascular Pharmacology*, 53, 77–87.

[76] Herceg, Z and Wang, Z.Q., (2001) Functions of poly(ADP-ribose) polymerase (PARP) in DNA repair, genomic integrity and cell death. *Mutational Research*, vol. 477, pp. 97–110.

[77] Berthold, C.L., Wang, H.L., Nordlund, S and Högbom, M., (2009) Mechanism of ADP-ribosylation removal revealed by the structure and ligand complexes of the dimanganese mono-ADP-ribosylhydrolase DraG. *Proceedings of the National Academy of Sciences of the United States of America*, 106, 14247–14252.

[78] Wang, M., Wu, W., Rosidi, B., Zhang, L., Wang, H and Iliakis, G., (2006) PARP-1 and Ku compete for repair of DNA double strand breaks by distinct NHEJ pathways. *Nucleic Acids Research*, 34, 6170–6182.

[79] Swindall, A.F., Stanley, J.A and Yang, E.S., (2013) PARP-1: Friend or foe of DNA damage and repair in tumorigenesis? *Cancers*, 5, 943–958.

[80] Sandhu, S.K., Yap, T.A and de Bono, J.S., (2010) Poly(ADP-ribose) polymerase inhibitors in cancer treatment: a clinical perspective. *European Journal of Cancer*, 46, 9–20.

[81] Bourton, E.C., Plowman, P.N., Harvey, A.J., Zahir, S.A and Parris, C.N., (2013) The PARP-1 Inhibitor Olaparib Causes Retention of γ -H2AX Foci in BRCA 1 Heterozygote Cells Following Exposure to Gamma Radiation. *Journal of Cancer Therapy*, 4, 44–52.

[82] Nijman, S.M.B., (2011) Synthetic lethality: general principles, utility and detection using genetic screens in human cells. *FEBS Letters*, 585, 1–6.

[83] Dedes, K.J., Wilkerson, P.M., Wetterskog, D., Weigelt, B., Ashworth, A and Reis-Filho, J.S., (2011) Synthetic lethality of PARP inhibition in cancers lacking BRCA1 and BRCA2 mutations. *Cell Cycle*, 10, 1192–1199.

[84] Bryant, H.E and Helleday, T., (2006) Inhibition of poly (ADP-ribose) polymerase activates ATM which is required for subsequent homologous recombination repair. *Nucleic Acids Research*, 34, 1685–91.

[85] Rottenberg, S., Jaspers, J.E., Kersbergen, A., van der Burg, E., Nygren, A.O.H., Zander, S.A.L., Derksen, P.W.B., de Bruin, M., Zevenhoven, J., Lau, A., Boulter, R., Cranston, A., O'Connor, M.J., Martin, N.M.B., Borst, P and Jonkers, J., (2008) High sensitivity of BRCA1-deficient mammary tumors to the PARP inhibitor AZD2281 alone and in combination with platinum drugs. *Proceedings of the National Academy of Sciences of the United States of America,* 105, 17079–84.

[86] Peter, P.D., Fong, C., Boss, D.S., Yap, T.A., Tutt, A., Wu, P., Mergui-Roelvink, M., Mortimer, P., Swaisland, H., Lau, A., O'Connor, M.J., Ashworth, A., Carmichael, J., Kaye, S.B., Schellens, J.H.M., and de Bono, J.S., (2009) Inhibition of Poly(ADP-Ribose) Polymerase in Tumors from BRCA Mutation Carriers. *New England Journal of Medicine*, 361, 123–134.

[87] Gelmon, K.A., Tischkowitz, M., Mackay, H., Swenerton, K., Robidoux, A., Tonkin, K., Hirte, H., Huntsman, D., Clemons, M., Gilks, B., Yerushalmi, R., Macpherson, E., Carmichael, J and Oza, A., (2011) Olaparib in patients with recurrent high-grade serous or poorly differentiated ovarian carcinoma or triple-negative breast cancer: a phase 2, multicentre, open-label, non-randomised study. *Lancet Oncoloy*, 12, 852–61.

[88] Tuli, R., Surmak, A.J., Reyes, J., Armour, M., Hacker-Prietz, A., Wong, J., DeWeese, T.L and Herman, J.M., (2014) Radiosensitization of Pancreatic Cancer Cells In Vitro and In Vivo through Poly (ADP-ribose) Polymerase Inhibition with ABT-888. *Translational Oncology*, 7, 439–445.

[89] Senra, J.M., Telfer, B.A., Cherry, K.E., McCrudden, C.M., Hirst, D.G., O'Connor, M.J., Wedge, S.R and Stratford, I.J., (2011) Inhibition of PARP-1 by olaparib (AZD2281) increases the radiosensitivity of a lung tumor xenograft. *Molecular Cancer Therapy*, 10, 1949–58.

[90] Boyd, M., Cunningham, S.H., Brown, M.M., Mairs, R.J and Wheldon, T.E., (1999) Noradrenaline transporter gene transfer for radiation cell kill by 131I meta-iodobenzylguanidine. *Gene Therapy*, 6, 1147–1152.

[91] Gaze, M.N., Huxam, I.M and Mairs, R.J., (1991) Intracellular localization of metaiodobenzyl guanidine in human neuroblastoma cells by electron spectroscopic imaging. *International Journal of Cancer*, 47, 875–880.

[92] Costanzo, V., (2011) Brca2 , Rad51 and Mre11 : Performing balancing acts on replication forks. *DNA Repair,* 10, 1060–1065.

[93] Fernet, M., Mégnin-Chanet, F., Hall, J and Favaudon, V., (2010) Control of the G2/M checkpoints after exposure to low doses of ionising radiation: Implications for hyper-radiosensitivity. *DNA Repair*, 9, 48–57.

[94] Lomax, M.E., Folkes, L.K and O'Neill, P., Biological consequences of radiation-induced DNA damage: Relevance to radiotherapy. *Clinical Oncology*, 25, 578–585.

[95] Collis, S.J., Schwaninger, J.M., Ntambi, A.J., Keller, T.W., Nelson, W.G., Dillehay, L.E and DeWeese, T.L., (2004) Evasion of early cellular response mechanisms following low level radiation-induced DNA damage. *Journal of Biological Chemistry*, 279, 49624–49632.

[96] Parplys, A.C., Petermann, E., Petersen, C., Dikomey, E and Borgmann, K., (2012) DNA damage by X-rays and their impact on replication processes. *Radiotherapy and Oncology*, 102, 466–471.

[97] Fuks, Z., Persaud, R.S., Alfieri, A., McLoughlin, M ., Ehleiter, D., Schwartz, J.L., Seddon, A.P., Cordon-Cardo, C and Haimovitz-Friedman, A., (1994) Basic fibroblast growth factor protects endothelial cells against radiation-induced programmed cell death in vitro and in vivo. *Cancer Research*, 54, 2582–2590.

[98] Russo, A.L., Kwon, H.C., Burgan, W.E., Carter, D., Beam, K., Weizheng, X., Zhang, J., Slusher, B.S., Chakravarti, A., Tofilon, P.J and Camphausen, K., (2009) In vitro and in vivo radiosensitization of glioblastoma cells by the poly (ADP-ribose) polymerase inhibitor E7016. *Clinical Cancer Research*, 15, 607–612.

[99] Paull, T.T., Rogakou, E.P., Yamazaki, V., Kirchgessner, C.U., Gellert, M and Bonner, W.M., (2000) A critical role for histone H2AX in recruitment of repair factors to nuclear foci after DNA damage. *Current Biology*, 10, 886–95.

[100] An, J., Huang, Y.C., Xu, Q., Zhou, L., Shang, Z., Huang, B., Wang, Y., Liu, X., Wu, D.C and Zhou, P.K., (2010) DNA-PKcs plays a dominant role in the regulation of H2AX phosphorylation in response to DNA damage and cell cycle progression. *BMC Molecular Biology*, 11, 18.

[101] Rainey, M.D., Charlton, M.E., Stanton, R.V and Kastan, M.B., (2008) Transient inhibition of ATM kinase is sufficient to enhance cellular sensitivity to ionizing radiation. *Cancer Research*, 68, 7466–7474.

[102] Mirzaie-Joniani, H., Eriksson, D., Sheikholvaezin, A., Johansson, A., Lobroth, P.O., Johansson, L and Stigbrand, T., (2002) Apoptosis induced by low-dose and low-dose-rate radiation. *Cancer*, 94, 1210–1214.

[103] Gildemeister, O.S., Sage, J.M and Knight, K.L., (2009) Cellular redistribution of Rad51 in response to DNA damage: Novel role for Rad51C. *Journal of Biological Chemistry*, 284, 31945–31952.

[104] McCluskey, A.G., Boyd, M., Pimlott, S.L., Babich, J.W., Gaze, M.N and Mairs, R.J., (2008) Experimental treatment of neuroblastoma using [131I]meta-iodobenzylguanidine and topotecan in combination. *British Journal of Radiology*, 81, 28-35.

[105] Rajecki, M., Hällström, T.A., Hakkarainen, T., Nokisalmi, P., Hautaniemi, S., Nieminen, A.I., Tenhunen, M., Rantanen, V., Desmond, R.A., Chen, D.T., Guse, K., Stenman, U.H., Gargini, R., Kapanen, M., Klefström, J., Kanerva, A., Pesonen, S., Ahtiainen, L and Hemminki, A., (2009) Mre11 inhibition by oncolytic adenovirus associates with autophagy and underlies synergy with ionizing radiation, *International Journal of Cancer*, 125, 2441–2449.

[106] Dale, R., (2004) Use of the linear-quadratic radiobiological model for quantifying kidney response in targeted radiotherapy. *Cancer Biotherapy and Radiopharmaceuticals*, 19, 363–370.

[107] Hall E.J and Giaccia, A.J., (2012) *Radiobiology for the Radiologist*, 7th ed. Philadelphia: Lippincot Williams & Wilkins.

[108] Yuan, S.S.F., Hou, M.F., Hsieh, Y.C., Huang, C.Y., Lee, Y.C., Chen, Y.J and Lo, S., (2012) Role of MRE11 in cell proliferation, tumor invasion, and DNA repair in breast cancer, *Journal of the National Cancer Institute*, 104, 1485–1502.

[109] Ying, S., Hamdy, F.C and Helleday, T., (2012) Mre11-dependent degradation of stalled DNA replication forks is prevented by BRCA2 and PARP1. *Cancer Research*, 72, 2814–21.

[110] Furuta, T., Takemura, H., Liao, Z.Y., Aune, G.J., Redon, C., Sedelnikova, O.A., Pilch, D.R., Rogakou, E.P., Celeste, A., Chen, H.T., Nussenzweig, A., Aladjem, M.I., Bonner, W.M and Pommier, Y., (2003) Phosphorylation of histone H2AX and activation of Mre11, Rad50, and Nbs1 in response to replication-dependent DNA double-strand breaks induced by mammalian DNA topoisomerase I cleavage complexes. *Journal of Biological Chemistry*, 278, 20303–20312.

[111] Friesner, J.D., Liu, B., Culligan, K., (2005) Ionizing Radiation–dependent γ-H2AX Focus Formation Requires Ataxia Telangiectasia Mutated and Ataxia Telangiectasia Mutated and Rad3-related. *Molecular Biology of the Cell*, 16, 2566–2576.

[112] Burma, S., Chen, B.P., Murphy, M., Kurimasa, A and Chen, D.J., (2001) ATM phosphorylates histone H2AX in response to DNA double-strand breaks. *Journal of Biological Chemistry*, 276, 42462–42467.

[113] Cariveau, M.J., Tang, X., Cui, X and Xu, B., (2007) Characterization of an NBS1 C-terminal peptide that can inhibit ataxia telangiectasia mutated (ATM)-mediated DNA damage responses and enhance radiosensitivity. *Molecular Pharmacology*, 72, 320–326.

[114] Yuan, J., Adamski, R and Chen, J., (2010) Focus on histone variant H2AX: to be or not to be. *FEBS Letters*, 584, 3717–24.

[115] You, Z., Chahwan, C., Bailis, J., Hunter, T and Russell, P., (2005) ATM activation and its recruitment to damaged DNA require binding to the C terminus of Nbs1. *Molecular and Cellular Biology*, 25, 5363–5379.

[116] Zhang, X., Shahid, T., Soroka, J., Kong, E.H., Malivert, L., McIlwraith, M.J., Pape, T., (2014) Structure and mechanism of action of the BRCA2 breast cancer tumor suppressor. *Nature Structural and Molecular Biology*, 21, 962–968.

[117] Cousineau, I., Abaji, C and Belmaaza, A., (2005) BRCA1 regulates RAD51 function in response to DNA damage and suppresses spontaneous sister chromatid replication slippage: Implications for sister chromatid cohesion, genome stability, and carcinogenesis. *Cancer Research*, 65, 11384–11391.

[118] Carson, C.T., Schwartz, R.A., Stracker, T.H., Lilley, C.E., Lee, D.V and Weitzman, M.D., (2003) The Mre11 complex is required for ATM activation and the G 2 / M checkpoint, *EMBO Journal*, 22.

[119] Tomimatsu, N., Mukherjee, B and Burma, S., Distinct roles of ATR and DNA-PKcs in triggering DNA damage responses in ATM-deficient cells. *EMBO Reports*, 10, 629–35.

[120] Hickson, I., Zhao, Y., Richardson, C.J., Green, S.J., Martin, N.M.B., Orr, A.I., Reaper, P.M., Jackson, S.P., Curtin, N.J and Smith, G.C.M., (2004) Identification and characterization of a novel and specific inhibitor of the ataxia-telangiectasia mutated kinase ATM. *Cancer Research*, 64, 9152–9159.

[121] Gaze, M.N., Chang, Y.C., Flux, G.D., Mairs, R.J., Saran, F.H and Meller, S.T., (2005) Feasibility of dosimetry-based high-dose 131I-meta-iodobenzylguanidine with topotecan as a radiosensitizer in children with metastatic neuroblastoma. *Cancer Biotherapy and Radiopharmaceuticals*, 20, 195–9.

[122] Chalmers, A., Johnston, P., Woodcock, M., Joiner, M and Marples, B., (2004) PARP-1, PARP-2, and the cellular response to low doses of ionizing radiation. *International Journal of Radiation Oncology and Biological Physics*, 58, 410–419.

[123] Thomas, H.D., Calabrese, C.R., Batey, M.A., Canan, S., Hostomsky, Z., Kyle, S., Maegley, K.A., Newell, D.R., Skalitzky, D., Wang, L.Z., Webber, S.E and Curtin, N.J., (2007) Preclinical selection of a novel poly(ADP-ribose) polymerase inhibitor for clinical trial. *Molecular Cancer Therapy*, 6, 945–956.

[124] Hirai, T., Shirai, H., Fujimori, H., Okayasu, R., Sasai, K and Masutani, M., (2012) Radiosensitization effect of poly(ADP-ribose) polymerase inhibition in cells exposed to low and high liner energy transfer radiation. *Cancer Science*, 103, 1045–50.

[125] van Vuurden, D.G., Hulleman, E., Meijer, O.L.M., Wedekind, L.E., Kool, M., Witt, H., Vandertop, P.W., Würdinger, T., Noske, D.P., Kaspers, G.J.L and Cloos, J., (2011) PARP inhibition sensitizes childhood high grade glioma, medulloblastoma and ependymoma to radiation. *Oncotarget*, 2, 984–96.

[126] Tewari, K.S., Eskander, R.N and Monk, B.J., (2015) Development of Olaparib for BRCA-Deficient Recurrent Epithelial Ovarian Cancer. *Clinical Cancer Research,* 21, 3829-3835.

[127] Lee, H.J., Yoon, C., Schmidt, B., Park, D.J., Zhang, A.Y., Erkizan, H.V., Toretsky, J.A., Kirsch, D.G and Yoon, S.S., (2013) Combining PARP-1 inhibition and radiation in ewing sarcoma results in lethal DNA damage. *Molecular Cancer Therapy*, 12, 2591–600.

[128] Karnak, D., Engelke, C.G., Parsels, L.A., Kausar, T., Wei, D., Robertson, J.R., Marsh, K.B., Davis, M.A., Zhao, L., Maybaum, J., Lawrence, T.S and Morgan, M.A., (2014) Combined inhibition of Wee1 and PARP1/2 for

radiosensitization in pancreatic cancer. *Clinical Cancer Research*, 20, 5085–96.

[129] Jelinic P and Levine, D.A., (2014) New insights of PARP inhibitors' effect on cell cycle and homology-directed DNA damage repair. *Molecular Cancer Therapy*, 13, 1645–54.

[130] Deckbar, D., Jeggo, P.A and Löbrich, M., (2011) Understanding the limitations of radiation-induced cell cycle checkpoints. *Critical Reviews in Biochemistry and Molecular Biology*, 46, 271–83.

[131] Helleday, T., (2010) Homologous recombination in cancer development, treatment and development of drug resistance. *Carcinogenesis*, 31, 955–60.

[132] Redon, C.E., Nakamura, A.J., Zhang, Y.W., Ji, J., Bonner, W.M., Kinders, R.J., Parchment, R.E., Doroshow, J.H and Pommier, Y., (2010) Histone H2AX and Poly(ADP-Ribose) as Clinical Pharmacodynamic Biomarkers. *Clinical Cancer Research*, 16, 4532–4542.

[133] Park, K.S., Yoon, S.W., Kim, D.K and Kim, K.P., (2014) Rad51 Regulates Cell Cycle Progression by Preserving G2/M Transition in Mouse Embryonic Stem Cells. *Stem Cells Development*, 23, 1–12.

[134] Bartek, J and Lukas, J., (2001) Mammalian G1- and S-phase checkpoints in response to DNA damage. *Current Opinions in Cell Biology*, 13, 738–747.

[135] Lee, J., Goodarzi, A.A., Jeggo, P.A and Paull, T.T., (2009) 53BP1 promotes ATM activity through direct interactions with the MRN complex. *EMBO Journal,* 29, 574–585.

[136] Mairs, R.J., Ross, S.C., McCluskey, A.G and Boyd, M., (2007) A transfectant mosaic xenograft model for evaluation of targeted radiotherapy in

combination with gene therapy in vivo. *Journal of Nuclear Medicine*, 48, 1519–1526.

[137] Czornak, K., Chughtai, S and Chrzanowska, K.H., (2008) Mystery of DNA repair: the role of the MRN complex and ATM kinase in DNA damage repair. *Journal of Applied Genetics*, 49, 383–396.

[138] Richard, D.J., Cubeddu, L., Urquhart, A.J., Bain, A., Bolderson, E., Menon, D., White, M.F and Khanna, K.K., (2011) HSSB1 interacts directly with the MRN complex stimulating its recruitment to DNA double-strand breaks and its endo-nuclease activity. *Nucleic Acids Research*, 39, 3643–3651.